

COMPUTER AIDED PROCESS PARAMETER
SELECTION FOR HIGH SPEED MACHINING

I.F. DAGILOKE

Ph.D. Thesis

1995

TABLE OF CONTENTS

	PAGE
Abstract	vi
Acknowledgement	viii
List of tables	ix
List of figures	x
Notation	xiv
1.0 Introduction	1
1.1 Need for the research	2
1.2 Objectives	4
1.3 Scope of the investigation	4
2.0 Literature review	7
2.1 Introduction	7
2.2 Experimental investigation	8
2.3 Analytical models	13
3.0 Theory	19
3.1 Introduction	19
3.2 Theoretical foundation	20
3.2.1 Geometry of the milling process	21
3.2.2 The chip thickness	24
3.2.3 Shear angle determination	27
3.2.4 Strain analysis in machining chips	29
3.2.5 Workpiece material properties	31
3.2.6 Cutting forces and power	32
(i) Low and high cutting force model	33
(ii) Low speed power and cutting forces	33
(iii) Momentum, power and high speed cutting forces	36
3.2.7 Cutting energy	39

3.2.8	Cutting temperature	41
3.3	The theoretical model of high speed machining	44
3.3.1	Modification to hsm cutting forces analysis	45
(i)	Comparison of modified main cutting force with Arndt's [8] main cutting force	47
(ii)	Comparison of modified feed force with Arndt's [8] feed force	49
3.4	Discussion and required level of accuracy	51
4.0	Numerical modelling of HSM and program design	52
4.1	Introduction	52
4.2	Numerical techniques	52
4.3	Numerical modelling structure	53
4.4	Design of the process analysis program	55
4.4.1	System resources flow chart	57
4.4.2	New input data flow chart	58
4.4.3	Change data option flow chart	59
4.4.4	Cutting process calculation module flow chart	60
4.4.5	Graphical output construction flow chart	61
4.5	Conceptual algorithm of the main program	62
4.6	General discussion on the simulation model	62
5.0	Numerical prediction results and discussion	64
5.1	Introduction	64
5.2	Prediction techniques	64
5.3	Prediction 1: The relationship between metal removal rate and the cutting speed.	64
(i)	Aim of prediction	64
(ii)	Input data	64
(iii)	Prediction results	65
(iv)	Discussion on the author's predicted and Schulz's [60] results	66

	(v) Comparison of prediction with published results	66
5.4	Prediction 2: The relationship between power and the cutting speed.	68
	(i) Aim of prediction	68
	(ii) Input data	68
	(iii) Prediction results	68
	(iv) Discussion on the author's predicted and Schulz's [60] results	69
	(v) Comparison of prediction with published results	71
5.5	Prediction 3: The relationship between specific removal rate and the cutting speed.	71
	(i) Aim of prediction	71
	(ii) Input data	71
	(iii) Prediction results	72
	(iv) Discussion on the prediction results	72
	(v) Comparison of prediction with published results	74
5.6	Simulation 4: The relationship between the cutting speed and the cutting forces.	74
	(i) Aim of prediction	74
	(ii) Input data	75
	(iii) Prediction results	76
	(iv) Discussion on the prediction results	76
	(v) Comparison of prediction with published results	79
5.7	Prediction 5: The relationship between the cutting speed and the momentum forces.	79
	(i) Aim of prediction	79
	(ii) Input data	79
	(iii) Prediction results	80
	(iv) Discussion on the prediction results	80
	(v) Comparison of simulation with published results	82
5.8	Prediction 6: The relationship between the cutting speed and the cutting temperatures.	82

6.3.2	Data processing	99
6.3.3	Dynamometer and charge amplifier calibration	100
6.4	Workpiece material selection	102
6.5	Machine tool and cutting tool selection	102
6.6	Experimental procedure	103
6.7	Cutting forces experimental technique	105
6.8	Experimental results analysis	107
6.8.1	Cutting power, metal and specific metal removal rates results analysis	109
7.0	Discussion and comparison of experimental work	111
7.1	Introduction	111
7.2	Measured forces in relation to the rotational angle using 50 mm diameter cutter	112
7.3	Experiment and predicted principal cutting force against cutting speed using 50 mm diameter cutter	122
(i)	Aims	122
(ii)	Input data	123
(iii)	Discussion on experiment and predicted results	123
7.3.1	The cutting forces	123
7.3.2	The cutting power	125
7.3.3	The metal removal rate	126
7.3.4	The specific metal removal rate	129
7.4	Results of measured forces in relation to the rotational angle using 25 mm diameter cutter	130
7.5	Discussion on the 25 mm diameter cutter experiment and predicted results	138
7.5.1	The cutting forces	138
7.5.2	The cutting power	140
7.5.3	The specific metal removal rate	142
7.6	General discussion on the results	143

8.0	Conclusions and recommendation for future work	145
8.1	Recommendation for future work	148
	List of references	149
	List of published papers and conferences attended	156
	Appendices	

Computer Aided Process Parameter Selection for High Speed Machining

I.F.Dagiloke

ABSTRACT

A high speed machining software package has been developed and experimentally verified. The software package demonstrated the influence of momentum force on cutting force at very high cutting speed applications.

The software package is interactive and available to explore the viability of high speed machining.

A theoretical analysis of high speed machining has been synthesised from published literature. The model has been experimentally verified and proves without doubt that the principal cutting force and power increases as the cutting speed increases.

The influence of the cutting speed, feed and rake angle on process parameters such as metal removal rate, cutting forces, temperatures and power are discussed.

In all some seventeen input variables are identified connected with cutting conditions, workpiece and tool geometry, workpiece thermal properties and mechanical properties. The importance of these input variables to the software package is discussed in some detail. The software package has fifty seven output parameters, some of which have been experimentally verified. The information in this study should assist in providing a foundation upon which adaptive optimisation strategies for high speed machining may be developed by integrating process parameter selection and manufacturing system element constraints in process planning.

ACKNOWLEDGEMENTS

I would like to thank Dr. A.Kaldos my academic director of studies, without whose constant encouragement and support this thesis would never have been completed. Secondly, I would like to thank Dr S.Douglas my second academic supervisor for his contribution setting up this project. Also I would like to thank Professor B.Mills - Director of the School of Engineering and Technology Management for his assistance and arranging funding for the completion of the project through Liverpool John Moores University.

I would like to acknowledge the help and financial support of British Aerospace Commercial Aircraft Division Chadderton - Manchester at the earlier part of the work, British Aerospace Military Aircraft Ltd Samlesbury for providing high speed machining system for the experimental work, and in particular Mr. Tony Silcock for his effort and encouragement regarding the experimental work. To all my colleagues and laboratory engineering staff at the School of Engineering and Technology Management, Joseph Okpala from the School of Pharmacy and Dr. J. S.Garr I would like to say thank you for your support and encouragement. Finally I would like to express special thanks to my children Toyin and Bukola for their kind understanding and support, and my wife, Janet, for her patience while this work was undertaken.

Israel Dagiloke

January 1995

LIST OF TABLES		Page
3.1	Main cutting force comparison data	48
3.2	The feed cutting force comparison data	50
5.1	Predicted metal removal rate and Schulz's result	65
5.2	Predicted cutting power and Schulz's result	69
5.3	Predicted specific removal rate and Schulz, result	72
5.4	Predicted cutting force and Okushima's et al result	76
5.5	Predicted momentum force and Arndt's result	80
5.6	Predicted temperatures and Schmidt's result	84
5.7	Predicted cutting force and Schulz's result	87
5.8	Predicted cutting force and Brown's result	90
5.9	Predicted temperature and Schmidt's result	93
6.1	Details of cutting test using 50 mm diameter cutter	106
6.2	Details of cutting test using 50 mm diameter cutter	106
7.1	Acquired cutting forces data at 2827 m/min	113
7.2	Acquired cutting forces data at 3142 m/min	114
7.3	Acquired cutting forces data at 3778 m/min	115
7.4	Acquired cutting forces data at 4084 m/min	116
7.5	Acquired cutting forces data at 4398 m/min	117
7.6	Acquired cutting forces data at 4712 m/min	118
7.7	Prediction and measured forces results	123
7.8	Prediction and experimental cutting power results	125
7.9	Prediction and experimental metal removal rate result	127
7.10	Prediction and experimental specific removal rate result	129
7.11	Acquired cutting forces data at 1570 m/min	131
7.12	Acquired cutting forces data at 1855 m/min	132
7.13	Acquired cutting forces data at 2042 m/min	133
7.14	Acquired cutting forces data at 2199 m/min	134
7.15	Acquired cutting forces data at 2356 m/min	135
7.16	Prediction and measured forces results	139
7.17	Prediction and experimental cutting power results	140
7.18	Prediction and experimental specific removal rate result	142

LIST OF FIGURES		Page
2.1	Momentum force and its components	11
3.1	Cutting energy model used in analysis	20
3.2	General milling geometrical model	23
3.3	Force resolution	23
3.4	Illustration of chip thickness	25
3.5	Size of cut variation for peripheral milling	25
3.6	Tool position for maximum force and undeformed chip thickness in peripheral milling	27
3.7	The velocity diagrams	28
3.8	Strain in chip formation	30
3.9	Force geometry for two dimensional low, high and ultra-high speed machining	34
3.10	Variation of momentum force and centrifugal force with cutting speed	36
3.11	Distribution of momentum force by controlled rake face radius	37
3.12	Flow chart showing parameters for numerical simulation	44
3.13	Momentum force components	46
3.14	Arndt's [8] and modified main cutting force	49
3.15	Arndt's [8] and modified feed cutting force	50
4.1	The structure of the simulation model	54
4.2	Computer model flow chart	56
4.3	System resources flow chart	57
4.4	New input data flow chart	58
4.5	Edit input data flow chart	59
4.6	Cutting process calculation modules flow chart	60
4.7	Graphical output construction flow chart	61
4.8	Conceptual algorithm for cutting process analysis over a wide cutting speed range	63
5.1a	The relationship between the cutting speed and	

the predicted metal removal rate	67
5.1b The relationship between the cutting speed and metal removal rate (after Schulz [60])	67
5.2a The relationship between the cutting speed and the predicted cutting power	70
5.2b The relationship between the cutting speed and the cutting power (after Schulz [60])	70
5.3a The relationship between the cutting speed and the predicted specific removal rate	73
5.3b The relationship between the cutting speed and the specific removal rate (after Schulz [60])	73
5.4a The relationship between the cutting speed and the predicted cutting forces	77
5.4b The relationship between the cutting speed and the cutting forces (after Okushima et al [19])	77
5.5a The relationship between the cutting speed and predicted momentum force	81
5.5b The relationship between the cutting speed and momentum force (after Arndt [59])	81
5.6a The relationship between the cutting speed and the predicted cutting temperature	85
5.6b The relationship between the cutting speed and cutting temperature (after Schmidt [71])	85
5.7a The relationship between the feed and the predicted cutting forces	88
5.7b The relationship between the cutting forces and the feed (after Schulz [60])	88
5.8a The relationship between the rake angle and the predicted cutting forces	91
5.8b The relationship between the rake angle and the cutting forces (after Brown [27])	91
5.9a The relationship between the rake angle and	

the predicted cutting temperature	94
5.9b The relationship between the rake angle and cutting temperature (after Schmidt [74])	94
6.1 The photographic illustration of the testing rig	98
6.2 Schematic representation of the signal processing equipment	99
6.3 Photograph picture of the 50 mm diameter cutter	103
6.4 Cutting forces experimental setup	104
6.5 Photograph picture of the forces measurement setup	105
7.1 Forces against rotational angle at 2827 m/min	119
7.2 Forces against rotational angle at 3142 m/min	119
7.3 Forces against rotational angle at 3770 m/min	120
7.4 Forces against rotational angle at 4084 m/min	120
7.5 Forces against rotational angle at 4398 m/min	121
7.6 Forces against rotational angle at 4712 m/min	121
7.7 The relationship between the cutting force and the cutting speed (predicted and experimental)	124
7.8 The relationship between the cutting power and the cutting speed (predicted and experimental)	126
7.9 The relationship between the metal removal rate and the cutting speed (predicted and experimental)	128
7.10 The relationship between the specific removal rate and the cutting speed (predicted and experimental)	130
7.11 Forces against rotational angle at 1570 m/min	136
7.12 Forces against rotational angle at 1885 m/min	136
7.13 Forces against rotational angle at 2042 m/min	137
7.14 Forces against rotational angle at 2199 m/min	137
7.15 Forces against rotational angle at 2356 m/min	138
7.16 The relationship between the cutting force and the cutting speed (predicted and experimental)	139
7.17 The relationship between the cutting power and the cutting speed (predicted and experimental)	141

7.18 The relationship between the specific removal rate
and the cutting speed (predicted and experimental)

143

NOTATION

V_c	cutting speed	m/s
V_s	shear velocity	m/s
V_o	chip velocity	m/s
V_m	momentum velocity	m/s
ϕ	shear angle	rad
Θ	tool contact angle	rad
α	rake angle	rad
s_1	shear zone thickness	m
a_c	undeformed chip thickness	m
b_1	width of cut	m
t_1	depth of cut	m
t_2	instantaneous chip thickness	m
f	feed	m
D	tool diameter	m
R	tool radius	m
z	number of teeth	[1]
n	spindle speed	1/s
ZW	metal removal rate	m^3/s
ZWS	specific metal removal rate	$m^3/s \text{ kW}$
P_{ch}	power at the cut	kW
r_c	cutting ratio	[1]
β	friction angle	rad
l_c	length of contact per tooth per revolution	m
γ	shear strain	[1]
$\dot{\gamma}$	strain rate	1/s
BH	Brinell hardness	N/m^2
σ_y	uni-axial tensile dynamic yield stress	N/m^2
ϵ_p	natural plastic strain	[1]
Ψ	work hardening coefficient	N/m^2
τ_s	dynamic shear stress	N/m^2

τ_y	shear yield stress	N/m ²
τ_{se}	effective dynamic shear strength	N/m ²
σ_s	true flow stress	N/m ²
ρ	workpiece density	kg/m ³
SHC	specific heat capacity	J/kgK
T_{con}	thermal conductivity	W/mK
F_{sh}	shear force at low speed	N
F_m	momentum force	N
F_{cm}	momentum principal cutting force	N
F_{fm}	momentum feed force	N
F_{ffm}	momentum frictional force	N
F_{tm}	momentum tangential force normal to the tool face	N
F_c	low speed principal cutting force	N
F_{ff}	low speed frictional force	N
F_f	low speed feed force	N
F_n	low speed tool face normal force	N
F_{sn}	low speed shear plane normal force	N
F_R	low speed resultant force	N
F_x	required instantaneous force in X direction	N
F_y	required instantaneous force in Y direction	N
F_{tp}	low speed force normal to the tool face	N
F_{tph}	force normal to the tool face	N
F_{ch}	high speed principal cutting force	N
F_{fh}	high speed feed force	N
F_{ffh}	high speed frictional force	N
F_{shh}	high speed shear force	N
F_{nh}	high speed tool face normal force	N
F_{snh}	high speed force normal to the shear plane	N
F_{fhn}	high speed shear plane normal force	N
F_{RH}	high speed resultant force	N
R_t	thermal number of the workpiece	[1]

H_f	rate of heat generated by friction between the chip and tool	J/s
H_T	rate of total heat generated	J/s
H_s	rate of heat generated by shearing	J/s
T_{ave}	average temperature of the chip resulting from the secondary deformation	K
δT_{max}	maximum temperature rise in the chip due to frictional heat source in the secondary deformation zone	K
L_o	length of heat source divided by the chip thickness	[1]
T_o	initial workpiece temperature	K
T_m	workpiece melting temperature	K
H_{cw}	heat conducted into the workpiece	J
δT_s	average rise in shear zone temperature	K
T_{max}	maximum temperature on the tool rake face	K

CHAPTER 1

1.0 INTRODUCTION

This study is concerned with the investigation of high speed machining of aluminium alloys using the milling process and with the development of cutting software package capable of predicting the cutting forces, power, metal removal rate, cutting energies and temperatures at high cutting speeds. High speed machining (HSM) is one of the emerging cutting processes that are employed either directly or indirectly in the metal cutting industry. However, because of the high speeds involved the process requires a special purpose machine tool, tools, jig and fixtures. Milling is an intermittent cutting process whereby the primary motion is provided by the tool and the secondary motion is provided by the workpiece. The primary motion is rotational and continuous while the secondary motion is normally linear resulting in variable chip thickness that may be classified into two types: (i) Peripheral (or plane) milling and (ii) Face (or end) milling.

Defining high speed machining is not an easy task, since the actual cutting speed that can be achieved depends upon the workpiece material, the type of cutting operation and the cutting tool used. This has led to several definitions being suggested in the literature. The most general definition is the economical utilization of resources and functions to remove mechanically the greatest amount of material in the shortest time span as suggested by Chasteen [1]. It is also essential to define the cutting speed quantitatively leading to the following according to von Turkovich [2]:

- (i) Low speed machining (LSM) 0 - 10 m/s;
- (ii) High speed machining (HSM) 10 - 30 m/s;
- (iii) Very high speed machining (VHSM) 30 - 300 m/s;
- (iv) Ultra-high speed machining (UHSM) being faster still (> 300 m/s).

The need to reduce manufacturing costs is an ever present challenge to industry. Processes are continuously being developed and new processes introduced to improve productivity and to meet the product specifications. It is recognised that conventional machining processes cannot always meet the technology of these new production challenges. Therefore, considerable interest in high speed machining technology arises due to the possibility that it can dramatically increase metal removal rates according to Flom et al [3]. For example, in the aerospace industry the wing spars are machined from expensive forged aluminium billets while the stringers are machined from milled bars. The final geometry of the spar and the stringer requires up to 90 percent of the original material to be removed. A typical front spar for the A320 aircraft has to be milled from 1895 kg down to 117 kg and stringer from 396 kg to 47 kg. Consequently the economics of the process largely depends on the metal removal rates. The ability to maintain high removal rates also depends on the ability to control the chips from the machining area. This implies that applying high speed machining techniques to large aerospace components is economically very attractive.

1.1 NEED FOR THE RESEARCH

It is well documented by King and Vaughn [4] that as the cutting speed increases above the conventional speed range, new dynamic effects are encountered in the cutting process. For example, the basic chip morphology changes due to the momentum force. Taylor's empirical equations are no longer valid since they are not velocity dependent as stated by King et al [4]. It has been suggested by Schulz and Moriwaki [5] that this momentum effect arises when additional energy has to be supplied to accelerate the chip past the shear zone.

In addition the implementation of high speed machining presents a challenge since various factors limit the extent to which cutting speeds may be advantageously increased. These factors include the cutting temperature, the

cutting tool material, the workpiece material, the machine tool design, the cutting geometry, the cutting power and also after machining the surface integrity and metallurgical condition of the workpiece.

Given the above considerations, experimental data and a mathematical model are essential in determining the factors which influence productivity at high cutting speed. Detailed information on the cutting process is necessary to improve understanding of high speed machining and enhance the possibility of the process being accepted by industrialists.

Fundamentally, the purpose of HSM has been based on process economics, however, a literature review coupled with the study into the manufacture of large aerospace component suggested that most previously published investigations have focused on the difference in the cutting mechanism between high and low speed machining rather than in improving production economy. Early works [6 - 10] have been directed towards understanding the deformation of materials at high impact rates based on the theory of plastic wave propagation established by von Karman et al [11]. More recent works [3, 12 - 14] have been concerned with studies of cutting mechanisms, including chip formation mechanics, temperatures and cutting forces determination.

To-date there has been no significant published work relating to simulation of the HSM process which includes cutting forces, momentum force, cutting energies and cutting temperatures. This can be attributed to the fact that the high speed machining process is a complex manufacturing method to understand. It involves various input and output parameters linked together through a multitude of complex internal interactions.

1.2 OBJECTIVES

The aim of the work was to develop a computer based simulation of the milling process at cutting speeds above 10 m/s using a two dimensional cutting model and to compare the predictions with experimental results.

The particular objectives may be summarized as follows:

- (i) To undertake an analytical and experimental investigation of the effects of independent cutting parameters such as cutting speed, feed, rake angle and depth of cut on the cutting process, selection of machine tools, cutting tools and workpiece materials at high cutting speeds.
- (ii) To develop a computer program based on the above analysis which includes momentum force and is capable of predicting the milling process parameters at both low and high cutting speeds.
- (iii) To measure cutting forces and cutting temperatures experimentally at high speed range.
- (iv) To validate the analytical model by comparison with experiment and to use the results to attempt to overcome some of the manufacturing engineering community reservations about high speed machining.

1.3 SCOPE OF THE INVESTIGATION

In the present study, a computer based mathematical cutting process model with an integrated database and experimental work based on a peripheral milling operation using a cutter with two tips at both low and high speed machining ranges is proposed, developed and verified.

In developing the proposed software program, several areas of metallurgy and machining mechanics were explored. As part of this research work, literature on HSM was reviewed and relevant cutting models related to this study were compiled and critically analysed. The philosophy adopted was

to create, implement a comprehensive theoretical model, based mathematically on basic cutting process parameters. Such a model makes it possible to simply investigate the dependency of each cutting parameter and its effect within the simulated results. The theoretical formulation and the program design methodology are discussed in chapter 3 and 4. Understandably such a model requires experimental validation. This was achieved by extensively milling aluminium alloy workpieces on a proper high speed machining system. The test rig used for such a validation obviously needs to be of the highest quality with excellent data acquisition control over the independent variables and good repeatability. It must also provide a great deal of highly detailed data on the cutting process. The equipment used, the experimental procedures and results analysis are described in chapter six.

In order to establish a broad data base for future use, all the acquired data for workpiece and tooling mechanical and thermal properties, cutting conditions, workpiece geometries, tooling geometries, machine tool parameters, generated numerical and graphical results data were stored on a DEC Vax computer system. Also a software package suitable for modelling orthogonal milling using single point HSM process was designed, developed, tested and discussed.

The thesis itself is divided into eight chapters. In chapter 2 a comprehensive review of the published theoretical and experimental work on HSM is discussed. Conclusions are drawn from the literature survey and its influence on the research is presented. Chapter 3 discusses the theoretical foundation for HSM of a peripheral milling operation and the computational analysis required. Individual parameters required for HSM are discussed, these include the metal removal rate, power, cutting forces, cutting energy and cutting temperature. Chapter 4 discusses numerical modelling and program design. This includes a structure for numerical modelling, creation of an input module database, a physical simulation module, an output module and flow chart for the simulation program. Chapter 5 discusses the method employed

in the simulation tests and choice of the simulation input variables. Results from the simulation are discussed. Chapter 6 presents the experimental work and equipment. Chapter 7 discusses the experimental results and comparison of experimental and simulation results. Finally, in chapter 8, general conclusions are presented and suggestions are made for further future work.

CHAPTER 2

LITERATURE REVIEW OF HIGH SPEED MACHINING

2.1 INTRODUCTION

The basic reservations to high speed machining as suggested by Aggarwal [7] are:

- (i) the fear of excessive maintenance problems, problems in swarf control and the basic apprehension associated with fast machining;
- (ii) industry's continuing tendency to use low speeds and feeds on the shop floor;
- (iii) belief that the major part of the manufacturing cost is in the material and handling process, therefore, HSM cannot possibly provide significant cost saving;
- (iv) the controversy over the claim that there is a reduction in cutting forces and temperature at high cutting speed;
- (v) uncertainty about how to select optimum cutting parameters and machine tool specifications for high speed machining.

The first stage of the research was aimed at addressing these issues.

Numerous high speed machining studies have been reported in the literature covering a variety of work materials including steels, cast iron, lead, aluminium alloys and titanium. The tool materials used in previous studies included carbon steels, high speed tool steels, carbides and oxide, whilst the cutting speeds ranged from 0.08 to 1217 m/s (5 to 73,000 m/min) according to Flom et al [3].

HSM requires a knowledge of a wide area of engineering including machine tool design, spindle design, cutting tool design, feed control, software

applications and cutting process parameters. It would be difficult to combine the study of all these topics and use it to draw conclusions regarding HSM capabilities and suitability as an alternative manufacturing process compared to conventional low speed machining. Therefore, the review will be restricted to cutting process analysis with special attention to two topics, namely: experimental investigations and analytical models that can be used to describe the geometry of the metal cutting process. It is believed that the background for the current research undertaken can be developed by focusing attention on these two topics.

2.2 EXPERIMENTAL INVESTIGATIONS

Arndt [9] suggested that the origin of the interest in HSM was based on the findings of Salomon in 1931, who proposed that metal removal rates increase with cutting speeds depending on particular conditions such as:

- tool life,
- adequate power,
- machining systems which are rigid enough
not to cause vibrations.

Arndt [9] stated in Salomon's study of high-speed milling of copper, bronze and aluminium at speeds up to 25.4 m/s (1524 m/min), concentrating on temperature measurement using a tool-chip thermocouple technique that the tool temperature increased with speed, reaching a peak, close to the melting temperature of the workpiece material and then decreased rapidly at very high speeds. It was concluded that better machining features can be obtained at very high cutting speeds. For machining steel and cast iron, it was predicted that the cutting temperatures should drop off at machining speeds over 752 m/s (45,110 m/min) for steel and 650 m/s (39,014 m/min) for cast iron. It was further concluded that a critical cutting speed exists for each material at which the temperature reaches a maximum and beyond which the cutting temperature falls rapidly to a low value. While this

hypothesis is informative, none of these predictions were substantiated in the literature according to Arndt [9], Wright and Bagchi [54].

No significant work on HSM was reported until von Karman [11] made a study of the stress waves arising from a longitudinal impact at the end of a cylindrical bar. It was shown that at high impact speeds metals undergo a small amount of plastic deformation. It was suggested that a critical velocity may exist beyond which all materials fail with negligible stress and that the concept of plastic strain propagation may bring about a better understanding of some anomalies encountered in HSM. It is apparent from these observations that metals experience a transition between shear deformation modes when the strain rate exceeds a critical value after which the shear stress begins to decrease rapidly. It appears that the idea of a reduction in cutting forces and temperatures as the cutting speed increases was based on this result.

Schmidt [16] reported the results of high speed milling tests up to 75 m/s (4500 m/min) on SAE 4340 steel hardened to 500 BHN and SAE 1020 hardened to 180 BHN using carbide and high speed tools. A decrease in metal removal rate was claimed as the cutting speed increased from 5 m/s (300 m/min) to 50 m/s (3000 m/min) and also that the tool-chip interface temperature increased. These findings are in total contradiction to Salomon's work as reported by Arndt [9]. Schmidt's results are not conclusive because the results were affected by rapid tool wear and critical tool deflection was experienced during the experiments. This might explain why reductions in metal removal rates were observed as the cutting speed increased.

By 1958, it had become apparent that high temperature and high tool wear were the major obstacles to using high machining speeds. This was manifested in the experimental work conducted by Siekmann [17] at cutting speeds up to 92 m/s (5,500 m/min) on AISI 1045 steel hardened to 180 BHN using alumina ceramic tools and cemented tungsten carbide tools. The

rate of tool wear was found to be extremely high at high speed. A 0.6 minute tool life was obtained at 92 m/s based on a 0.3 mm flank wear criterion. Due to high tool wear rate these experiments were limited. A more precise conclusion could not be given other than to confirm the problem posed by high temperature and tool wear at high cutting speeds.

In 1965 Tanaka and Kitano [18] conducted high speed machining tests up to 127 m/s (7,600 m/min) on mild steel and on an aluminium alloy using an ultra high-precision lathe with carbide and oxide tools. Both the carbide and oxide tools were found to wear extremely rapidly. However, it was found that the ceramic tools wore at a slightly lower rate. In 1966 similar results were reported at even lower speeds of 30 m/s (1,800 m/min) by Okushima et al [19]. Okushima et al found the tool life to be affected by the high cutting temperatures and the vibrations of the machine tools. The results reported here and those of Siekmann [17] make it clear that there is no evidence for a reduction in cutting temperatures at higher cutting speed.

In 1972 Arndt and Brown [20] published results taken from an experimental ballistic machining facility that could machine at speeds from 150 to 2433 m/s (9,000 to 146,000 m/min). Their aim was to use the upper speed to investigate whether or not metals exhibit brittle behaviour in high speed machining, that is, at speeds exceeding the elastic wave propagation velocity. Most of the tests were conducted on aluminium, however, a few were conducted on steel and lead materials. It was reported that most of the tests resulted in severely chipped cutting edges while some led to complete fracture of the tool, especially at higher cutting speeds. The chipping of the tools at high cutting speeds were attributed to impact loading of the tool and the momentum force that is concentrated at the tool tip. Arndt and Brown determined the cutting ratio (r_c) for each test by dividing the depth-of-cut by the maximum measured chip thickness. The shear angle was then

determined from the orthogonal cutting relationship as shown in equation:

$$\Phi = \arctan \left(\frac{\cos \alpha}{(1/r_c) - \sin \alpha} \right) \dots \dots \dots (2.1)$$

Knowing the shear angle and using figure 2.1, it was possible to calculate the momentum force F_m and its components parallel and normal to the cutting direction. The change in momentum caused by the transformation of uncut chip material into the chip gives rise to the momentum force which was derived as :

$$F_m = \frac{b_1 t_1 V_c^2 \rho}{\cos \phi} \left(\frac{1}{1 + \tan \phi \tan \alpha} \right) \dots \dots \dots (2.2)$$

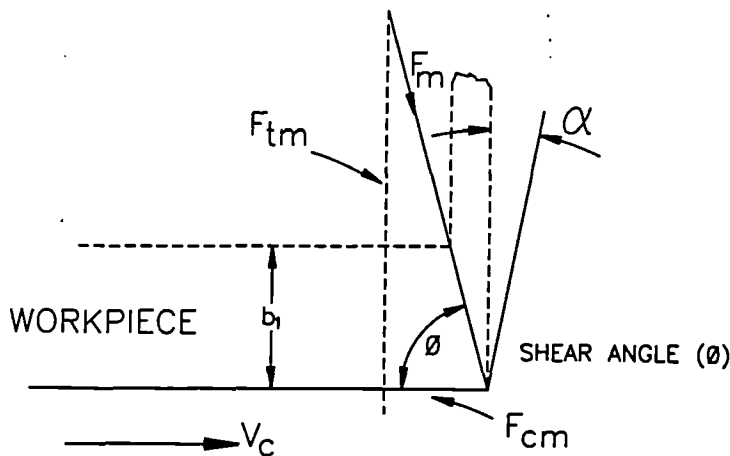


Fig. 2.1: Momentum force and its components after Arndt [20]

The reported result shows that the cutting ratio, shear angle, momentum and other cutting forces increase with an increase in cutting speeds. They suggested that the influence of this momentum force is insignificant compared to the shear force and other cutting forces at conventional low speed machining. However, at high cutting speeds its value may become significantly high since it varies with the square of the cutting speed.

Although Arndt and Brown's [20] work demonstrated that the cutting forces increase with an increase in cutting speed and gave an insight to the

influence of the momentum force in HSM, however, the authors did not comment on the tool flank and rake face wear except a mention of the dark discoloration observed at the rake face and light discoloration at the flank.

Chaplin [21] reported that the side load on a carbide end mill cutting aluminium was reduced as the cutting speed was increased. For the same chip load and depth of cut, the side load was reduced by 70 percent when the spindle speed was increased from 67 to 333 rev/s (4,000 to 20,000 rev/min) during roughing operations, thus enabling milling of thinner sections with deeper cuts and closer tolerance than were previously considered possible. Further findings were that the surface texture obtained was better than with conventional machining. The metal removal rates when machining aluminium was approximately doubled compared to conventional rates. These findings proved that significant savings can be made by using HSM as compared to conventional low speed machining and contradicted the findings of Schmidt [16]. However, the reported results lacked details on how to establish optimum cutting conditions for high speed machining and an implementation procedure for the shopfloor.

Komanduri et al [22] conducted experiments on an AISI 4340 steel hardened to 325 BHN at various speeds up to 41.7 m/s (2,500 m/min). Longitudinal midsection of the chips was examined metallurgically to determine the differences in the chip formation characteristics at various speeds. Shear-localized chips were observed at all cutting speeds above 4.6 m/s (275 m/min). At cutting speeds higher than 16.7 m/s (1000 m/min) the segments were found to separate completely due to extensive shear in the primary shear zone; at lower speeds they were held intact. Finally, the speed at which catastrophic shear was found to completely develop and the speed at which individual segments were found to separate completely by intense shear were found to depend on the hardness of the material used. The results of this experiment were useful in that it gave an insight into chip formation at high cutting speeds. However, nothing was reported on the

temperatures, tool wear or cutting forces.

Nieminen et al [23] conducted an experimental milling of polymer-matrix composites such as carbon and glass fibre by using advanced carbide and diamond tools. Flank wear resulting from the abrasive wear mechanism was reported as the dominant wear form of the cemented carbide tools when graphite was milled. There was no report of any crater wear on the rake face of the tools. When the ball-nose end mills were used in the milling of the tool steel, it was reported that the tool materials used display an excellent wear resistance and the surface texture of the workpiece was good. This result justified the use of HSM over conventional machining for achieving better surface finish, although, nothing was reported on the power consumption of the machine tool.

2.3 ANALYTICAL MODELS INVESTIGATION

Analytical modelling has been conducted of the chip formation process in HSM [2, 24 - 28]. The theoretical and metallurgical features of chip formation have been organised into four areas. The main features are: (i) chip geometry and morphology, (ii) kinematics, (iii) deformation zones, and (iv) cutting forces. The theory applies both to continuous and segmental (discontinuous) types of chips.

The earliest model of the orthogonal metal cutting process which applied to both conventional and high speed machining was developed by Merchant [24]. Part of this work was the derivation of shear angle based on the principle of minimum energy. Critical analysis of this theory indicates that the effects of cutting speeds and cutting energy which are crucial in HSM has not been taken into consideration and thus makes its application to HSM ineffective.

Recht [29] conducted an ultra high-speed machining feasibility study. Recht

theoretically analyzed the variation of tool-chip interface temperature as a function of speed. Recht suggested that since the heat generation at the tool-chip interface must be conducted into the chip, an increase in cutting velocity would mean an increase in heat conducted away with the chip during unit time. As a result, the tool-chip interface temperature should rise very rapidly with cutting velocity and should approach the melting point of the workpiece material. This theory is however limited in scope since no attempt was made to address the influence of the cutting speed on the cutting forces especially the momentum (inertia) effect and the surface integrity of the machined workpiece.

Fenton et al [30] used strain-rate dependent machining theory to predict the cutting forces for a low carbon mild steel for cutting speeds in the range 0.5 to 50.8 m/s (30 to 3048 m/min). In this study the workpiece material flow stress characteristics were expressed in the form:

$$\sigma_{eff} = \sigma_1 E_{eff}^n \dots \dots \dots (2.3)$$

where σ_{eff} and E_{eff} are the effective stress and effective strain respectively and the "constant" σ_1 and n are strain-rate dependent. Values of σ_1 and n were obtained from tensile tests and machining tests for strains in the range 10^{-6} to 10^5 per second were used in the calculations, however, for the very high cutting speeds (strain-rate greater than 10^5 per second) these results were extrapolated. The forces calculated in this way showed that the force in the direction of cutting reduces up to approximately 5.08 m/s (305 m/min) and then started to increase as the speed is further increased to 50.8 m/s (3048 m/min). In view of the author's use of extrapolated stress-strain data at very high cutting speeds the results from this study must be treated with some caution particularly in regard to the reduction of cutting forces with an increase in the cutting speed.

Tanaka et al [31] studied high speed cutting of mild steel, brass and aluminium in the speed range of 16.7 to 133 m/s (1000 to 8000 m/min). The

authors investigated the influence of high cutting speed on chip formation, shear angle, shear stress and cutting forces. It was reported that the cutting deformation behaviour is significantly influenced by the temperature gradient in the shear zone and at the tool-chip interface. A further finding was that with increase in cutting speed, the shear angle increases and that the specific cutting force and shear energy remain constant irrespective of cutting speed. These results were not surprising because the influence of the momentum at high cutting speed were not taken into consideration. Also the theory was deficient in that it took no account of the temperature rise in cutting and its influence on flow stress.

Matthew et al [15] predicted the effect of very high cutting speeds up to 100 m/s (6000 m/min) on cutting forces, temperatures and stresses based on plane strain orthogonal machining under steady state conditions. Unlike the results of Fenton et al [30], these results indicated that the cutting forces will keep reducing with increase in speed up to the maximum speed (100 m/s) considered. The reason given was that the increase in temperature at the tool-chip interface with increase in speed is sufficiently large compared with the increase in strain rate for velocity modified temperature at the interface to keep increasing, thus in effect reducing the chip thickness and the principal cutting force. The reported results are very questionable because the material properties were extrapolated and the effect of inertia forces that take place at high cutting speed was ignored.

Recht [13] developed for HSM force diagrams and a model of energy balances that treats the chips as a free body for continuous chip formation in high speed machining. This model properly considers the effect of chip momentum change. This analysis showed that Merchant's [24] equation $((\phi = 90 - \tau + \alpha) / 2)$ which describes for conventional machining the relationship between rake angle, shear angle and friction angle applies also to high speed continuous chip formation process. The reported results gave insight into the effect of workpiece material properties and also accounted

for the momentum force effects at high cutting speed. However, Recht's suggestion that Merchant's model for conventional machining applies to HSM as well is surprising when it has been suggested by King et al [4] that Merchant's model is independent of cutting speed.

An analytical model developed by von Turkovich [2] relates the onset of shear localization to cutting speed through the effect of the latter on strain rate. This analysis led to the formulation of a stability principle based on the properties of the stress-strain-rate surface under adiabatic deformation conditions. The author demonstrated that the model can be used to identify a speed at which the chip formation mechanism becomes unstable and chip segmentation begins. By comparing theoretical results with limited experimental data, it was concluded that chip formation is not a main problem in hsm. However, tool wear posed a severe restriction on cutting mechanism investigation. Further conclusion from the study was that the cutting forces, chip geometry and deformation process in the shear zone were not substantially changed by a large increase of the cutting speed up to the speed of the order of 333 m/s. The reported results were useful in that it provides techniques of using the energy balance equation to analyse the influence of very high cutting speed on chip formation in hsm. However, the level of accuracy of these results was questionable because strain rates higher than 10^5 per second which are central to cutting forces and temperature calculation were based on approximate estimates.

Sedgwick, [32] employed a two-dimensional finite difference computer program to model the high speed machining process. This is an explicit version of a Hydrodynamic Elastic-Plastic continuum mechanics program. The program solves the basic equations of continuum mechanics throughout a fixed mesh to obtain the deviatoric stress components, pressure, mass density, material velocity components and internal energy as functions of space and time. The material model includes an equation-of-state which gives the pressure as a function of mass density and internal energy, an

elastic-plastic constitutive relation and a material failure model. The reported results showed the configuration of the chip during its formation process, the material velocity fields, the mass density distribution and the total stress distribution. This model only applies to continuous chip formation and it is only effective at lower machining speed calculations.

From the literature study three important issues arise as follows:

- (i) Some work has been undertaken to establish the difference between HSM and LSM.
- (ii) As yet a numerical algorithm allowing the HSM cutting process parameters to be predicted and verified by reliable experimental data has not been developed.
- (iii) It is apparent that a practical solution to predicting high speed cutting process parameters can only be acquired by the inclusion of momentum effect in the analysis.

Hence, from the above expositions it becomes evident that many unresolved questions still exist in the field of HSM. There is a clear need for further research into generic computer cutting models verified by experimental data that describes the hsm processes, which can be related to milling operations regardless of workpiece materials. This would provide a powerful tool to assess the economic justifications, safety aspects and implementation implications of HSM technology for manufacturing process engineers to use.

Apart from the theoretical interest in explaining the complicated phenomena that arise in high speed machining, there is a wide range of important applications of the computer aided process parameters selection software package proposed in this study; such as selecting optimum cutting parameters, spindle and machine tool requirements which will help to reduce setup time, tape proving time and production costs significantly.

The direction of research needed for the advancement of knowledge in the

field of high speed machining lies in the development of more refined analytical models. The models should not represent just one aspect of cutting process determination as have been the case in all previous works but should synthesise elements of the cutting process including cutting conditions, forces, temperatures and power. Through the use of these models the cutting process may be more accurately represented.

CHAPTER 3

3.0 THEORY

3.1 INTRODUCTION

The power consumed in metal cutting is largely converted into heat near the cutting edge of the tool and many of the economic and technical problems of machining are caused directly or indirectly by this heating action. The cost of machining is very strongly dependent on the rate of metal removal and may be reduced by increasing the cutting speed and/or the feed rate. However, there are limits to the speed and feed above which the life of the tool is shortened excessively. The limitations imposed by cutting speeds have been the spur to both the research community and industry in the last 70 years to find the optimum cutting speed and techniques to model HSM.

Based on established theoretical analysis, Boothroyd and Bailey [33] suggested that chip formation consists of shearing in the primary deformation zone and sliding of the chip along the rake face of the tool in the secondary deformation zone and that these are the two principal zones of energy dissipation occurring in machining. This is illustrated in Figure 3.1 and it is, therefore, important to understand the factors which affect the cutting process and this chapter presents and discusses the dynamics of high speed milling. The various forces that influence the milling process in both low and high speed cutting due to interactions of the cutting tool and the workpiece material are quantified using trigonometric relations. Equations for cutting energies, temperatures and other process parameters are presented in terms of the general principles of mechanics of metal cutting. The equations are further developed to include the momentum force and energy that takes place at high cutting speed.

Also based on established theoretical analysis, theoretical modelling of the

HSM process and modifications to mathematical equations of the cutting force in HSM are presented.

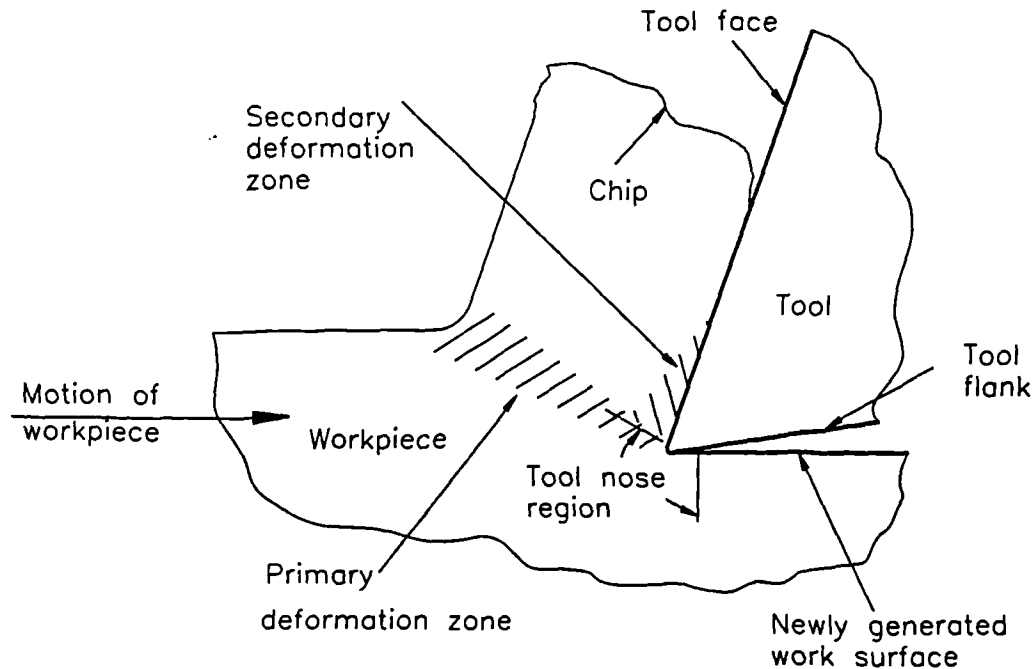


Fig. 3.1: Cutting energy model used in analysis [33]

3.2 THEORETICAL FOUNDATION

Representation of the milling process for both low and high speed machining involves the penetration of the tool into the surface of the workpiece in such a way as to separate the undeformed chip in a continuous manner resulting in the production of a deformed chip. It has been suggested by Zorev [34] that during the metal machining process, the tool experiences severe frictional conditions along its rake face and that in the region of chip-tool contact close to the tool cutting edge, conditions of so-called sticking friction exist. This is where the shear stress is constant and equal to the shear strength of the chip. In the remaining region of chip-tool contact sliding frictional conditions exist. This is where the coefficient of friction is constant. Beyond the sliding region, the chip curls away from the tool face.

The reason for the existence of the sticking and sliding region has been explained by Albrecht [35]. The tool forces exert bending stresses several times the magnitude of the shear stress over the shear plane. The bending stresses cause the chip initially to flatten out as it contacts the tool and then to curl away from the tool as it moves up the tool face. This accounts for the existence of the sticking region along the lower part of the tool as well as the high normal stresses in this region. Beyond the sticking region the chip curves away from the tool producing a sliding region.

A complete dynamic description of the milling process requires a determination of the chip thickness and the shear angle produced when the cutting tool first penetrates the surface of the workpiece. There is no simple analysis to this and the dynamics are further complicated by the fact that the geometry of the chip formation process is controlled by the conditions of strain, strain rate and temperature in the cutting zone. These parameters are themselves controlled by the input cutting conditions such as the cutting speed and the tool rake angle. The solution to this dynamic problem requires the establishment of selection of all the necessary equations that describe both low and high speed milling operations to form a cutting model. The areas where process equations were selected are:

- (i) Strain and strain rate in machining of chips;
- (ii) Machining stresses;
- (iii) Cutting power and forces;
- (iv) Cutting energies and temperatures.

3.2.1 GEOMETRY OF THE MILLING PROCESS

To accomplish the objectives of this work, it is necessary to develop a model that correctly predicts the stress level at which separation occurs, to determine the chip thickness and shear angle which can be used to calculate the cutting forces, energies and temperatures. To derive these required equations it is necessary to analyse the geometry of the chip section since

the sectional area of the chip changes continuously as the cutter tooth moves along the workpiece. Furthermore, in the case of the helical cutter, the width as well as the thickness of the chip changes with the angle of advancement of the cutter tooth in the workpiece material. At present insufficient knowledge exists to enable a three dimensional geometric model that can describe accurately the complete chip formation process at high cutting speed to be developed. For example, there is lack of adequate knowledge on how to predict the influence of cutting fluid and how many cuts have to be made before the tool wear criterion could be taken into consideration. It was, therefore, necessary to develop a two dimensional model.

Figure 3.2 as presented by Kaldos et al [38] illustrates schematically the geometry of the cutting process. Its associated force resolution diagram is shown in Fig 3.3 subject to the following assumptions being made as suggested by Dagiloke et al [36-37]:

- (i) that the operation is two dimensional peripheral milling and no cutting fluid is applied.
- (ii) that each chip particle formed follows an identical curved path through a shear deformation zone of finite thickness and its velocity changes progressively from the cutting velocity to shearing velocity and finally to chip velocity.
- (iii) that the workpiece is at room temperature.
- (iv) that there is no wear on the tool. This is important so that errors due to tool wear can be eliminated.

Having described the assumptions made and the idealized geometry of the cutting process, the remainder of this chapter describes the analysis of the general equations selected for the cutting process parameters.

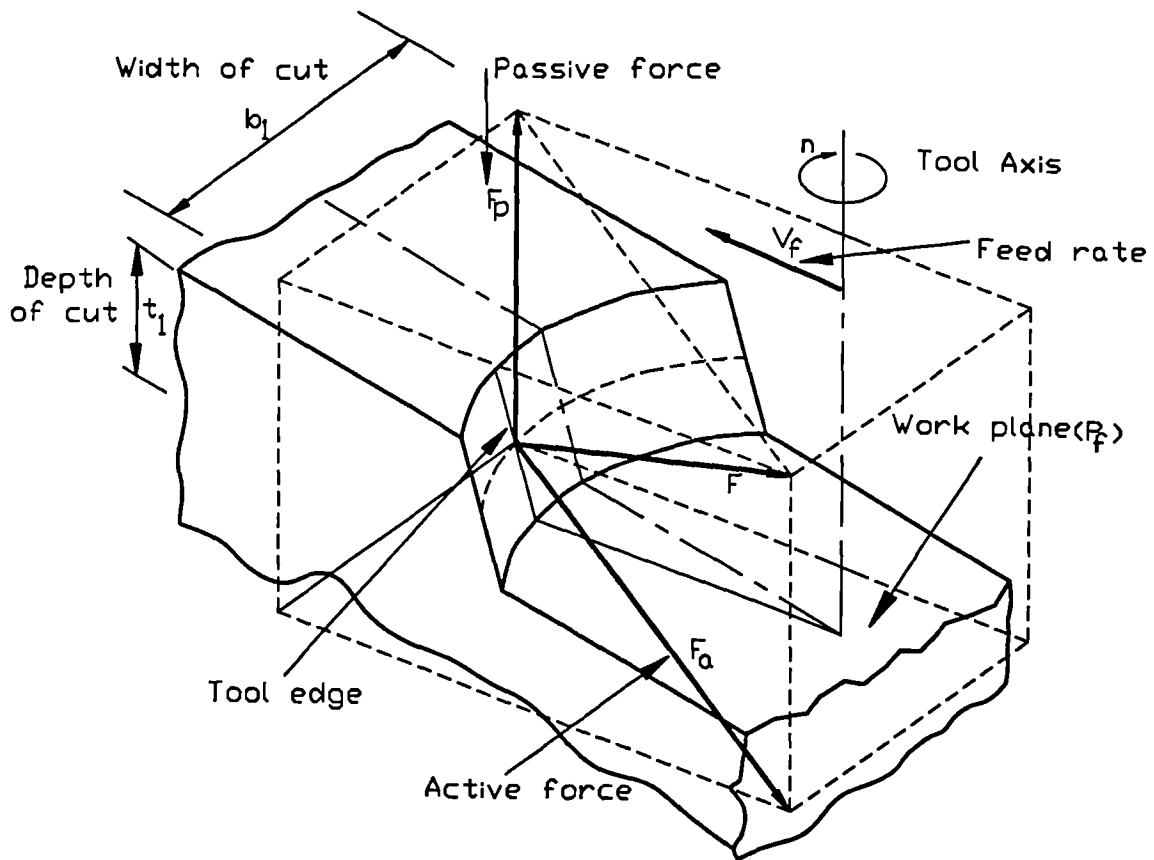


Fig. 3.2: General milling geometrical model [38]

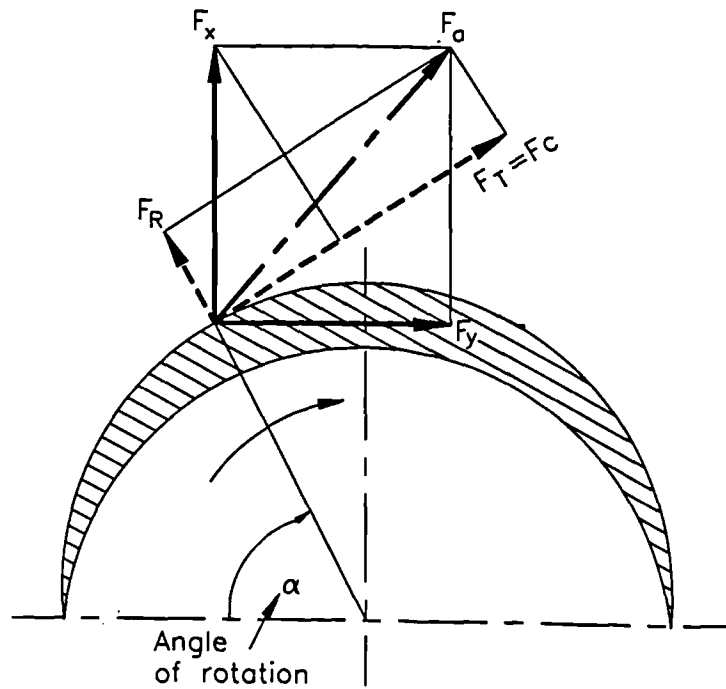


Fig. 3.3: Force resolution [38]

The determination of the low speed general equations in milling are well known [38 - 41]. A thorough analysis has been presented by Martellotti [42] and Armarego et al [43]. The analysis that follows shows the standard equations that cater for both low and high speed machining.

3.2.2 THE CHIP THICKNESS

An element central to the prediction of the cutting forces is the chip load on the cutter. Martellotti [40] presented a detailed analysis of the mechanics of the milling process which provides the basis for the chip load calculation. The basic equation for the instantaneous chip thickness is:

$$t_2 = f \sin\theta \dots\dots\dots (3.1)$$

where t_2 is the instantaneous chip thickness, f is the feed (mm/tooth) and θ is the angular position of a tooth in the cut.

A complete representation of the chip load on a slab mill at any instant is obtained by considering thin, disc-like sections along the axis of the cutter as presented by Martellotti [40]. The location of each flute on each disc is determined and for each flute engaged in the cut, the chip thickness multiplied by the thickness of the disc yields the chip load. As the angular position of the cutter is incremented, the chip load is recomputed. This is shown in Fig 3.4 which shows the cut geometry and co-ordinate system for down milling.

To derive the instantaneous chip thickness, it is essential to know the angular position and this is derived as follows. Figure 3.5 shows the thickness variation of the cut for a circular tooth path. The maximum undeformed chip thickness is defined by a_c and various methods have been used to determine its value. From the geometry shown, Armarego et al [43] has shown that the maximum undeformed chip thickness can be given as:

$$a_c = 2 f \sqrt{\frac{t_1}{D} \left(1 - \frac{t_1}{D}\right)} \dots\dots\dots (3.2)$$

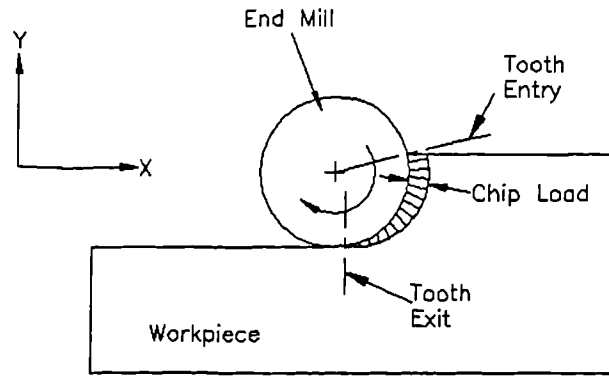


Fig. 3.4: Illustration of chip thickness

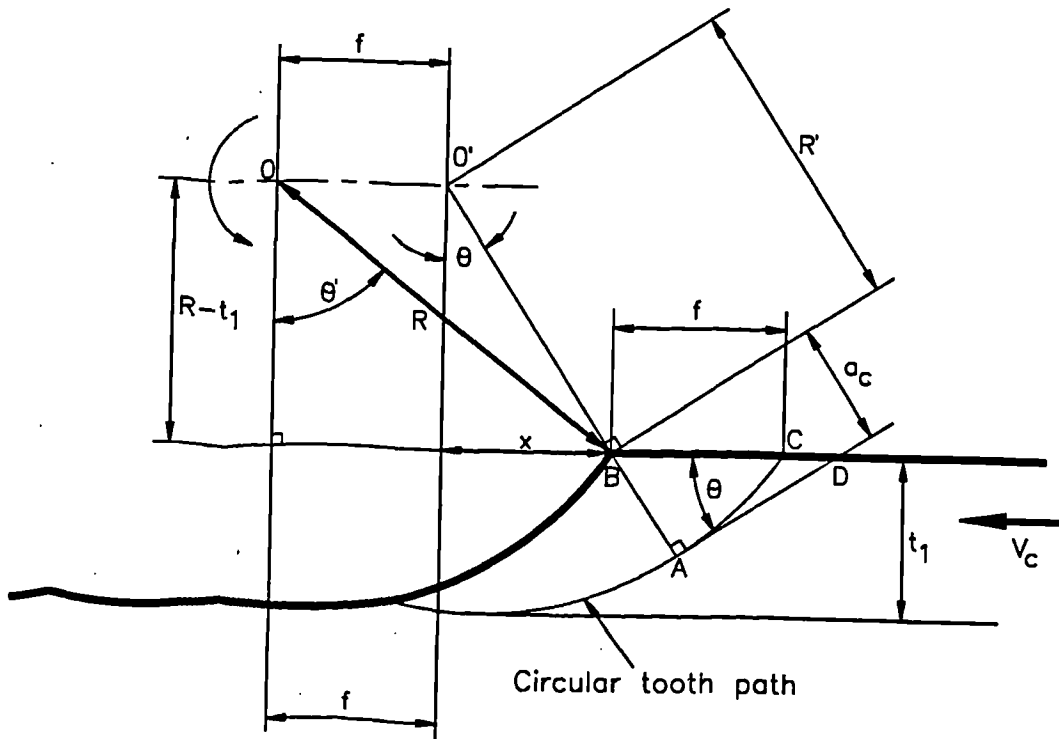


Fig. 3.5: Size of cut variation for peripheral milling [41]

The length of contact per tooth per revolution according to Armarego et al [43] is given by:

$$L_c = R \theta = R \cos^{-1} \left(\frac{R-t_1}{R} \right) = \frac{D}{2} \cos^{-1} \left(\frac{D-2t_1}{D} \right) \dots\dots (3.3)$$

The average undeformed chip thickness is given by:

$$t_{ave} = \frac{f t_1}{L_c} = \frac{2 f t_1}{D \cos^{-1} \left(\frac{D-2t_1}{D} \right)} \dots\dots\dots (3.4)$$

Armarego et al [43] suggested that further approximations may be made if $D \gg t_1$, so that the maximum undeformed chip thickness can be given as:

$$a_c = 2 f \sqrt{\frac{t_1}{D}} \dots\dots\dots (3.5)$$

and by expanding $\cos \theta'$ in terms of θ' and equating to $(D-2t_1)/D$

$$\theta = 2 \sqrt{\frac{t_1}{D}} \dots\dots\dots (3.6)$$

Hence

$$L_c = R \theta = \sqrt{t_1 D} \dots\dots\dots (3.7)$$

Similarly

$$t_{ave} = f \frac{t_1}{L_c} = f \sqrt{\frac{t_1}{D}} = \frac{a_c}{2} \dots\dots\dots (3.8)$$

From the Armarego et al [43] analysis shown in equations 3.2 to 3.8, it is observed that even when a circular path is assumed a number of approximations are required to arrive at simple relationships. Assuming a circular tooth path implies that the workpiece feed is intermittent, so that the workpiece is stationary during a tooth engagement and then moves suddenly by feed (f) before the next tooth starts a cut.

3.2.3 SHEAR ANGLE DETERMINATION

An important parameter to determine cutting forces, energies and temperatures is the shear angle produced during the cut as illustrated in figure 3.6.

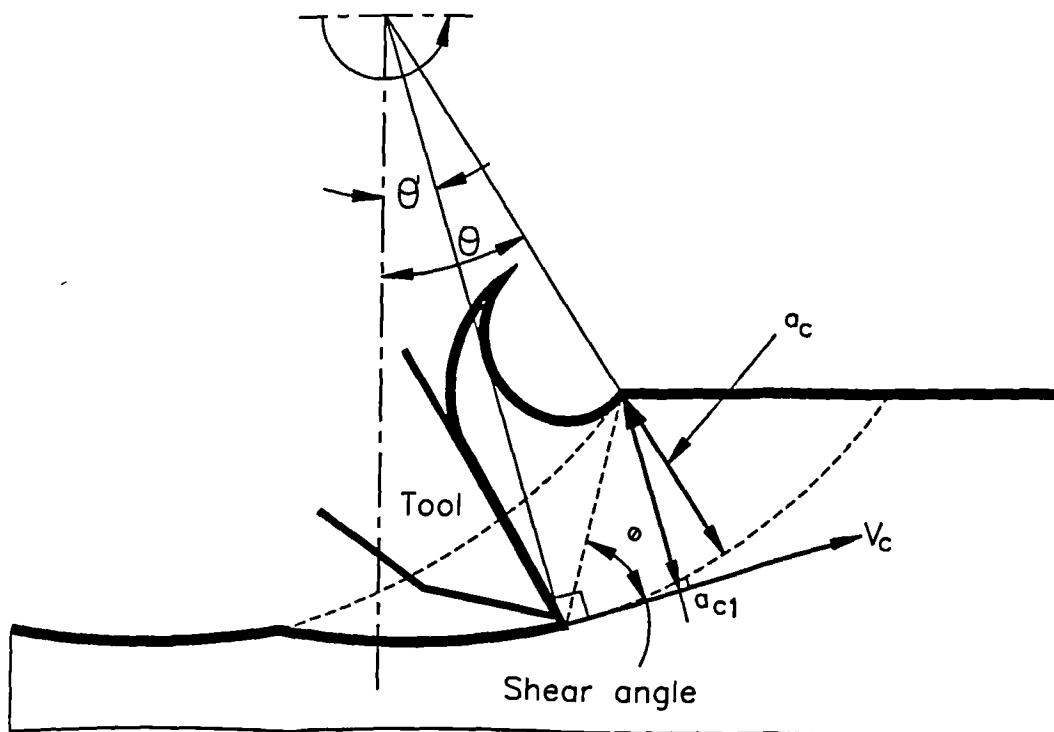


Fig. 3.6: Tool position for maximum force and undeformed chip thickness in peripheral milling [43]

It has been shown that the size of cut varies during the tooth contact. It is also noted that for peripheral milling, cutting is performed with a single cutting edge. The theories of cutting normally consider the undeformed chip thickness to be uniform.

However, when the thin-plane model developed by Armarego [43] is applied to peripheral milling the deformation is as shown in Figure 3.6, from which the shear angle for each position can be calculated as the chip thickness

varies. For illustration two positions of change in undeformed chip thickness were shown as a_c which is the initial undeformed chip thickness, whilst a_{c1} shows the position of the maximum undeformed chip thickness. Because of the important role the shear angle plays in simulation accuracy, it is essential to specify the type of undeformed chip thickness incorporated i.e initial/minimum, average or maximum undeformed chip thickness.

From equation 3.1, t_2 is known and the depth of cut is given as one of the input variables, therefore, the cutting ratio r_c can be calculated as:

$$r_c = \frac{t_1}{t_2} \dots\dots\dots (3.9)$$

If the chip is assumed to remain attached to the workpiece and increases in length only, any point in its interior must have a velocity V_s , which is a vector sum of the velocities V_c and V_o .

Thus

$$\vec{V}_s = \vec{V}_c + \vec{V}_o \dots\dots\dots (3.10)$$

as illustrated in figure 3.7.

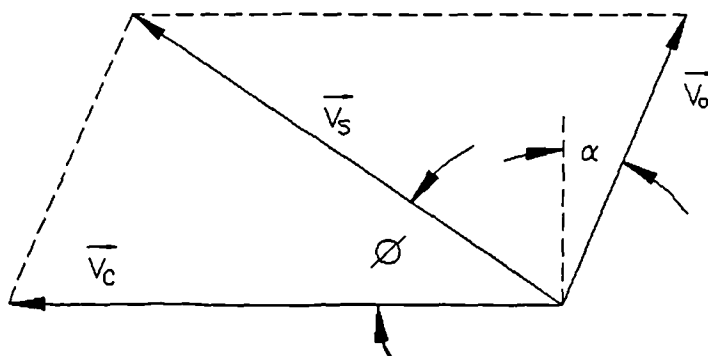


Fig. 3.7: The velocity diagrams

The angle ϕ between the vectors V_c and V_s is called the shear angle and is given by:

$$\tan\phi = \frac{V_o \cos\alpha}{V_c - V_o \sin\alpha} = \frac{r_c \cos\alpha}{1 - r_c \sin\alpha} \dots\dots\dots (3.11)$$

Thus it is sufficient to calculate the instantaneous chip thickness t_2 and using equation 3.11 determine the value of ϕ . Once the shear angle relationship is known the strain, strain rate and force variation during a cut may be found.

3.2.4 STRAIN ANALYSIS IN MACHINING CHIPS

In the cutting process as a volume of metal passes through the shear zone, it is plastically deformed to a new shape before moving away from the cutting zone. Therefore, it is necessary to know the amount of plastic deformation (shear strain) and the strain rate which is itself related to the shearing velocity and the machining stresses of the workpiece which are temperature dependent. These parameters have a controlling effect on the surface texture of the workpiece.

Chips with varying thicknesses as in the milling process present special problems for strain quantification as they may take several forms as suggested by Komanduri and Brown [44]. Typical forms are continuous, sawtooth and discontinuous chips. A precise description of the strain distribution in machining chips is required to advance the understanding of the metal cutting process.

The method of determination of the strain and strain rates in metal cutting is well known. Several workers [44 - 47] have published accounts of the mathematical formulation and experimental methods required in determining these parameters. A more thorough analysis has been presented by von Turkovich [47] whose work has been critically analysed and found to be

suitable for the present study as illustrated in figure 3.8.

In figure 3.8, the line AB represents the boundary between the chip and the workpiece. Below this line the workpiece material is not deformed, and above it the chip is fully formed. It is therefore, convenient to imagine this line as a thin layer. The layer AA'B'B is deformed by shear into the layer ACDB, as the tool progresses from the right to the left in the figure. The layer AA''B''B is the next layer to be deformed. The shear strain can therefore be defined as:

$$\gamma = \frac{A'C}{AE} = \frac{A'E}{AE} + \frac{CE}{AE} = \cot\phi + \tan(\phi - \alpha) \dots\dots\dots (3.12)$$

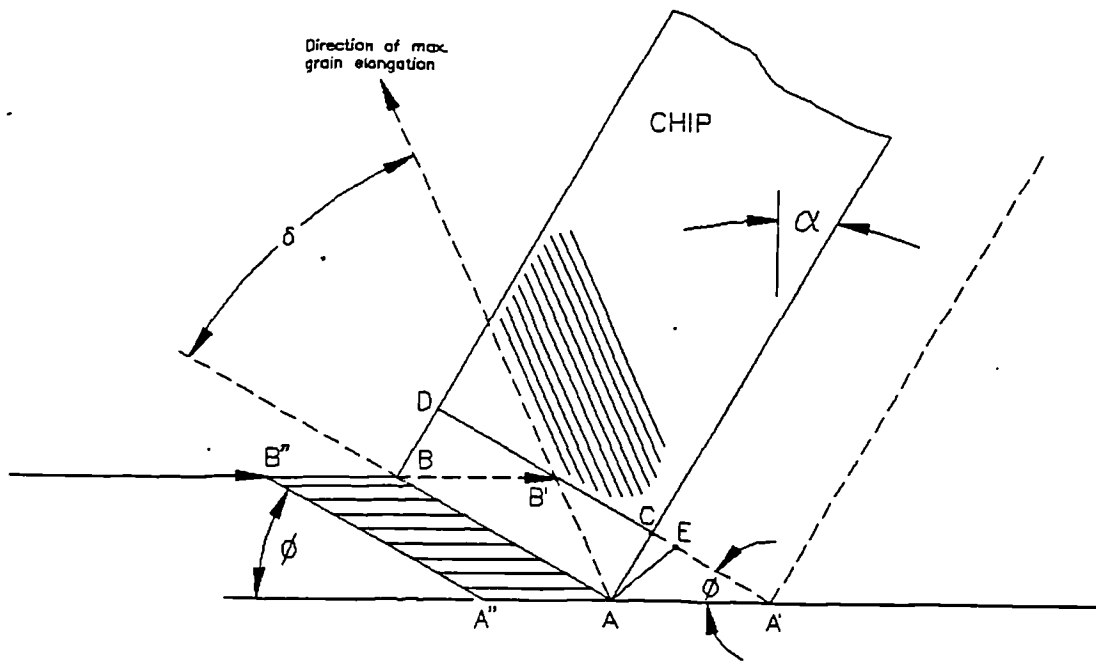


Fig. 3.8: Strain in chip formation [47]

The strain rate is determined from the shearing velocity V_s and the thickness of the shear zone. If the distance AE in fig 3.8 is the shear zone thickness s_1 then

$$\dot{\gamma} = \frac{V_s}{s_1} \dots\dots\dots (3.13)$$

The accuracy of the above analysis is limited by the irregularities in the chip surface and the extent of the influence of the secondary deformation zone. However, the accuracy can be improved significantly if experimentally determined chip thickness is used.

3.2.5 WORKPIECE MATERIAL PROPERTIES

For a computer simulation, it is necessary to know the relevant workpiece material properties such as flow stress, yield stress, Brinell hardness and shear stress for the appropriate conditions of strain, strain rate and temperature as these are the parameters that indicate the metallurgical state of the machined workpiece. The dynamic behaviour of steel, aluminium and titanium alloys has been examined by Recht [48]. Recht studied the relationships between elastoplastic dynamic stress and strain behaviour in uniaxial tension. By applying the von Mises plasticity theory to convert shear and stresses, Recht provided the following equations which give a good estimate of the dynamic strength as a function of Brinell hardness (BH):

$$\sigma_y = 3.92 BH \quad \dots \dots \dots (3.14)$$

$$\Psi = 4.55 BH \quad \dots \dots \dots (3.15)$$

$$\sigma_s = \sigma_y + \Psi \epsilon_p \quad \dots \dots \dots (3.16)$$

where σ_y is the uni-axial tensile dynamic yield stress, σ_s is the dynamic flow stress, ϵ_p is the natural plastic strain, Ψ is the work hardening coefficient, 3.92 and 4.45 are the conversion factors.

For prediction purposes, an ability to determine the dynamic yield and flow stresses from the above equations make it possible to determine the machining stresses without the experimental measured forces. Therefore, by

applying the deformation theory of plasticity to equation 3.16 as suggested by Recht [13] in this case using a conversion factor of 1.732, the dynamic shear stress is computed by :

$$\tau_s = \frac{\sigma_y + \psi \left(\frac{\gamma}{1.732} \right)}{1.732} \dots\dots\dots (3.17)$$

Similarly, the dynamic shear yield stress is computed by :

$$\tau_y = \frac{\sigma_y}{1.732} \dots\dots\dots (3.18)$$

In a uniform continuous chip, if the total strain is given by equation 3.12, the maximum dynamic shear stress is computed using equation 3.17 and the dynamic shear yield stress τ_y is determined by equation 3.18, then the effective dynamic shear strength can be taken to be the average value given by the following equation:

$$\tau_{se} = \frac{\tau_s + \tau_y}{2} \dots\dots\dots (3.19)$$

3.2.6 CUTTING FORCES AND POWER

The forces acting on the tool play an important role in the economics of the metal cutting process. For those concerned with the manufacture of machine tools, a knowledge of the forces is needed for estimation of power requirements and to design machine tool structures adequately rigid to be free from vibration. In the case of those concerned with tool design an accurate determination of forces would be helpful in optimising tool design because the cutting forces vary with the tool angles. Knowledge of the forces is needed for the estimation of the cutting power and the temperatures in the cutting zone for the analysis of the metallurgical state of the surface of the machined workpiece and productivity analysis. It is, therefore, important to understand the factors which influence cutting

forces. The forces and power in milling are often determined by empirical methods according to von Turkovich [47], however, this approach is not adequate since it excludes provision to calculate the momentum forces both on the workpiece and on the tool face. Therefore, an improved model is required that would allow the determination of all the cutting forces at both low and high cutting speed ranges.

(i) Low and High Cutting Speed Forces Model

The hypothesis is based on the work of Arndt [8] who produced a combination of conventional and high speed cutting forces as illustrated in Figure 3.9. In this diagram the momentum force and its resolved component have been added vectorially to the force vectors arising from the cutting mechanism to determine the resultant forces acting on the cutting tool. To fully understand these phenomena, the conventional and the high cutting forces need to be analyzed separately as follows:

(ii) Low Speed Power and Cutting Forces

From established machining theory according to Boothroyd and Knight [49] and Shaw [50] it is known that the shear force is one of the factors responsible for all forces created by interaction of the tool and chip. The shear force itself is produced by the action of shear deformation in combination with the shear angle. For the purpose of this investigation, the magnitude of this shear force is computed by the following expression:

$$F_s = \frac{\tau t_1 b_1}{\sin \phi} \dots\dots\dots (3.20)$$

If the value for the shear stress on the shear plane can be obtained from Equation 3.19 and the friction angle is known then by applying trigonometrical relationships as suggested by von Turkovich [47] to the model shown in Fig 3.9 it is possible to find the other cutting forces as

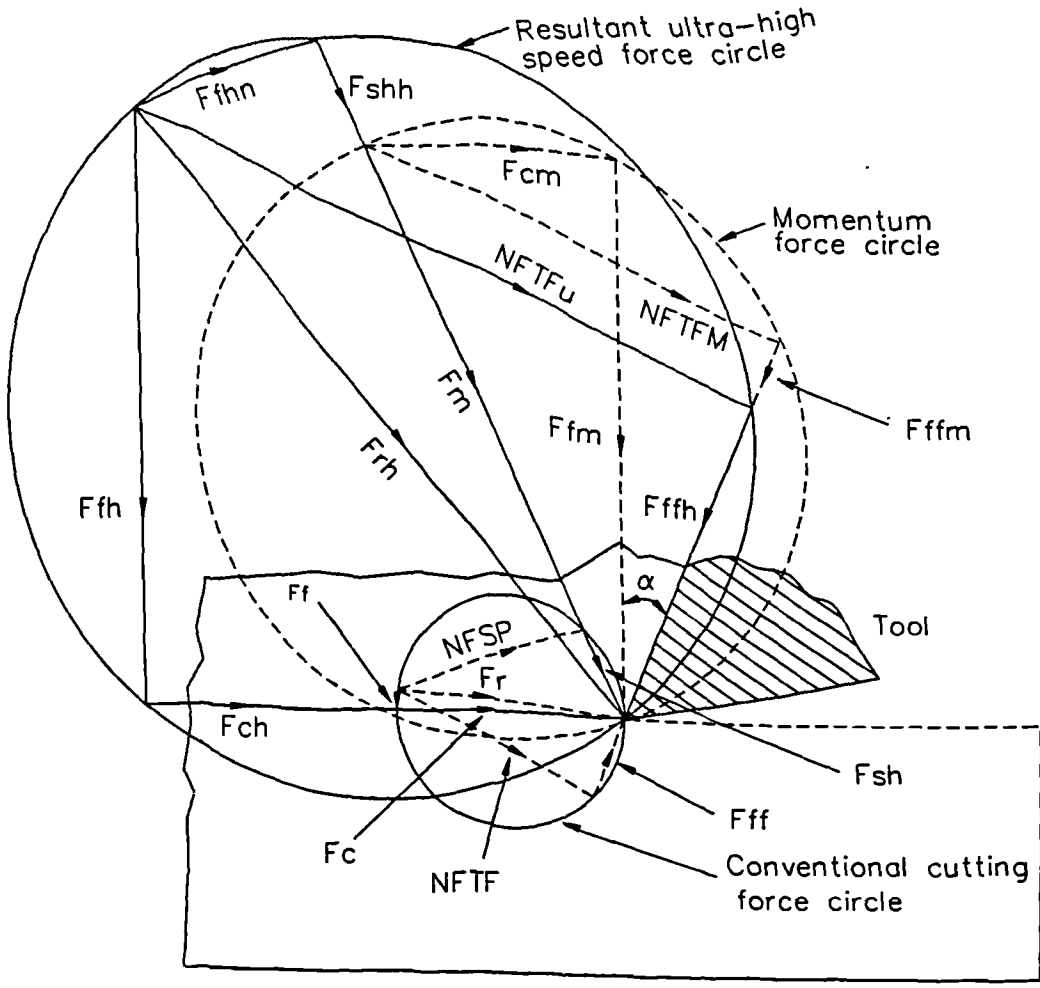


Fig. 3.9: Force geometry for two dimensional low, high and ultra-high speed machining [8]

follows. The main cutting force is computed by :

$$F_c = \frac{\tau b_1 a_c \cos (\beta - \alpha)}{\sin \phi \cos (\phi + \beta - \alpha)} \dots \dots \dots (3.21)$$

The feed force is given by:

$$F_f = \frac{\tau b_1 a_c \sin (\beta - \alpha)}{\sin \phi \cos (\phi + \beta - \alpha)} \dots \dots \dots (3.22)$$

The low speed shear plane normal force is given by:

$$F_{sn} = F_c \sin \phi + F_t \cos \phi \quad \dots\dots\dots (3.23)$$

The low speed tool face normal force is given by:

$$F_n = F_c \cos \alpha - F_t \sin \alpha \quad \dots\dots\dots (3.24)$$

The low speed frictional force is computed by:

$$F_{ff} = F_c \sin \alpha + F_t \cos \alpha \quad \dots\dots\dots (3.25)$$

The low speed resultant force is:

$$F_R = \frac{\tau b_1 a_c}{\sin \phi \cos (\phi + \beta - \alpha)} \quad \dots\dots\dots (3.26)$$

If this cutting force find good correlation with practical experiments then it will be possible to use the model to determine the cutting power, metal removal rate and the specific metal removal rate. This will ensure a correct prediction of machining times, allow a comparison of selected cutting conditions and make a judgement as to whether the machine tool and available spindle power will withstand the selected cutting conditions.

The metal removal rate (ZW) can be expressed mathematically as:

$$ZW = t_1 b_1 f n Z \quad \dots\dots\dots (3.27)$$

The cutting power is:

$$P_{ch} = F_c V_c \quad \dots\dots\dots (3.28)$$

The specific metal removal rate is:

$$ZWS = \frac{ZW}{P_{ch}} \quad \dots\dots\dots (3.29)$$

(iii) Momentum, Power and Cutting Forces

The significant difference between low speed machining and high speed machining is the influence of the momentum force on the cutting forces at high cutting speeds. This momentum arises when the workpiece is cut and the chip is generated, additional energy or force has to be supplied to the cutting process in order to accelerate the chip past the shear zone as suggested by Schulz and Moriwaki [5]. This momentum force is thought to act parallel to the shear velocity vector or along the shear plane according to Arndt [8].

Figure 3.10 illustrates the centrifugal and momentum force acting on the surface layers of a workpiece. In this diagram the position of the tool can be

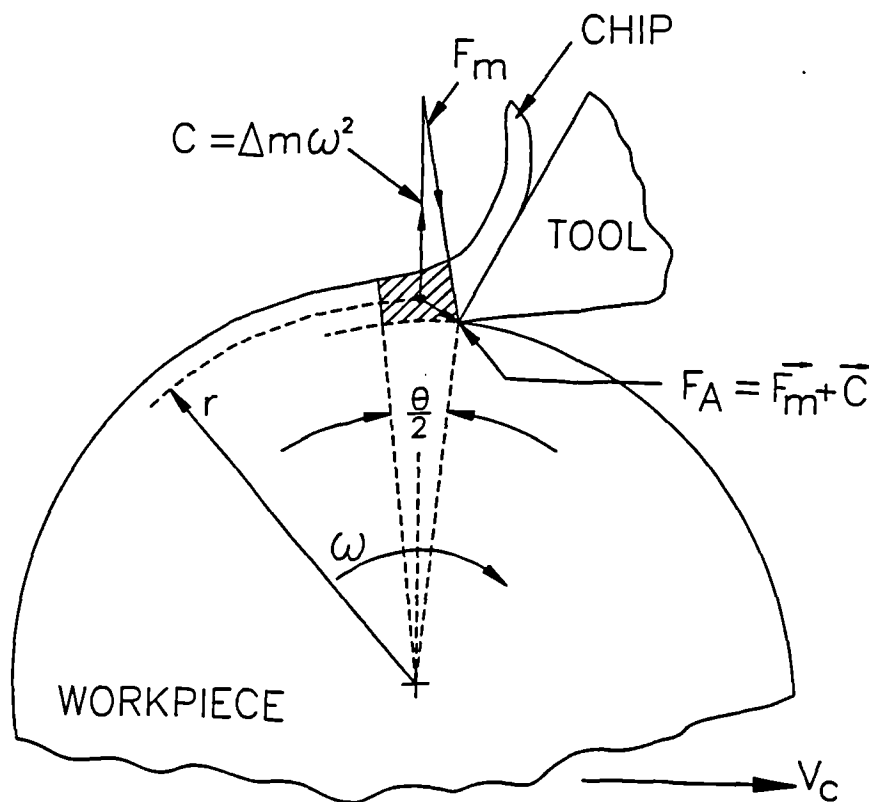


Fig. 3.10: Variation of momentum force (F_m) and centrifugal force (C) with cutting speed [51]

seen as well as the directions of both the momentum and centrifugal forces which shows that both forces act in opposite direction to each other. The

resultant of F_m and the centrifugal force is a new force component F_A which can be absorbed by the tool as stated by Arndt [51].

One of the problem arising from the HSM process is impact of tool wear caused by the high momentum force as suggested by Arndt [51]. A number of methods can be used to overcome this problem such as a gradual increase in depth of cut and a suitable radius at the tool rake face as illustrated in figure 3.11. All these measures lead to a more distributed tool loading according to Arndt [51].

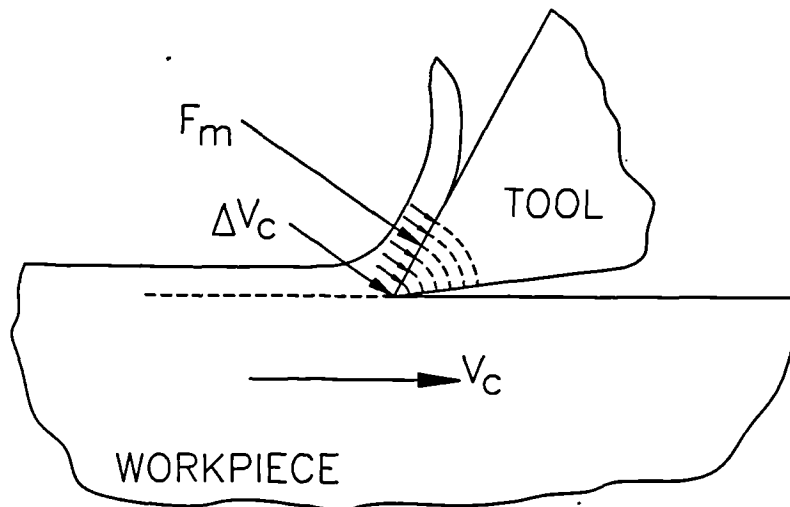


Fig. 3.11: Distribution of momentum force by controlled rake face radius [51]

Having shown the geometrical and momentum force components, a mathematical expression is required for its representation in simulation model. Using Figure 3.9 the momentum force and its resolved component have been added vectorially to the forces arising from the cutting mechanism to arrive at the resultant forces acting on the cutting tool. With increasing cutting speed, the ratio of F_m circle diameter to cutting force diameter increases and F_{Rh} can be seen to approach F_m in both magnitude and direction.

The value of this momentum force according to Arndt [8] is given by :

$$F_m = \frac{b_1 t_1 V_c^2 \rho}{\cos(\phi)} \left(\frac{1}{1 + \tan(\phi) \tan(\alpha)} \right) \dots\dots\dots (3.30)$$

From the above equation it can be seen that if the value of the cutting speed is low then the value of the momentum force would be low compared to shear force and other cutting forces. From a geometrical point of view, the cutting speed does not affect the cutting forces at low speed. The reason for this is because the values of the momentum force is small and if its vector sum is added to the other cutting forces it would not make much difference. However, as the cutting speed increases the momentum force increases and it may become exceedingly high since it varies with the square of cutting speed according to Arndt [8] as shown in equation 3.30. Therefore, if the vector sum of this momentum force is added to other cutting forces an increase in cutting forces will be experienced.

Hence, with momentum effects included, it is now possible to find the other cutting forces at high cutting speed. By applying trigonometrical relationships to Figure 3.9 and accounting for momentum force according to Arndt [8] the following forces can be calculated as follows:

The principal cutting force is suggested by Arndt [8] to be $F_c + F_{cm}$ and this force is computed by:

$$F_{ch} = a_c b_1 \left[\frac{\tau \cos(\beta - \alpha)}{\sin\phi \cos(\phi + \beta - \alpha)} + \frac{\rho V_c^2}{\cos\phi + \tan(\alpha)} \right] \dots (3.31)$$

The high speed feed force ($F_c + F_{tm}$) is given by:

$$F_{fh} = a_c b_1 \left[\frac{\tau \sin(\beta - \alpha)}{\sin\phi \cos(\phi + \beta - \alpha)} + \frac{\rho V_c^2}{1 + \tan\phi \tan\alpha} \right] \dots (3.32)$$

The high speed shear force is:

$$F_{shh} = F_m + F_c \cos \phi - F_f \sin \phi \quad \dots\dots\dots (3.33)$$

The high speed friction force is:

$$F_{fth} = F_m \cos (90 - \phi + \alpha) + F_c \sin \alpha + F_f \cos \alpha \quad \dots (3.34)$$

The high speed tool face normal force is given by:

$$F_{nth} = F_m \sin(90-\phi+\alpha) + F_c \cos \alpha - F_f \sin \alpha \quad \dots\dots (3.35)$$

Having derived the cutting forces, it is possible to find the cutting power and the specific metal removal rate. Equation 3.27 for the metal removal rate is applicable to both low and high speed cutting. Therefore, the cutting power at the cut is:

$$P_{ch} = F_{ch} V_c \quad \dots\dots\dots (3.36)$$

The specific metal removal rate is defined as:

$$ZWS = \frac{ZW}{P_{ch}} \quad \dots\dots\dots (3.37)$$

3.2.7 CUTTING ENERGY

The interaction between the tool and the workpiece during high speed machining is extremely complex because the material being machined undergoes high localized deformation and the temperature in the primary deformation zone increases. Although the tool undergoes very little deformation it is subjected to significant frictional forces and heating which cause rapid tool wear which may lead to eventual failure according to Sedgwick [32].

It is, therefore, important to understand the factors which influence the

generation of heat, the flow of heat and the temperature distribution in the tool and work material near the tool edge. Several workers Shaw [14], Boothroyd and Bailey [33], Sadat [52] and Hsu [53] have published accounts of the mathematical formulation required. Therefore, the analysis that follows is basically standard. The energy in low speed machining is derived using the following equations :

The rate of energy consumption (U) is:

$$U = F_c V_c \dots\dots\dots (3.38)$$

The specific cutting energy (U_e) is:

$$U_e = \frac{F_c}{a_c b_1} \dots\dots\dots (3.39)$$

The shear energy (U_s) is computed by:

$$U_s = \frac{F_{sh} V_s}{V_s a_c b_1} \dots\dots\dots (3.40)$$

The friction energy (U_f) is:

$$U_f = \frac{F_c r_c}{a_c b_1} \dots\dots\dots (3.41)$$

In high speed machining, one of the possible limiting factors is the momentum energy associated with the momentum force. As the cutting speed increases the momentum energy in the cutting zone also increases which may result in increase in cutting zone temperature. Sadat [48] has suggested that any excessive increase in cutting zone temperature could have great influence on the surface finish of the workpiece. Therefore, as the cutting speeds increases the cutting zone temperatures need to be monitored for any excessive increase. This specific momentum energy (U_m) is computed by :

$$U_m = \frac{F_m V_s}{V_c t_1 b_1} \dots\dots\dots (3.42)$$

The above equations are for low speed machining, however, by replacing cutting force F_c in equations 3.38, 3.39 and 3.41 with F_{ch} obtained from high speed force analysis, the high speed energies can be predicted. Equation 3.40 is applicable to both low and high speed machining. In equation 3.42 the variation in the cutting speed is the dominant factor.

3.2.8 CUTTING TEMPERATURE

The chip formation is predominantly and most frequently explained by means of plasticity theory and when necessary supplemented by the analysis of fracture. Plastic flow theory implies that the strain and strain rate must be quite high for the chip to form because of the geometry of the process. Since the mechanical work supplied by the tool motion converts into heat and therefore raises the temperature of the deformation zone, the temperature has a very specific effect on the entire cutting operation, in particular in limiting the rates of metal removal when cutting iron, steel and other metals and alloys of high melting point.

Therefore, the measurement and calculation of these temperatures is of utmost importance and becomes even more critical when high cutting speeds are involved. The physical features of these shear zones have been investigated by a number of workers [2, 31, 54, 55]. The analysis presented by Boothroyd et al [49] allows the calculation of temperatures from readily measured cutting data. This approximate method is based on heat transfer in a moving material. The theory considers the heat generated in the primary zone and the standard heat transfer equations for a moving heat source with one boundary condition which is the heat flux due to secondary shear. This method gives rise to the following equations which were used in this study and also further consideration for chosen these equations is that they incorporates the thermal properties of the workpiece material which are critical to the prediction model proposed in this study.

The method of finding the fraction heat that goes into the plane is know as thermal number which is a function of dimensionless factors describing the undeformed chip thickness, cutting speed, material density and the ratio of thermal conductivity. This thermal number of the material (R_t), is given by:

$$R_t = \frac{\rho V_c SHC a_c}{T_{con}} \dots\dots\dots (3.43)$$

The rate at which heat is generated by friction between the chip and tool is :

$$H_f = F_{ff} V_o = F_{ff} V_c r_c \dots\dots\dots (3.44)$$

However, if the rake angle (α) = 0, then $F_{ff} = F_f$ and

$$H_f = F_f V_c r_c \dots\dots\dots (3.45)$$

The rate of total heat generated is :

$$H_T = F_{ch} V_c \dots\dots\dots (3.46)$$

The rate of heat generation by shearing is :

$$H_s = H_T - H_f \dots\dots\dots (3.47)$$

The average temperature of the chip resulting from the secondary deformation is :

$$T_{av} = \frac{H_f}{\rho SHC V_c a_c b_1} \dots\dots\dots (3.48)$$

The maximum temperature rise in the chip due to the frictional heat source in the secondary deformation zone is :

$$\delta T_{max} = T_{av} 1.13 \ln \left(\frac{R_t}{L_o} \right) \dots\dots\dots (3.49)$$

$$\text{where } L_o = \frac{L_c r_c}{a_c} \dots\dots\dots (3.52b)$$

In developing a predictive theory for estimating the heat conducted into the workpiece (H_{cw}), it has been suggested [56 - 57] that an empirical equation (57) based on a compilation of experimental data by Boothroyd [58] can be used as shown:

$$H_{cw} = 0.5 - 0.35 \log (R_t \tan \phi)$$

$$\text{for } 0.04 \leq R_t \tan \phi \leq 10.0$$

and $\dots\dots\dots (3.51)$

$$H_{cw} = 0.3 - (0.15 \log (R_t \tan \phi))$$

$$\text{for } R_t \tan \phi > 10.0$$

The rate of heat generation in the primary deformation zone is H_p and a fraction of this heat H_{cw} , is conducted into the workpiece, the remainder, $((1 - H_{cw}) H_p)$ is transported with the chip. Therefore, the average temperature rise (δT_s), of the material passing through the primary deformation zone is :

$$\delta T_s = \frac{(1 - H_{cw}) H_p}{SHC V_c a_c b_1} \dots\dots\dots (3.52)$$

The maximum temperature along the tool rake face is :

$$T_{max} = T_m + T_s + T_o \dots\dots\dots (3.53)$$

Equations 3.44 to 3.46 can be used for HSM temperature predictions by replacing the cutting forces values with high cutting speed forces.

3.3 THE THEORETICAL MODEL OF HIGH SPEED MACHINING

The theoretical modelling structure for the design and the development of the numerical model for cutting process evaluation in this study is as shown in figure 3.12. This model does not include any constraints such as resource considerations, the manufacturing environment or tooling feasibility. However, these factors could be incorporated into the model in the future.

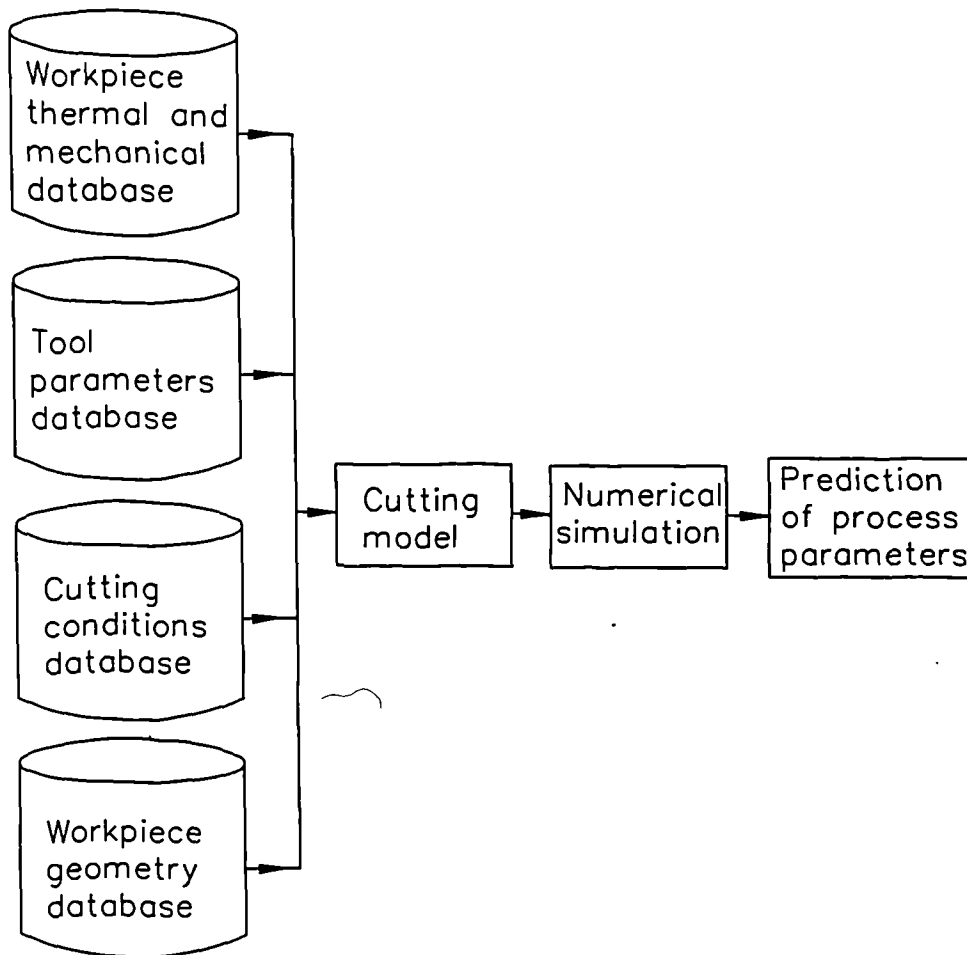


Fig. 3.12: Flow chart showing parameters for numerical simulation

The strategy adopted was firstly to set up databases for the input data as shown in figure 3.12. This would enable the input cutting data to be retrieved during simulation and the calculated results to be displayed numerically and graphically or alternatively, the results can be stored in the database.

The set of equations of the milling process covering both LSM and HSM presented in the first part of this chapter are considered to be justifiable for description of the cutting process subject to the following modifications.

3.3.1 MODIFICATIONS TO HSM CUTTING FORCES ANALYSIS

The relationship between cutting forces and momentum force developed by Arndt [8] expressed in equations 3.31 to 3.35 in this chapter gave insight to process parameters prediction at high cutting speed. However, when these equations were applied to a wide range of machining data in HSM using the software program developed in this study, the accuracy of predicted cutting forces becomes poor.

Arndt [8] has shown that in HSM the principal cutting force (F_{ch}), the feed force (F_{fh}), frictional force (F_{ffh}) and the normal or radial force on the tool (F_{nh}) can be calculated, this implies that all these forces would increase with increasing cutting speed. Studying of these equations reveals that as the cutting speed increases, the cutting forces predicted results became unrealistic. For example at cutting speed below 8.3 m/s (500 m/min), these equations were found to predict normal behaviour from the prediction, however, at cutting speed above 8.3 m/s the predicted results were found to be abnormal in some cases the resulting values were found to be extremely large. The reason for the abnormal value of the main principal cutting force (F_{ch}) and the feed force F_{fh} may be attributed to the errors in deriving equations for both forces. Therefore, the analysis of the correct equations and comparison of the new equations with Arndt [8] are as follows:

From figure 3.9, figure 3.13 is derived to simplify how F_{ch} and F_{th} are derived. According to Arndt and Brown [59] in order to obtain meaningful forces at high cutting speed, the shear angle need to be kept constant, therefore, it is assumed that the shear angle at conventional force circle

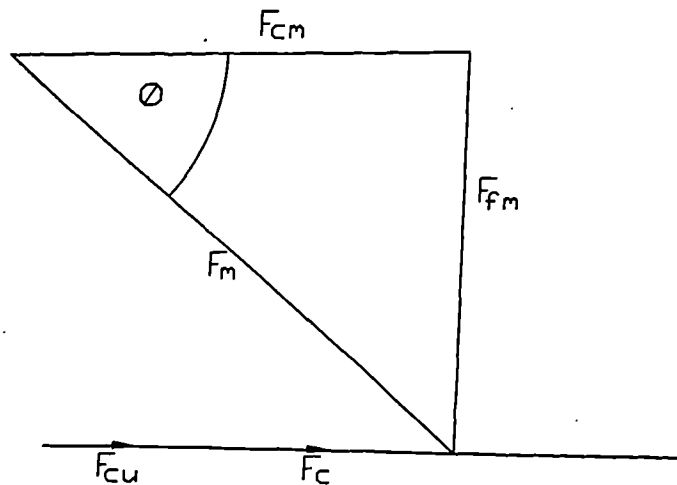


Fig. 3.13: Momentum force components.

diagram in figure 3.9 is applicable at high speed force circle diagram shown in figure 3.9 as well. Therefore, from figure 3.13, if the shear angle is known and the momentum force F_m is known from equation 3.30.

Then $F_{cm} = \cos(\phi) F_m$

and since $F_{ch} = F_c + F_{cm}$

then F_{ch} equation can be derived as follows:

$$F_{ch} = F_c + \cos\phi F_m \dots\dots\dots (3.54)$$

If the above equation is simplified then it becomes:

$$F_{ch} = a_c b_1 \frac{\tau \cos(\beta - \alpha)}{\sin\phi \cos(\phi + \beta - \alpha)} + \frac{\cos\phi a_c b_1 \rho V_c^2}{\cos\phi(1 + \tan\phi \tan\alpha)} \dots (3.55)$$

If the above equation is re-arranged then it becomes:

$$F_{ch} = a_c b_1 \left[\frac{\tau \cos(\beta - \alpha)}{\sin\phi \cos(\phi + \beta - \alpha)} + \frac{\rho V_c^2}{1 + \tan\phi \tan(\alpha)} \right] \dots (3.56)$$

Mathematically it is not understood how Arndt [8] derived equation 3.31 from $F_{ch} = F_c + F_{cm}$ based on figure 3.9, there appears to be an error in the analysis.

Similarly, a thorough analysis shows an error in equation 3.32. Using figure 3.13 derived from figure 3.9, the shear angle (ϕ) is known and the momentum force F_m is known from equation 3.30. Therefore,

$$F_{tm} = \sin(\phi) F_m$$

$$\text{and since } F_{fh} = F_c + F_{tm}$$

then F_{fh} equation can be derived as follows:

$$F_{fh} = F_c + \sin\phi F_m \dots\dots\dots(3.57)$$

which then becomes

$$F_{fh} = \frac{a_c b_1 \tau \sin(\beta - \alpha)}{\sin\phi \cos(\phi + \beta - \alpha)} + \frac{\sin\phi a_c b_1 \rho V_c^2}{\cos\phi (1 + \tan\phi \tan\alpha)} \dots(3.58)$$

If the above equation is re-arranged then it becomes:

$$F_{fh} = a_c b_1 \left[\frac{\tau \sin(\beta - \alpha)}{\sin\phi \cos(\phi + \beta - \alpha)} + \frac{\rho V_c^2 \tan\phi}{1 + \tan\phi \tan\alpha} \right] \dots(3.59)$$

(i) COMPARISON OF MODIFIED MAIN CUTTING FORCE WITH ARNDT'S [8]
MAIN CUTTING FORCE

To compare the new modified equations with those given by Arndt [8], the following input data similar to those used for the experiment in chapter 6 are entered into the software program:

Workpiece - AL L168:1978

Cutter dia. - 50 mm

Depth of cut - 4 mm

Width of cut - 25 mm

Feed - 0.3 mm

Rake angle - 12 (deg)

Number of tips - 2

Based on the above input data, table 3.1 shows the main cutting force predicted data, whilst figure 3.14 illustrate the plotted result. It can be clearly seen in table 3.1 that as the cutting speed increases the value of Arndt result using equation 3.31 gets larger than the result obtained from the modified equation 3.56.

Table 3.1 : Main cutting force comparison data

Cutting speed (m/min)	Arndt's [8] Main force (N) (Equation 3.31)	Modified Main force (N) (Equation 3.56)	Difference (N)
2827	583	547	36
3142	722	679	43
3456	874	822	52
3778	1044	982	62
4084	1218	1145	73
4398	1415	1331	84
4712	1623	1527	96

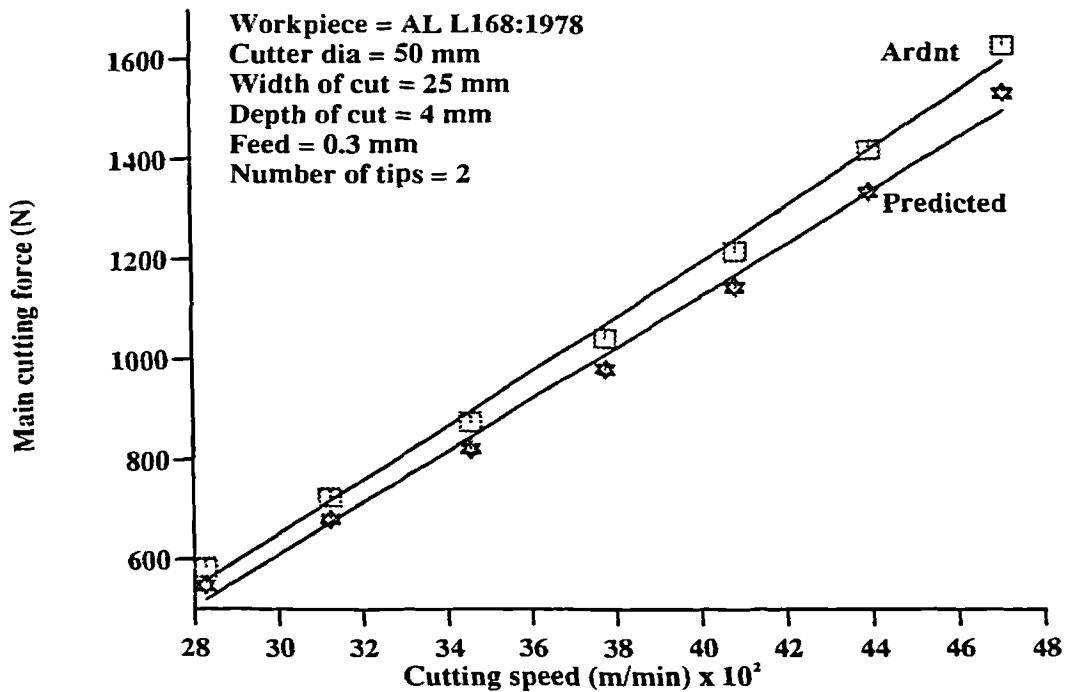


Figure 3.14: Arndt's [8] and modified main cutting forces

(ii) COMPARISON OF MODIFIED FEED FORCE WITH ARNDT'S [8]
 FEED FORCE RESULT

Based on the same input data as the those used above, table 3.2 shows Arndt [8] and the modified feed cutting force data, whilst figure 3.15 illustrate the plotted result. It can be clearly seen in table 3.2 that as the cutting speed increases the value of Arndt result using equation 3.32 gets larger than the result obtained from the modified equation 3.59.

Provided the modified equations are used, the equations presented in this chapter are more likely to cover a large range of machining data at high cutting speed. However, experimental work is obviously required to find the level of accuracy.

Table 3.2 : The feed cutting force comparison data

Cutting speed (m/min)	Arndt's [8] Feed force (N) (Equation 3.32)	Modified Feed force (N) (Equation 3.59)	Difference (N)
2827	547	339	208
3142	679	421	258
3456	822	509	313
3778	982	608	374
4084	1145	710	435
4398	1331	824	507
4712	1527	944	583

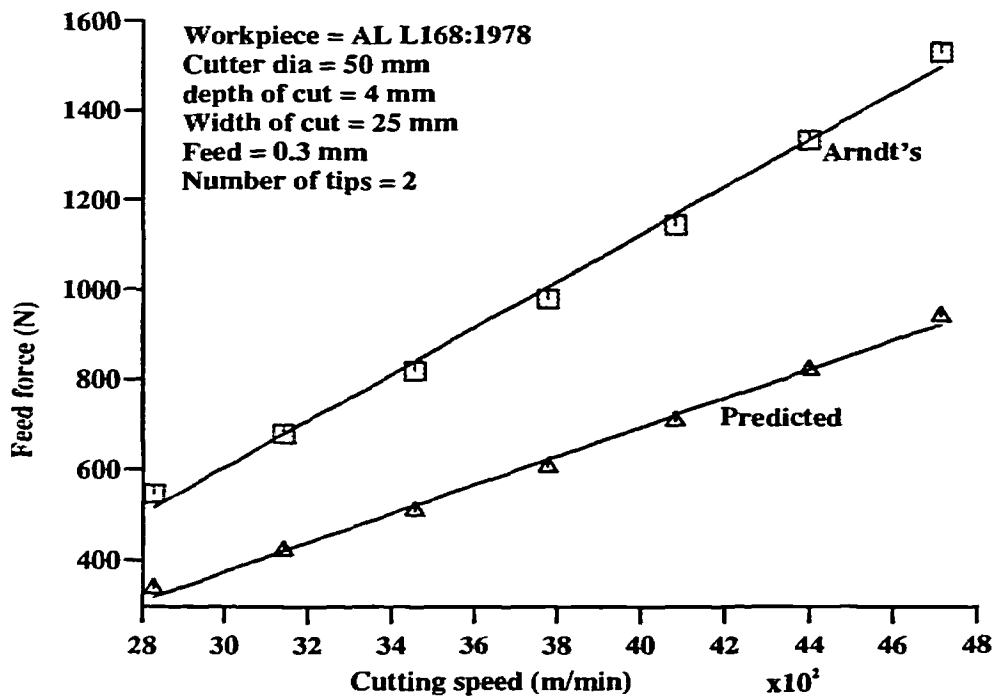


Figure 3.15: Arndt's [8] and modified feed cutting forces

3.4 DISCUSSIONS AND REQUIRED LEVEL OF ACCURACY

This chapter has considered the body of the equations required to model high cutting speed process. It has been shown that the momentum force increases with increase in cutting speed and this causes other forces to increase. Also the cutting temperature equations has shown that the tool rake face and chip temperatures will increase as the cutting speed increases, whilst the heat conducted to the workpiece may decrease with increased cutting speed.

In addition, the theoretical analysis has shown that there are discrepancies in the equations available from the literature. However, extreme care has been taken to select equations used in this study from authors whose works are widely regarded and well quoted in the literature.

Therefore, the equations presented in this chapter are believed to adequately describe cutting process parameters encounter at high cutting speed. However, there is a parameter which can critically influence the determination of the cutting force, this is the chip thickness. Normally the chip thickness is determined experimentally and the forces evaluated. In terms of a simulation model chip thickness must be approximated. Therefore the analysis presented here needs to be compared with experimental results. Nonetheless, from a mathematical modelling point of view, these equations provide a basis to model the cutting process in HSM, provided that there is good agreement between results from the numerical simulation and experimental results.

CHAPTER 4

4.0 NUMERICAL MODELLING OF HSM AND PROGRAM DESIGN

4.1 INTRODUCTION

The equations presented to model high speed machining processes based on figures 3.1 to 3.4 in chapter 3 require a numerical solution before they can be used for simulation. This chapter presents a numerical modelling technique developed to reformulate the equations of mechanics of cutting to obtain the workpiece material stresses, strain and strain rates, metal removal rate, cutting power, cutting forces, energies and cutting temperatures. The main objective is for the model to be able to be used to predict optimum cutting process parameters at both low and high cutting speeds by the process engineers and research community. With the advantage of reducing setup time, tape proving time and production cost significantly.

A Fortran program was written as a tool to obtain a better understanding of the process parameters in HSM. The selection of Fortran was based on the belief that this language is ideally suited for the solution of problems that involve large quantities of numerical data known to occur during high speed machining simulation. A development of the theory behind the application of the program as well as the description of the sub-routine used in this work are discussed.

4.2 NUMERICAL TECHNIQUES

The philosophy used was to create and implement an extensive and comprehensive theoretical model, based mathematically on basic cutting process parameters. Application of such a model makes it possible to show the dependency of the cutting parameters and their effect within the

simulated results. Further, by solving the equations, simultaneously as a set, it is possible to show how the user's choices of inputs influence the hsm process.

In order to establish a broad data base for future access, all the data acquired for workpiece and tooling, mechanical and thermal properties, cutting conditions, workpiece geometries, tooling geometries, machine tool parameters, generated numerical and graphical results data were stored on a DEC Vax computer system.

4.3 NUMERICAL MODELLING STRUCTURE

Figure 4.1 illustrates the structure of the cutting simulation system which consists of three major modules: integrated input database, numerical simulation and output modules. The input module has an integrated database including the following modules:

- (i) Workpiece materials: density, thermal conductivity, specific heat capacity, initial workpiece temperature and Brinell hardness.
- (ii) Tool materials: Coated/uncoated, density, thermal conductivity, specific heat capacity, initial temperature and Brinell hardness.
- (iii) Tool geometry: Tool diameter, number of teeth or flutes, tool shank diameter, rake angle and flute length.
- (iv) Workpiece geometry: Blank size, length, height, width and geometrical features.
- (v) Cutting parameters: Feed, feed rate, depth of cut, width of cut, and cutting speed.
- (vi) Machine tool parameters: Range of operation for feed rate in x,y and z axes, spindle speed and power, tool length/diameter in x,y and z axes, i.e. working envelope.

Having identified the input information required, the coded program was designed to transform the geometric, mechanical and thermal properties

information of the workpiece, tools, machine tool and cutting conditions from the databases into a suitable form for simulation. Alternatively, a new set of input data can be entered into the model. The workpiece, tools, machine tool and cutting conditions data files in the modules can be edited making it possible to update and expand the databases. The input module can also be edited prior to cutting simulation.

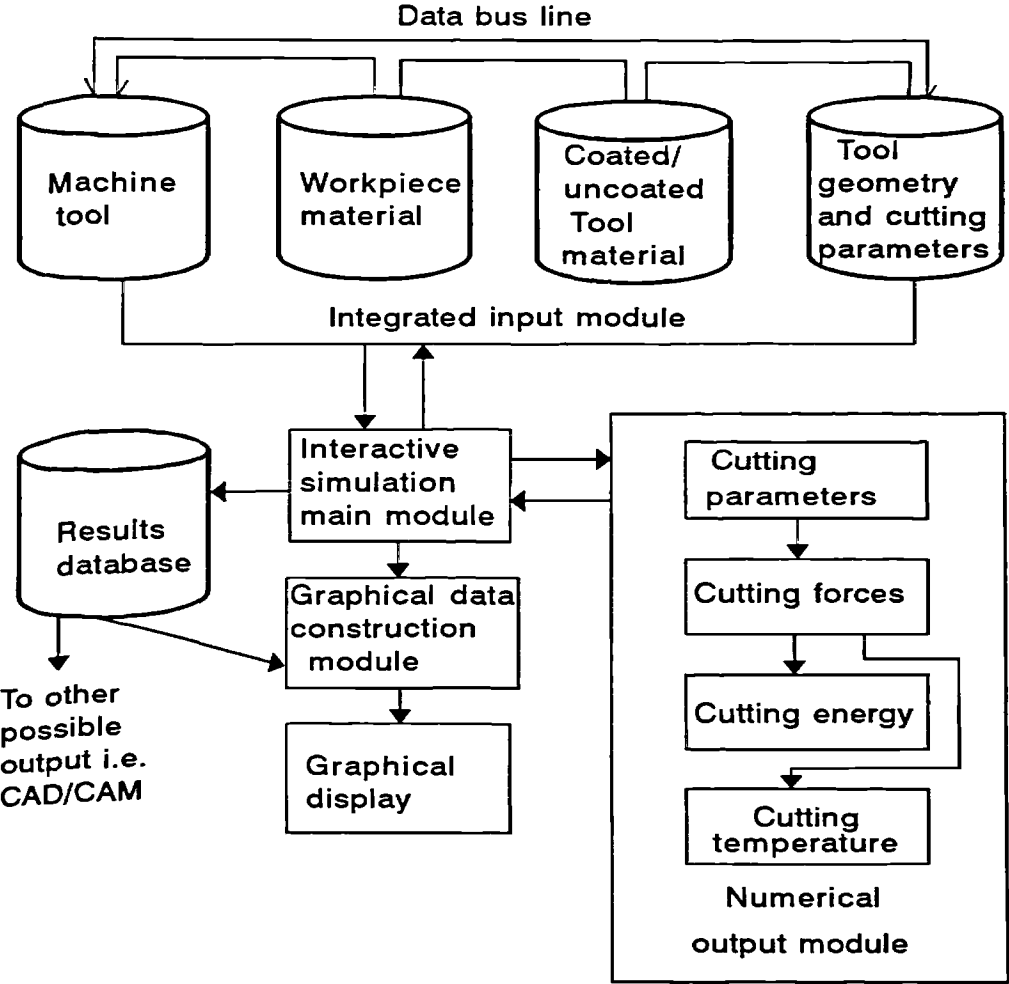


Fig. 4.1: The structure of the simulation model

The numerical simulation module has an inbuilt numerical data controller with four sub-modules, which determines the cutting parameters, cutting forces, cutting energy and cutting temperatures respectively. Once the input data is entered, the numerical simulation takes approximately 20-25

seconds. However the simulation sub modules have to be selected in the following pre-determined order:

- (i) cutting parameters; (ii) cutting forces,
- (iii) cutting energy; (iv) cutting temperature.

The reason for this is that the cutting forces cannot be calculated without getting some essential information from the cutting parameters sub-routine. Also the cutting energy and the cutting temperature depend on results from the cutting parameter and cutting force sub routines.

The output module generates the numerical output data and graphical representation of the cutting process based on the numerical data obtained through the "Results database".

4.4 DESIGN OF THE PROCESS ANALYSIS PROGRAM

Figure 4.2 describes the simplified algorithm of the main body of the program with ten major subroutines. This program is menu driven with ten possible options. Within the main program there is an inbuilt data pool controller which has direct communication access to the input databases, cutting speed indicator module, the cutting process calculation subroutines and output results data file. Its main function is to ensure that correct data are passed effectively within the main program and all the subroutines.

As for the cutting simulation itself, the program is designed in such a way that the simulation can be carried out repeatedly as required and its results displayed numerically without saving. However, if the results are to be displayed graphically or used at a later time, then it needs to be stored each time the simulation is effected. The program termination module is included to ensure simulation at any stage during program running time can be terminated.

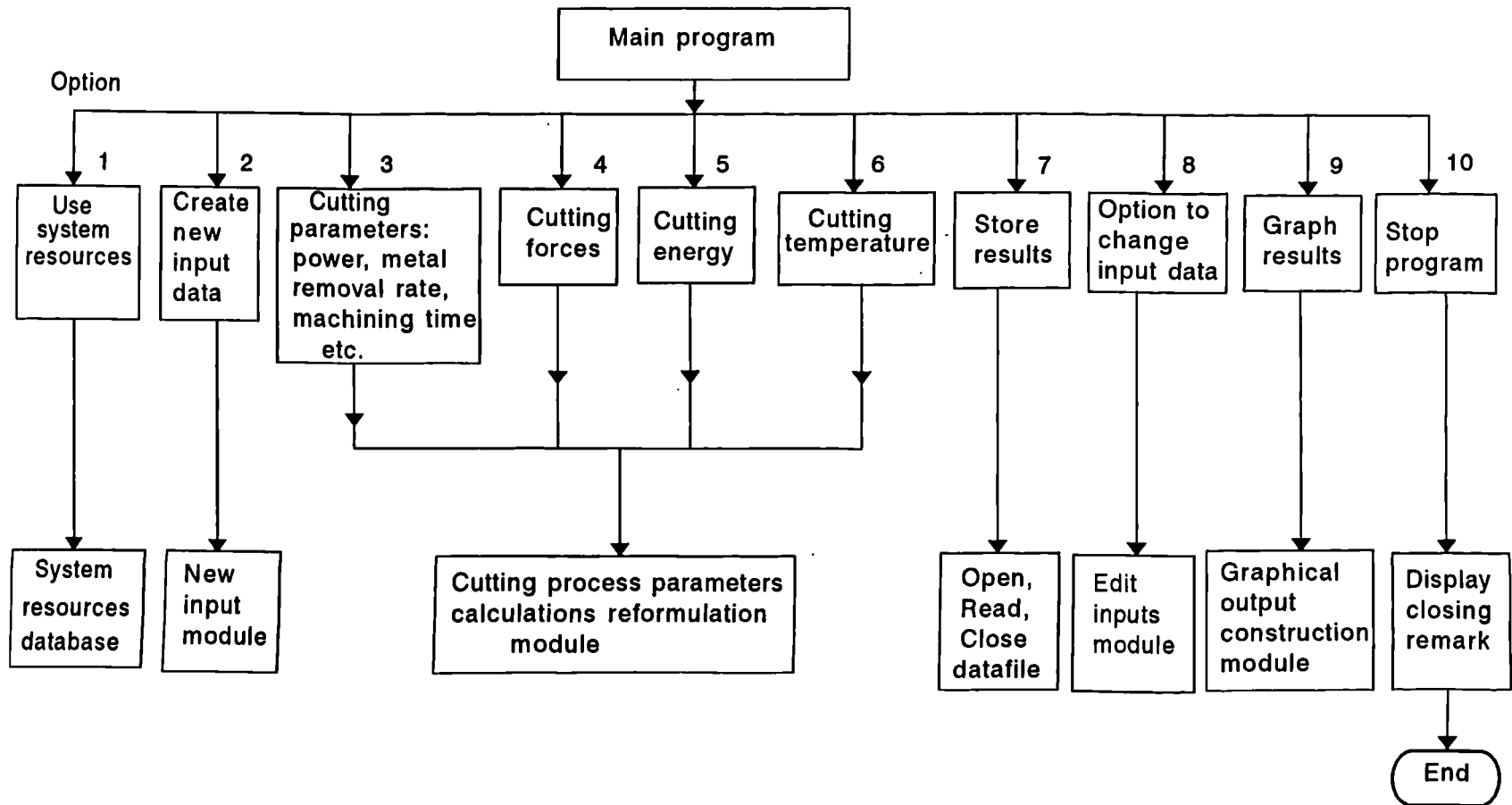


Figure 4.2: Computer model flow chart

4.4.1 SYSTEM RESOURCES FLOW CHART

Figure 4.3 illustrates the flow chart of the system resources designed for this study. The aim is to provide the potential user with readily available data to run the cutting simulation and obtain results. However, if the user is not satisfied with the supplied data, the system editing option can be selected

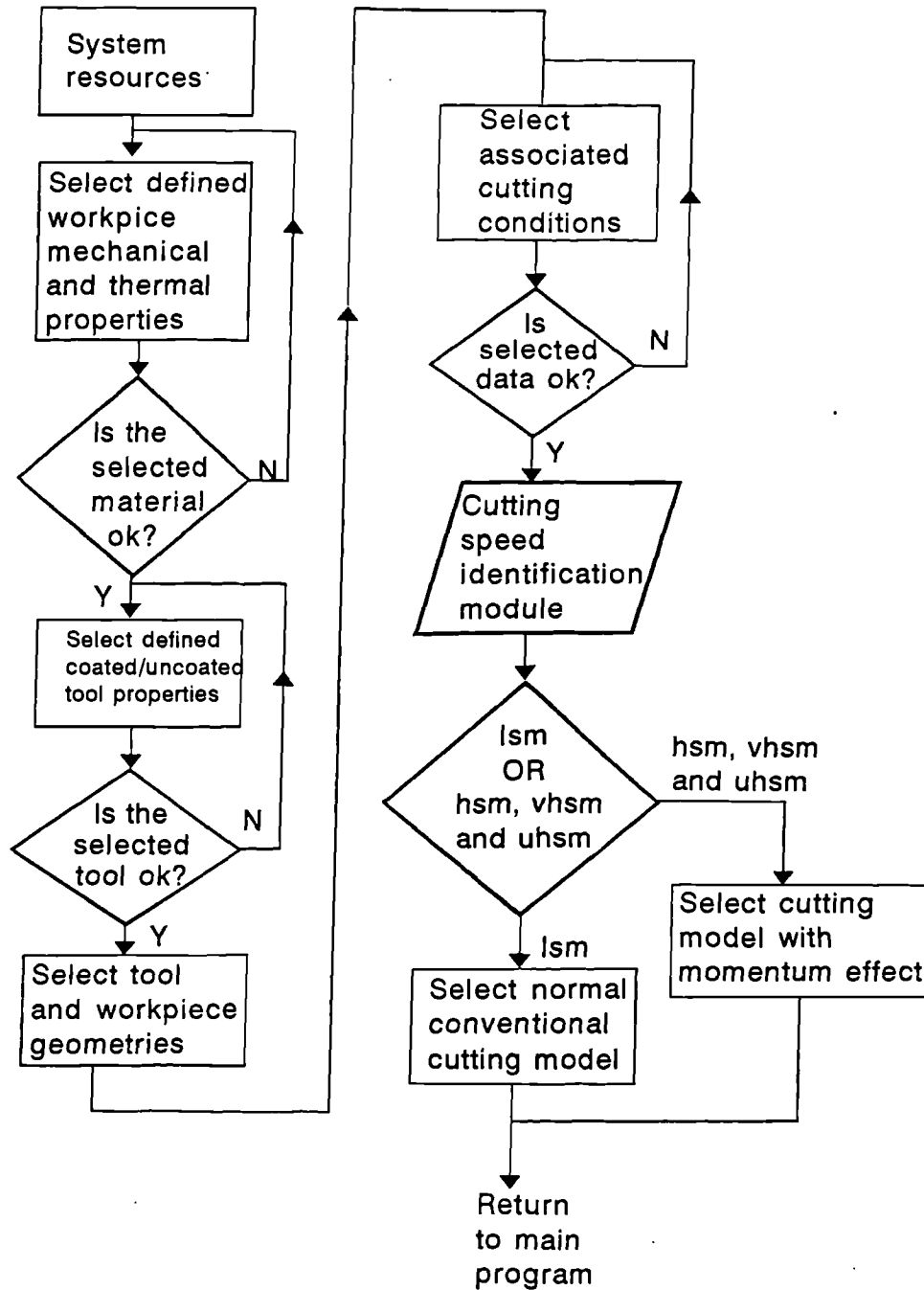


Fig. 4.3: System resources flow chart

to change the supplied data within the main program. As a precaution against data corruption, there is an inbuilt safety mechanism to prevent the user changing the original data in the databases. In a situation where the objective is to add or edit the systems resources data, this can be done by quitting the main program and the executing system resources data file separately.

4.4.2 NEW INPUT DATA FLOW CHART

This module offers the potential user the opportunity to input a new set of data as suited. The schematic representation of this module flow chart is as shown in figure 4.4. Six options are available and the input data can be entered in any particular order. When data are entered for the first time, the

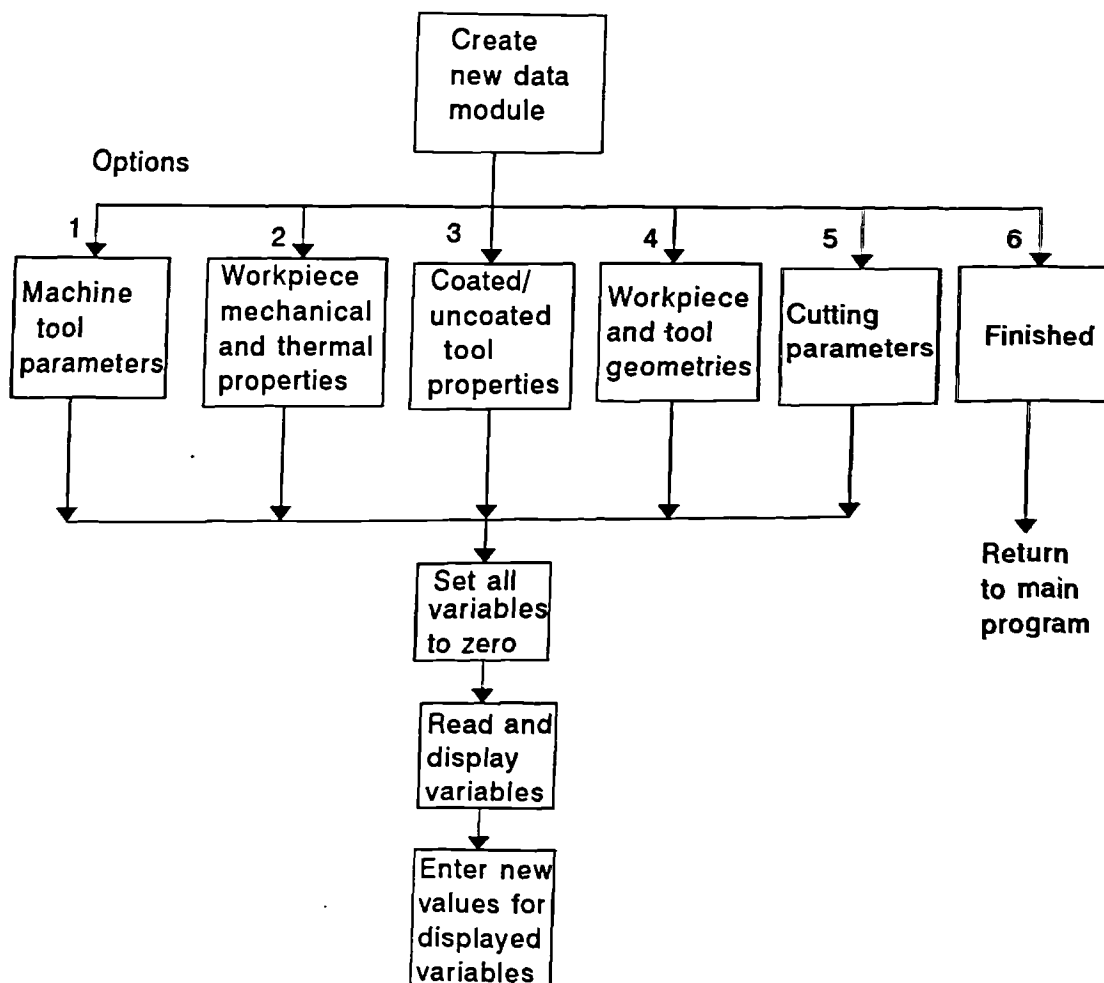


Fig. 4.4: New input data flow chart

system is designed to set all input variables to zero and start accepting data afresh. This ensures that all the data within the main program at that particular time are the ones the user entered. Once the user is satisfied with the input data, the finish option can be selected which will take the user back to the main program.

4.4.3 CHANGE DATA OPTION FLOW CHART

Figure 4.5 illustrates the flow chart of the editing or change option module. The objective is to make it possible to change any of the input variables before or after cutting simulation. When this option is selected, the system will display the inbuilt input variables as shown previously in figure 4.4. Once the input variable data modules are displayed, it can be edited in any particular order and the new set of data will automatically be returned to the main program for simulation.

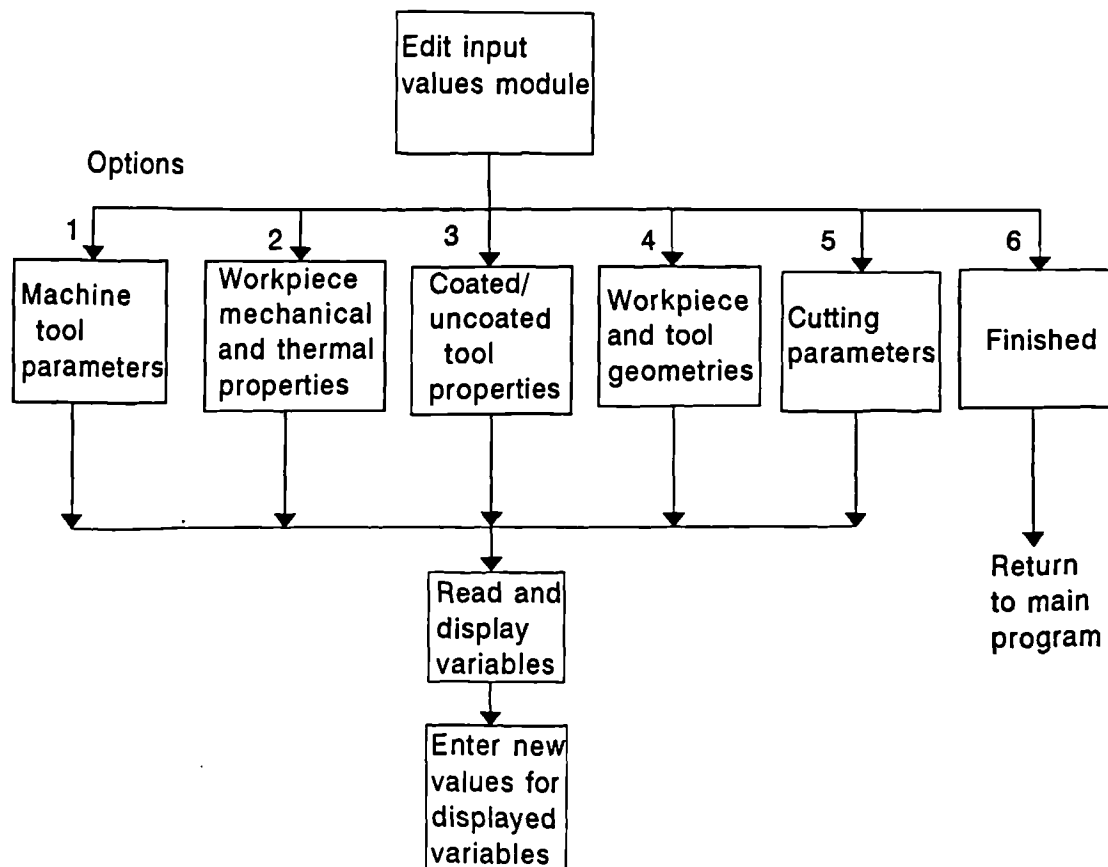


Fig. 4.5: Edit input data flow chart

4.4.4 CUTTING PROCESS CALCULATION MODULE FLOW CHART

Figure 4.6 shows the cutting process calculation flow chart. The cutting parameters, forces, energies and temperatures can be simulated and analyzed with the aid of inbuilt equations as discussed earlier. The cutting simulation itself has an inbuilt data pool controller subroutine which main objective is to ensure that the correct data are retrieved and sent to the appropriate destination within the program. Also there is an inbuilt numeric data supervisor subroutine which main purpose is to ensure that the simulated results data are sent to the appropriate output module. Finally, the simulated results can be displayed numerically, graphically and stored to an external data file if required.

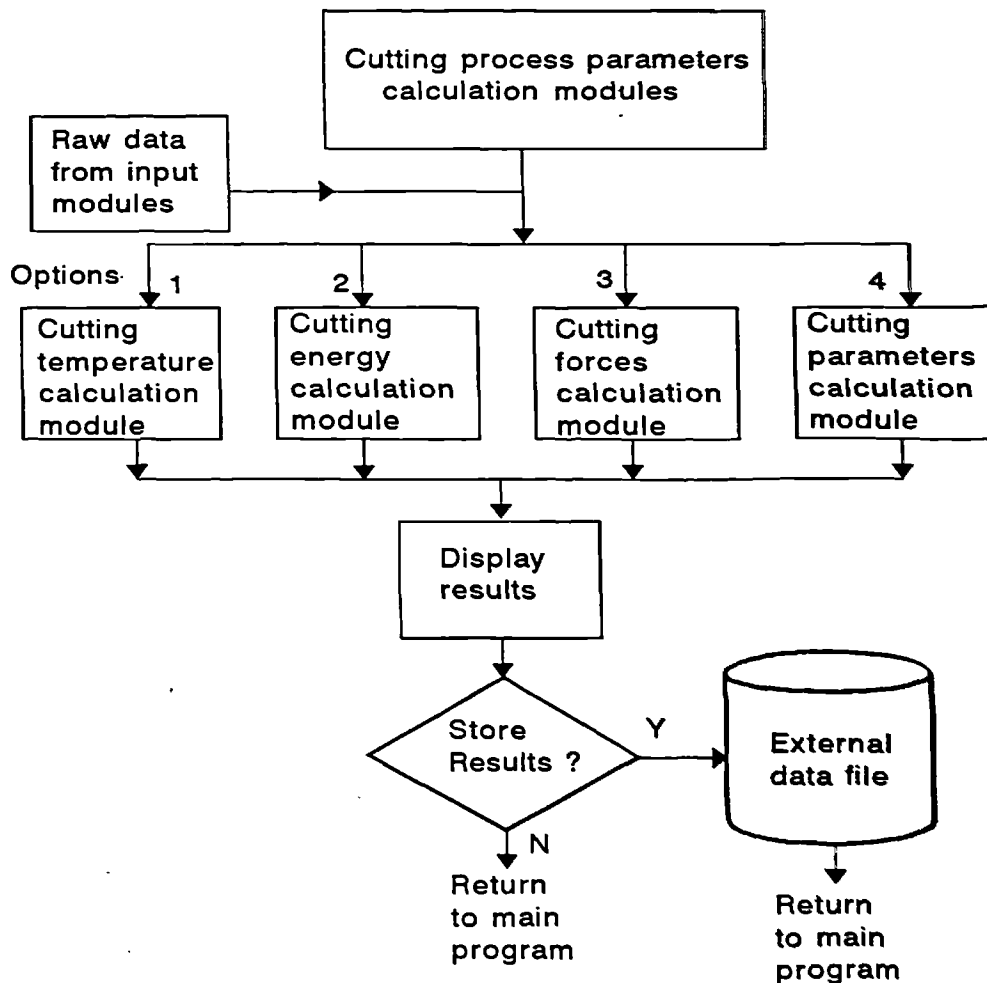


Fig. 4.6: Cutting process calculation modules flow chart

4.4.5 GRAPHICAL OUTPUT CONSTRUCTION FLOW CHART

Figure 4.7 describes the schematic representation of the graphical output construction flow chart. The objective of this module is to present the potential user with the options of displaying the results on line, which offers

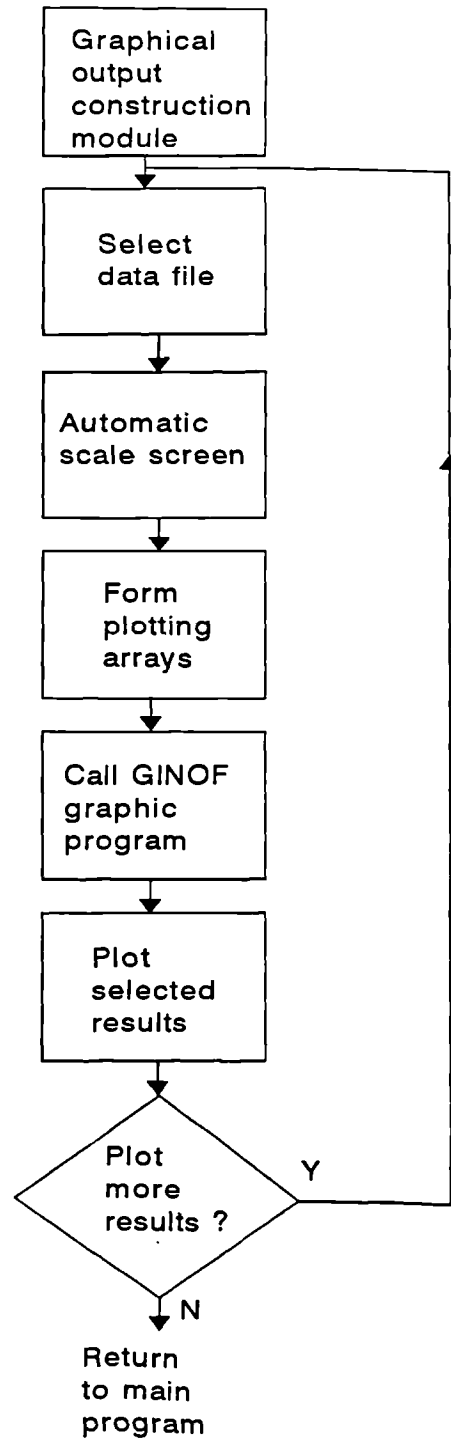


Fig. 4.7: Graphical output construction flow chart

an advantage over numerical viewing as it enables the user to have graphical verification of the results.

4.5 CONCEPTUAL ALGORITHM OF THE MAIN PROGRAM

In order to enhance understanding of the work that which have been described in this chapter, Figure 4.8 shows the full conceptual algorithm of the simulation model for the cutting process analysis of both conventional and high speed machining. As discussed earlier, the program is menu driven and all the available menu are shown in figure 4.8. The program is designed to have a cutting speed flag indicator as part of its input subroutine as shown in figure 4.8. The objective of this cutting speed indicator is to indicate to the main program which section of the cutting equations to use every time there are changes in the input data that affect the value of the cutting speed.

The main program itself has an inbuilt data pool controller subroutine the main objective of which is to ensure that the correct data are retrieved and sent to the appropriate destination within the program. Also there is an inbuilt numeric data supervisor subroutine which ensure that the simulated results data are sent to the appropriate output module.

4.6 GENERAL DISCUSSION ON THE SIMULATION MODEL

In this chapter a computer based software program has been developed based on the equations analysed in chapter 3. This software program should provide a method to predict cutting process parameters which will allow a comparison of selected cutting conditions and make a judgement as to whether the machine tool and available spindle power will withstand the selected cutting conditions. To facilitate this, the software program have been developed interactively to allow for selection of the process parameters from the created database. In addition, the system database and the programming structure are designed to allow for future expansions or modifications.

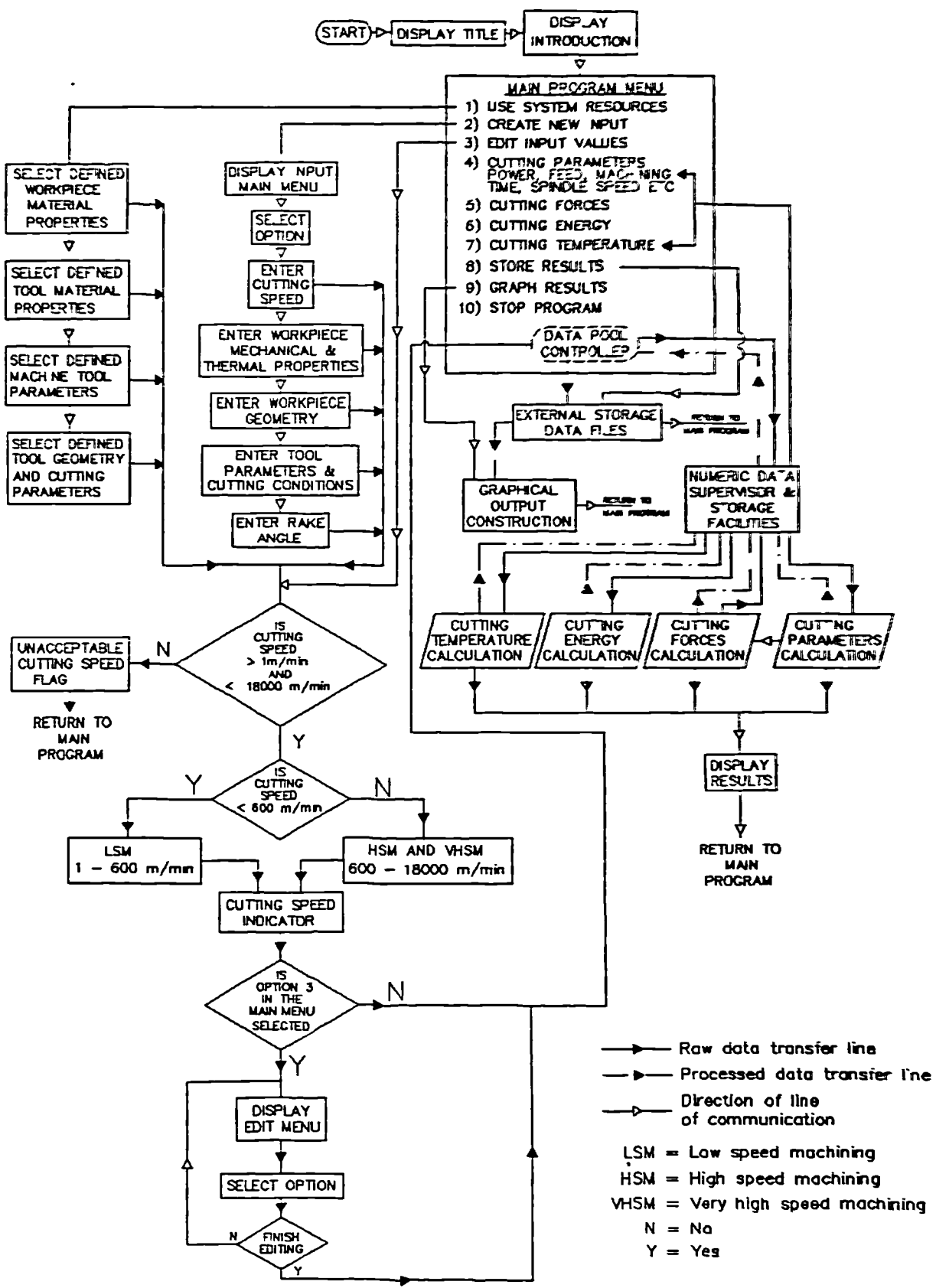


Fig. 4.8: Conceptual algorithm for cutting process analysis over a wide cutting speed range

CHAPTER 5

5.0 NUMERICAL PREDICTION RESULTS AND DISCUSSION

5.1 Introduction

This chapter describes how the computer program can be applied to model the HSM process. A number of results are presented and compared with published results. Their significance in high speed machining is discussed. The results presented serve to validate the cutting model and simulation aspects of the developed software.

5.2 PREDICTION TECHNIQUES

The input data for each set of results are selected from the published results from the literature. These data are then entered into the software package and the output results saved in files and analysed using Annotate and Harvard graphic software packages. There are 33 input variables to this software package which can be applied individually or in combination with others to simulate the model and can generate 75 different output results. To demonstrate and verify the model effectiveness approximately 5000 predictions were made, details of some of the results are presented as follows:

5.3 PREDICTION 1: THE RELATIONSHIP BETWEEN METAL REMOVAL AND THE CUTTING SPEED.

(i) AIM OF PREDICTION

To establish the influence of increase in cutting speed on the metal removal rate. The result of this analysis can be used to determine the type of swarf removal technique to be employed.

(ii) THE INPUT DATA

The selected input data are from the experimental work of Schulz [60] as

follows:

Workpiece material - Aluminium AlCuMgPb

Cutting speed - 0 - 6000 m/min,

Depth of cut - 1.5 mm,

Width of cut - 1 mm,

Feed - 0.52 mm,

cutter diameter - 40 mm,

Rake angle - 12 (deg),

Number of tips - 2

(iii) PREDICTION RESULTS

The predicted metal removal rate, the experimental result from the work of Schulz [60] and the percentage error between both results are shown in table 5.1.

TABLE 5.1: PREDICTED METAL REMOVAL RATE AND SCHULZ'S RESULT

Cutting speed (m/min)	Schulz's ZW (cm ³ /min)	Author's Predicted ZW (cm ³ /min)	Error (%)
0.0	0.0	0.0	0.0
1000	12.0	12.4	-3.33
2000	24.0	24.8	-3.33
3000	37.0	37.23	-0.62
4000	49.0	49.65	-1.3
5000	62.0	62.05	-0.08
6000	75.0	74.47	0.62

(iv) DISCUSSION ON THE AUTHOR'S PREDICTED AND SCHULZ'S RESULTS

Figure 5.1a shows the predicted result of the relationship between the metal removal rate (ZW) and cutting speed (V_c), whilst figure 5.1b (feed = 5.2 mm graph 7) shows the experimental result of Schulz [60]. It can be observed in both figures 5.1a and 5.1b that the metal removal rate increases almost linearly with the increase in cutting speed, this can be ascribed to the fact that the metal removal rate is a function of the cutting speed.

The significance of this result is that it can provide the process engineer the information needed to estimate the quantity of swarf that can be produced during a cutting operation. Once this information is known, adequate swarf removal system can be designed.

(v) COMPARISON OF PREDICTION WITH PUBLISHED RESULTS

Using the same input data, the predicted result shown in figure 5.1a compared positively well with the experimental result of Schulz[60] graph 7 (feed = 0.52 mm) shown in figure 5.1b. The average percentage error between both the predicted and Schulz's results as shown in table 5.1 was -1.34 percent.

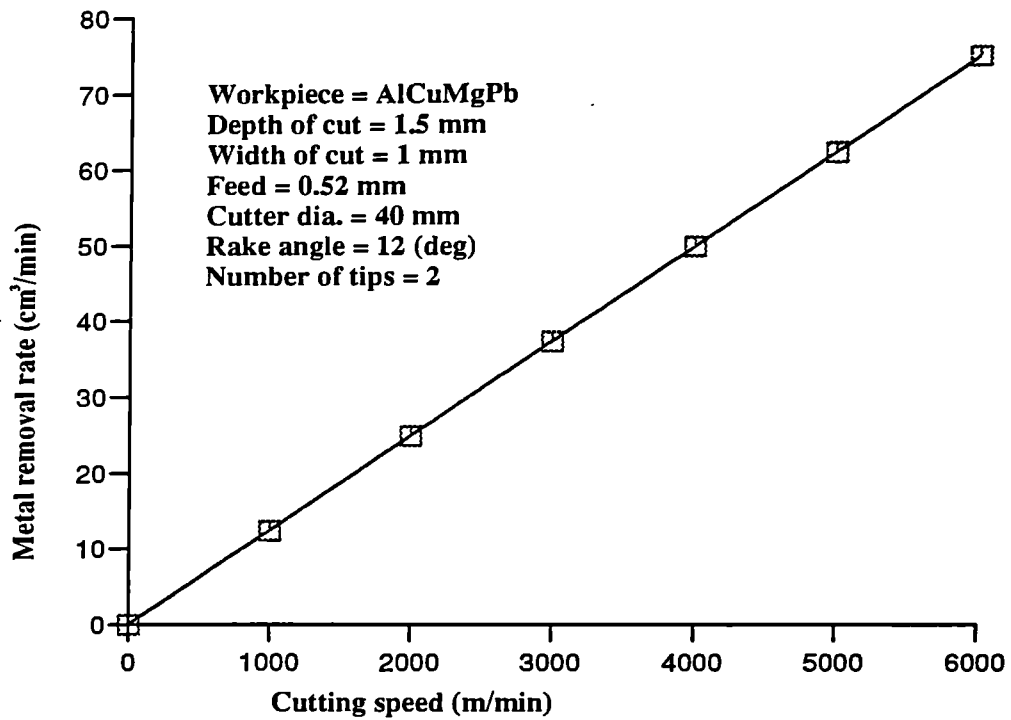


Fig. 5.1a: The relationship between the cutting speed and the predicted metal removal rate

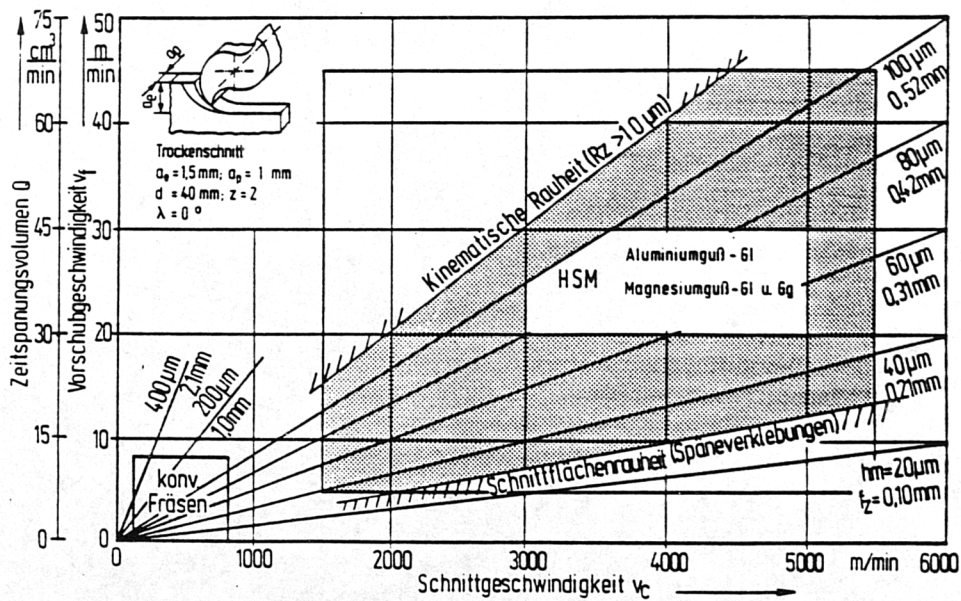


Fig. 5.1b: The relationship between the cutting speed and the metal removal rate according to Schulz [60]

5.4 PREDICTION 2: THE RELATIONSHIP BETWEEN POWER AND THE CUTTING SPEED.

(i) AIM OF PREDICTION

To establish the influence of increase in cutting speed on the cutting power so that the power consumption during cutting operation and the power requirement of the machine tool can be determined.

(ii) THE INPUT DATA

The selected input data are from the experimental work of Schulz [60] as follows:

Workpiece material - Aluminium AlCuMgPb

Cutting speed - 1500 - 9500 m/min,

Feed rate - 6 m/min (graph e figure 5.2b),

Depth of cut - 3 mm,

Width of cut - 1 mm,

Cutter dia. - 16 - 100 mm,

Rake angle - 12 (deg),

Number of tips - 2

(iii) PREDICTION RESULTS

The predicted cutting power, the experimental result from the work of Schulz [60] and the percentage error between both results are shown in table 5.2.

TABLE 5.2: PREDICTED CUTTING POWER AND SCHULZ'S RESULT

Cutting speed (m/min)	Schulz's Result (kW/mm)	Author's Predicted Result (kW/mm)	Error (%)
1500	1.9	2.03	-6.8
3100	2.7	2.89	-7
4700	4.36	4.79	-9.9
6300	7.36	8.02	-8.9
7900	10.36	11.18	-7.9
9500	13.36	14.29	-7

(iv) DISCUSSION ON THE PREDICTED RESULTS

Figure 5.2a shows the predicted result on the relationship between the power (P_{ch}) and cutting speed (V_c), whilst figure 5.2b (graph e) shows the experimental result of Schulz [60].

The results shown in both figures 5.2a and 5.2b indicates that the cutting power increases with cutting speed because power is a product of the principal cutting force and the cutting speed. As evident at cutting speed below 1500 m/min although not shown clearly in the figures above, the power did not increase much due to the relatively constant values of the cutting force. However, at higher cutting speed when the momentum force comes into action, the principal cutting force increases, thereby causing a sharp increase in power.

The results show that the cutting power and spindle speed increase with cutting speed. Therefore, when specifying the cutting speed for any given workpiece material, the power capability of the machine tool and the available spindle speed should be taken into consideration.

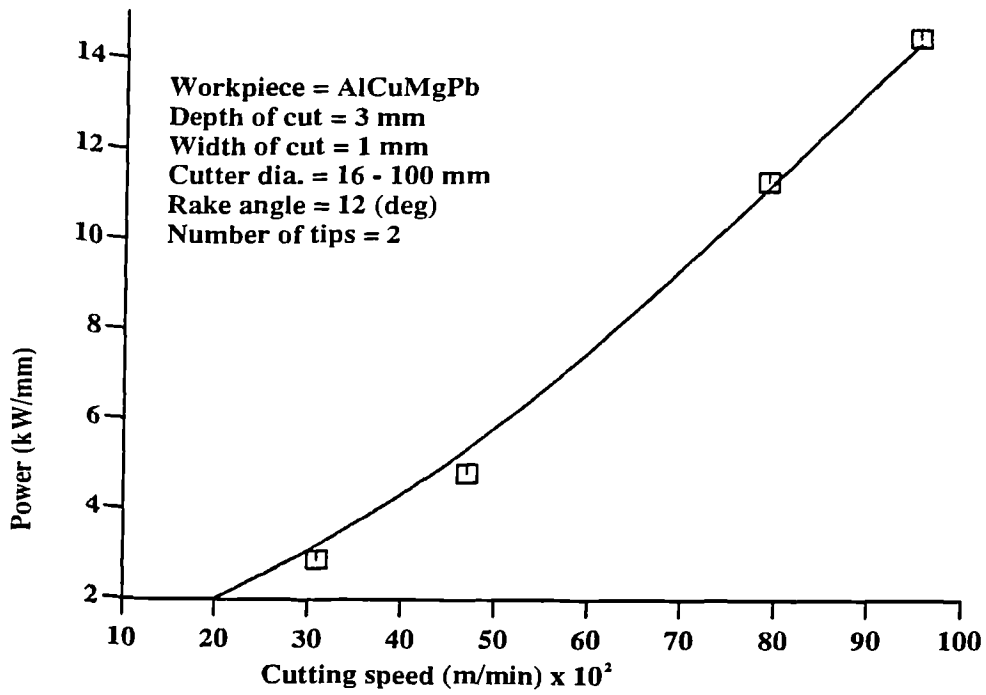


Fig. 5.2a: The relationship between the cutting speed and the predicted cutting power

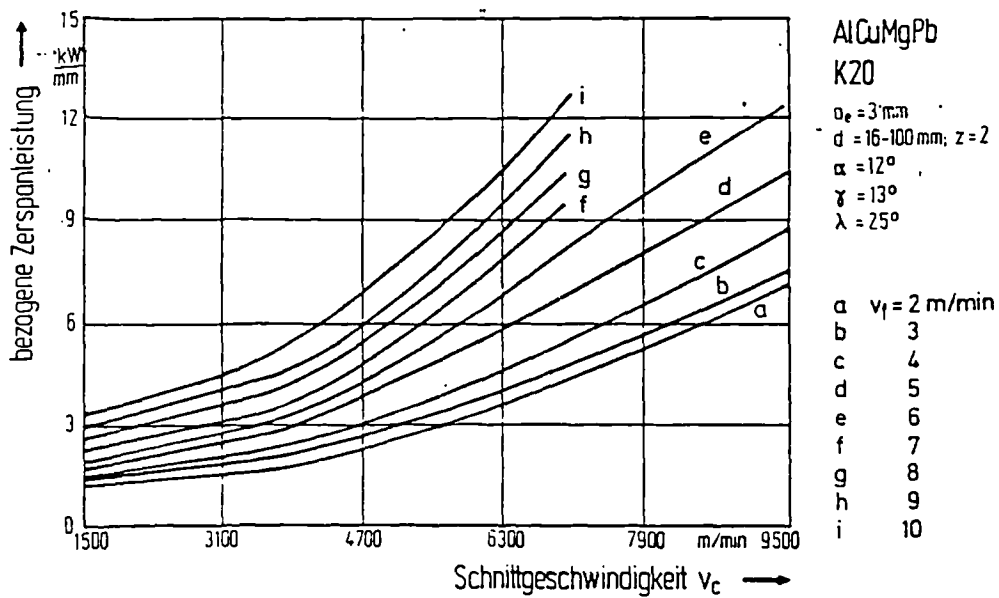


Fig. 5.2b: The relationship between the cutting speed and the cutting power (after Schulz [60])

(v) COMPARISON OF PREDICTION WITH PUBLISHED RESULTS

The experimental findings Aggarwal [61] in the cutting speed between 300 to 2100 m/min indicated that the cutting power reduces gradually as the cutting speed is increased. However, based on the observation in this study and the experimental findings of Schulz [60], there is nothing to suggest that the power would be reduced. The predicted result illustrated in figure 5.2a can be seen to correlate with the experimental graph by Schulz [60] shown in figure 5.2b. The percentage error between the two set of results as shown in table 5.2 was 8 percent. The slight discrepancy could be attributed to the selection of some of the workpiece material properties which were not given in the cutting data supplied by Schulz [60]. The data shown in table 5.2 suggests that aluminium alloys can be milled at cutting speeds up to 9500 m/min. The only limiting factors appears to be the design of the part being machined and the capability of the machining systems in terms of adequate power and speed of control.

5.5 PREDICTION 3: THE RELATIONSHIP BETWEEN THE SPECIFIC REMOVAL RATE AND THE CUTTING SPEED.

(i) AIM OF PREDICTION

To establish the influence of increase in cutting speed on the specific metal removal rate.

(ii) THE INPUT DATA

The selected input data are from the work of Schulz [60] as follows:

Cutting speed - 3000 - 5000 m/min,

Depth of cut - 3 mm,

Width of cut - 20 mm,

Feed - 0.3 mm, cutter dia. = 50 mm,

Rake angle - 12 (deg),

Number of tips - 2

(iii) PREDICTION RESULTS

The predicted specific removal rate and the experimental result of Schulz [60] graph c in figure 5.3b are shown in table 5.3

TABLE 5.3: PREDICTED SPECIFIC REMOVAL RATE AND SCHULZ'S RESULT

Cutting speed (m/min)	Schulz's ZWS (Graph c) (cm ³ /mm/kW)	Author's Predicted ZWS (cm ³ /mm/kW)	Error (%)
3000	75.0	100.5	-34
3400	83.5	98	-17
3800	87.5	95	-8.57
4200	85.0	93.5	-10
4600	79.0	86.9	-10
5000	70	77	-10

(iv) DISCUSSION ON THE PREDICTION RESULTS

Figure 5.3a illustrates typical relationship between the specific metal removal rate (ZWS) and cutting speed (V_c). Whilst figure 5.3b (aluminium AlCuMgPb graph c) shows the experimental result from Schulz [60].

It can be seen clearly from the predicted result in figure 5.3a that the specific metal removal rate reduces, however not linearly, whilst the power to remove the undeformed chips increase as illustrated in figure 5.2a. This can be attributed to the effect of the momentum force which operates at

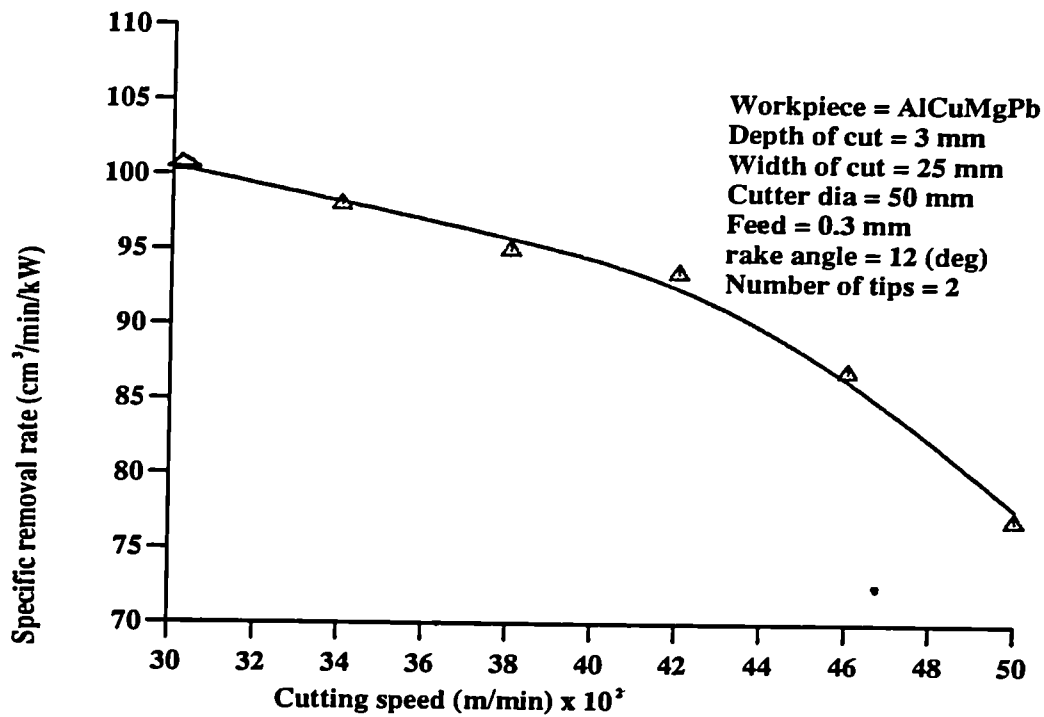


Fig. 5.3a: The relationship between the cutting speed and the predicted specific metal removal rate

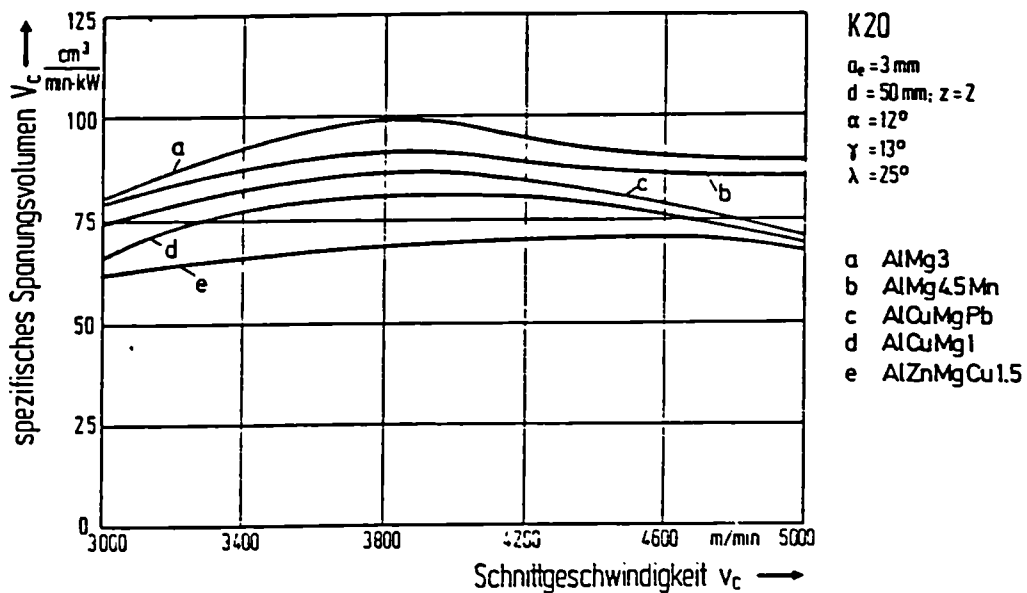


Fig. 5.3b: The relationship between the specific metal removal rate and the cutting speed (after Schulz [60])

high cutting speeds which requires an additional energy input. However figure 5.3b by Schulz shows that at cutting speeds below 3800 m/min the specific energy increase with an increase in cutting speeds. Whilst as the cutting speed increases above 3800 m/min, the specific energy reduces as the cutting speed increases. No theoretical explanation was given for the increase in the specific energy with an increase in cutting speed up to 3800 m/min.

(v) COMPARISON OF SIMULATION WITH PUBLISHED RESULTS

The predicted result above 3800 m/min compared well with Schulz [60]. The error between the two results was about 10 percent. However, based on Schulz's metal removal rate illustrated in figure 5.1b and cutting power shown in figure 5.2b it is not clear why Schulz observed an increase in the specific cutting energy between 1500 m/min and 3800 m/min as shown in figure 5.3b ($ZWS = ZW/P_{ch}$). The trend of the predicted result was also in agreement with the suggestions of Miller [62].

5.6 PREDICTION 4: THE RELATIONSHIP BETWEEN THE CUTTING SPEED AND THE CUTTING FORCES

(i) AIM OF PREDICTION

The variation of the cutting forces with cutting speed has been the subject of many investigations, but as yet no definite trend has emerged. Findley and Reed [63] found a large decrease in force by increasing the cutting speed from 1.8 to 1152 m/min for a lead-antimony alloy. Similar trends were reported by Fenton and Oxley [30] when machining steel in the cutting speed ranges from 60 to 311 m/min. However, on the other hand, Okushima [19] found that with medium carbon steel, the cutting forces remain constant up to approximately 2012 m/min and then increase. This agrees

with the results obtained by Tanaka et al [31] who, apart from the initial force reduction at below 91 m/min, report steady force increase with increasing cutting speed. The need for a more thorough analysis of cutting forces and perhaps of their relations to momentum force is clearly needed before definite conclusions on their behaviour at high speeds are possible. Therefore, the aim is to find the influence of the increase in cutting speed on the cutting forces.

(ii) INPUT DATA

The selected input data are from the work of Okushima et al [19] as follows:

Workpiece material - Steel S45C

Cutting speed - 0 - 2000 m/min,

Depth of cut - 0.5 mm,

Width of cut - 20 mm,

Feed - 0.05 mm,

Cutter diameter - 40 mm

Rake angle - 12 (deg),

Brinell Hardness - 274

(iii) PREDICTION RESULTS

Based on the supplied inputs, the simulated cutting force results data are as shown in table 5.4.

TABLE 5.4: PREDICTED CUTTING FORCES AND OKUSHIMA'S ET AL RESULTS

Cutting speed (m/min)	Principal force (N) Okushima	Predicted Principal force (N)	Feed force (N) Okushima	Predicted feed force (N)
0	0	0	0	0
200	88	97	29	40
400	78	97	21.5	40
600	73.5	97	19.6	40
800	68	97	19.6	40
1000	68	105	24.5	45
1200	108	118	29.4	55
1400	147	164	59	65
1600	196	210	98	108
1800	264	275	147	163
2000	343	355	186	205

(iv) DISCUSSION OF PREDICTION RESULTS

Figure 5.4a shows the relationship between the principal cutting force (F_{ch}), feed force (F_{fh}) and the cutting speed (V_c). It was observed that the cutting forces remain relatively constant up to 1000 m/min. However, as the effect

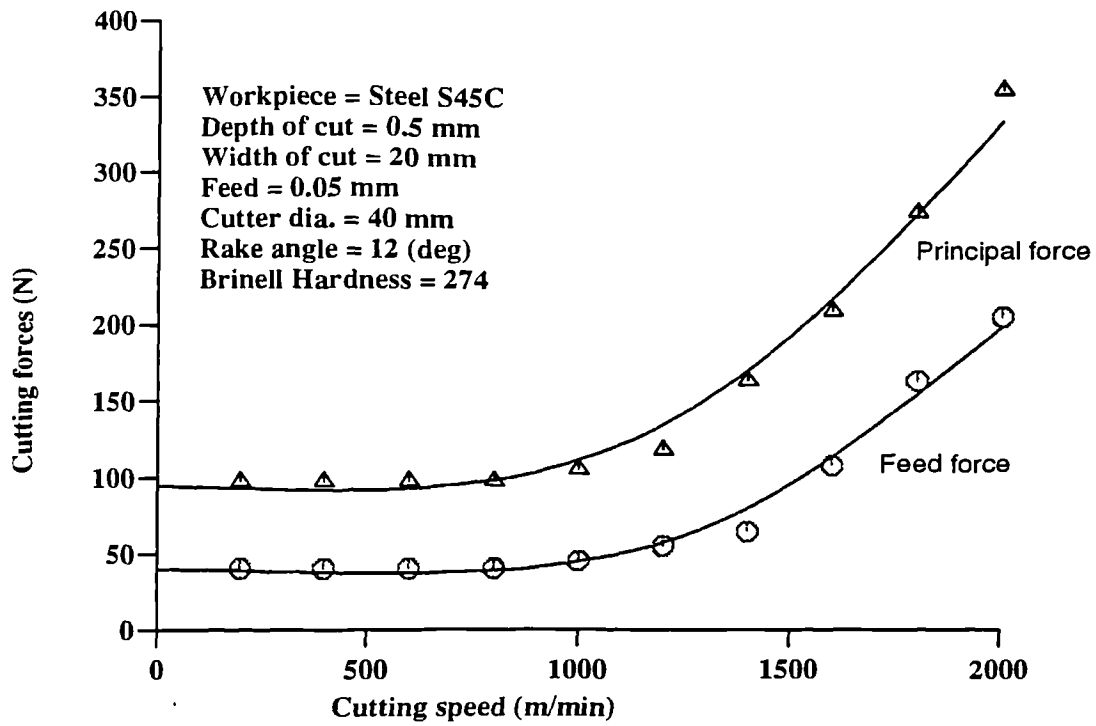


Fig. 5.4a: The relationship between the cutting speed and the predicted cutting forces

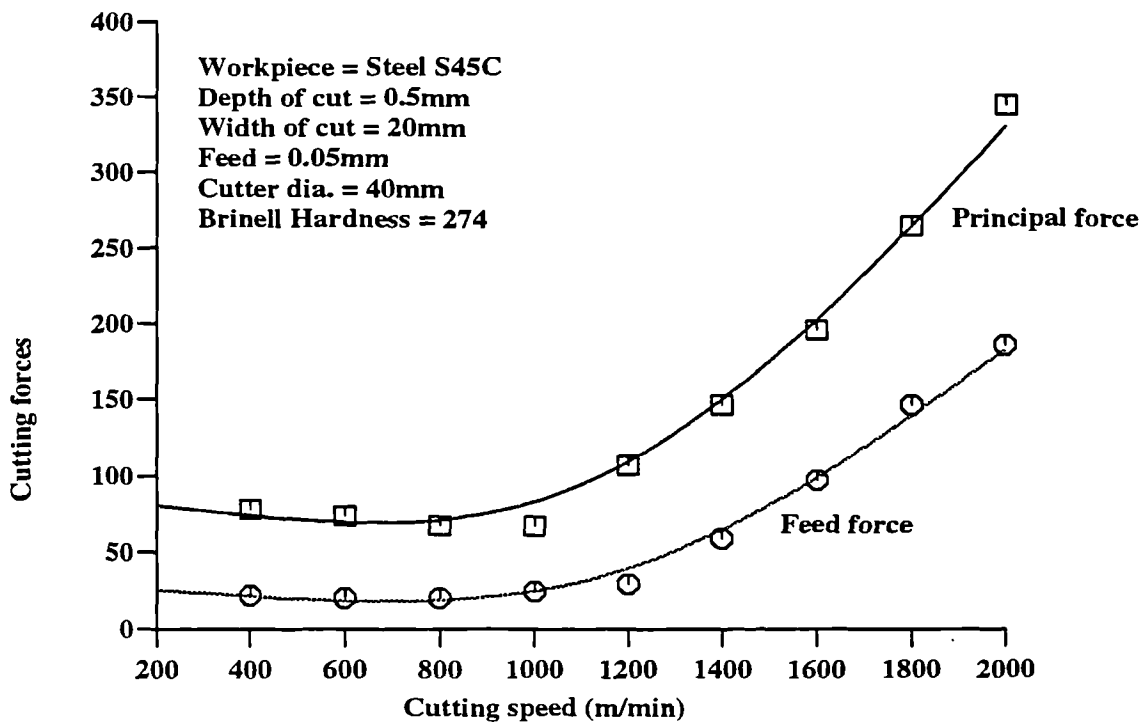


Fig. 5.4b: Relationship between cutting speed and tool forces (after Okushima et al [19])

of the momentum force (F_m) was taken into consideration, both cutting forces started to increase except the normal force on the tool face which remained relatively constant, due to the independence of the cutting forces on cutting speeds. Figure 5.4b illustrates the experimental result of Okushima et al. It was observed that a slight decrease in both forces occurred between 400 to 1000 m/min before the forces started to increase. No explanation was given for the observed reduction in cutting forces. However, it was explained that in order to measure the tool wear, the cutting operation was constantly interrupted.

Further observations from the results are as follows :

(i) The initial rise in cutting force at low cutting speed in the experimental graphs found in the literature can be associated with the formation of built-up edge Wright [55]. The cutting speed and cutting forces appear to be independent of each other within the cutting speed limits of the various tool and workpiece materials up to 1200 m/min after which the effect of momentum force takes place. This finding accords with Armitage et al [64]. Although it must be stressed that the two quantities depend on material properties such as hardness and tensile strength.

(ii) The cutting force can be said to be proportional to the Brinell hardness of the workpiece material, feed and depth of cut. This view agrees with the findings of Radford et al [65].

(iii) The product of cutting speed and cutting force determines the power which is consumed at the cutting edge. Therefore, it is evident that the utilization of the power of a given machine tool requires a reduction in cutting speed if the cutting force increases and vice versa.

(iv) In milling, a decrease of cutting force with increase of cutting speed is not always obtained [66, 67] and this is in agreement with the findings in this study where an increase in cutting force was experienced.

(v) COMPARISON OF SIMULATION WITH PUBLISHED RESULTS

The cutting speed and cutting forces appear to be independent of each other within the cutting speed limits of the various tool and workpiece materials up to 1000 m/min after which the effect of momentum force takes place. This finding accords with Schlesinger, Armitage et al and Okochi et al as reported by Kronenberg [68], [64], also with earlier work of Okushima et al [10] as shown in Fig. 5.4b and most recently with that of Ber et al in 1988 [69] and Armarego et al in 1991 [70].

5.7 PREDICTION 5: THE RELATIONSHIP BETWEEN THE CUTTING SPEED AND THE MOMENTUM FORCE

(i) AIM OF PREDICTION

The main aims of this part of the study were to elucidate the influence of the momentum force on cutting forces, establish the cutting speed range at which its significance should be considered and finally to compare the result with some of the earlier results published in the literature.

(ii) INPUT DATA

The selected input data from Arndt and Brown [59] are as follows:

Workpiece material - Aluminium

Workpiece density - 2777 kg/m³

Cutting speed - 0 - 1500 m/s,

Depth of cut - 0.508 mm,

Width of cut - 9.5 mm (0.375 inch),

Rake angle - 10 (deg),

Shear angle - 45 (deg)

(iii) PREDICTION RESULTS

Based on the supplied inputs, the simulated momentum force results data are as shown in table 5.5.

TABLE 5.5: PREDICTED MOMENTUM FORCE AND ARDNT'S RESULT

Cutting speed (m/s)	Arndt's et al Result (N)	Author's Predicted Result (N)	Error (%)
0	0.0	0.0	0
300	2207	1453	34
600	11036	5812	47
900	26487	13078	50.6
1200	58271	23250	60
1500	77255	36326	53

(iv) DISCUSSION OF THE PREDICTION RESULTS

The force F_m arising from momentum change was calculated using equation 3.30. The author's predicted results is shown in figure 5.5a whilst Arndt et al [59] experimental result is shown in figure 5.5b. In figure 3.9 the momentum force and its components in the direction of cutting F_{cm} and perpendicular to it F_{fm} are shown. According to Arndt and Brown [59] the graph in figure 5.5b are lines-of-best-fit through the experimental points. The order of magnitude of this force is extremely high compared to cutting forces for aluminium at conventional speeds and the predicted result plotted in figure 5.5a. Based on the data presented in table 5.5, it is expected that the forces would be even higher for a higher density material such as steel.

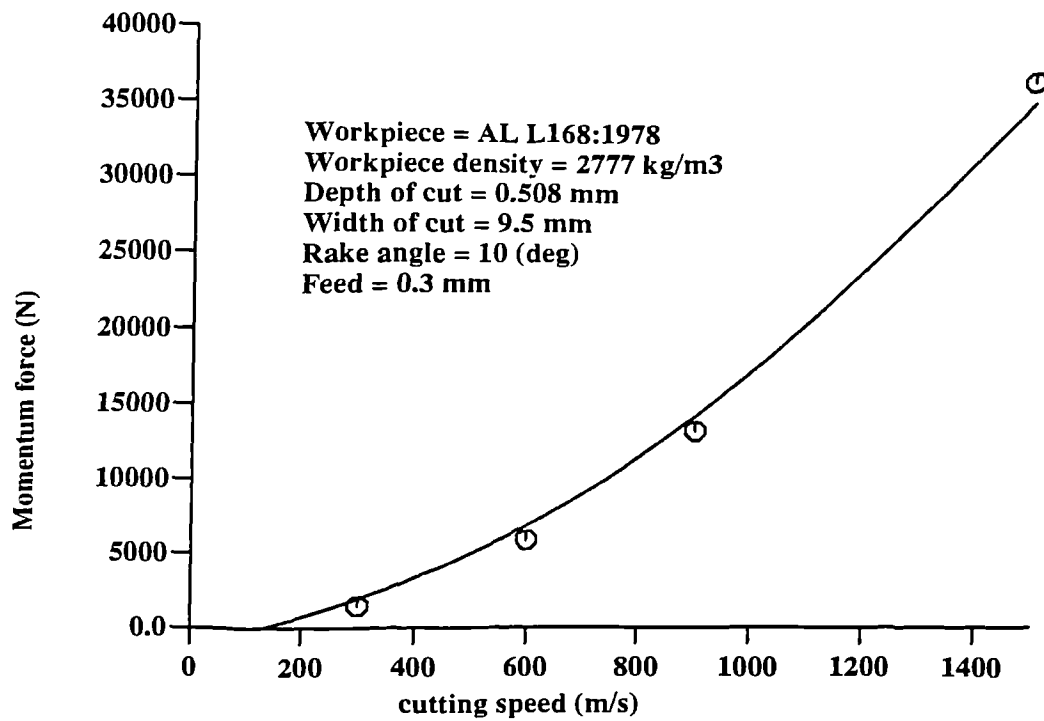


Fig. 5.5a: The predicted relationship between the cutting speed and the momentum force

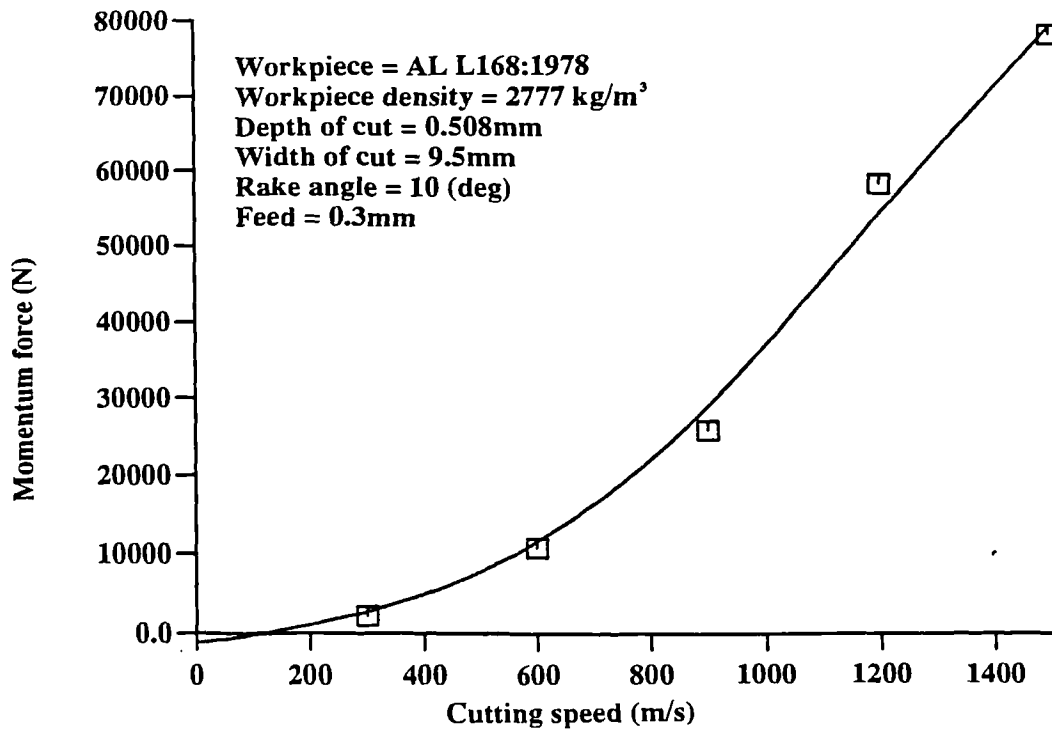


Fig. 5.5b: Relationship between cutting speed and momentum force (after Arndt [59])

According to Arndt et al [59], for a practical application, the very high values of momentum force as shown in both figure 5.5a and 5.5b indicate some of the problems in applying ultra-high speed machining. The energy required for cutting will be very high and there may be some difficulties in designing a tool sufficiently strong to withstand the forces involved. Therefore, the cutting speed used here is not normal cutting application it was used by Arndt et al only for research purposes.

(v) COMPARISON OF PREDICTION WITH PUBLISHED RESULTS

The prediction result plotted in figure 5.5a was based on the limited input data supplied by Arndt et al [59]. For example the shear angle and the workpiece material which are crucial to prediction software program were not given. This might probably account for the lower values of F_m in figure 5.5a as compared to Arndt et al [59] result plotted in figure 5.5b. Another reason for the difference between the two results could be the measuring technique and equipment used to measure F_m at such higher cutting speeds. Having said that, it can be seen that both graphs follow the same trend.

5.8 PREDICTION 6: THE RELATIONSHIP BETWEEN THE CUTTING SPEED AND THE CUTTING TEMPERATURE

(i) AIM OF PREDICTION

Arndt [9] states that Salomon in 1931 reported an increase in tool temperature with cutting speed, reaching a peak close to the melting temperature of the work material under consideration and then a rapid decrease at very high cutting speeds, thus manifesting better machining features at high cutting speed. However, from the literature survey, it appears that there is no clear method for estimating the cutting temperature, most of the earlier and recent works are still based on empirical equations. This can be attributed to the complexity of machining at high cutting speeds

and most importantly on available measuring equipment. Therefore, the principal aim of this part of the study was to establish whether there is scientific justification for the earlier findings that there exists a critical cutting speed for each material at which temperature reaches a maximum and beyond which the tool temperature falls rapidly to a low value and also to establish a mechanism for calculating cutting temperature for a wide range of workpiece materials at a given cutting speed.

(ii) INPUT DATA

The selected input data are from the work of Schmidt [71] as follows:

Workpiece material - Steel S45C,

Workpiece density - 7200 kg/m³

Depth of cut - 3.175 mm,

Width of cut - 5 mm,

Feed - 0.2032 mm,

Cutter diameter - 40 mm,

Rake angle - -6 (deg),

(iii) PREDICTION RESULTS

Based on the supplied inputs, the simulated cutting temperature results data are as shown in table 5.6. Keys to the table are as follows:

- A - Schmidt's [71] workpiece temperature
- B - Schmidt's [71] Average chip temperature
- C - Schmidt's [71] Chip/tool interface temperature
- A1 - Predicted workpiece temperature
- B2 - Predicted Average chip temperature
- C3 - Predicted Chip/tool interface temperature

TABLE 5.6 : PREDICTED TEMPERATURES AND SCHMIDT'S RESULT

Cutting speed (m/min)	A (°C)	B (°C)	C (°C)	A1 (°C)	B2 (°C)	C3 (°C)
0	0	0	0	0	0	0
60	33.8	415	649	37	459	680
120	31	418	760	36	459	798
180	31	418	815	36	459	860
240	31	421	871	36	456	920
300	31	421	926	35	456	985
360	31	421	973	35	456	1021

(iv) DISCUSSION OF THE SIMULATION RESULTS

Figure 5.6a shows the relationship between the cutting speed and the workpiece temperature (H_{cw}), the average shear zone temperature (T_s), the chip temperature (T_{chip}) and the maximum temperature along the tool rake face. This figure and table 5.6 indicates that up to 1000 m/min, H_{cw} and T_s remains relatively constant, whilst T_{chip} increases significantly. However, as the cutting speed increases above 1000 m/min H_{cw} and T_s begins to decrease modestly whilst T_{chip} continue increasing. The reduction in H_{cw} and T_s can be attributed to the fact that as the cutting speed increases there is less time available for plastic deformation and the mode of heat transfer changes from conduction to convection where the majority of the heat generated is transferred with the chip. This is in accord with Recht [29], Stock and Thompson [72] and Kuznetsov [73]. The increase in the chip and tool rake face temperature can be attributed to the frictional force which increases with the cutting speed and also with the effect of secondary deformation due to the interaction between the chip and the tool rake face.

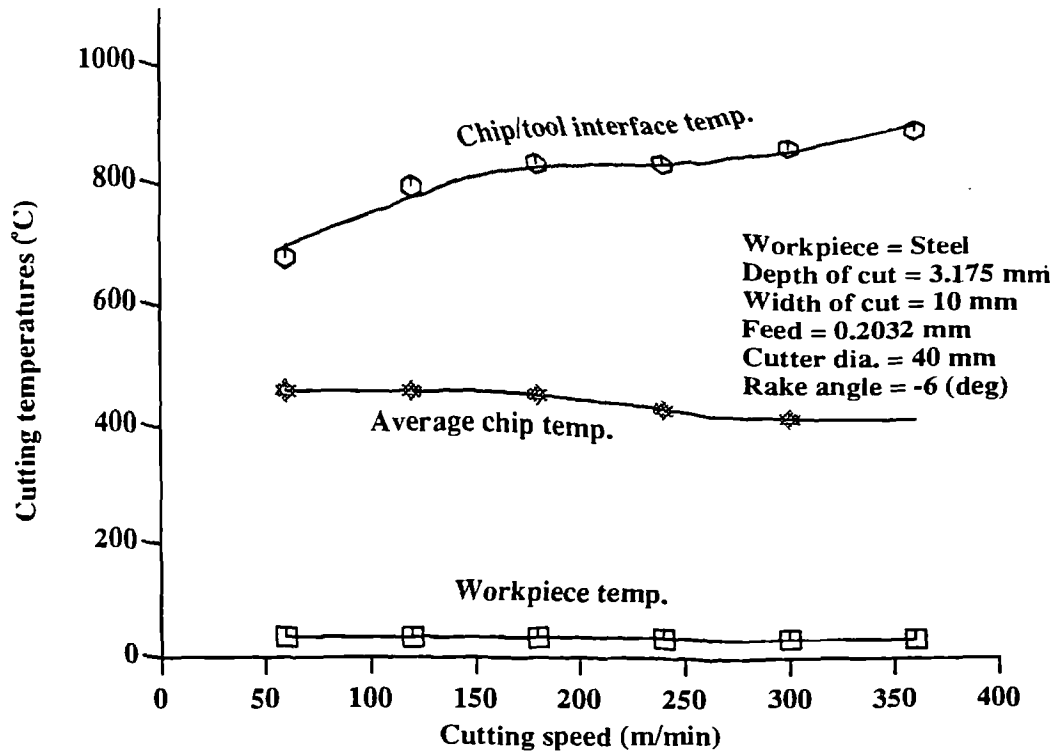


Fig. 5.6a: The predicted relationship between the cutting speed and cutting temperatures

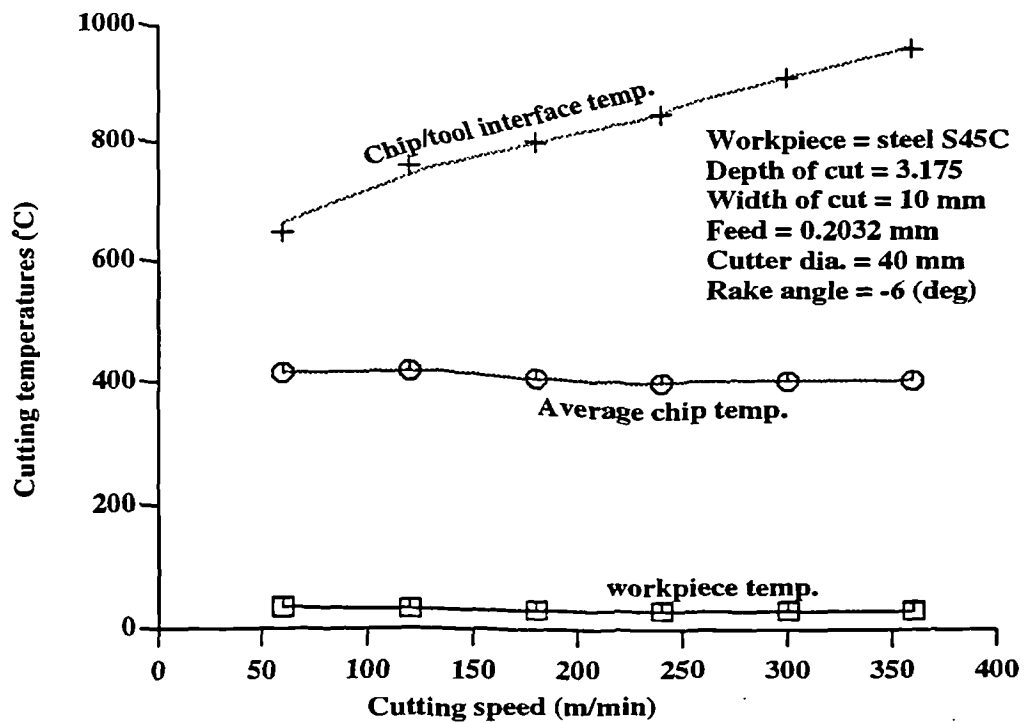


Fig. 5.6b: Effect of cutting speed on temperature of workpiece, chip and chip/tool interface (after Schmidt [71])

This finding clarifies the controversy amongst the earlier investigators regarding the influence of cutting speed on cutting temperature. Those who observed a reduction in cutting temperature were referring to H_{cw} and T_s . Whilst those who claimed to observe increased cutting temperature with cutting speeds were referring to T_{chip} .

(v) COMPARISON OF SIMULATION WITH PUBLISHED RESULTS

The result of this study shown in figure 5.6a compared well with the finding of Schmidt [71] plotted in figure 5.6b and also in agreement with the findings of von Turkovich [47], Boothroyd et al [49], Tay et al [56], Tanaka and Kitano [18], Okushima et al [19], Merchant [24], Recht [29], Stock and Thompson [72] and Kuznetsov [73].

5.9 PREDICTION 7: THE RELATIONSHIP BETWEEN CUTTING FORCES AND THE FEED.

(i) AIM OF THE PREDICTION

Theoretically an increase in feed should increase the shear angle thereby resulting in lower cutting forces. As a result of this perception there has been much research activity in this area. However, from the literature survey, clear trends are not yet established regarding the influence of feed on cutting forces in HSM. Therefore, the principal aim of this part of the study was to establish the effect of feed on the cutting forces.

(ii) THE INPUT DATA

The selected input data are from the experimental work of Schulz [60] as follows:

Workpiece material - Aluminium AlCuMgPb

Cutting speed - 1000 m/min,

Depth of cut - 1.5 mm,

Width of cut - 5 mm,
 Cutter diameter - 40 mm,
 Rake angle - 12 (deg),
 Number of tips - 1

(iii) PREDICTION RESULTS

The predicted cutting force, the experimental result from the work of Schulz's [60] and the percentage error between both results are shown in table 5.7.

Table 5.7 : PREDICTED FORCES AND SCHULZ'S RESULTS

Feed (mm)	Schulz's main force (N)	Schulz's feed force (N)	Predicted main force (N)	Predicted feed force (N)
0.0	0.0	0.0	0.0	0.0
0.1	390	300	417	320
0.2	450	400	485	428
0.3	700	600	750	640
0.4	820	700	878	745
0.5	1200	780	1280	830

(iv) DISCUSSION ON THE PREDICTION RESULTS

Figure 5.7a shows the predicted result on the relationship between the principal cutting force, the feed force and the feed, whilst figure 5.7b shows the experimental result of Schulz [60]. It can be seen in both figures that the cutting forces increase almost linearly with the feed. These

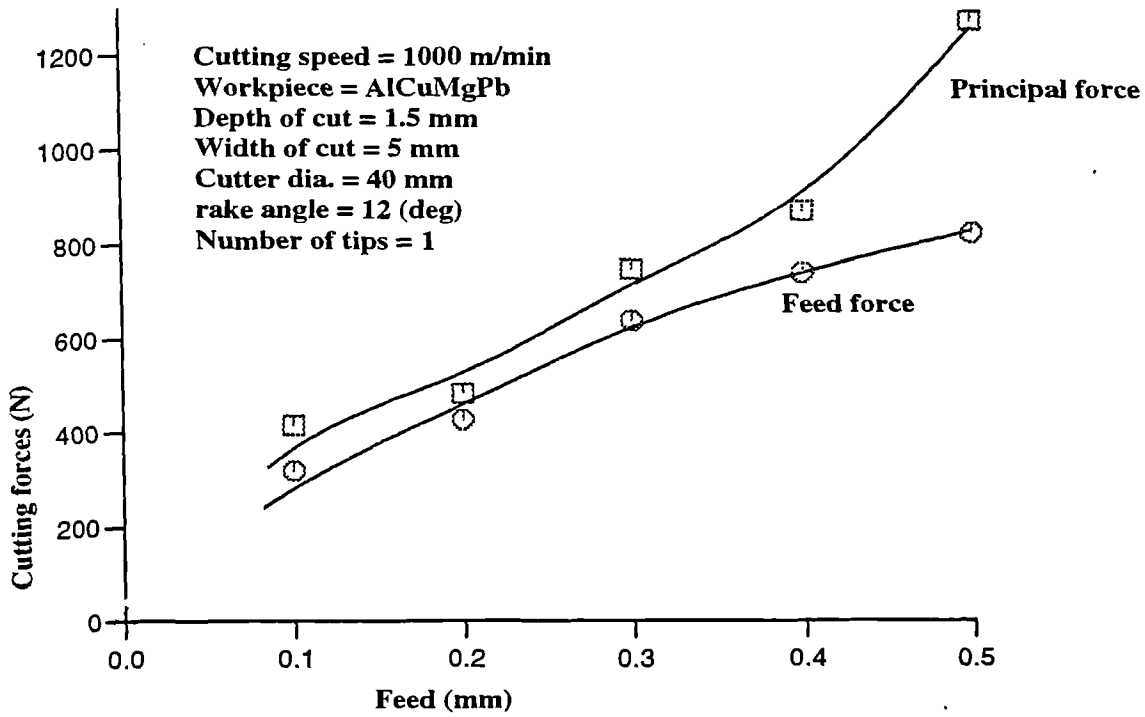


Fig. 5.7a: The relationship between the predicted cutting forces and the feed

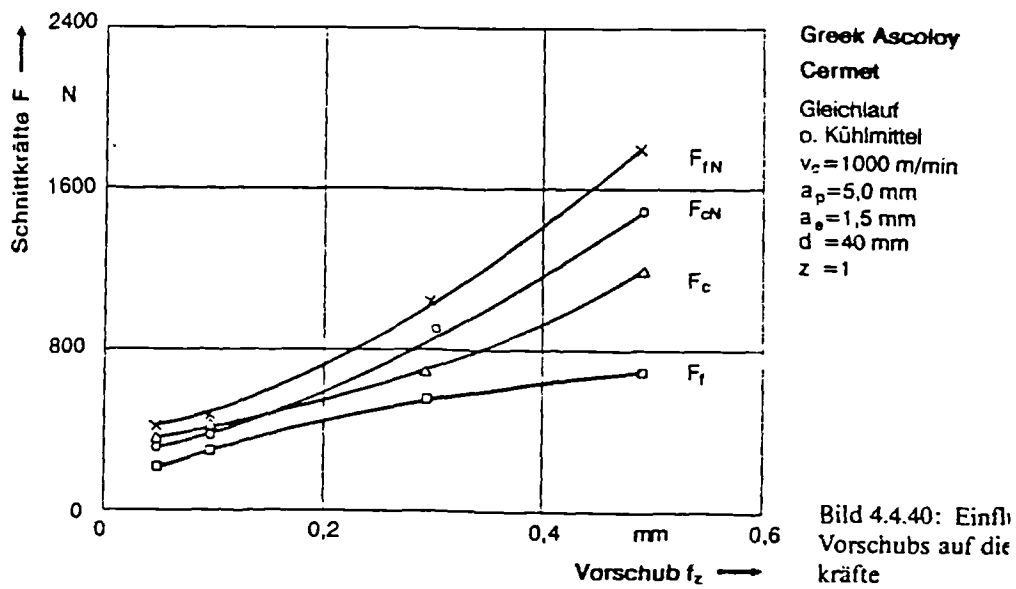


Fig. 5.7b: The relationship between the cutting forces and the feed (after Schulz [60])

results indicate that the cutting forces are proportional to feed, the brinell hardness of the workpiece and the depth of cut. This view agrees with the findings of Radford et al [65].

(v) COMPARISON OF SIMULATION WITH PUBLISHED RESULTS

The results compare well with the experimental results of Schulz [60] plotted in figure 5.7b and also Martellotti [42] and Brown [27] observed an increase in both main cutting force and the feed force in their studies. The percentage error between the predicted and Schulz's [60] result was about 10 percent.

5.10 PREDICTION 8: THE RELATIONSHIP BETWEEN THE RAKE ANGLE AND THE CUTTING FORCES

(i) AIM OF PREDICTION

The effect of rake angle on cutting forces are of interest since if the forces are less with large or positive rake angle the power requirement will be less. Therefore the aim of this part of the study was to establish the influence of rake angle on cutting force and how it affects the power requirement in HSM.

(ii) INPUT DATA

The selected input data are from the experimental work of Brown [27] as follows:

Workpiece material = Aluminium 2017 T4

Cutting speed - 1000 m/min,

Depth of cut - 2.54 mm and 3.05mm,

Width of cut - 5 mm,

Cutter diameter - 40 mm,

Rake angle - -20, -15, -5, 0, 6 (deg),

Number of tips - 1

(iii) PREDICTION RESULTS

The predicted cutting forces and the experimental result from Brown's work are shown in table 5.8.

Table 5.8: PREDICTED FORCES AND BROWN'S RESULTS

Rake Angle	measured Fc	measured ft	Predicted fc (N)	Predicted ft (N)
-15	211	112	235	125
-10	198	96	211	107
-5	190	74	210	82
0	185	70	205	78
6	190	55	210	60

(iv) DISCUSSION OF PREDICTION RESULTS

Figure 5.8a illustrates the relationship between the principal cutting force (F_{ch}), feed force (F_{th}) and the rake angle (α). The results obtained suggested that the negative rake angles produce higher principal cutting force and feed force. These results were attributed to the reduction in shear angle suggesting a high cutting power requirement. However an increase in the positive value of rake angle gave a reduction in both forces although the reduction in the principal cutting force is not dramatic as the reduction in the feed force. These reductions in forces are attributed to an increase in shear angle with the implication being a lower power requirement.

(v) COMPARISON OF SIMULATION WITH PUBLISHED RESULTS

The prediction results plotted in figure 5.8a compared well with experimental work of Brown [27] shown in figure 5.8b. Decreases in force with increasingly positive rake angle, have also been reported by von Turkovich [47] and Fenton et al [30].

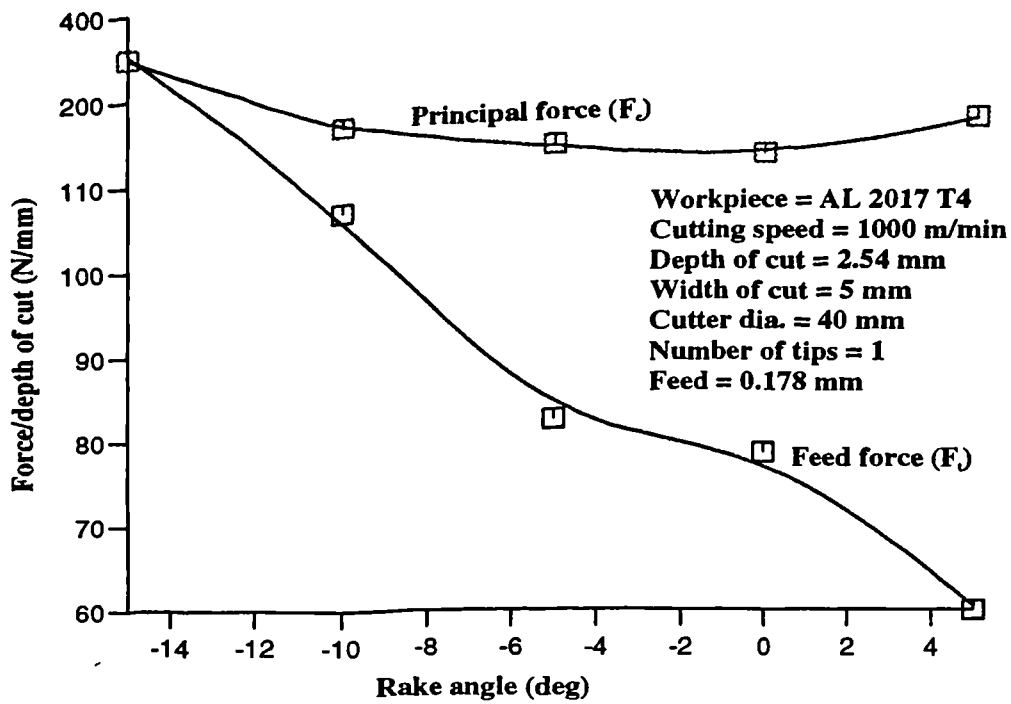


Fig. 5.8a: The relationship between the rake angle and the predicted cutting forces

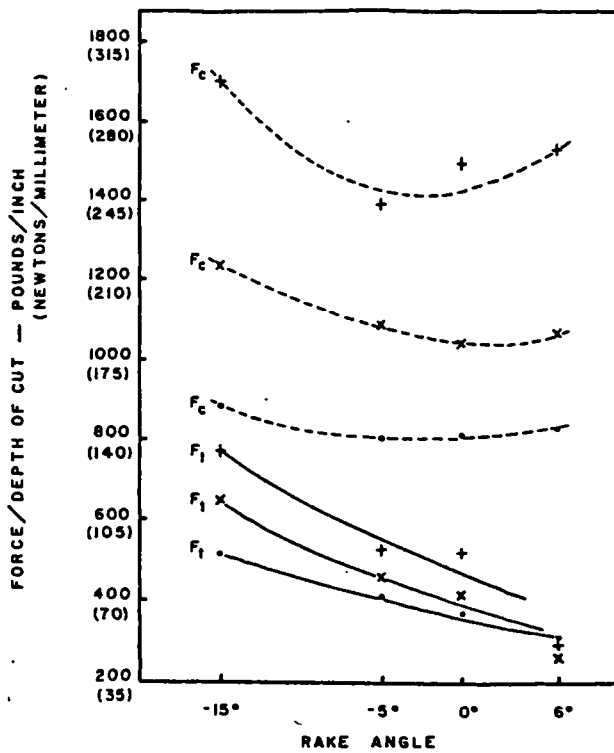


Fig. 5.8b: Forces versus rake angle at three feeds
 (Feed = 0.279 mm, 0.178 mm, 0.127 mm (after Brown [27]))

5.11 PREDICTION 9: THE RELATIONSHIP BETWEEN THE RAKE ANGLE AND THE CUTTING TEMPERATURE

(i) AIM OF PREDICTION

Shaw [71] has suggested that lower temperature may lead to longer tool life, however, from the relationship between the rake angle and the cutting forces by Brown [27] plotted in figure 5.8b, it has been shown that negative rake angle produces higher forces. Therefore, the aim of this aspect of the study was to establish the correlation between the rake angle and the cutting temperature and determine the most suitable rake angle for cutting at HSM.

(ii) INPUT DATA

The selected input data from Schmidt [74] experimental work are as follows:

Workpiece = steel S45C

Cutting speed = 400 m/min,

Depth of cut = 1.5 mm,

Width of cut = 2 mm,

Feed = 0.177 mm

Cutter dia. = 40 mm

Number of tips = 2

(iii) PREDICTION RESULTS

Based on the supplied inputs, the predicted results data are as shown in table 5.9. It can be seen that the maximum average chip temperatures decrease with increasing rake angle.

TABLE 5.9 : PREDICTED TEMPERATURE AND SCHMIDT'S RESULTS

Rake angle (deg)	Schmidt's maximum average chip temp. (°C)	Predicted maximum average chip temp. (°C)
5	454	481
0	468	496
-5	493	518
-10	527	553
-15	568	596
-20	621	650
-25	637	665
-30	678	705

(iv) DISCUSSION OF SIMULATION RESULTS

Figure 5.9a shows the predicted relationship between the rake angle and the maximum average chip temperature along the tool rake face, whilst figure 5.9b illustrates Schmidt's [74] experimental result. Both plotted results indicate that negative rake angles cause higher cutting temperatures and hence a shorter tool life than positive rake angles.

The general conclusion from these results is that the work done, the cutting forces and the temperature generated, decreased with increase in rake angle through negative rake cutting to positive rake cutting therefore requiring less power.

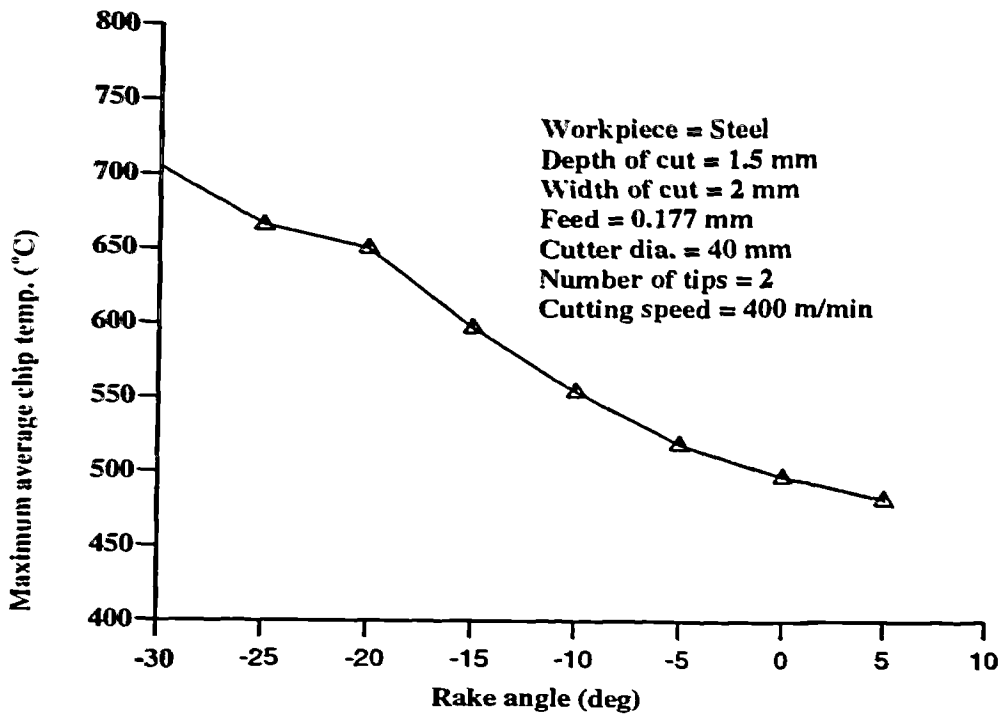


Fig. 5.9a: The relationship between the rake angle and the predicted cutting temperature

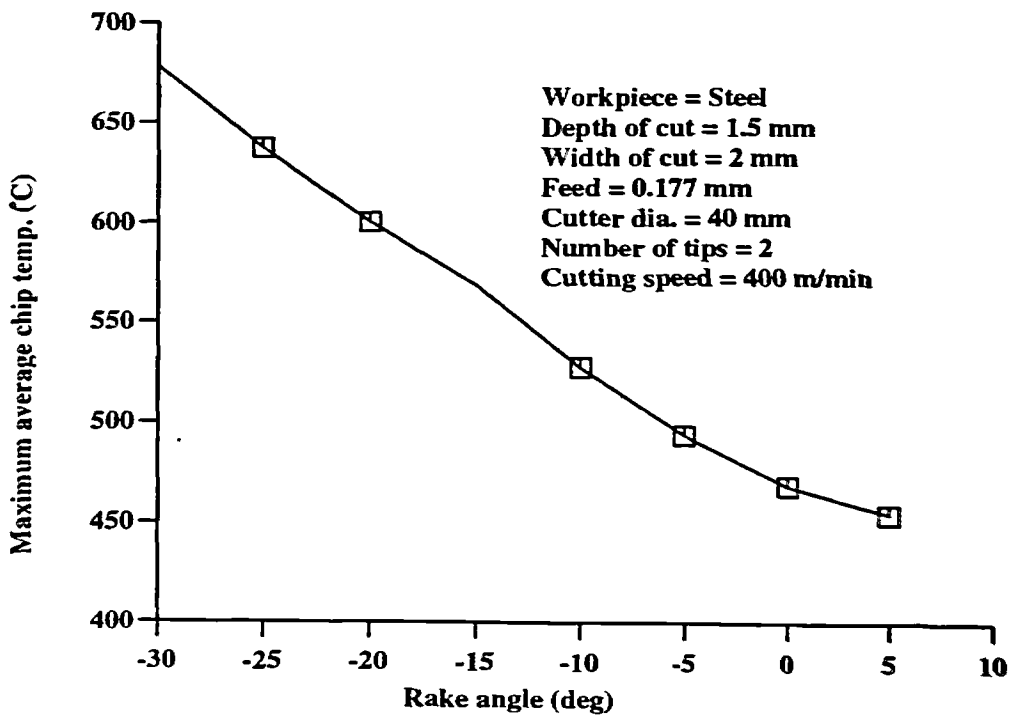


Fig. 5.9b: Effect of rake angle on chip and workpiece temperature for various feeds when milling steel (after Schmidt [74])

(v) COMPARISON OF SIMULATION WITH PUBLISHED RESULTS

The predicted results shown in figure 5.9a are comparable with the experimental findings of Armitage and Schmidt [74] plotted in figure 5.9b. The error between the two results was about 10 percent. The results also correlate with findings of a number of workers [75-79].

CHAPTER 6

EXPERIMENTAL WORK IN HIGH SPEED MACHINING

6.1 INTRODUCTION

Although the simulation results compared with published results, obviously before the simulation package can be used it needs to be verified with experimental results since most of the published work in milling has either (i) been concerned with cutting at low speed, especially in its simplest form using one tip cutter [38] and [69], or (ii) the results extrapolated to high cutting speed range [30] and (iii) the graphical results have not been accompanied with qualitative data as presented by Arndt [8,9], Brown [27], Recht [29] and Tanaka et al [31]. The results such as these are not adequate to describe what really happens in practical milling operations because operations such as milling which are intermittent and exhibit complicated cutting geometries as well as varying chip thickness, demand special experimental care. This special care becomes more critical in high speed milling.

Therefore, there is a need to establish the degree of correlation between the mathematical cutting simulation model result predictions developed at the first stage of this study and the actual cutting experimental results. In this chapter the experimental programme developed to verify the predicted results in detailed are discussed. The collaborative experimental work was carried out at the Research and Development Centre at British Aerospace Samlesbury.

6.2 AIMS AND OBJECTIVES OF THE EXPERIMENTAL WORK

The aim of the experiments was to measure the forces induced during high speed milling to help in assessing the practical application, prediction of accuracy and providing important cutting data to further improve the cutting

simulation model development. This should enable the model to provide a foundation upon which adaptive optimisation strategies may be developed by integrating process parameter selection and manufacturing system element constraints in the process planning. The model may then become a vital useful tool for the process engineers. Therefore, the main objective of this part of the work was to describe the necessary experimental equipment, setup procedures and tests undertaken for the measurement of the cutting forces.

6.3 EXPERIMENTAL EQUIPMENT

The initial task involved the identification of all the necessary experimental equipment and the construction of a test rig which was mobile enough to be transported between the University and British Aerospace. The design and commissioning of a reliable test rig were carried out and developed to provide enough data to meet the objectives of this investigation.

The test rig consisted of the following:

- Dynamometer (Kistler 9240) for force measurement;
- Milling machine tool;
- 30000 rpm spindles;
- Aluminium workpiece material;
- 25 and 50 mm diameter cutters;
- Charge amplifier;
- Digital oscilloscope;
- Personal computer with data acquisition card.
- Infrared camera (VideoTherm 94);
- Portable video cassette recorder;
- Signal conditioning system for both cutting forces and temperature measurements.

The photographic illustration of the testing rig is as shown in figure 6.1. As it can be seen, to the left side of the computer is the signal conditioning unit

placed on top of the charge amplifier box and the dynamometer is on the right hand side of the computer.

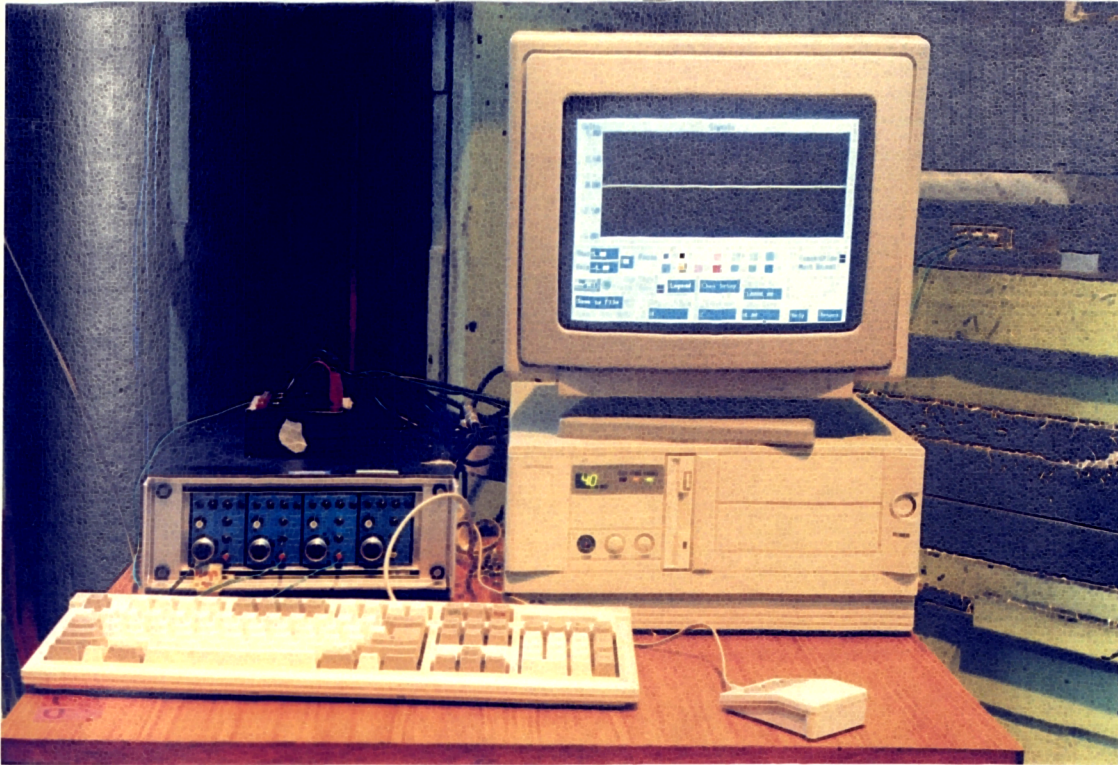


Fig. 6.1 :The photographic illustration of the testing rig

6.3.1 EXPERIMENTAL RIG DESIGN

For the force measurements, the signal conditioning system was designed and developed. This system formed the link between the incoming signals from the dynamometer, charge amplifiers and the data acquisition card in the computer. The benefits of this signal conditioning system was that it provided a mechanism to measure the incoming signal off line with a volt meter or oscilloscope independent of the data acquisition card in the computer, thereby acting as safety device. Also the number of the incoming signal channels to the computer can be controlled manually or electronically through the data acquisition card.

6.3.2 DATA PROCESSING

The processing of the experimental signals was performed by a personal computer illustrated in a schematic diagram figure 6.2. The analogue to digital converter used in this investigation was a 12-bit data acquisition card known as Lab PC Plus and the data capturing was achieved by the aid of

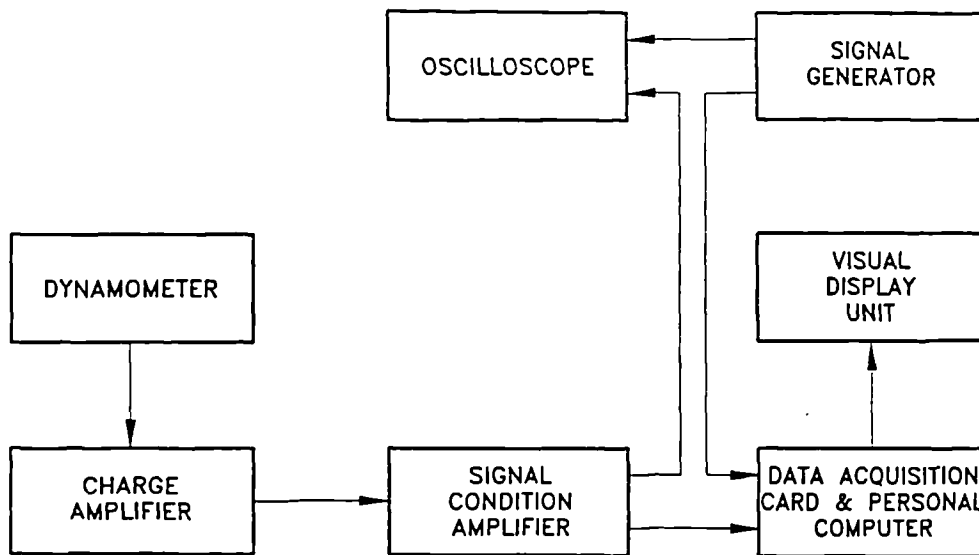


Fig. 6.2: Schematic representation of the signal processing equipment

off-the-shelf software called Daqware. Both the data card and the software were supplied by National Instruments. The card has a sample and storage amplifier which allows event acquisition rate between 1HZ to 83Khz. When a data acquisition cycle is triggered manually or through the internal programmable timer clock then the input data are multiplexed into 512 byte first-in-first-out buffer by the control and timing logic on the card. These signals are then transferred independently to the host computer memory using a direct memory access process. One of the limitations of this card is that its buffer is not big enough to store large data at high sampling rate, however, since only the quality of the data is of great interest rather than the quantity, the starting time to start capturing data was controlled manually and the termination of data storing process was left to the time the

memory buffer is full at which point the storing operation will stop. At this stage it is possible to store the data into the computer hard drive or a floppy disk in either ASCII, BINARY, or in Lotus 1-2-3 format suitable for analysis.

An IBM compatible personal computer model 386DX 40 with 128K Cache, 8 megabyte of memory and installed with 12-bit data acquisition card was used as central data control system. Once the data is stored in the computer hard disk or floppy disk it can either be analyzed directly 'on-line' or stored for later use. Analysis of the measured force, power and temperature signals was achieved by the aid of a program specifically written in Minitab software and Harvard Graphic software package was used to plot the results.

Several preliminary checks of the data acquisition system were made to ensure that the data logger, signal conditioning system and the software were operating correctly. A check of both the computer and the acquisition program were performed by feeding simulated signals from a signal generator. The amplitude limit control or voltage level on the data acquisition card which sets the minimum and maximum level of the incoming signal was set at $-/+ 5$ volts. The reason for this was that any incoming signal below $- 5$ volt and above $+ 5$ volts could be rejected thereby protecting the data acquisition card.

Once it was established that the computer, data acquisition, signal conditioning and the software were working correctly the following equipment were calibrated:

6.3.3 DYNAMOMETER AND CHARGE AMPLIFIER CALIBRATION

The dynamometer is one of the most successful tools used in the study of tool forces generated during metal cutting. It allows investigation of the effects of changes in cutting conditions on the forces developed during machining of various materials. Since this is a three component

dynamometer it is ideally suited for the milling process. During this process the dynamometer was used to measure the instantaneous forces in X and Y directions (F_x and F_y), which are the components of the resultant or the principal cutting force parallel and normal to the cutting direction. The force in the Z direction (F_z) were not measured since it does not play any significant role in determining the tangential force. The dynamometer that is described here is an off-the shelf type 9240 supplied by Kistler Instrument Ltd.

The calibration procedure employed was that the gain on the charge amplifier was set at 50 which was the highest gain setting possible on the charge amplifier. Then the signal cable was connected to the dynamometer and a known load or weight was placed on the dynamometer and the correspond output voltage readings was taken from the charge amplifier. The following formula was used to find the equivalent force in kilo newton of the voltage readings:

$$1 \text{ kilogram of load} = 0.0066 \text{ mV} = 9.8 \text{ newton force}$$

Several readings were taken before arriving at an average reading of 0.0066 mV = 1 kilogram of load.

When the Z axis on the dynamometer had been successfully calibrated, the dynamometer was repositioned to calibrate its X and Y axes as well. On average the same value of 0.006 mV per 1 kilogram of load was recorded which indicated the level of accuracy of the dynamometer.

After calibration, the dynamometer was clamped tightly on top of the milling machine table by means of the two flanges attached to the dynamometer and the workpiece was placed on top of the dynamometer and clamped tightly. Finally, the BNC end of the signal cables were connected to the x, y and z socket on the dynamometer and the other ends to the charge amplifiers. A series of cutting trials were then performed.

6.4 WORKPIECE MATERIAL SELECTION

Since one of the objectives of this study was to investigate milling of aluminium alloys suitable for aerospace components at high cutting speeds, aerospace aluminium alloys type L168:1978 whose basic mechanical and thermal properties were known were employed in these experiments. The reason for selecting this type of material instead of commercial aluminium alloys was that it has better machinability factors and its properties are better detailed than commercial materials. The workpiece material was received in the form of rectangular bar with cross section measuring approximately 300 mm by 300 mm by 45 mm, whilst the material used for the video demonstration was 700 mm by 300 mm by 45 mm. The mechanical and thermal properties of this material are given in Appendix 1.

6.5 MACHINE TOOL AND CUTTING TOOLS SELECTION

The machine tool used was a Marwin vertical milling machine equipped with a 30000 rpm high speed spindle with ceramic ball bearings and operating power of 25 kW. It has a maximum feedrate in X, Y and Z direction of 20 m/min, however, this depends on the length of the program. The controlling system has execution times of about 20 ms. The accuracy of positioning and repeatability is within 10 microns for the X, Y and Z axes. However, this depends on the mechanical parts of the machine.

The cutting tool material selected is tungsten carbide brazed on high speed steel body based on the recommendation of British Aerospace Military Aircraft Division. This material can be easily machined in its annealed state to the required shape, then heat treated to produce the desired mechanical properties suitable for metal cutting. The cutters chosen were 50 mm and 25 mm diameter with 2 tips. The tungsten carbide is ideally suited for machining soft metals. The photographic illustration of the 50 mm diameter cutter is as shown in figure 6.3.

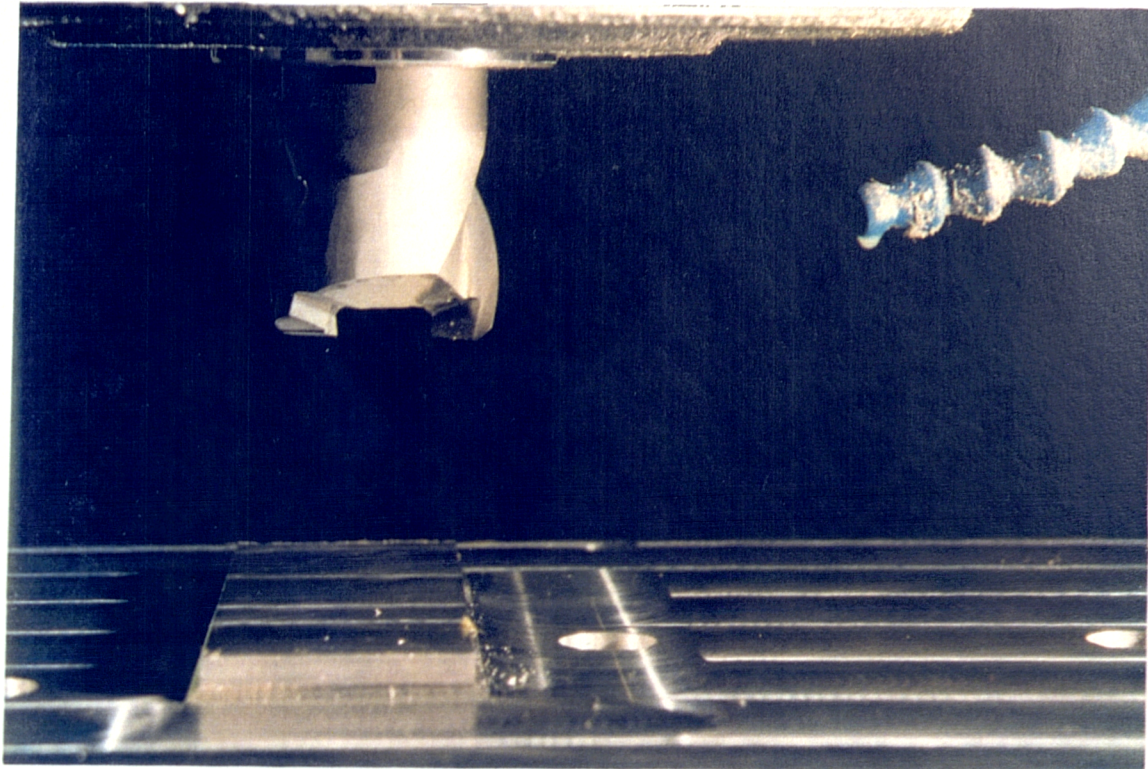


Fig. 6.3: The photographic picture of the 50 mm diameter cutter.

6.6 EXPERIMENTAL PROCEDURE

The three component dynamometer was mounted on the milling table and the aluminium workpieces were mounted and bolted down on top of the dynamometer. The dynamometer was used to measure the tangential, feed and the radial forces produced during machining. The force measurement schematic setup arrangement is as illustrated in figure 6.4, whilst the photographic illustration is as shown in figure 6.5.

The aluminium workpieces were machined using a cutting fluid. The reason for the lubricant was that at high speed the heat generated was much higher than that generated at low speed. For the purpose of this study, the influence of the increase in cutting speed on cutting process parameters was tested.

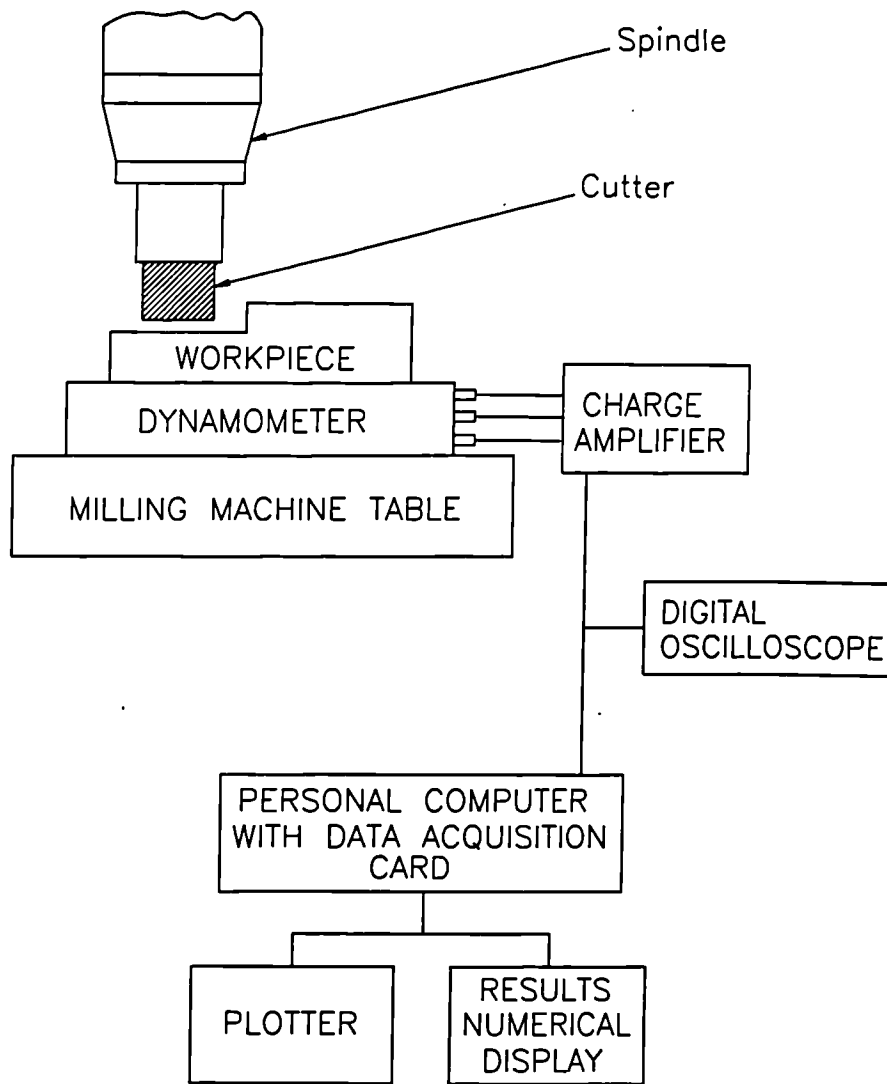


Fig. 6.4: Cutting force measurement experimental setup

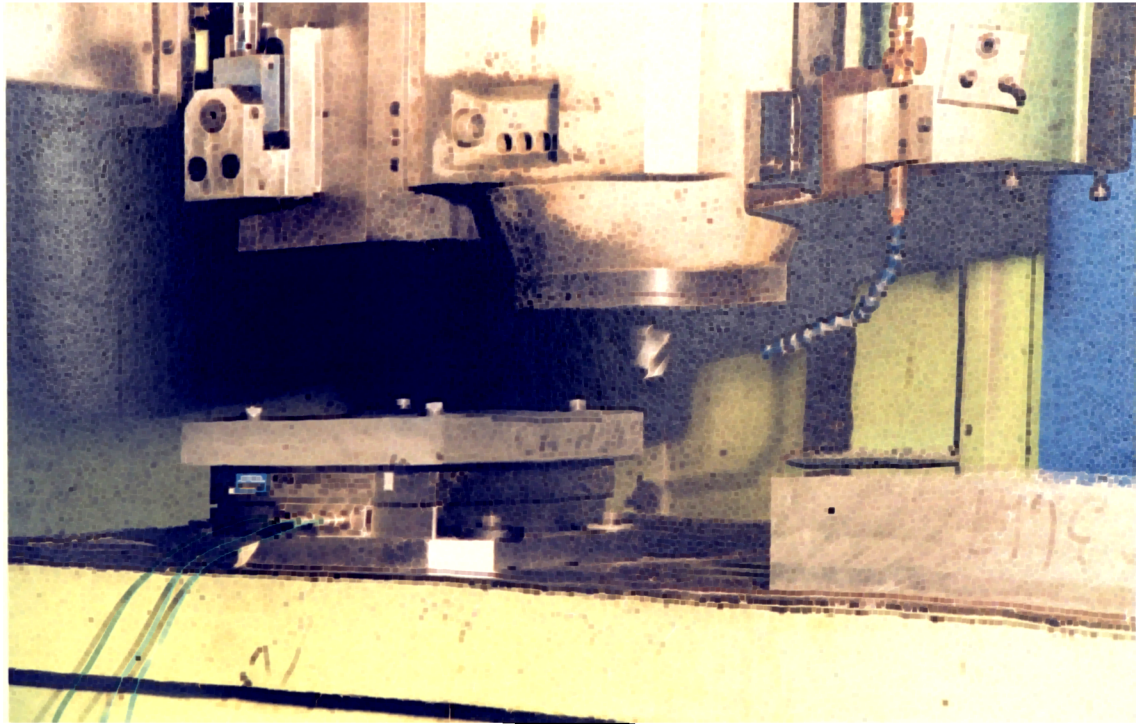


Fig. 6.5: The photograph picture of the force measurement setup

6.7 CUTTING FORCE EXPERIMENTAL TECHNIQUE

Prior to the experimental test all the instruments were switched on and simulated by the signal generator for a period of 90 minutes to ensure that they were working correctly and a steady operating state was reached. A further test was carried out to establish that the signals coming from the dynamometer 3 channels were correct. This was achieved by applying loads with known weights on the dynamometer and observing the output readings on the computer to see whether they were similar to the readings obtained when the dynamometer was initially calibrated.

Once it was established that all instruments were working, the influence of the cutting speed on the cutting forces as discussed earlier was measured.

The principle of measuring these forces is that when the machine tool is switched on and the cutter makes contact with the workpiece it will apply some pressure on the workpiece. This pressure is transmitted through the dynamometer X, Y and Z axis to the charge amplifier and the charge amplifier converts the pressure to an electrical voltages and these are passed to the data card which are then stored by the computer. The X force is tangential, the Y force is in the feed direction and the Z force is radial.

A number of cutting tests were carried out using the 50 mm diameter cutter as shown in table 6.1 whilst table 6.2 shows the cutting speed tests performed using the 25 mm diameter cutter.

Test no	Spindle speed (1/min)	Cutting speed (m/min)	Feedrate (m/min)	Feed (mm)	Depth (mm)	Cutter dia. (mm)	No of tip (1)
1	18000	2827	10.8	0.3	4	50	2
2	20000	3142	12	0.3	4	50	2
3	22000	3455	13.2	0.3	4	50	2
4	24000	3770	14.4	0.3	4	50	2
5	26000	4084	15.6	0.3	4	50	2
6	28000	4398	16.8	0.3	4	50	2
7	30000	4712	18	0.3	4	50	2

Table 6.1: Details of cutting speed test using 50 mm dia. cutter

Test no	Spindle speed (1/min)	Cutting speed (m/min)	Feedrate (m/min)	Feed (mm)	Depth (mm)	Cutter dia. (mm)	No of tip (1)
1	18000	1414	10.8	0.3	4	25	2
2	20000	1570	12	0.3	4	25	2
3	22000	1728	13.2	0.3	4	25	2
4	24000	1885	14.4	0.3	4	25	2
5	26000	2042	15.6	0.3	4	25	2
6	28000	2199	16.8	0.3	4	25	2
7	30000	2356	18	0.3	4	25	2

Table 6.2: Details of cutting speed test using 25 mm dia. cutter

To demonstrate the capability of this machine tool a cutting demonstration was carried out which was filmed with the following cutting parameters:

Spindle speed	- 26000 rpm
Cutting speed	- 4084 m/min
Feed rate	- 15 m/min
Feed	- 0.3 mm
Depth of cut	- 4 mm
Width of cut	- 40 mm
Cutter dia	- 50 mm
No of tips	- 2

Workpiece size = 700 by 300 mm and a square box size 200 by 100 mm with 4 mm height was machined.

6.8 EXPERIMENTAL RESULTS ANALYSIS

Analysis of the measured force, power and temperature signals was achieved by the aid of a program specifically written in Minitab software. Once the analysis was completed it was imported to a Harvard Graphic software package to plot the results. The procedure for the analysis was as follows:

The first step was to load the file to be analysed. Once the file was loaded, the Minitab program displayed the number of columns which corresponded to the number of channels plugged into the dynamometer and also the number of data rows in each column were displayed.

Once the information was displayed, three important calculations were needed. The first calculation was to use the sampling time to break down the data capture per channel. This is illustrated by the following example. Supposing a file with the following data is loaded:

Spindle speed = 30000 rpm;
 Sampling rate = 10000 samples per second;
 Number of channels = 2
 Number of data rows = 290
 Cutting frequency = 30000/60 = 500Hz
 Total samples per revolution = 10000/500 = 20 data
 In 360 deg it samples at 360/20 = 18 deg for both channels. However for each channel, it samples at 360/10 = 36 deg.
 Total data per channel = 20/2 = 10 data points.

It is now possible to divide the data in each column by 10 to find the profile of the signal. This is achieved by dividing 290 by 10 = 29 which means that this particular file has 29 complete revolutions with 10 data points each.

Once each revolution data have been found, this can be converted to forces by using the equation:

$$Force1 = \frac{Volt1}{0.0073} \quad 9.8 \quad (6.1)$$

where force1 = the instantaneous force in Y direction, Volt1 = voltage signal from the dynamometer, 0.0073 is the constant value obtained during the dynamometer calibration and 9.8 is the conversion factor to newton. The same method was used to find the instantaneous force in the X direction.

Once the forces were known the next task was to find the rotational angle. This is achieved by using the expression:

$$RK = \frac{Force1 \cdot 360}{C} \quad (6.2)$$

where Force1 = the values obtained in equation 6.1 and the preferred equation for C =

and not

where n = spindle speed and z = number of cutting tips and C is the tooth

$$C = \frac{1}{n/60} \quad (6.3)$$

$$C = \frac{1}{n \cdot z/60} \quad (6.4)$$

frequency.

Since the cutter used has two tips where one is bigger than the other, analysis has shown that if equation 6.4 is used it will show one signal profile in one complete revolution and it is possible that the small tip profile will be displayed which will result in a wrong impression of the peak maximum cutting forces. However, if equation 6.3 is used, analysis has shown that both tips signal profiles may be displayed in which it would be easier to choose the bigger tip signal profile for analysis purposes.

Finally since it was known that the signals F_y and F_x were not captured instantaneously by the data acquisition card, the angle α needs to be the same to find the principal cutting force. Therefore an analysis program was written in Minitab software package to make the correction possible. Once the common angle α was found the following expression was used to find the principal cutting force or the tangential force:

$$F_t = F_y \sin \alpha + F_x \cos \alpha \quad (6.5)$$

where F_y = measured feed and F_x = measured tangential force

6.8.1 CUTTING POWER, METAL AND SPECIFIC METAL REMOVAL RATES ANALYSIS

Once the tangential force was known, it was possible to calculate the cutting power, metal removal rate and specific removal rates using the equations presented in chapter 3. However, a different approach from those discussed in chapter 3 is required to find the cutting power. Kaldos et al [36]

have shown that for a full width of cut in milling the average tangential force to be used should be one third of the maximum peak tangential force. Therefore, for half the width of cut, the value of the main force to be used is 1/6 by F_t . The cutting power is given by:

$$P_c = \left(\frac{F_{tmax}}{6} \right) V_c \dots\dots\dots (6.6)$$

From the results of the experimental analysis, graphs were plotted of the cutting forces, power, metal and specific metal removal rates which are presented and discussed in chapter 7.

CHAPTER 7

DISCUSSION AND COMPARISON OF EXPERIMENTAL RESULTS

7.1 INTRODUCTION

Although the errors in the prediction results presented in chapter 5 on average was between 6 to 10 percent of the results from the literature, however, some of the input cutting data such as shear angle, width of cut and feed which are crucial to the prediction software program were not given in some of the published results. Therefore, a number of assumptions were made for the values of the missing input data before the prediction software package could be executed and this might explain the discrepancy between the predictions and the published results. This chapter presents an opportunity to compare the prediction software program results with the experimental work conducted in this study with the main emphasis on the influence in change in cutting speed on the process parameters.

Cutting forces play an important role in the economics of the milling process. The forces control the energy consumed as well as the power requirements of the process. The cutting forces consist of the thrust force F_y and feed force F_x measured parallel and perpendicular to the direction of relative work-tool motion. The third force is the radial force F_z which is the force in the z direction, this particular force is not important since it does not play any significant role in the overall process analysis.

For a given material, the cutting forces depend on the tool geometry, volume of material removed, depth of cut, rake angle, cutting speed and the type of chip produced. In order to select an appropriate variable against which to compare the cutting forces, an understanding of the mechanisms involved in the milling process is necessary. Various cutting force models have been developed [2, 8, 10, 13, 15, 20, 38]. One of the best known

models is that proposed by Arndt [8] the illustration of which was shown in chapter 3 figure 3.9. The basis of Arndt's theory was the suggestion that the momentum force and its components should be added vectorially to the forces arising from the cutting mechanism to arrive at the resultant forces acting on the cutting tool. There are conflicting views on the influence of the increase in cutting speed on cutting forces in the past. For example, Matthew et al [15] suggested a reduction in cutting forces as the cutting speed increases, whilst others, Arndt [8] and Fenton et al [30], observed an increase in cutting forces with increased cutting speed. Therefore, it seems appropriate to examine the variation of the experimentally determined tool forces with the variation in the cutting speed.

The analytical strategy was based upon the following assumptions:

(i) It is relatively unimportant to know the rotational position angle of tangential or the main principal cutting force F_t during cutting since this depends on the values of F_y and F_x and their corresponding angles. In practice the author found that in milling both F_y and F_x varies in the positive and negative directions which implied that the tangential force would rotate in both positive and negative directions.

(ii) It is important to know the peak or average magnitude of both F_y and F_x since these value will determine F_t which is used to calculate the cutting power and metal removal rates.

Since two different sizes of cutters namely, 50 mm and 25 mm diameter were used the results for the 50 mm diameter cutter would be discussed first and followed by the results for the 25 mm cutter.

7.2 RESULTS OF THE MEASURED FORCES IN RELATION TO THE ROTATIONAL ANGLE USING 50 MM DIAMETER CUTTER

Representative cutting force behaviour pattern encountered in milling operation using the 50mm diameter cutter are shown in tables 7.1 to 7.6,

whilst its graphical representation are shown in figures 7.1 to 7.6. Each figure illustrates the nature of the "raw data" acquired for analysis in milling aluminium alloys type L168:1978 at a constant cutting speed given in the figures as a function of rotational angle.

TABLE 7.1: ACQUIRED CUTTING FORCES DATA AT 2827 M/MIN

Rotationa angle (deg)	Force Y (N)	Force X (N)
0	-61	-150
22	-220	212
44	-302	691
66	150	873
87	536	619
109	720	270
130	150	-121
152	79	-244
174	-170	-93
196	-290	42
218	-256	152
240	-10	355
261	238	437
283	396	305
305	475	86
327	-38	-104

(i) INPUT DATA

The selected input data used to produce tables 7.1 to 7.6 at different cutting speeds are from the experimental work undertaken in the present study and they are as follows:

Workpiece material = AL L168:1978, tool material = tungsten carbide,
cutting speed = 2827 to 4712 m/min, depth of cut = 4 mm,
width of cut = 25 mm, feed = 0.3 mm,
cutter diameter = 50 mm, rake angle = 12 (deg),
Number of tips = 2

TABLE 7.2: ACQUIRED CUTTING FORCES DATA AT 3142 M/MIN

Rotational angle (deg)	Force Y (N)	Force X (N)
0	370	0
24	118	-84
48	-10	-150
72	-120	-28
96	-195	100
120	-216	428
144	102	850
168	491	830
192	661	359
216	88	-252

TABLE 7.3: ACQUIRED CUTTING FORCES DATA AT 3778 M/MIN

Rotational angle (deg)	Force Y (N)	Force X (N)
0	167	0
28.8	-124	-412
57.8	88.6	-420
86	161	-55
115	-307	634
144	16	727
172.8	425	137
201	38	-252
230	-143	-343
259	36	-124

TABLE 7.4: ACQUIRED CUTTING FORCES DATA AT 4084 M/MIN

Rotational angle (deg)	Force Y (N)	Force X (N)
0	229	0
31	-307	-183
62	-173	75
93	22	319
125	180	719
156	496	710
187	491	49
219	-202	-261
250	-190	-61
281	36	69

TABLE 7.5: ACQUIRED CUTTING FORCES DATA AT 4398 M/MIN

Rotational angle (deg)	Force Y (N)	Force X (N)
0	-472	-150
34	-579	-500
68	-157	980
102	825	1016
137	930	177
171	-422	-437
205	-377	-380
240	220	126
274	480	573
308	416	488

TABLE 7.6: ACQUIRED CUTTING FORCES DATA AT 4712 M/MIN

Rotational angle (deg)	Force Y (N)	Force X (N)
0	279	-230
36	484	349
72	154	630
108	-361	217
144	-229	-281
180	163	32
216	586	645
252	806	622
288	-363	198
324	-557	-402

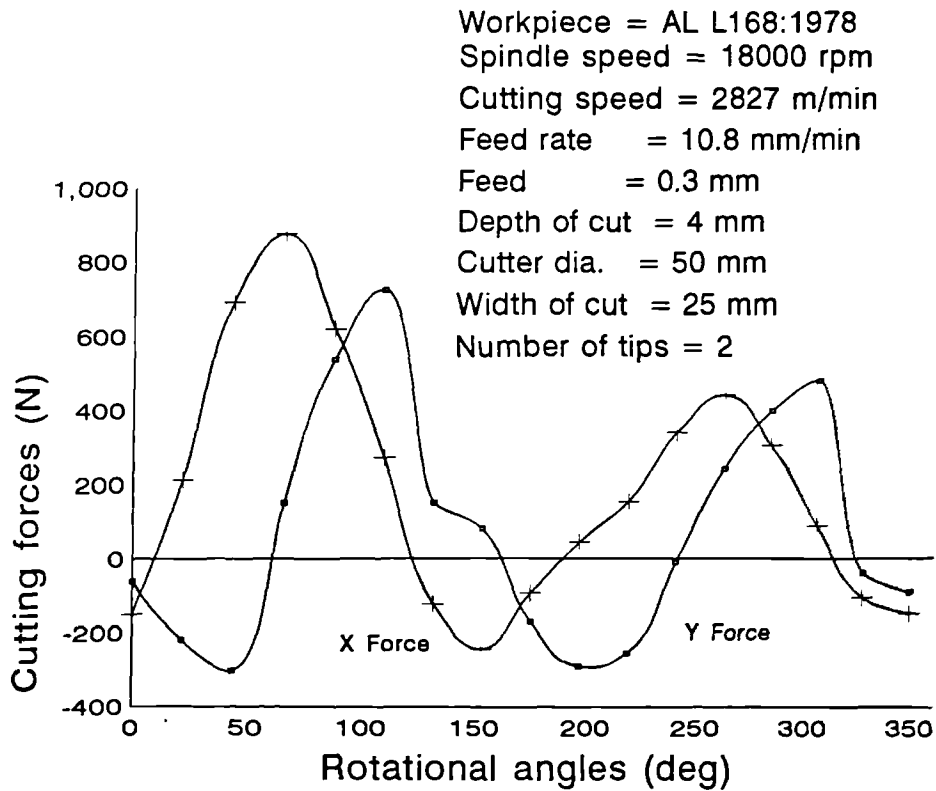


Fig. 7.1: Forces against rotational angle at 2827 m/min

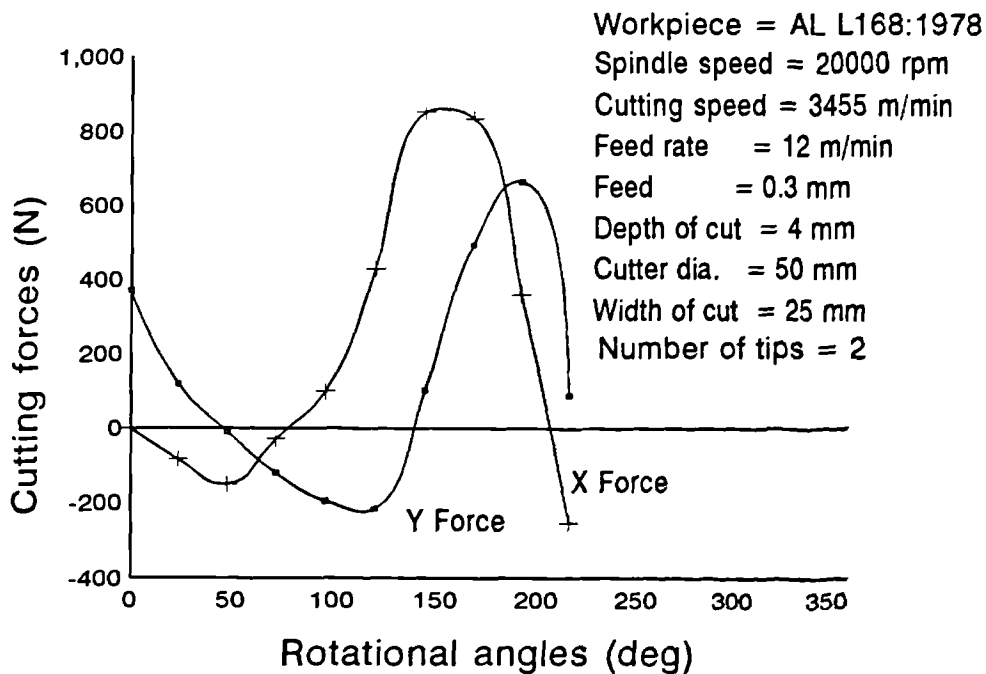


Fig. 7.2: Forces against rotational angle at 3142 m/min

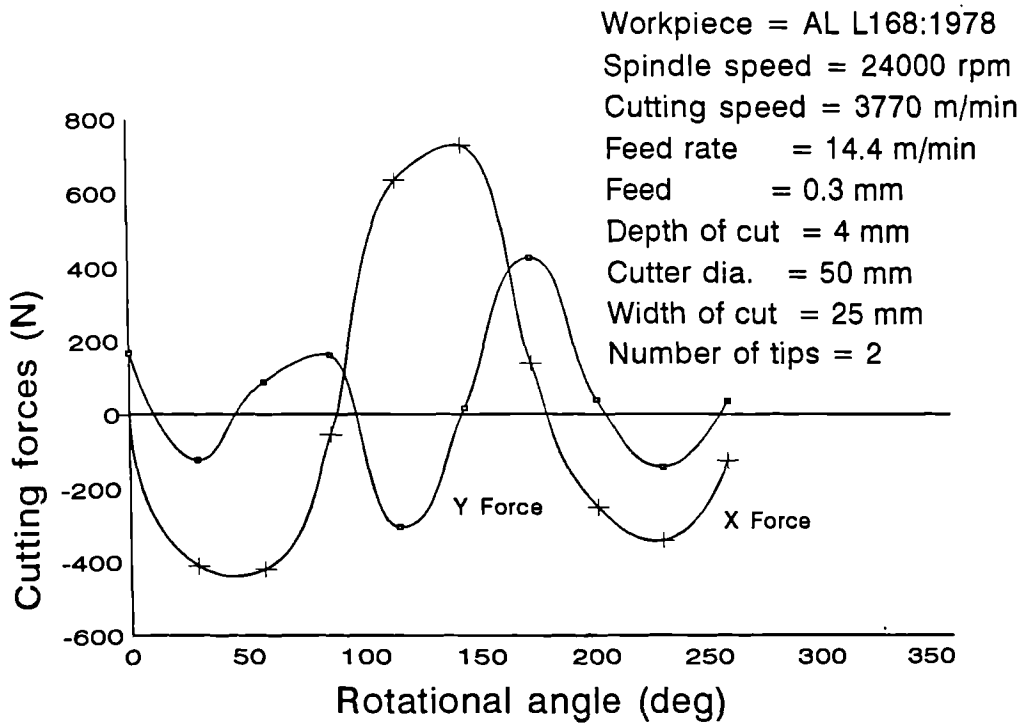


Fig. 7.3: Forces against rotational angle at 3770 m/min

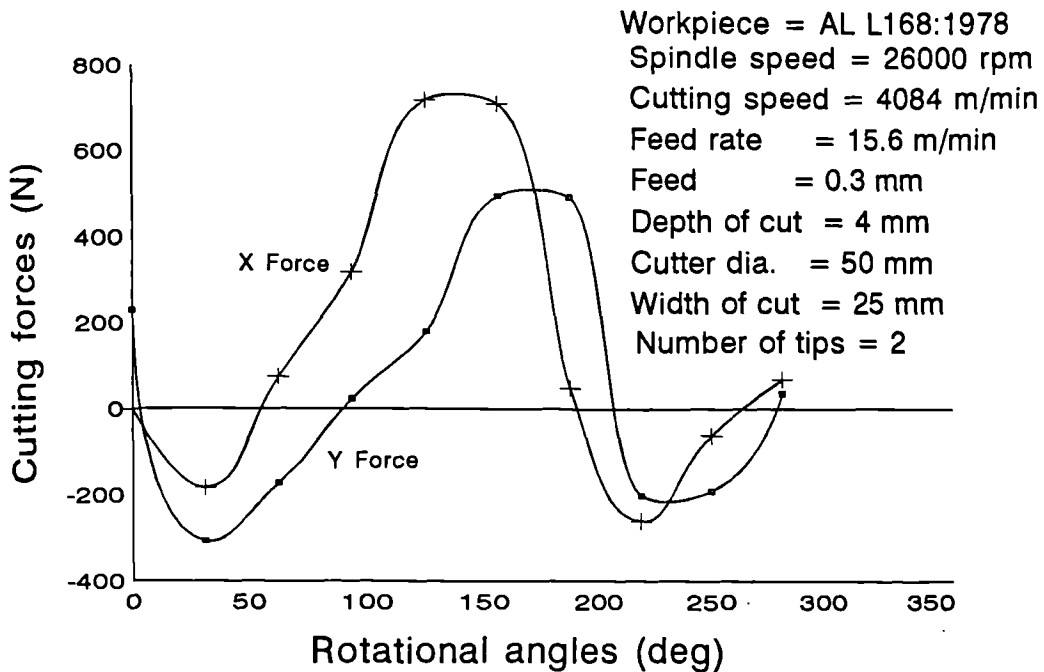


Fig. 7.4: Forces against rotational angle at 4084 m/min

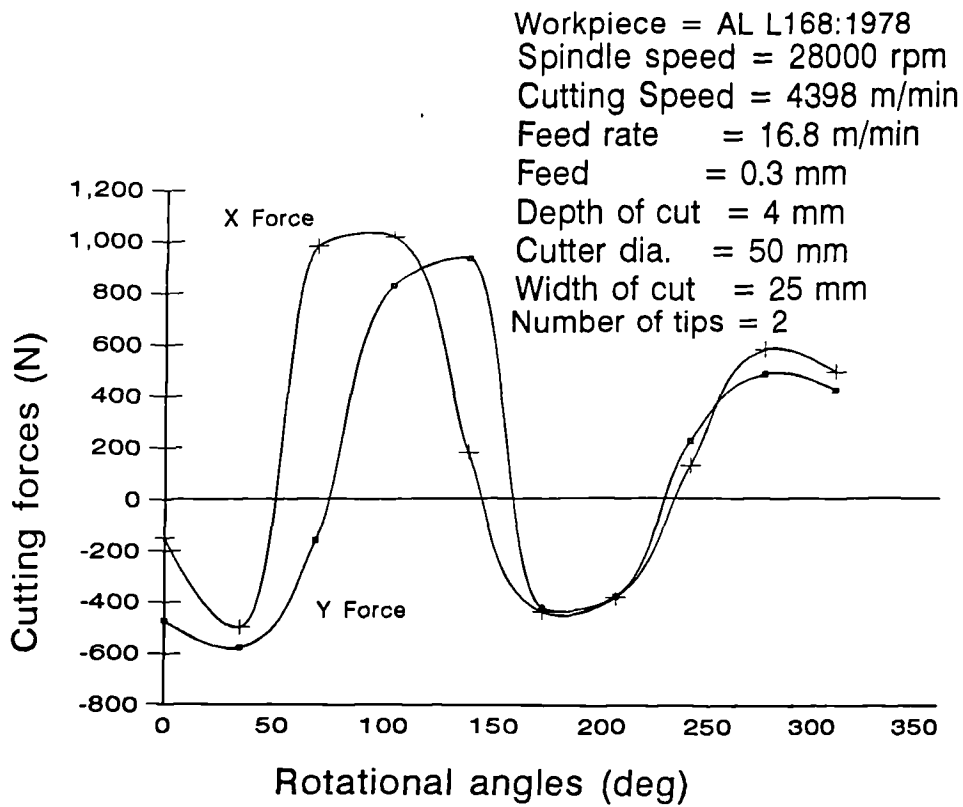


Fig. 7.5: Forces against rotational angle at 4398 m/min

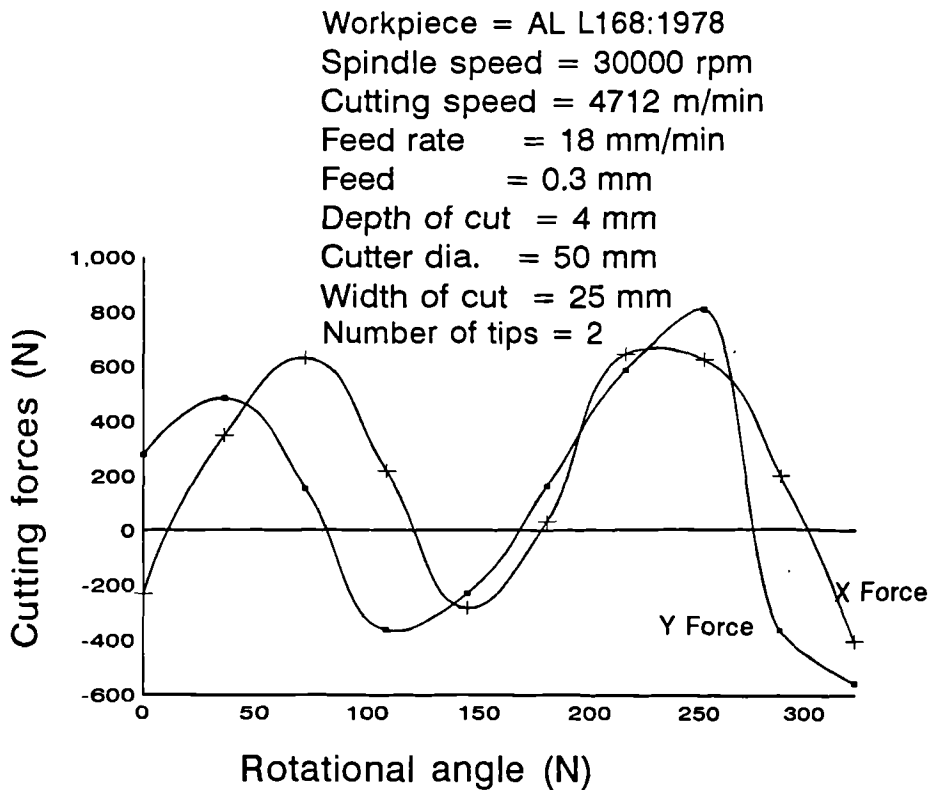


Fig. 7.6: Forces against rotational angle at 4712 m/min

As it can be seen from these figures, for each particular cutting speed it is possible to find the measured force X and Y which can be used to calculate the main cutting force at any particular cutter rotational position within one complete revolution. The figures show that from the cutting speed 2827 m/min to 4712 m/min the pattern of both forces followed the same trend and from the results, the magnitude of the measured forces was bigger in the positive direction when the cutter was cutting and smaller in the negative direction when it was not cutting.

The reasons for the observed forces in the negative direction can be attributed to:

- (i) The cutter was rubbing on the workpiece when it was supposed to disengage, however, whilst this was possible, the magnitudes of the forces obtained in the negative direction suggested that other factors might be responsible in addition to the rubbing effect;
- (ii) A further possible reason could be a noise effect of the measuring system i.e the dynamometer, the charge amplifier and data acquisition card;
- (iii) another possible reason could be the tool and workpiece geometry arrangement.

7.3 EXPERIMENT AND PREDICTED PRINCIPAL CUTTING FORCE AGAINST CUTTING SPEED USING 50 MM DIAMETER CUTTER

(i) AIM OF EXPERIMENT

To find correlation between the measured and the predicted main cutting forces. The need for a more thorough analysis of cutting forces and perhaps of their relations to momentum force is clearly needed before definite conclusions on their behaviour at high speeds are possible. Therefore, the aim is to find the influence of the increase in cutting speed on the cutting forces.

(ii) INPUT DATA

The selected input data are from the experimental work undertaken in the present study and they are as follows:

Workpiece material = AL L168:1978, tool material = tungsten carbide,
cutting speed = 2827 - 4712 m/min, depth of cut = 4 mm,
width of cut = 25 mm, feed = 0.3 mm, cutter diameter = 50 mm
rake angle = 12 (deg), number of tips = 2

(iii) DISCUSSION ON EXPERIMENT AND PREDICTED RESULTS

7.3.1 The Cutting Forces

Based on the supplied inputs, the experiment and the predicted principal cutting force results data are as shown in table 7.7.

TABLE 7.7: PREDICTED AND MEASURED FORCE RESULTS

Cutting speed (m/min)	Predicted principal force (N)	Measured principal force (N)	Error (%)
2827	648	711	-9.7
3142	695	741	-6.6
3456	820	855	-4.2
3778	980	905	10
4084	1146	1031.4	10
4398	1329	1196	10
4712	1524	1371.6	10

For the purpose of this study, after employing equation 6.5 to find the main cutting force F_c , the average peak force over 6 complete revolutions was chosen. Having found the average peak main cutting force for each cutting speed, figure 7.7 shows the relationship between the principal cutting force over a wide range of cutting speeds for both experimental and the predicted results. As can be seen, the cutting force increased with increase in cutting speed.

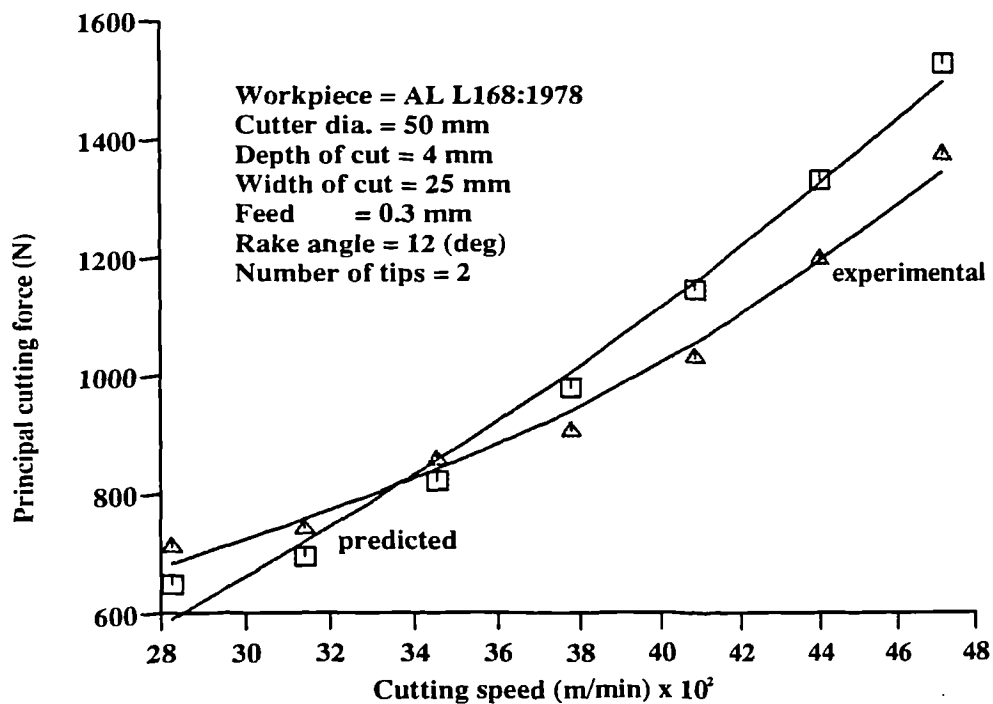


Fig. 7.7: The relationship between the cutting force and the cutting speed

In figure 7.7 and table 7.7 it can be seen that the experimental cutting force is bigger than the predicted cutting force between 2800 to 3300 m/min. This may be due to under estimation of the shear angle and the friction angle in the prediction analysis. However, the maximum percentage error between the experiment and the predicted results was 15 percent. Both results show an increase in cutting force with increased cutting speed. This finding is in agreement with earlier experimental findings of a number of workers [10, 30,

58, 62, 63]. This can be attributed to the effect of the momentum force as discussed in chapter 3 and 5.

7.3.2 The Cutting Power

Table 7.8 shows the prediction and experimental power results calculated using the measured cutting forces.

TABLE 7.8: PREDICTION AND EXPERIMENTAL CUTTING POWER RESULTS

Cutting speed (m/min)	Predicted cutting power (kW)	Experimental power (kW)	Error (%)
2827	5.08	5.58	-9.8
3142	6.06	6.47	-6.76
3456	7.87	8.2	-4.19
3778	10.28	9.49	7.7
4084	13.0	11.7	10
4398	16.23	14.6	10
4712	19.95	17.95	10

Based on the data in table 7.8, Figure 7.8 shows the relationship between the power and the cutting speed for both the experimental and the predicted results. The result of this experiment and the prediction results showed that the power increased as the cutting speed increased.

The reason for this is that power is the product of the principal cutting force F_t and the cutting speed. Both results correlate positively with the experimental result of Schulz plotted in figure 5.2b and earlier findings of King and McDonald [6].

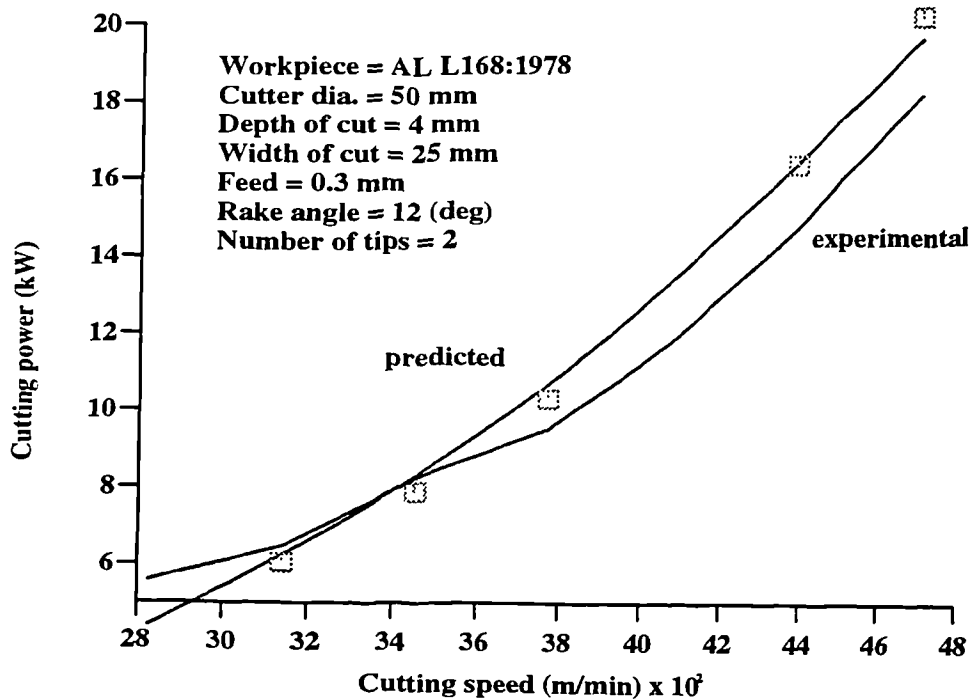


Fig. 7.8: The relationship between the power against the cutting speed.

7.3.3 The Metal Removal Rate

In order to determine the amount of swarf produced so that an adequate swarf removal technique can be design it is necessary know the actual amount of swarf generated. Table 7.9 shows the predicted and experimental metal removal rates, whilst the relationship between the metal removal rate and the cutting speed is illustrated in figure 7.9. It was observed in both experimental and the predicted results that the metal removal rate increased linearly with increase in speed. This can be ascribed to the fact that the metal removal rate is a function of the cutting speed. The predicted results correlate positively with the experimental results and earlier findings of Schulz [60].

TABLE 7.9: PREDICTION AND METAL REMOVAL RATE
EXPERIMENTAL RESULTS

Cutting speed (m/min)	Predicted metal removal rate (cm ³ /min)	Experimental metal removal rate (cm ³ /min)	Error (%)
2827	1080	1080	0
3142	1232	1200	2.6
3456	1308	1320	-0.9
3778	1415	1440	-1.74
4084	1536	1560	-1.4
4398	1690	1680	0.6
4712	1767	1800	-1.83

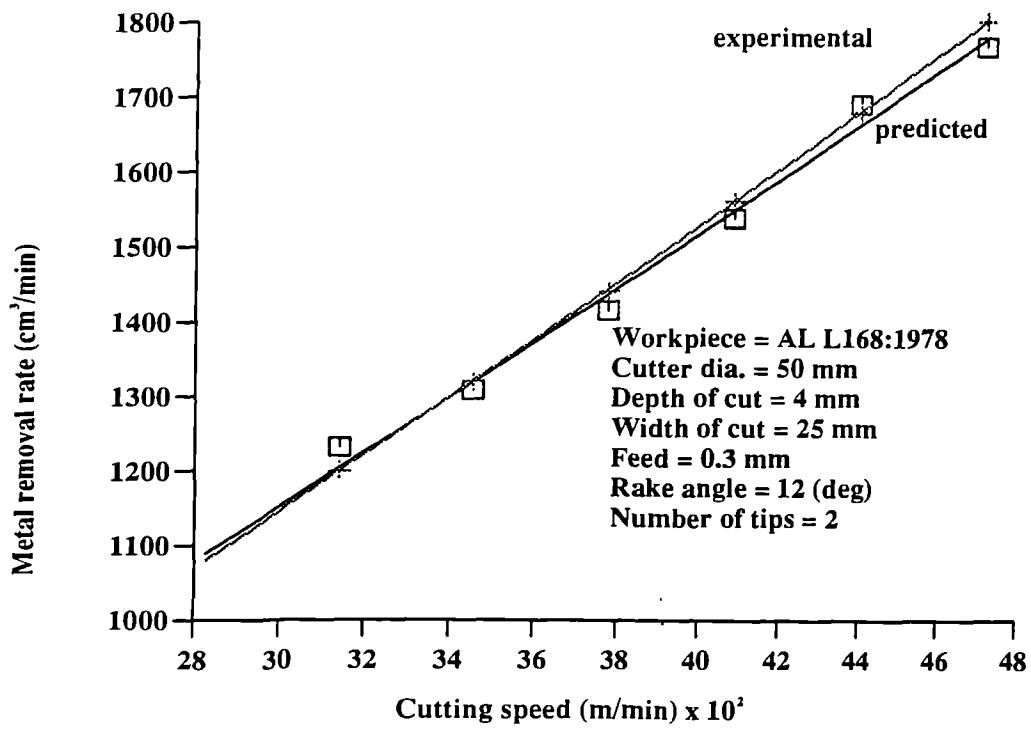


Fig. 7.9: The relationship between the metal removal rate and the cutting speed

7.3.4 The Specific Metal Removal Rate

Table 7.10 illustrates the predicted and the experimentally determined specific metal removal rate based on the measured cutting forces.

TABLE 7.10: PREDICTION AND SPECIFIC REMOVAL RATE
EXPERIMENTAL RESULTS

Cutting speed (m/min)	Predicted specific metal removal rate (cm ³ /min/kW)	Experimental specific metal removal rate (cm ³ /min/kW)	Error (%)
2827	213	193.5	8.4
3142	203	186	8.3
3456	166	161	3
3778	138	152	-10
4084	118	133	-12.7
4398	104	115	-10.8
4712	88	100	-13.6

Figure 7.10 illustrates the relationship between the specific metal removal rate and the cutting speed. It is found that as the cutting speed is increased the specific removal rate decreases. It means that the removal of unit volume of undeformed material per unit time requires increasing power. Alternatively, with the increase in cutting speed, unit energy removes smaller amount of material. However, the change is not linear, because the power required to remove the undeformed chips increases in a non-linear way. This can be explained by the effect of the momentum force which dominantly operates at high cutting speeds requiring an additional energy input. The predicted results compared well with the experimental result as shown in

figure 7.10. The error found is due to the process equations in the cutting model and in the light of this, the present process model and the database require a slight modification to meet accuracy requirements.

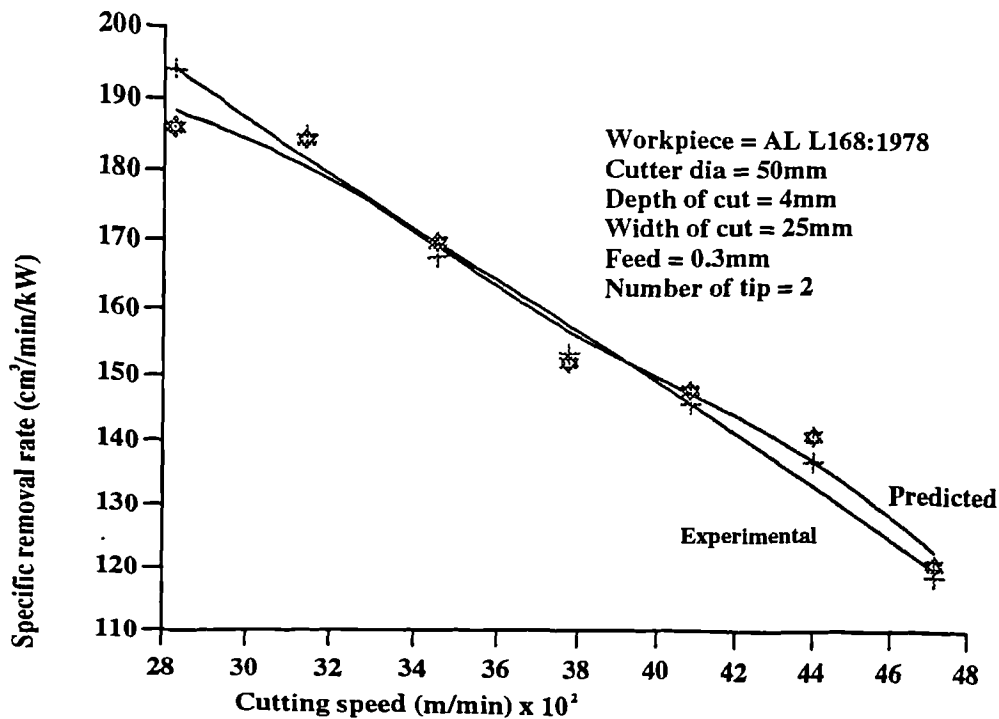


Fig. 7.10: Specific metal removal rate against the cutting speed

7.4 RESULTS OF THE MEASURED FORCES IN RELATION TO THE ROTATIONAL ANGLE USING 25 MM CUTTER

Cutting force behaviour pattern acquired during the milling operation using the 25 mm diameter cutter are shown in tables 7.11 to 7.15, whilst its graphical representation are illustrated in figures 7.11 to 7.15. Similar to 50 mm diameter cutter, each figure illustrates the nature of the "raw data" acquired for analysis in milling aluminium alloys type L168:1978 at a constant cutting speed given in the figures as a function of rotational angle.

INPUT DATA

The selected input data used to produce tables 7.11 to 7.15 at different

cutting speeds are as follows:

Workpiece material = AL L168:1978

Tool material = Tungsten carbide, cutting speed = 1570 to 2356 m/min,

depth of cut = 4 mm, width of cut = 12.5 mm, feed = 0.3 mm,

cutter diameter = 25 mm, rake angle = 12 (deg), Number of tips = 2

TABLE 7.11: ACQUIRED CUTTING FORCES DATA AT 1570 M/MIN

Rotational angle (deg)	Force Y (N)	Force X (N)
0	-275	-256
24	-26	-129
48	129	93
72	289	701
96	373	1050
120	514	748
144	609	76
168	-32	-337
192	-240	-178
216	-88	189
240	265	386
264	290	451
288	150	351
312	50	106
336	-166	-85

TABLE 7.12: ACQUIRED CUTTING FORCES DATA AT 1855 M/MIN

Rotational angle (deg)	Force Y (N)	Force X (N)
0	-148	-160
28	-269	184
58	-214	694
87	183	917
115	884	400
144	535	-107
172	42	-59
201	-141	27
230	-332	169
260	-460	484
289	91	568
316	888	183
345	409	-78

TABLE 7.13: ACQUIRED CUTTING FORCES DATA AT 2042 M/MIN

Rotational angle (deg)	Force Y (N)	Force X (N)
0	-96	405
31	-151	582
63	272	799
94	626	411
125	134	-102
156	-66	-117
188	-20	133
219	250	360
250	390	548
282	249	345
314	38	-45
344	-26	5

TABLE 7.14: ACQUIRED CUTTING FORCES DATA AT 2199 M/MIN

Rotational angle (deg)	Force Y (N)	Force X (N)
0	-237	-220
34	-367	-103
69	-45	729
103	571	1157
137	875	557
171	-171	-248
206	-255	-397
240	131	155
274	650	797
309	550	791
343	211	130

TABLE 7.15: ACQUIRED CUTTING FORCES DATA AT 2356 M/MIN

Rotational angle (deg)	Force Y (N)	Force X (N)
0	-150	-451
36	-257	-252
72	102	117
108	636	654
144	299	648
180	-321	99
216	10	-486
252	250	-229
288	199	565
324	-150	722

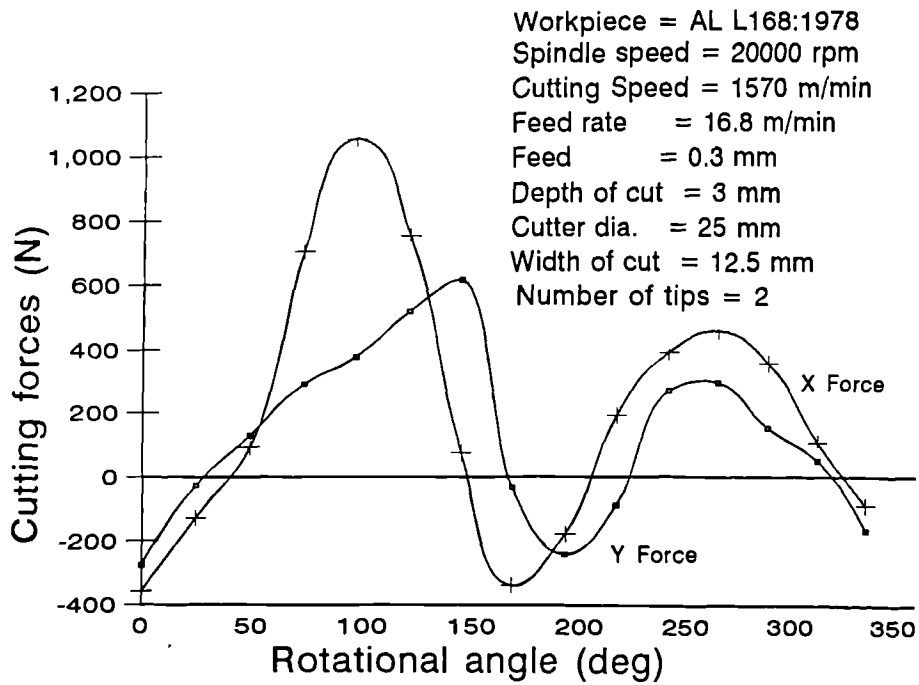


Fig. 7.11: Forces against rotational angle at 1570 m/min

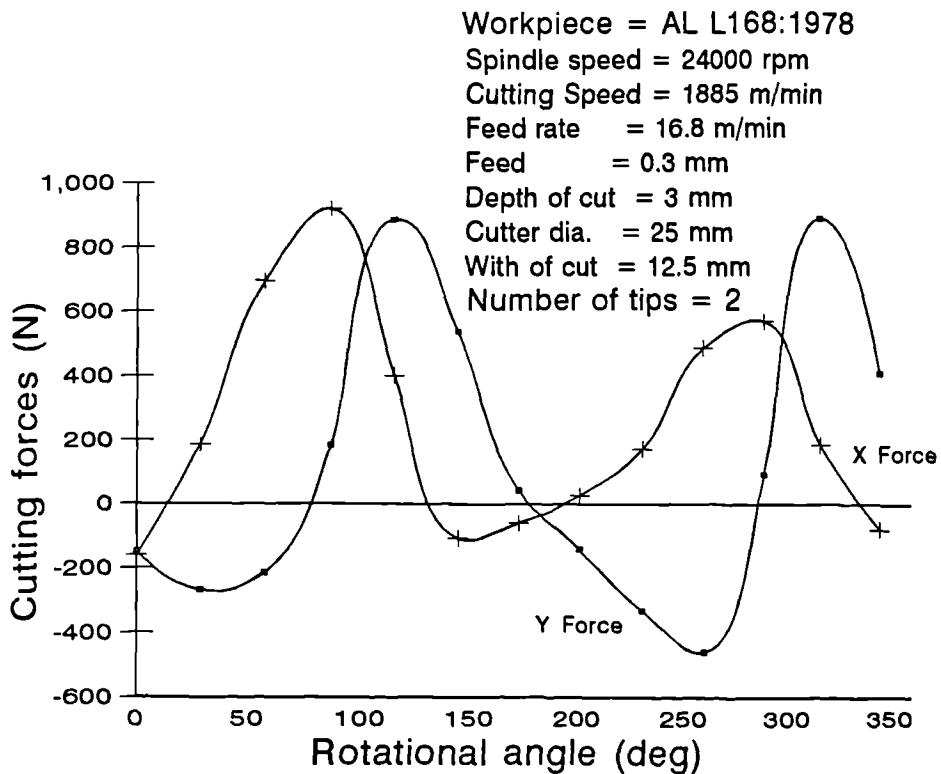


Fig. 7.12: Forces against rotational angle at 1885 m/min

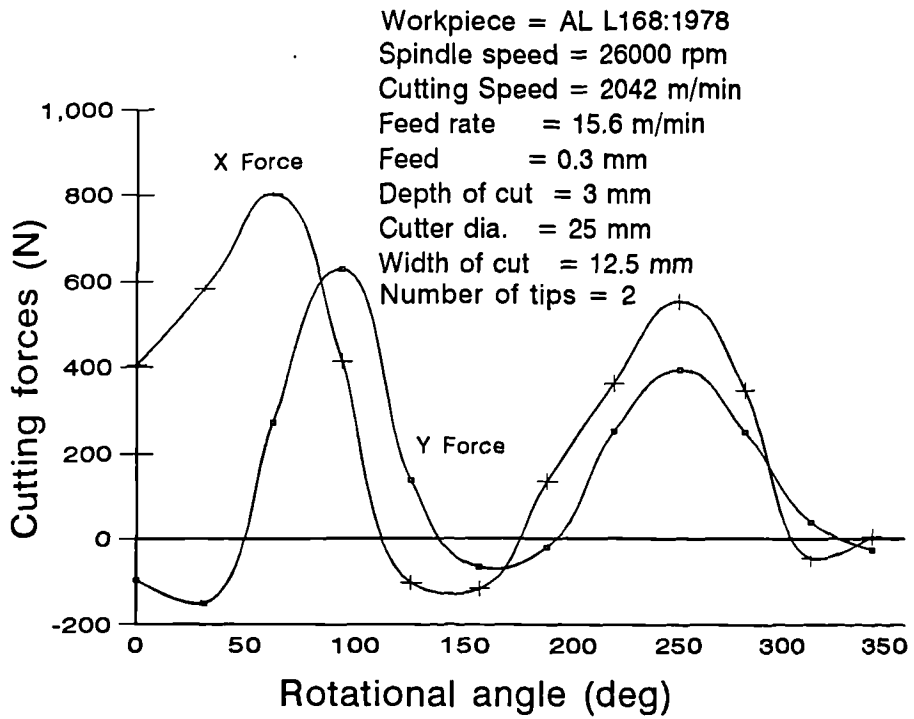


Fig. 7.13: Forces against rotational angle at 2042 m/min

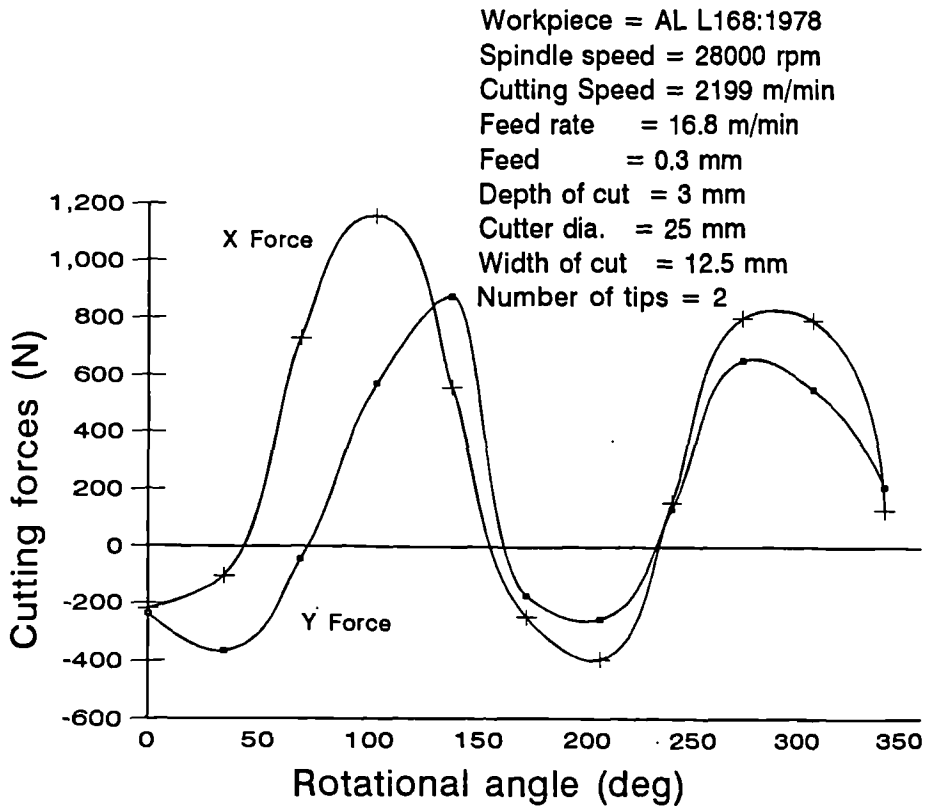


Fig. 7.14: Forces against rotational angle at 2199 m/min

Workpiece = AL L168:1978
 Spindle speed = 30000 rpm
 Cutting speed = 2356 m/min
 Feed rate = 18 m/min
 Feed = 0.3 mm
 Depth of cut = 4 mm
 Cutter dia. = 25 mm
 Width of cut = 12.5 mm
 Number of tips = 2

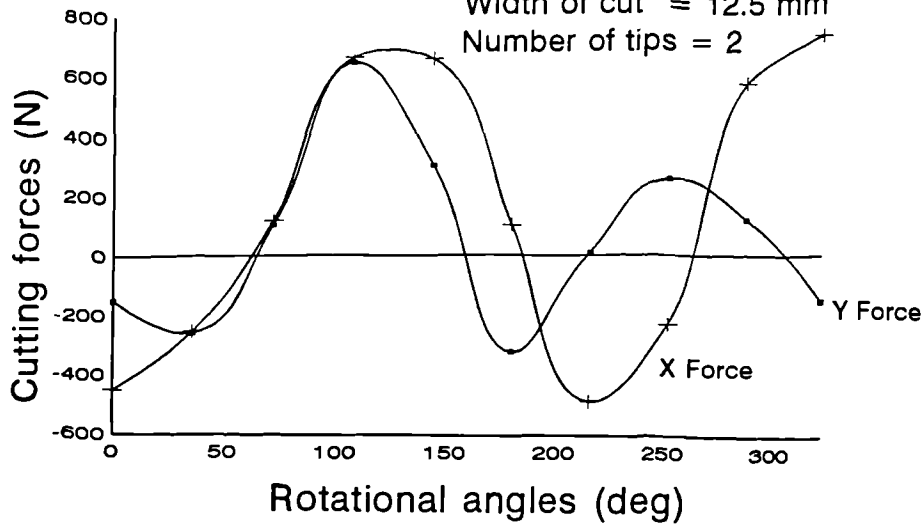


Fig. 7.15: Forces against rotational angle at 2356 m/min

As it can be seen from figures 7.11 - 7.15, for each particular cutting speed, it is possible to find the measured force X and Y which can be used to calculate the principal cutting force at any particular cutter rotational position within one complete revolution.

7.5 DISCUSSION ON THE 25 MM DIAMETER CUTTER'S EXPERIMENT AND THE PREDICTED RESULTS

7.5.1 The Cutting Forces

Based on the supplied inputs, the experiment and the predicted principal cutting force results data are as shown in table 7.16.

TABLE 7.16: PREDICTED AND MEASURED FORCE RESULTS

Cutting speed (m/min)	Predicted principal force (N)	Measured principal force (N)	Error (%)
1570	705	811	- 13
1728	735	845	- 13
1885	774	880	- 12
2042	791	920	- 14
2199	850	985	- 14
2351	920	1042	- 12

Similar to the method used for the 50 mm diameter cutter results, equation 6.5 was employed to find the principal cutting force F_c . Having found the average peak principal cutting force for each cutting speed, figure 7.16

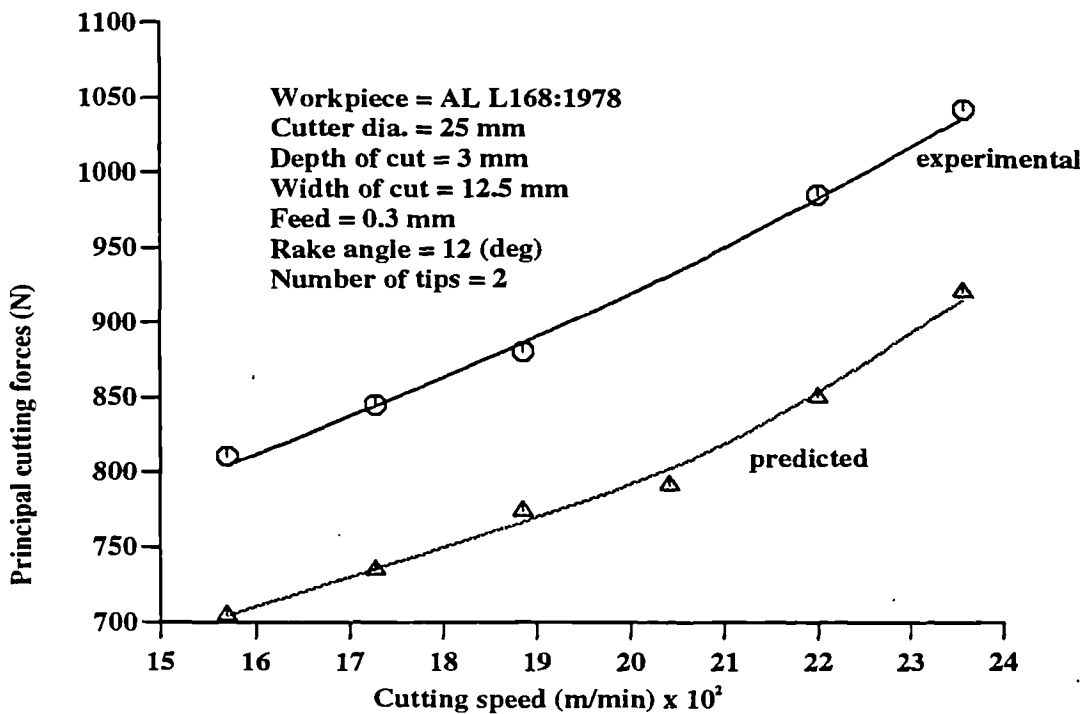


Fig. 7.16: The relationship between the cutting force and the cutting speed

shows the relationship between the principal cutting force over a wide range of cutting speeds for both experimental and the predicted results. As can be seen, the cutting force increased with increase in cutting speed.

In figure 7.16 and table 7.16 it can be seen that the experimental cutting force is bigger than the predicted cutting force. This is due to the under estimation of the shear angle and the friction angle in the prediction analysis. However, the maximum percentage error between the experiment and the predicted results is 15 percent. Both results show an increase in cutting force with increased cutting speed.

7.5.2 The Cutting Power

Table 7.17 shows the prediction and experimental power results calculated using the measured cutting forces.

TABLE 7.17: PREDICTION AND EXPERIMENTAL CUTTING POWER RESULTS

Cutting speed (m/min)	Predicted cutting power (kW)	Experimental cutting power (kW)	Error (%)
1570	3.1	3.5	13
1728	3.5	4.1	13
1885	4.05	4.6	12
2042	4.5	5.2	14
2199	5.2	6	14
2356	6.0	6.8	12

Based on the data in table 7.17, Figure 7.17 shows the relationship between the power and the cutting speed for both the experimental and the predicted results. The result of this experiment and the prediction results showed that the power increased as the cutting speed increased.

The reason for this is that power is the product of the principal cutting force F_c and the cutting speed. Both results were similar to the 50 mm diameter cutter and correlate positively with the experimental result of Schulz [60] plotted in figure 5.2b and earlier findings of King and McDonald [6].

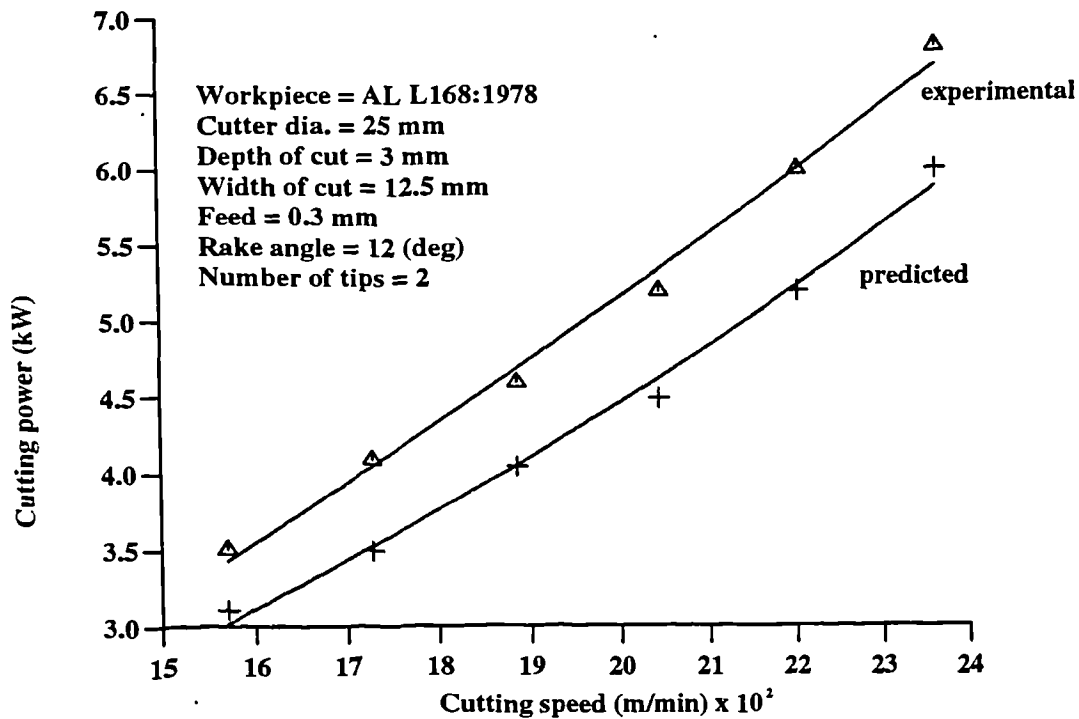


Fig. 7.17: The relationship between the power against the cutting speed

7.5.3 The Specific Metal Removal Rate

Table 7.18 illustrates the predicted and the experimentally determined specific metal removal rates based on the measured cutting forces.

TABLE 7.18: PREDICTION AND METAL REMOVAL RATE
EXPERIMENTAL RESULTS

Cutting speed (m/min)	Predicted specific metal removal rate (cm ³ /min/kW)	Experimental specific metal removal rate (cm ³ /min/kW)	Error (%)
1570	145	129	-12.4
1728	141	121	-16.5
1885	133	117	-13.6
2042	130	112	- 16
2199	121	105	- 15
2356	112	99	- 13

Figure 7.18 illustrates the relationship between the specific metal removal rate and the cutting speed. Similar to the result of the 50 mm diameter cutter, it is found that as the cutting speed is increased the specific removal rate decreases. It means that the removal of unit volume of undeformed material per unit time requires increasing power. However, the increase is not linear, because the power required to remove the undeformed chips increases in a non-linear way. This can be explained by the effect of the momentum force which dominantly operates at high cutting speeds requiring

an additional energy input. The predicted results compared well with the experimental result as shown in figure 7.18.

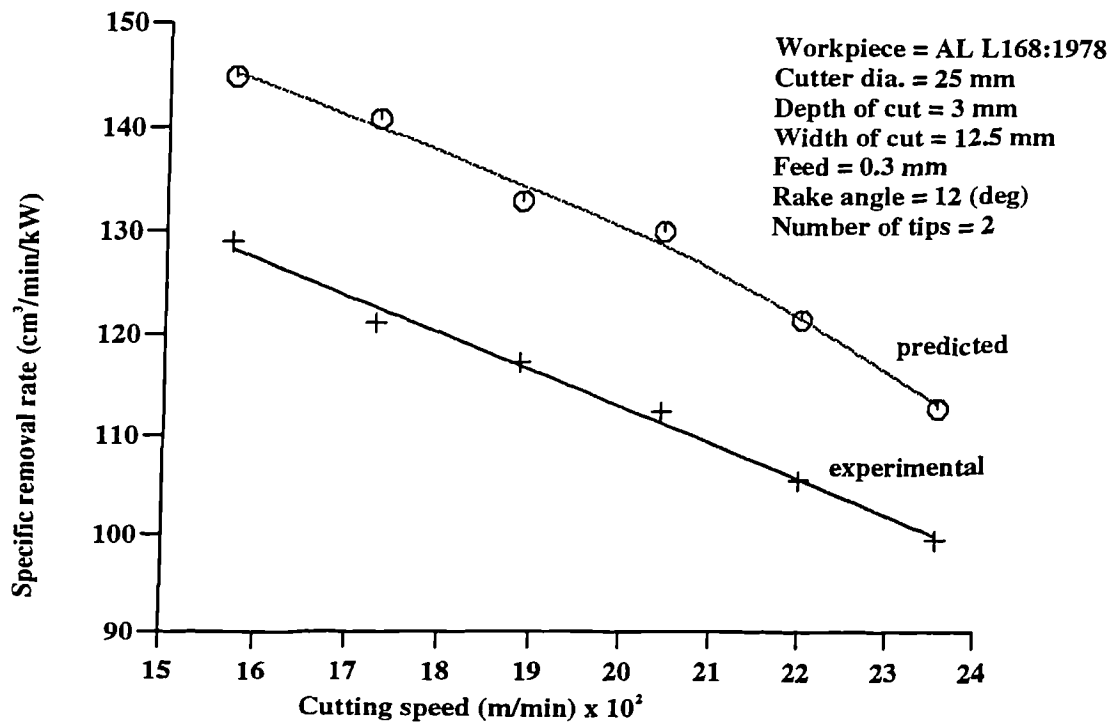


Fig. 7.18: Specific metal removal rate against the cutting speed

7.6 GENERAL DISCUSSION ON THE RESULTS

There has been much controversy surrounding the effect of increase in cutting speed on the cutting forces. Albrecht [80] in his study observed a reduction in cutting forces with an increase in cutting speed. Albrecht attributed the decrease in cutting forces with an increase in the cutting speed to the decrease of the ploughing force with an increase in the cutting speed. However, since a sharp tool was used in the present investigation, the effect of the ploughing force was negligible. A more likely reason for the variation was given by Boothroyd and Bailey [81], also by Kobayashi and Thomsen [82]. Based on their research on the orthogonal machining of 85/15 brass, it was determined that the cutting ratio increased with an increase in cutting speed. This meant that the chip became thinner and the area of the shear plane smaller thus the cutting forces required to produce

the chip must decrease.

However, in this study it was established beyond reasonable doubt that the cutting forces increase as the cutting speed increases. The forces trend data obtained strongly suggests that the forces do increase due to the effect of the momentum force as discussed in chapter 3. Similar trends have been observed by Schulz et al [5], Arndt [8], Arndt [9], Arndt and Brown [20] and most recently by Schulz [60].

The results of this study suggested that the power increases with cutting speed. The reason is that the principal cutting force increases with the cutting speed as shown in equation 6.6, figure 7.7 and figure 7.16.

Regarding the 25 mm diameter cutter, it was found that the X and Y components of the principal cutting force varied in a similar manner to that observed with 50 mm diameter cutter. However, no cutting test could be performed at 1413 m/min because the cutter broke due to the fact that the spindle speed of 18000 rpm was too slow.

Basically, the explanations given for the 50mm diameter cutter are considered to be valid for the 25 mm diameter cutter also. It was observed with the 50 mm diameter cutter that the cutting operation was more stable.

CHAPTER 8

8.0 CONCLUSIONS AND RECOMMENDATION FOR FUTURE WORK

From the literature survey and the detailed study of HSM undertaken in this work it is clear that there are benefits to be derived in using HSM. However, there are various factors which impose physical limitations on the application of HSM technology on the shop-floor such as cutting temperature and tool life, tool and workpiece materials, machine tool design, cutting geometry, chip removal techniques and management. Also the safety of personnel within the machining area is most important of all.

A mathematical model has been developed based on single point milling operation and the average chip thickness which satisfies the objectives of this study.

It must be stressed that, although the average percentage error between the predicted results, the published and the experimental results conducted in this study were within 15 percent mainly because of the uncertainties inherent in some empirical equations employed. Therefore, the results from the experimental work need to be used to modify the model and make it more representative of the real situation.

About 5000 process parameter predictions have been made in this study and by comparing the simulation results with published experimental graphs and data generated in the experimental work, the following conclusions can be drawn :

(i) According to the proposed algorithm, the values for process parameters can be predicted in terms of the material properties, tool parameters, workpiece geometry and cutting conditions.

(ii) There are many controversies over the influence of cutting speed on cutting forces. However, the prediction results of this study revealed that the cutting forces remain relatively constant up to 16.6 m/s (1000 m/min) before their values start to increase significantly. Also in the experimental work in milling aluminium type AL L168:1978 an increase in cutting forces was observed up to 78.6 m/s (4720 m/min). This increase in cutting forces can be attributed to the effect of the momentum force and also suggests that there is no scientific basis for the earlier claims that cutting forces reduce at high cutting speed.

(iii) Power and metal removal rates increase almost linearly with increase in cutting speed. There is no evidence that less power would be required at high cutting speed as a continuous increase in power is observed right up to 78 m/s (4712 m/min) which was the highest cutting speed used when milling aluminium alloy type L168:1978 in this study.

(iv) Regarding the specific removal rates, it is found that as the cutting speed is increased the specific removal rate decreases. It means that the removal of unit volume of undeformed material per unit time requires increasing power. Alternatively, with the increase in cutting speed, unit energy removes smaller amount of material. However, the change is not linear, because the power required to remove the undeformed chips increases in a non-linear way. This can be explained by the effect of the momentum force which dominantly operates at high cutting speeds requiring an additional energy input.

(v) Regarding the relationship between the cutting speed and the cutting temperature, it was found in the predicted results that the workpiece temperature (H_{cw}) and the average shear zone temperature (T_s) decrease with increase cutting speeds, whilst the chip and the tool rake face temperatures (T_{chip} and T_{max}) increase as the cutting speed increases. Therefore, these findings clarify the controversy amongst the earlier investigators regarding

the influence of cutting speed on cutting temperature. Those who suggested observing reduction in cutting temperature were referring to H_{cw} and T_s . Whilst those who claimed observing increased cutting temperature with cutting speeds were referring to T_m and T_{max} . The reduction in H_{cw} and T_s can be attributed to the fact that as cutting speeds increase there is less time available for plastic deformation and the mode of heat transfer changes from conduction to convection. This is in accord with suggestion of Arndt [9], Turkovich et al [26] and Kuznetsov [73]. The increase in chip and tool rake face temperature can be attributed to the frictional force which increases with the cutting speed.

(vi) From the prediction results it was noticed that an increase in the feed also increases the metal removal rate and the cutting power. This implies that either the feed or the cutting speed can be varied to achieve the same aim. However, it must be stressed that any increase in cutting speed will have greater effect than increase in feed.

(vii) Utilization of the numerical and the graphical results makes it possible to apply the model to complex machining analyses. The results also can help in the determination of a suitable chip removal system based on volume of metal removed per given time, and spindle and machine tool specification.

(viii) Comparisons between the limited simulation results and experimental results with the published experimental results from the literature showed that the model can predict the cutting process adequately. The errors found are due to the process equations in the cutting model and in the light of this, the present process model and the database require a slight modification to meet accuracy requirements.

(ix) The model and the experimental work described here allows the identification of material/process interactions that might otherwise be overlooked.

The major significant feature of this coherent detailed study is that the mechanics of cutting approach employed in this investigation has been shown to be a sound scientific and quantitative and qualitative basis for machining performance predictions in HSM. HSM will be feasible only if the tool cutting edge can sustain the applied normal load and the temperature in the shear zone.

Finally, the application of the prediction model described here is expected to contribute significantly to the fundamental understanding of HSM process over a wide range of cutting speeds, yielding a valuable insight into the complexity of cutting process and the influence of process variables on chip management, spindle specification, and machine tool control systems especially when machining expensive components like spars and stringers in the aerospace industry.

8.1 RECOMMENDATION FOR FUTURE WORK

Following on from the results of this project, recommended future work is as follows:

(i) Refinement of the present single point geometrical milling model to multi-teeth face milling model with the application of integration functions program to model the cutting forces.

(ii) Integration of the cutting simulation model to computer aided design (CAD) system, first by modelling the workpiece shapes using suitable software and then using the developed cutting model to predict the instantaneous, average and peak forces, power, energy and temperature.

(iii) A comprehensive study of the temperature measurement techniques in HSM.

REFERENCES

- [1] D.M. Chasteen : High Speed Machining - Implementation : A User's Point-of-View, Proc. of ASME high speed machining conf. PED 12, 1984, p460.
- [2] B.F. von Turkovich : Influence of Very High Cutting Speed on Chip Formation Mechanics, 7th NAMRC Proc. May 1979, SME. Tech. 1979, pp241-247.
- [3] D.G. Flom, R. Komanduri and M. Lee: High Speed Machining of Metals, Annual Review of Materials Science, Vol 4, 1984, p231.
- [4] R.I. King and R.L. Vaughn : A Synoptic Review of High Speed Machining from Salomon to the Present, Proc. of ASME High Speed Machining Conf., PED 12, 1984, p2.
- [5] H.Schulz and T.Moriwaki: High Speed Machining, Annals of CIRP Vol. 41/2, August, 1992, pp
- [6] R.I. King and J.G. McDonald : Production Design Implications of New High-Speed Milling Techniques, Journal of Engineering for Industry, ASME, Nov. 1976, p176.
- [7] T.R. Aggarwal : A New Approach to Selecting Machining Parameters and Machine Tools for High Speed Milling of Aluminium, SME paper MR85 - 471, SME 1985 Int. Conf. Detroit, Michigan, May 6 - 9, 1985, pp1 - 13
- [8] G. Arndt Ultra-high Speed Machining : A Review and an Analysis of Cutting Forces, Proc. of Institute of Mech. Engineers (London), 1973, Vol. 187, No 44/73, 625-634.
- [9] G. Arndt : The Development of Higher Machining Speeds - Part 2, The Production Engineer, Vol 49, Dec 1970, pp517 - 529
- [10] K. Okushima, K. Hotomi, S. Ito and N. Narutaki : A Fundamental Study of Super-High Speed Machining, Bull Japanese Society of Mechanical Engineers, Vol 8, No 32, 1965, p702
- [11] T. von Karman and P. Duwez: The Propagation of Plastic Deformation in Solids, Journal of Applied Physics, Vol. 21, 1950, pp987 - 994

- [12] H. Schulz : High Speed Milling of Aluminium Alloys, Proc. of ASME High Speed Machining Conf., 1984, PED 12, pp241-244.
- [13] R.F. Recht: A Dynamic Analysis of High Speed Machining, Proc. of ASME High Speed Machining Conf., 1984, PED p12, pp83-93.
- [14] M.C. Shaw: Temperature in Cutting, ASME, Production Engineering Division, 1988, Vol 30, pp133-143.
- [15] P. Matthew and P.L.B. Oxley: Predicting the Effects of Very High Cutting Speeds Forces etc. Annals of CIRP Vol 31/1, 1982, pp49-52
- [16] A.O. Schmidt : Ultra-High Speed Machining - Panacea or Pipedream, The Tool Engineer, Nov. 1958, pp105-109
- [17] H.J. Siekmann: Proc. of ASME (now SME), 1958, No 82.
- [18] Y. Tanaka and M. Kitano : Metal Cutting with Extremely High Speeds, Technology Reports of the Osaka University, Vol 16, No 670, 1965, pp305-314
- [19] K. Okushima, K. Hitomi and S. Ito : A study of Super-High Machining, Annals of CIRP XIII, 1966, pp339-410
- [20] G. Arndt and R.H. Brown : Design and Preliminary Results from Experimental Machine Tool Cutting Metals At Up To 8000 Feet Per Second, Proc. 13th Int. M.T.D.R. Conf., London Pergamon, 1972, pp217-223
- [21] J. Chaplin, J.A. Miller and R.I. King: Summary of Recent Lockheed Research, Re: High speed machining, SME, Dearborn, Mich, USA, 1981, pp311-317.
- [22] R. Komanduri, T.A Schroeder, J. Hazra, von Turkovich and D. Flom: On the Catastrophic Shear Instability in High Speed Machining of an AISI 4340 Steel, Trans. ASME, J. of Eng. for Ind. Vol 104, 1982.
- [23] I. Nieminen, J. Paro and V. Kauppinen: High Speed Milling of Advanced Materials: Proc. of the Int. Conf. on Advances in Materials & Processing Technologies, AMPT'93, Dublin, 1993, Vol 1, pp21-32.
- [24] M.E. Merchant : Journal of Applied Physics, Vol 16, 1945, pp267-318
- [25] D.R. Durham and B.F. von Turkovich: Material Deformation Characteristic at Moderate Strains and High Strain Rates from Metal

- Cutting Data, Proc. of the 10th NAMRC 1982, pp324-331.
- [26] B.F. von Turkovich and D.R. Durham: Machining of Titanium and Its Alloys, Proc. of the Symposium on Advanced Processing Methods for Titanium, TMS-AIME Meeting, Louisville, 1981, pp241-256.
- [27] C.A. Brown: A Practical Method for Estimating Machining Forces from Tool-chip Contact Length, Annals of CIRP, 32/2, 1983, pp91-96.
- [28] D. Lee and W.W. Wilkening: Material Modelling and High Speed Machining, General Electric Report No 82CRD261, 1982, pp1- 15.
- [29] R.F. Recht : Catastrophic Thermoplastic Shear, Trans ASME, Journal of Applied Mechanics, Vol. 31, 1964, pp189-193.
- [30] R.G. Fenton and P.L.B. Oxley : Predicting Cutting Forces at Super-high Cutting Speeds from Work Material Properties and Cutting Conditions, Proc. 8th, M.T.D.R. Conf., (Pergamon Press Oxford), 1976, pp247-258
- [31] Y. Tanaka, H. Tsuwa and M. Kitano : Cutting mechanism in Ultra-high Speed Machining, ASME, Proc. of Prod. Engineering Conf., Cleveland Ohio, May 2-4, 1967, pp1-12
- [32] R.T. Sedgwick, Numerical Modelling of High Speed Machining Processes, Proc. of ASME High Speed Machining Conf., PED 12, 1984, pp141-155.
- [33] G. Boothroyd and J.A. Bailey : Effects of Strain rate and Temperature in Orthogonal Metal Cutting, Journal of Mech. Eng. Sci., Vol 8, No 3, pp264-275, 1966.
- [34] N.N. Zorev: Interrelationship Between Shear Processes Occurring Along Tool Face and on Shear Plane in Metal Cutting, Proc. Int. Prod. Eng. Res. Conf., ASME, Pittsburgh, Sept. 9-12, 1973, p42.
- [35] P.Albrecht: New Development in the Theory of the Metal Cutting Process - Part II, The Theory of Chip Formation, Trans. ASME, Vol 83, Nov. 1961, p557.
- [36] Israel Dagiloke, Andrew Kaldos, Steve Douglas and Ben Mills: A Generic Process Model For High Speed Milling Eurometalworking'94, The University of Udine, Italy, 28-30 Sept 1994

- [37] I.F.Dagiloke, A.Kaldos, S.Douglas and B.Mills: Developing High Speed Cutting Simulation Suitable for Aerospace Components Proc. of Aerotech '94, IMechE, Birmingham, 18-21 Jan. 1994
- [38] A.Kaldos, E.Nagy and J.Takacs: Cutting Technology and Cutting Tools, Technical Publishing Company, Budapest, 1981, J4-790
- [39] F. Koenigsberger and A.J.P. Sabberwal: Chip Section and Cutting Forces During the Milling Operation, Annals OF CIRP, 1960.
- [40] F. Koenigsberger and A.J.P. Sabberwal: An Investigation into the Cutting Force Pulsations During Milling Operation, Int. J. Mach. Tool Des. Res. Vol 1, 1961, p15
- [41] P.S. Houghton : The Milling Machine, Crosby Lockwood and Sons Ltd, 3rd ED., 1965, pp158-198
- [42] M.E. Martellotti : An analysis of the Milling Process, Part II - Down Milling, Trans ASME, Vol 67, 1945, p233
- [43] E.J.A. Armarego and R.H. Brown : The Machining of Metals, Prentice-Hall, Int. Inc. London, 1969, pp174-188
- [44] R.Komanduri and R.H.Brown: On the Mechanics of Chip Segmentation, Trans. ASME, Journal of Eng. for Industry, Vol. 103, 1981, pp33-51
- [45] C.R. Liu, Z.C. Lin and M.M. Barash: Effects of Plane Strain and Plane Stress Conditions on Stress Field in the Workpiece During Machining - An Elasto-Plastic Finite Element Analysis, Proc. of ASME High Speed Machining Conf., 1984, PED 12, pp167 - 180.
- [46] C.R. Liu, Z.C. Lin and M.M. Barash: Thermal and Mechanical Stresses in the Workpiece During Machining, Proc. of ASME High Speed Machining Conf., 1984, PED 12, pp181 - 191.
- [47] B.F. von Turkovich : Cutting Theory and Chip Morphology, Handbook of High Speed Machining Technology, Chapman and Hall, London, 1985, pp27-47
- [48] R.F. Recht : Taylor Ballistic Impact Modelling Applied to Deformation and Mass Loss Determination, Int. J. Eng. Sci. Vol. 16, 1978, pp809-827

- [49] G. Boothroyd and W. A. Knight : Fundamentals of Metal Machining and Machine tools, 2nd ED, Marcel Dekker, Inc., 1989, pp109 - 127
- [50] M.C. Shaw : Metal Cutting Principles, 3rd Ed., M.I.T. Press, Cambridge, Mass, 1965, pp -12-1 - -12-40
- [51] G.Arndt : Further Considerations of Ultra-High Speed Machining, Unpublished paper, 1975
- [52] A.B. Sadat : Effect of High Cutting Speed on Surface Integrity of AISI 4330 During Turning, Materials Sci. and Technology, April 1990, Volume 6, pp371 - 376.
- [53] T.C. Hsu : Analysis of the Plastic Deformation Due To Orthogonal and Oblique Cutting, Journal of Strain Analysis, Vol 1, part 5, 1966, pp375-378.
- [54] P.K. Wright and A. Bagchi: Tool Wear Process in High Speed Machining, Manuf. Eng. Trans 1980 North America Manuf. Res. Conf. Proc. 8th, 1980, 277- 284.
- [55] P.K. Wright and J.L. Robinson : Material Behaviour in Deformation Zone of Machining, Journal of Metal Technology, Vol. 4, 1977, p240
- [56] A.O.Tay, M.G.Stevenson, G. De Vahl Davis and P.L.B.Oxley : A Numerical Method for Calculating Temperature Distribution in Machining, From Force and Shear Angle Measurements, Int. J. of Machine Tool Des. and Res. Vol 16, 1978, pp335 - 349
- [57] P. Matthew: Use of Predicted Cutting Temperatures in Determining Tool Performance, Int. J. of Mach. Tools Manufacturing, 1989, Volume 29, No 4, 481-497.
- [58] G. Boothroyd : Proc. Inst. Mech. Engineers, Vol 177, 1963, p789.
- [59] G.Arndt and R.H.Brown: Design and Preliminary Results From An Experimental Machine Tool Cutting Metals at up to 8000 ft/sec, Pro. 13th International M.T.D.R. Conf., 1972, pp217-223.
- [60] H.Schulz: Hochgeschwindigkeitsfraesen Metallischer und Nichtmetallischer Werkstoffe, Carl Hanser Verlag Muenchen Wien, 1989, pp1-150

- [61] T.R. Aggarwal : General Theory and its Application in the High-Speed Milling of Aluminium, Handbook of High Speed Machining Technology, Chapman and Hall, London, 1985, pp197 - 239
- [62] J.A. Miller : High Speed Machining of Space Shuttle External Tank Panel, Tool Materials for High Speed Machining Conf. Proc., Soc. of Carbide and Tool Engineers, 1987, pp11-22
- [63] W.N. Findley and R.M. Reed: The influence of Extreme Speeds and Rake Angles in Metal Cutting, Trans ASME, Series B, Vol. 85, No 2, 1963, pp49-67
- [64] J.B. Armitage and A.O. Schmidt : Experimental Measurement of Cutting Forces and Speeds, Part II, Tool Engineer, Vol. 27 No 5, Nov. 1951, p50
- [65] J.d. Radford and D.B. Richardson : Production Engineering Technology, Macmillan and Co. Ltd, 1969, p127
- [66] Armitage J.B. and A.O. Schmidt : Radial Rake Angles in Face Milling, Mechanical Engineering, N.Y. Vol 66, 1944, p403 and p453
- [67] K.J. Trigger and B.T. Chao : Trans ASME, Vol 73, No 1, Jan 1951, p68
- [68] M. Kronenberg : Machining Science and Application, Pergamon Press, London, 1st ED,1966,pp217-219
- [69] A. Ber, J. Rotberg and S. Zombach : A Method for Cutting Force Evaluation of End Mills, Annals of the CIRP, Vol 37/1, 1988, p39
- [70] E.J.A. Armarego and N.P. Deshpande : Computerized End-Milling Force Predictions With Cutting Models Allowing For Eccentricity and Cutter Deflections, Annals of the CIRP, Vol 40/1, 1991, p27
- [71] A.O. Schmidt : Metal Cutting Temperatures and Tool Wear, Tool Engineer, Vol 29, No 1, July 1952, p33
- [72] T.A.C. Stock and K.R.L. Thompson : Penetration of Aluminium Alloys by Projectiles, Metall. Trans., Vol 1, 1970, pp219-224
- [73] V.D. Kuznetsov : Super High Speed Cutting of Metals, The Iron Age, May 10 1945, pp66-69 and p142
- [74] A.O. Schmidt: Workpiece and Surface Temperatures in Milling, Trans

- A.S.M.E., Vol 75, July 1953, pp883-890.
- [75] D.C. Drucker : An Analysis of the Mechanics of Metal Cutting, J. Appl. Phys. Vol 20 No 11, Nov. 1949, p1013
 - [76] M.C. Shaw and P.A. Smith : Tool Wear Results from Several Causes, American Machinist, New York, Vol 95, No 22, Oct. 1951, p100
 - [77] M.C. Shaw : Metal Cutting Principles, 3rd Ed., M.I.T. Press, Cambridge, Mass, 1965, p55
 - [78] O.W.Dillon, R.J. De Angelis, W.Y. Lu, J.S. Gunasekera and J.A. Deno: The Effects of Temperature on the Machining of Metals, J. Materials Shaping Technology, Vol. 8, No 1, 1990, pp23-29
 - [79] A.O. Schmidt and J.B. Armitage: An Investigation of Radial Rake Angles in Face Milling, Trans ASME, Vol 66, No 8, 1944, p633
 - [80] P.Albrecht: New Developments in the Theory of the Metal Cutting Process - Part 1 The Ploughing Process in Metal Cutting, Trans. ASME, Vol. 82, November 1960, p348
 - [81] G.Boothroyd and J.A.Baily: A Laboratory Course in Metal Cutting, Bull. Mech. Eng. Educ., Vol. 5, 1966, p9
 - [82] S.Kobayashi and E.G.Thomsen: Some Observations on the Shearing Process in Metal Cutting, Trans. ASME, Vol. 81, 1959, p251

LIST OF PUBLISHED PAPERS

- 1.0 I.F.Dagiloke, A.Kaldos and S.Douglas: A Method of Milling Cutting Process Evaluation at High Cutting Speed, Proc. of 8th National Conf. For Manufacturing Research, University of Central England, Birmingham, 8-10 Sept. 1992, p91-95

- 2.0 I.F.Dagiloke, A.Kaldos, S.Douglas and B.Mills: High Speed Machining: An Approach To Process Analysis Proc. of the International Conf. on Advances in Materials and Processing Technologies (AMPT'93), Dublin City University, 24-27 August 1993, p63-70

- 3.0 I.F.Dagiloke, A.Kaldos, S.Douglas and B.Mills:Developing High Speed Cutting Simulation Suitable for Aerospace Components Proc. of Aerotech '94, IMechE., Birmingham, 18-21 Jan. 1994

- 4.0 I.F.Dagiloke, A.Kaldos, S.Douglas and B.Mills:A Generic Computer Model for High Speed Machining With an Integrated Database. Proc. of 10th National Conf. on Manufacturing Research, Loughborough University of Technology, 5-7 Sept. 1994, p622-626

- 5.0 I.F.Dagiloke, A.Kaldos, S.Douglas and B.Mills:A Generic Process Model For High Speed Milling, Eurometalworking'94, The University of Udine, Italy, 28-30 Sept. 1994

A Method Of Milling Cutting Process Evaluation At High Cutting Speed

I.F. Dagiloke, A. Kaldos and S. Douglas

School Of Eng & Tech Management, Liverpool John Moores University.

ABSTRACT

This paper presents cutting process and related numerical method for evaluation of milling process for various workpiece materials subject to high speed machining conditions. The technique enables power, feed, feedrate, metal removal rates, cutting forces, cutting energies and cutting temperatures for peripheral milling operation at high cutting speed to be predicted.

1.0 INTRODUCTION

The need for more readily available and reliable quantitative machining performance information has been emphasised in a recent survey, Kahles, 1987 [1], and the problem becomes even more acute for high speed machining (HSM). HSM offers the potential to reduce production cycle times and obtain higher throughput across the manufacturing facility, however, prior to implementation of HSM strategies, an insight into the complexity of the process is necessary and the influence of the process variables understood. This paper presents the development of HSM model for a single point milling operation which includes the influence of momentum force. The development of HSM model for quantitative prediction of machining performance characteristics represents a formidable and complex task. However, by establishing HSM models it became possible to dispel some of the misconceptions which has arisen around HSM.

2.0 MECHANICS OF CUTTING APPROACH FOR HSM MODEL

The basic strategy for milling process models at HSM is to develop computer based analyses to predict the torque, cutting conditions, spindle speed, metal removal rates, cutter specifications, cutting forces, cutting energies, and cutting temperature among other cutting process parameters over any given cutting speed. However, it has been suggested that from the cutter and material point of view, that the basic chip formation changes as new cutting regimes are experienced making Taylor's empirical equations invalid since they are independent of energy and force [2]. Two dimensional mechanics of cutting, including the influence of momentum force and temperature analyses in the shear zone are used to predict the process parameters in this study. Fig.1 illustrates schematically the geometrical model of the cutting process employed based on the assumption that the tool is wear free and continuous chip is produced with no built up edge. In each tooth engagement with the workpiece, the milling cutter tooth removes a small piece of the material from the workpiece (determined by the depth and width of cut), and deforms it plastically into chip of a variable thickness. Because of this variable chip thickness effect, as initial approximation, the average chip thickness is employed in this study. Therefore, having described the assumptions made and

the idealized model of cutting process employed in the present theory, from [3 - 7] the mathematical procedure explained and the developed equations are found suitable for describing cutting process at HSM.

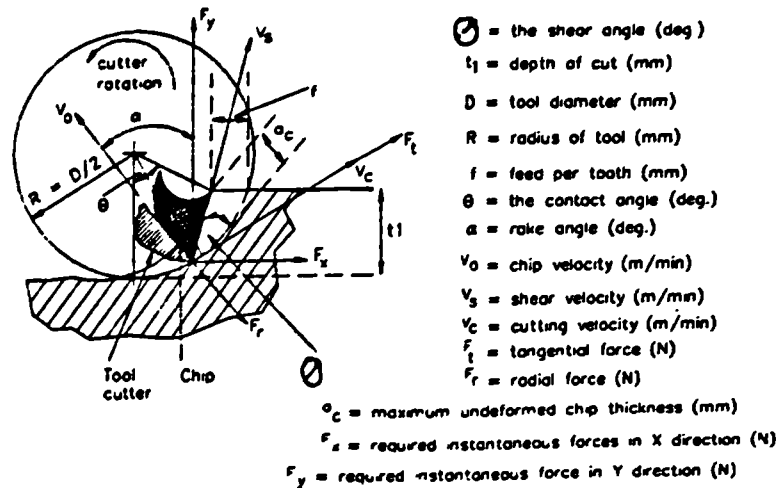


FIG.1 PERIPHERAL MILLING GEOMETRICAL TWO DIMENSIONAL MODEL

3.0 NUMERICAL SIMULATION OF HSM PROCESS

Fig. 2 describes the structure of cutting simulation system. The model is developed on a VAX main frame computer using Fortran and Ginof graphical

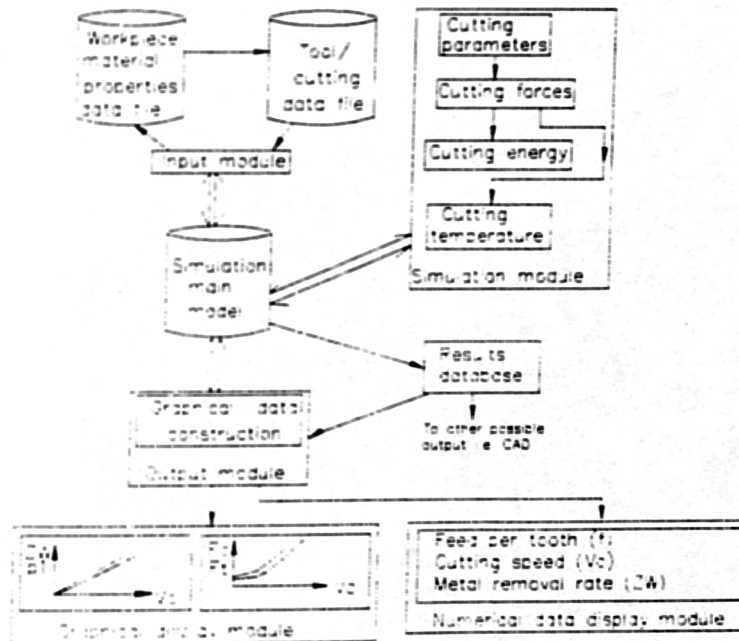


FIG.2 THE STRUCTURE OF THE CUTTING SIMULATION MODEL

software package. The model consists of three major modules viz: input, simulation and output module.

3.1 INPUT MODULE

Two methods are developed to enter data into the input module, the first method is for the input module to take the geometric, mechanical and thermal properties information of the workpiece, tools and cutting conditions from the databases and transforms them into suitable form for simulation. The second method is for new set of input data for the aforementioned parameters in the first method to be entered into the model. The workpiece, tool and cutting conditions data files can be edited making it possible to add more data, also the input module can be edited prior to cutting simulation.

3.2 THE PHYSICAL SIMULATION MODULE

The simulation module has a built-in numerical data controller with four sub-modules, which are for cutting parameters, cutting forces, cutting energies and cutting temperatures respectively. Once the input data have been supplied, the numerical simulation takes about 20-25 seconds.

3.3 THE OUTPUT MODULE

Based on the numerical data obtained through the "Results database", the output module can present the cutting process results numerically or graphically through built-in graphic image construction.

4.0 NUMERICAL SIMULATION RESULTS

Fig.3 illustrates typical relationship between cutting speed (V_c) and the power consumed at the cutting edge. It was observed that this parameter increase almost linearly with increase in cutting speed.

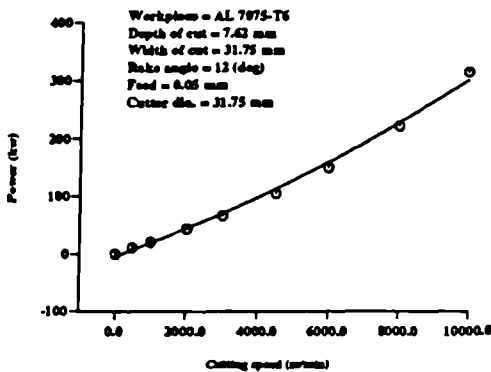


Fig.3 : The relationship between the cutting speed and the power consumed

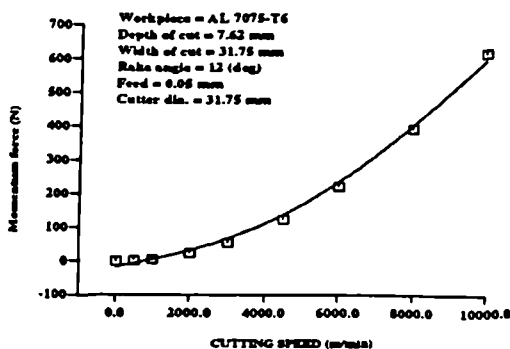


Fig.5 : The relationship between the cutting speed and momentum force

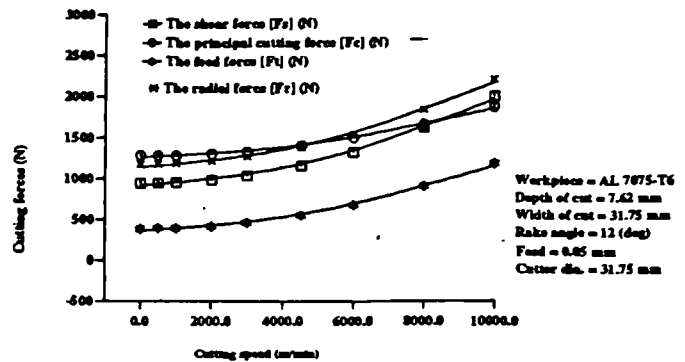


Fig.4 : The relationship between the cutting speed and cutting forces

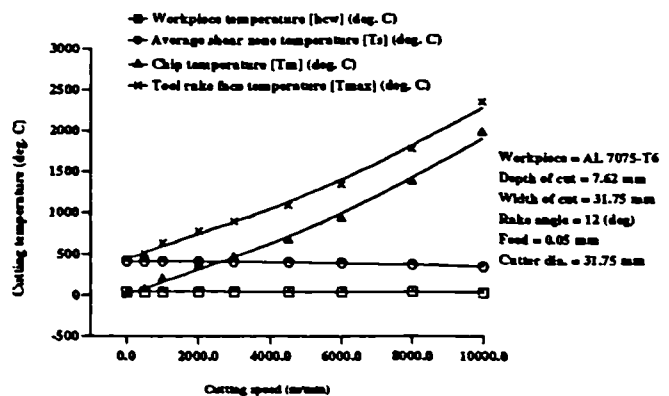


Fig.6 : The relationship between the cutting speed and cutting temperature

It was also observed that the feed rate and metal removal rate increases with increased cutting speed, ascribed metal removal rate and feedrate been proportionally related to the spindle speed whilst the spindle speed is also proportionally related to the cutting speed, suggesting that any effort to increase the cutting speed in order to maximize the metal removal rate should take the spindle speed and power requirements into consideration. Fig.4 showed the cutting forces remained relatively constant at low cutting speed, this can be ascribe to the fact that at low cutting speed the magnitude of the momentum force is insignificant compared to the other cutting forces, however, as the cutting speed approaches 1500 m/min, its magnitude started to increase causing the other forces to increase due to the indication that the vector sum of the momentum forces shown in Fig.5 has to be added to the values of other forces. Fig.6 illustrates the effect of increase in cutting speed on cutting temperature, it was found that the workpiece and the average shear zone temperatures decreases with increasing cutting speed whilst increasing cutting speed causes chip and tool rake face temperatures to increase. The increase in chip and tool rake face temperatures can be attributed to the increase in frictional force in the shear zone whilst decrease in workpiece and shear zone temperature can be attributed to the fact that as the cutting speed increases there is less time available for plastic deformation and the mode of heat transfer changes from conduction to convection.

5.0 DISCUSSION

From the cutting simulation results test it was observed that the metal removal rate increase as the cutting speed increases whilst the machining time was observed to reduce with increasing cutting speeds. These results support the case for machining at high speed, however, the results also shows that the power consumed at the cut and spindle speed increases with cutting speed. Therefore, when specifying the cutting speed for any given workpiece material, the power capability of the machine tool and the available spindle speed should be taken into consideration. The initial rise in cutting forces at low cutting speeds in the experimental graphs that appeared in the literature can be associated with the formation of built-up edges [8]. The cutting speed and cutting forces appear to be independent of each other within the cutting speed limits of the various tool and workpiece materials up to 1200 m/min where the effect of momentum force takes place. This finding accord with [9]. However, it must be stressed that the two quantities dependent on material properties such as hardness and tensile strength. The product of cutting speed and cutting force determines the power which is consumed at the cutting edge. Therefore, it is evident that the utilization of the power of a given machine tool requires a reduction in cutting speed if the cutting force increases and vice versa. With milling operation, a decrease of cutting force with increase of cutting speed is not always obtained [10] and it is suggested by [11] that increases of cutting force may be experienced with increase in cutting speed and this is in agreement with the findings in this study.

5.1 COMPARISON OF RESULTS

The findings of McGee and Stelson reported by Aggarwal [4] regarding the cutting parameters versus cutting speed indicated that the power consumed at cut reduces gradually as the cutting speed is increased. However, based on the observation in this study and the findings of King et al [12], there is nothing to suggest that the power would reduced. The probable reason why those earlier researchers observed gradual reduction in power was the failure to take the significance of the momentum force at high cutting speed into consideration as clearly demonstrated in this present study. The cutting speed against cutting forces appears to correlate with the findings of Schlesinger, Armitage et al and Okochi et al reported by Kronenberg [13], also with earlier work of Okushima et al [14] and most recently with that of Ber et al, 1988, [15] and Armarego et al, 1991, [16]. As for cutting speed against momentum force, the cutting simulation results correlate with the findings reported by Arndt [7]. The cutting speed against the maximum temperature in the chip and on the tool rake face, the obtained results correlate with the earlier findings of Wright [17] whilst obtained reduction in workpiece and shear zone temperatures correlate with the findings of Stock et al [18].

5.0 CONCLUSION

A computer based milling process simulation has been systematically developed.

First, a peripheral milling mathematical model which is suitable for application at low, high, very high and ultra-high speed machining is developed and discussed. The milling mechanics equations are then reformulated into analytical expressions tailored to a software package. The input module takes the workpiece geometric, mechanical and thermal properties information, tool parameters and cutting conditions from the databases and transforms them into suitable form for the simulation. The conclusions of the cutting simulation can be summarised as follows:

(i) The cutting simulation module provide a method of calculating and predicting the cutting parameters, cutting forces, cutting energies and cutting temperatures.

(ii) Utilization of the numerical and graphical results makes it possible to apply the model to complex machining analyses. The results also can help in the determination of suitable chip removal system, spindle and machine tool specifications for any particular operation.

(iii) Comparisons of the simulation results with the published cutting experiments showed that the model can predict the cutting process accurately and adequately.

(iv) The model described here is proposed as a valuable tool for the LSM/HSM process engineers and machine tool builders because it allows the identification of material/process interactions that might otherwise be overlooked.

REFERENCES

- [1] J.F. Kahles : CIRP Technical Report, Annals of CIRP, 36/2, 1987, p523
- [2] R.I. King and R.L. Vaughn : A Synoptic Review of High Speed Machining from Salomon to the Present, Proc. of ASME High Speed Machining Conf., PED 12, 1984, p2
- [3] R.F. Recht : A Dynamic Analysis of High Speed Machining, Proc. of ASME High Speed Machining Conf., PED 12, 1984, pp83-93.
- [4] T.R. Aggarwal : General Theory and Its Application in the High Speed Milling of Aluminium, Handbook of High Speed Machining Technology, Chapman and Hall, London, 1985, pp197-239.
- [5] B.F. von Turkovich : Cutting Theory and Chip Morphology, Handbook of High Speed Machining Technology, Chapman and Hall, London, 1985, pp27-47.
- [6] G.Boothroyd and W.A. Knight : Fundamentals of Metal Machining and Machine Tools, 2nd Ed, Marcel Dekker, Inc., 1989, pp109-127.
- [7] G. Arndt : Ultra-high Speed Machining : A Review and an Analysis of Cutting Forces, Proc. of Institute of Mech. Engineers (London), Vol 187, No 44/73, 1973, pp625-634.
- [8] J.D. Radford and D.B. Richardson : Production Engineering Technology, Macmillan and Co. Ltd, 1969, p127.
- [9] J.B. Armitage and A.O. Schmidt : Experimental Measurement of Cutting Forces and Speeds, Part II, Tool Engineer, Vol 27, No 5, Nov. 1951, p50.
- [10] J.B. Armitage and A. O. Schmidt : Radial Rake Angles in Face Milling, Mechanical Engineering, New York, Vol 66, 1944, p403 and p453.
- [11] K.J. Trigger and B.T. Chao : Trans ASME, Vol 73, No 1, Jan. 1951, p68
- [12] R.I. King and J.G. McDonald : Production Design Implications of New High Speed Milling Techniques, Journal of Engineering for Industry, ASME, Nov. 1976, p176.
- [13] M. Kronenberg : Machining Science and Application, Pergamon Press, London, 1st Ed, 1966, pp217-219.
- [14] K. Okusima, K. Hotomi, S. Ito and N. Narutaki : A Fundamental Study of Super-high Speed Machining , Bul. Japanese Society of Mechanical Engineers, Vol 8, No 32, 1965, p702
- [15] A. Ber, J. Rotberg and S. Zombach : A Method for Cutting Force Evaluation of End Mills, Annals of The CIRP, Vol 37/1, 1988, p39.
- [16] E.J.A. Armarego and N.P. Deshpande : Computerized End Milling Force Predictions with Cutting Models Allowing for Eccentricity and Cutter Deflections, Annals of the CIRP, Vol 40/1, 1991, p27
- [17] P.K. Wright and A. Bagchi : Tool Wear Process in High Speed Machining, Manuf. Eng. Trans 1980 North Americal Manuf. Res. Conf. Proc. 8th, 1980, pp277- 284.
- [18] T.A.C. Stock and F.R.L. Thompson : Penetration of Aluminium Alloys by Projectiles, Metall. Trans., Vol 1, 1970, pp219-224

HIGH SPEED MACHINING: AN APPROACH TO PROCESS ANALYSIS

I.F. Dagiloke, A. Kaldos, S. Douglas and B. Mills

*School of Engineering and Technology Management,
Liverpool John Moores University, U.K.*

ABSTRACT

A software package has been developed to describe high speed machining applied to a number of metal cutting operations. The formulations of the model and program are described and an example is presented applied to milling. This modular system incorporates a structured database that can be updated by the user in a dialogue operational mode and allows the user to obtain process parameters for changing cutting conditions in both conventional and high speed machining. The model described here also incorporates workpiece/tool thermal and mechanical properties amongst its input variables. This allows the outputs to be more representative of real life cutting and the outputs of the model are useful for both conventional and high speed machining.

1. INTRODUCTION

Of the many variables encountered in machining, cutting speed is the one that most seriously influences production rate and workpiece surface finish. Hence, interest in optimizing cutting speed as a means for higher production has gained momentum in recent years in both the research community and industry. A review of the literature indicated that the efficiencies of high speed machining have been investigated for the machining of aluminium alloys, steels, iron and titanium alloys [1-11]. Although the main purpose of high speed machining has been based on production economy, however, most of the previously published investigations have focused on the difference in cutting mechanism between high and conventional low speed machining rather than in improving production economics.

Early work [1,4,5] has been directed towards understanding the deformation of materials at high impact rates based on the theory of plastic wave propagation established by Karman and Duwez [7]. More recent work [8-10] has been concerned with studies of cutting mechanisms, including chip formation mechanics, temperatures and cutting force determinations. A neglected aspect of high speed machining technology has been the implementation of the technology in industry based on a total analysis of the high speed machining process.

The main aim of the present paper is to analyse the cutting process over a very wide speed range including the important momentum effect caused by the process of chip formation at high speed.

2. AN OVERVIEW OF HIGH SPEED MACHINING INPUT AND OUTPUT PARAMETERS

The basic strategy for high speed machining is to be able to select appropriate workpiece, tool and machining systems for a given cutting speed. To achieve this, it is imperative to understand the effect of increase in cutting

speed on the workpiece/tool mechanical and thermal properties. Secondly, to understand the effect of increase in cutting speed on the machining system such as the machine tool, the spindle and jigs/fixtures. Therefore, to give an insight into the formulation of this strategy and process complexity. Fig. 1 shows a schematic representation of the essential input and output elements of the machining process which the authors have

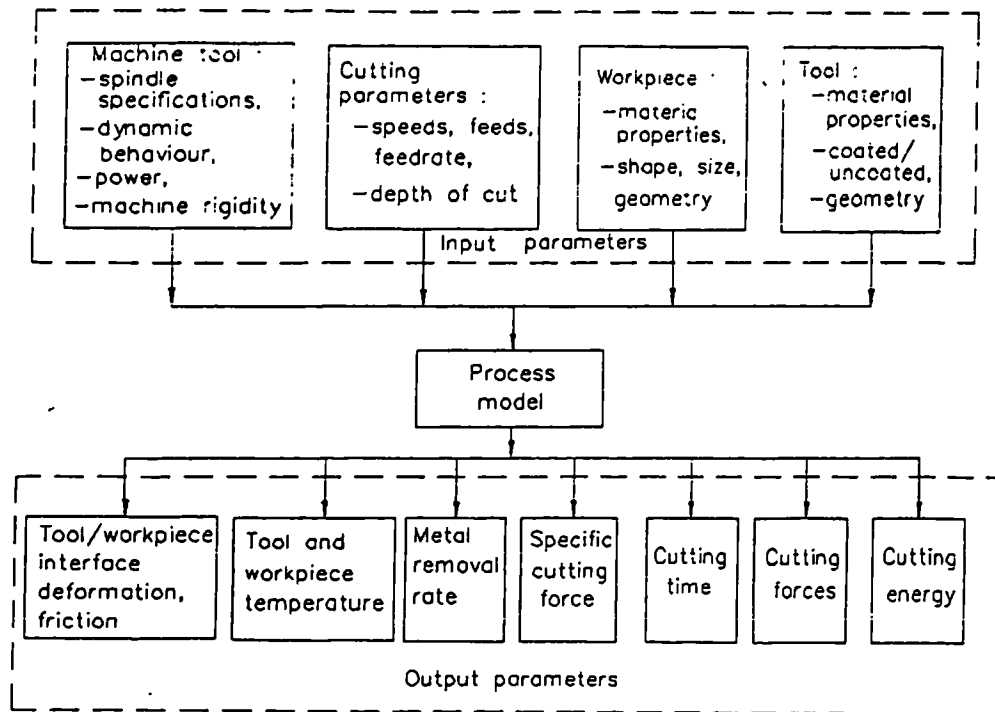


FIG. 1: MODEL INPUTS/OUTPUTS SCHEMATIC REPRESENTATION

identified as essential to the mathematical modelling of the high speed machining process. The information on the machine tool, the cutting conditions, the workpiece/tool geometries, the workpiece/tool thermal and mechanical properties are designated as inputs whilst the outputs are the computed cutting forces, cutting energy, cutting temperature, power requirements and metal removal rates.

In establishing the theoretical foundation for high speed machining, it is vital to be aware of the influence of the momentum force and energy Recht [11], also the effect of increase in cutting temperature on the workpiece and tool properties in the shear zone as cutting speed increases Shaw [9]. Based on these phenomena, the following equations and machining variables need to be established before any realistic high speed cutting simulation models can be constructed:

- (1) the equations for cutting parameters such as the feed, feed rate, metal removal rates, friction angle, shear angle etc.;
- (2) the cutting forces including the effect of momentum force;
- (3) the cutting energy and the cutting temperatures in both the primary and the secondary deformation zones.

The equations employed were derived from both theoretical and experimental studies [3-5, 11] and these are believed to adequately describe the cutting processes encountered at high metal removal rates.

3. ANALYTICAL PROCEDURE

Fig. 2 shows the conceptual algorithm proposed in this study for the cutting process analysis of both high speed and conventional machining based on the numerical modelling using a Fortran software package. Databases were created for future access for the cutting conditions, the tool material and geometry data, the workpiece material geometry, the workpiece thermal and mechanical properties. To determine the necessary cutting equations, a two dimensional cutting model based on the general principles of metal cutting mechanics for milling operations was employed. The power consumed at the cut, the metal removal rates, feed, feedrates, machining time, cutting energy, cutting forces, cutting temperatures and stress distributions in the deformation zones are first analyzed for a given set of cutting conditions and workpiece thermal and mechanical properties using a simulation of the cutting process developed in the Fortran software language. The results are then presented numerically and graphically for evaluation.

It can be clearly seen in this model that all relevant input parameters which influence the cutting process were accounted for, unlike some of the earlier models Armarego and Deshpande [21] which did not include workpiece/tool mechanical and thermal properties in their analysis.

4. ANALYTICAL RESULTS.

Fig.3 shows a typical relationship between the cutting speed (V_c) and the power consumed at the cutting edge. It was observed that this parameter increases almost linearly with increase in cutting speed. Fig.4 shows that the cutting forces remained relatively constant at low cutting speed, which can be ascribed to the fact that at low cutting speed, the magnitude of the momentum force is insignificant compared to the other cutting forces. However, as the cutting speed approaches 1500 m/min, its magnitude started to increase causing the other forces to increase due to the indication that the vector sum of the momentum forces shown in Fig.5 has to be added to the values of the other forces.

Fig.6 illustrates the effect of increase in cutting speed on cutting temperatures. It was found that the workpiece and the average shear zone temperatures decrease with increasing cutting speed whilst chip and tool rake face temperatures increase. The increase in chip and tool rake face temperatures can be attributed to the increase in energy dissipation at the tool face. The decrease in the workpiece and shear zone temperature at high speed may be due to the fact that as the cutting speed increases there is less time available for the heat generated to conduct into the workpiece, so that the heat is effectively carried away with the chip.

5. DISCUSSION

At high speed, metal removal rates increase, however, the present simulation shows that the power consumed during cutting increases with cutting speed. Thus, when specifying the cutting speed for any given workpiece material, the power capability of the machine tool and the available spindle speed should be considered. The initial rise in cutting forces at low cutting speeds from experimental data has been shown by Radford and Richardson [12] to be associated with the formation of built-up edge. In this study, it was found that the cutting speeds and cutting forces appear to be independent of each other within the cutting speed limits of the various tools and workpiece materials up to 1200 m/min when the effect of momentum force begins to take place. This finding is in agreement with the work of Armitage and Schmidt [13]. Since it is known that the product of the cutting speed and cutting force determines the power which is consumed at the cutting edge. Therefore, the utilization of the power of a given machine tool requires a reduction in cutting speed if the cutting force increases and vice versa. These findings agree with the work of Armitage et al and Trigger et al [14, 15] in which increase in the cutting forces with increased cutting speed were reported.

5.1 Comparison of results

In the relationship between the power consumed at the cut and the cutting speed, an increase in cutting power with increased cutting speed was observed and this result correlates with the findings of King and McDonald [16]. In the authors opinion there is nothing to suggest that the power would reduce as reported by Aggarwal [17]. The probable reason why these earlier researchers observed a gradual reduction in power was the failure

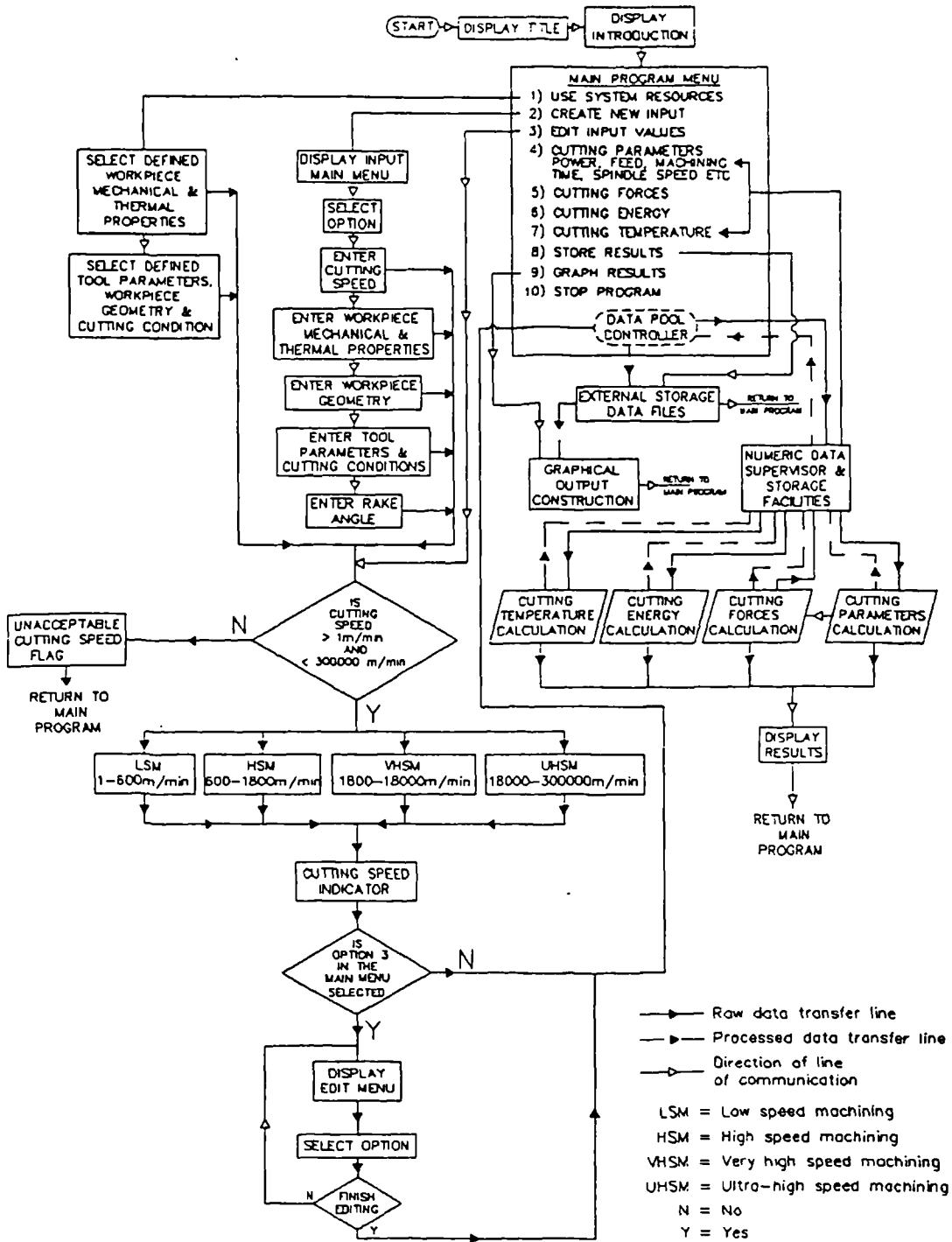


FIG.2. CONCEPTUAL ALGORITHM FOR CUTTING PROCESS ANALYSIS OVER A WIDE CUTTING SPEED RANGE

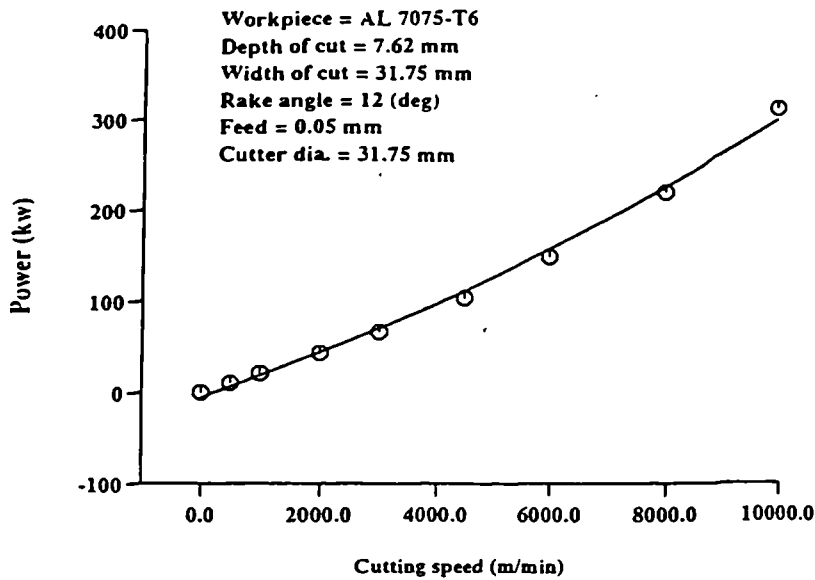


Fig.3 : The relationship between the cutting speed and the power consumed

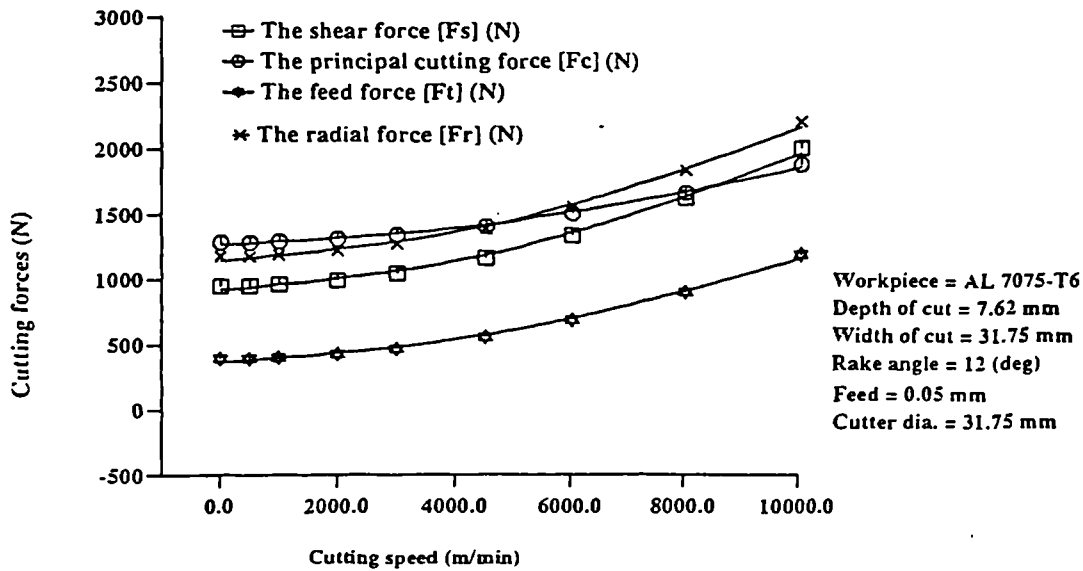


Fig.4 : The relationship between the cutting speed and cutting forces

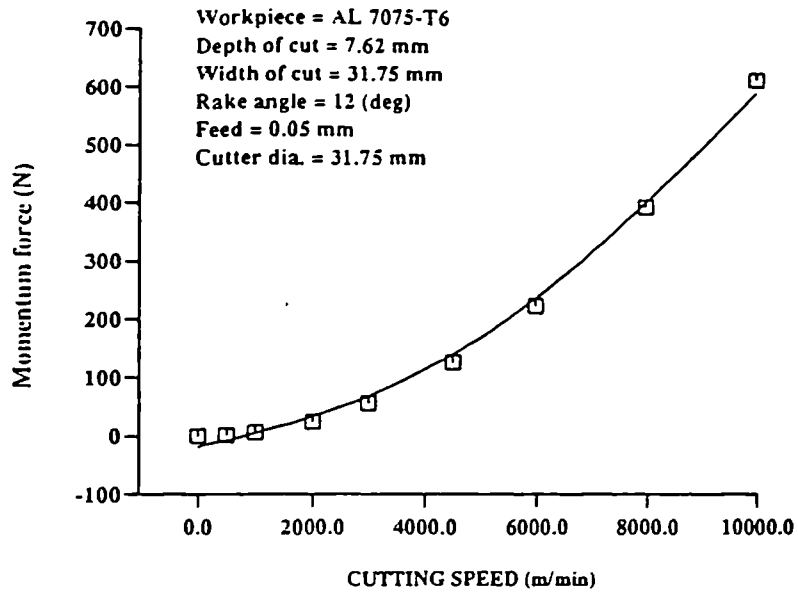


Fig.5 : The relationship between the cutting speed and momentum force

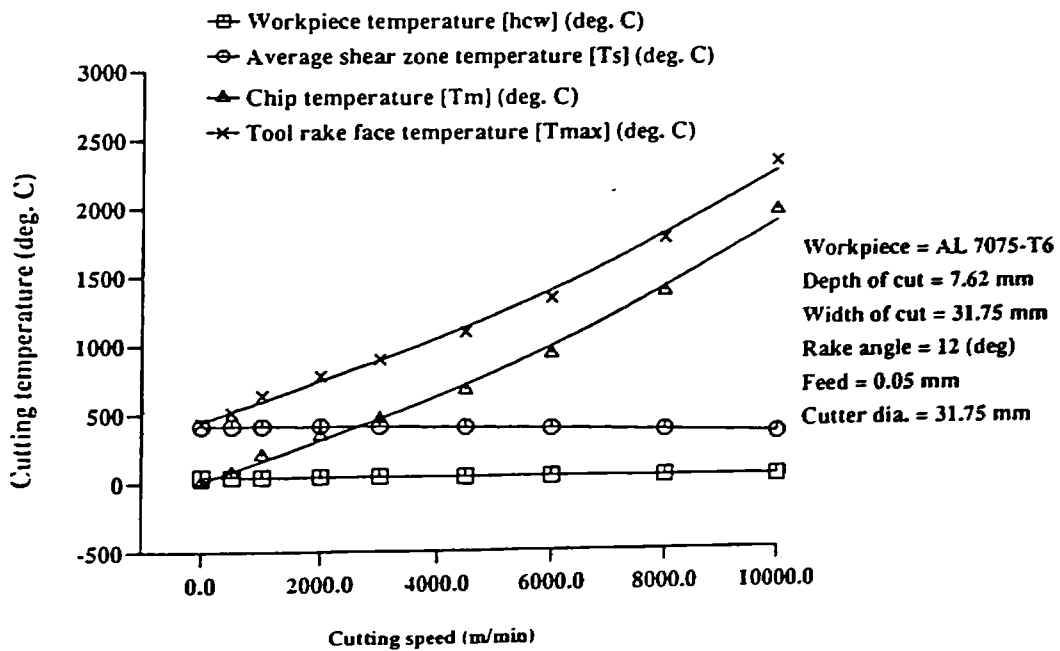


Fig.6 : The relationship between the cutting speed and cutting temperature

to consider the significance of the momentum force at high cutting speed as clearly demonstrated in this present study (Fig.3). The cutting force variation with cutting speed, Fig.4 appears to correlate with the earlier experimental findings of a number of workers [18-21]. The variation of momentum force with cutting speed (Fig.5) from our cutting simulation results correlate with the findings reported by Arndt [6]. In the case of the increase of the maximum temperature in the chip and on the tool rake face with cutting speed, Fig.6, the present results of the simulation are in agreement with the earlier findings of Wright and Bagchi [22]. The predicted reduction in workpiece and shear zone temperatures, Fig.6, also correlate well with the findings of Stock and Thompson [23].

6. CONCLUSION

In the present analysis of the cutting process over a wide cutting speed range, an approach has been described based on the numerical simulation concept. The method of formulating input and output variables has been presented and discussed, followed by an approach to selection of cutting equations for the process of high speed machining. In general the overall conclusions of the present cutting simulation can be summarised as follows:

- (1) The inclusion of the workpiece/tool mechanical and thermal properties as input data allows the simulation of the high speed machining process which is representative of real machining conditions.
- (2) The cutting simulation modules provide a method of calculating and predicting the cutting parameters, cutting forces, cutting energies and cutting temperatures.
- (3) Utilization of the numerical and graphical results makes it possible to apply the model to complex machining analyses. The results can also help in the determination of a suitable chip removal system and spindle and machine tool specification for any particular operation.
- (4) The model described here allows the identification of material and process interactions that might otherwise be overlooked.
- (5) The possibility of identifying material and process interactions in real time now provides a significant step towards the development of adaptive optimisation strategies for high speed machining.

REFERENCES

- [1] B.F. von Turkovich: Influence of Very High Cutting Speed on Chip Formation Mechanics, 7th NAMRC Proc. May 1979, SME. Tech. 1979, pp241-247.
- [2] K. Okushima, K. Hitomi and S. Ito : A Study of Super-High Speed Machining, Annals of CIRP XIII, 1966, pp339-410.
- [3] B.F. von Turkovich : Cutting Theory and Chip Morphology, Handbook of High Speed Machining Technology, Chapman and Hall, London, 1985, pp27-47.
- [4] G. Arndt: The Development of Higher Machining Speeds - Part 2, The Production Engineer, Vol 49, Dec 1970, pp517 - 529.
- [5] M.P. Kalashnikova: The Study of Cutting Processes at Very High Speeds, F13, Metallov Metallovedenie, Vol 10, No 30, 1960, pp425-434, Translation pp107 -116.
- [6] G. Arndt : Ultra-High Speed Machining : A Review and An Analysis of Cutting Forces, Proc. of Institute of Mech. Engineers (London), Vol 187, No 44/73, 1973, pp625 - 634.
- [7] T. von Karman and P. Duwez: The Propagation of Plastic Deformation in Solids, Journal of Applied Physics, Vol. 21, 1950, pp987 - 994.
- [8] D.G. Flom, R. Komanduri and M. Lee: High Speed Machining of Metals, Ann. Rev. Mater. Sci., 1984, Vol 14, pp231 - 278.
- [9] M. C. Shaw: Temperature in Cutting, ASME, Production Engineering Division, 1988, Vol 30, pp133-143.
- [10] H. Schultz: High Speed Milling of Aluminium Alloys, Proc. of ASME High Speed Machining Conf., PED 12, 1984, pp241-244.
- [11] R.F. Recht: A Dynamic Analysis of High Speed Machining, Proc. of ASME High Speed Machining Conf., PED 12, 1984, pp83-93.
- [12] J.D. Radford and D.B. Richardson: Production Engineering Technology, Macmillan and Co. Ltd, 1969, p127.

Advances in Materials and Processing Technologies

- [13] J.B. Armitage and A.O. Schmidt: Experimental Measurement of Cutting Forces and Speeds, Part II. Tool Engineer. Vol. 27, No 5, Nov. 1951, p50.
- [14] Armitage J.B. and A.O. Schmidt: Radial Rake Angles in Face Milling. Mechanical Engineering. N.Y., Vol 66, 1944, p403 and p453.
- [15] K.J. Trigger and B.T. Chao: Trans ASME. Vol 73, No 1, Jan 1951. p68.
- [16] R.I. King and J.G. McDonald: Production Design Implications of New High-Speed Milling Techniques. Journal of Engineering for Industry, ASME, Nov. 1976, p176.
- [17] T.R. Aggarwal: General Theory and Its Application in the High Speed Milling of Aluminium, Handbook of High Speed Machining Technology, Chapman and Hall, London, 1985, pp197-239.
- [18] M. Kronenberg: Machining Science and Application, Pergamon Press, London, 1st ED, 1966, pp217-219.
- [19] K. Okushima, K. Hotomi, S. Ito and N. Narutaki: A Fundamental Study of Super-high Speed Machining, Bul. Japanese Society of Mechanical Engineers, Vol 8, No 32, 1965. p702.
- [20] A. Ber, J. Rotberg and S. Zombach: A Method for Cutting Force Evaluation of End Mills, Annals of the CIRP, Vol 37/1, 1988, p39.
- [21] E.J.A. Armarego and N.P. Deshpande: Computerized End-Milling Force Predictions with Cutting Models Allowing for Eccentricity and Cutter Deflections, Annals of the CIRP, Vol 40/1, 1991, p27.
- [22] P.K. Wright and A. Bagchi: Tool Wear Process in High Speed Machining, Manuf. Eng. Trans 1980 North America Manuf. Res. Conf. Proc. 8th, 1980, pp277- 284.
- [23] T.A.C. Stock and K.R.L. Thompson: Penetration of Aluminium Alloys by Projectiles, Metall. Trans., Vol 1, 1970, pp219-224.

Developing High Speed Cutting Simulation Suitable for Aerospace Components

by I F Dagiloke, MSc; A Kaldos, Dipl Ing (Mech) Dipl Ing (Elec) PhD MSME; S Douglas, BSc MSc PhD MIMechE and B Mills, BSc MSc PhD CEng FIM, *Liverpool John Moores University*

SYNOPSIS

It is widely accepted that high speed machining has tremendous potential not only in increased metal removal rates but also in increased performance indicators such as excellent surface finish, dimensional accuracy and favourable surface stress states for components used in the aerospace industry. To fully understand the potential of this technology a computer based mathematical cutting simulation model for predicting process parameters at any given cutting speed regardless of what type of workpiece material is in use, is developed and discussed in this paper. Also the need for experimental work to establish the correlation of the simulation predictions with reliable experimental data is addressed.

NOTATION

V_c	Cutting speed	m/min	BHN	Brinell hardness number	N/mm ²
V_s	Shear velocity	m/min	σ_y	Uni-axial tensile dynamic yield stress	N/mm ²
V_o	Chip velocity	m/min	ϵ_p	Natural plastic strain	[1]
V_m	Momentum velocity	m/min	ψ	Work hardening coefficient	N/mm ²
ϕ	Shear angle	deg	τ_s	Dynamic shear stress	N/mm ²
Θ	The tool contact angle	deg	τ_y	Shear yield stress	N/mm ²
α	Rake angle	deg	σ_s	True flow stress	N/mm ²
t_1	Depth of cut	mm	τ	Effective dynamic shear strength	N/mm ²
S_1	Shear zone thickness	mm	ρ	Workpiece density	kg/m ³
b_1	Width of cut	mm	SHC	Specific heat capacity	J/kgK
D	Tool diameter	mm	T_{con}	Thermal conductivity	W/mK
f	Feed	mm	F_s	Shear force at low speed	N
Z	Number of teeth	[1]	F_m	Momentum force	N
n	Spindle speed	1/min	F_{cm}	Momentum principal cutting force	N
ZW	Metal removal rate	cm ³ /min	F_{fm}	Momentum feed force	N
ZWS	Specific metal removal rate	cm ³ /min kW	F_{fm}	Momentum frictional force	N
P_1	Power at the cut	kW	$NFTF_m$	Momentum tangential force parallel to the tool face	N
a_c	Undeformed chip thickness	mm	F_c	Low speed principal cutting force	N
r_c	Cutting ratio	[1]	F_r	Low speed frictional force	N
β	Friction angle	deg	F_t	Low speed feed force	N
L_c	Length of contact per tooth per revolution	mm			
γ	Shear strain	[1]			
$\dot{\gamma}$	Strain rate	1/sec			

F_n	Low speed tool face normal force	N
NFSP	Low speed shear plane normal force	N
R_r	Low speed resultant force	N
F_x	Required instantaneous force in X direction	N
F_y	Required instantaneous force in Y direction	N
NFTF	Tangential force parallel to the tool face at low speed	N
NFTF _h	Tangential force parallel to the tool face at high speed	N
F_{cu}	High speed principal cutting force	N
F_{fu}	High speed feed force	N
F_{fu}	High speed frictional force	N
F_{su}	High speed shear force	N
F_{nu}	High speed tool face normal force	N
NFSP _h	High speed shear plane normal force	N
R_{ru}	High speed resultant force	N
R_t	Thermal number of the workpiece	[1]
P_f	The rate of heat generated by friction between the chip and tool	J/s
P_m	The rate of total heat generated	J/s
P_s	Rate of heat generated by shearing	J/s
T_f	The average temperature of the chip resulting from the secondary deformation	°C
δT_m	The maximum temperature rise in the chip due to frictional heat source in the secondary deformation zone	°C
L_o	Length of heat source divided by the chip thickness	[1]
T_o	Initial workpiece temperature	°C
M_{temp}	Workpiece melting temperature	°C
H_{CW}	Heat conducted into the workpiece	°C
δT_s	Average rise in shear zone temperature	°C
T_{max}	Maximum temperature on the tool rake face	°C

1 INTRODUCTION

The need to reduce manufacturing costs is an ever-present challenge to the aerospace industry. New

processes must be developed to improve productivity and also to meet the stringent product specifications. In the aerospace industry the wing spars are machined from expensive forged aluminium billets while the stringers are machined from milled bars. The final geometry of the spar and the stringer mean that up to 90 percent of the original material needs to be removed. Consequently the economics of the process largely depends on the metal removal rates and the swarf control techniques for clearing the chips from the machining area. This implies that the concept of applying high speed machining (hsm) principles to large aerospace components is economically very attractive.

As high speed machining can dramatically increase metal removal rates resulting in reduced machining times and increased productivity there has been great interest in this technology. However, there are a number of issues including the effect of cutting speed on the machine tool, cutting tool materials and workpiece materials that need to be considered when contemplating the implementation of high speed machining.

A review of the literature reveals that the efficiencies of high speed machining have been investigated for the machining of aluminium alloys, steels, iron and titanium alloys (1-5). However, to date little published work relating to hsm mathematical/numerical simulation models which comprise the cutting parameters, cutting forces, cutting energies and cutting temperatures has been presented. Such models are required to assist the aerospace industry in the selection of cutting parameters and help allay the following misconceptions and reservations about hsm:

- (a) the fear of excessive maintenance problems, problems in swarf control and the basic apprehension associated with machining faster;
- (b) industry's continuing tendency to use the old established speeds and feeds on the shop floor;
- (c) belief that the major part of the manufacturing cost is in the material and handling process, therefore, hsm cannot possibly provide significant cost saving;
- (d) the controversy over the claim that there is reduction in cutting forces at high cutting speed;
- (e) uncertainty about how to select proper hsm cutting parameters and machine tool specifications.

In addition, the implementation of high speed machining presents a challenge since various factors limit the extent to which cutting speeds may be advantageously increased. These factors include the cutting temperature, the cutting tool material, the

workpiece material, the machine tool design, the cutting geometry, the cutting power and also after machining the surface integrity and metallurgical condition of the workpiece. For any machining system (machine/cutter/workpiece combination) it may be difficult to predict which element would be the dominant limitation. For example, will the spindle or machine tool control stall as the cutting speed increases? Will the cutter deflect and break? To address these questions requires a thorough understanding of the high speed machining process which is one of the purposes of this paper.

In view of these controversies and uncertainties associated with high speed machining technology there is a need for a mathematical simulation model that is capable of describing high speed cutting processes.

Therefore, the main aim of this paper is to describe the development of a high speed cutting simulation model for milling operations. In addition, the model aims to assist in understanding the high speed machining process and provide valuable insight into chip management, spindle specifications and machine tool requirements.

2 HIGH SPEED MACHINING GEOMETRICAL MODEL

When considering the milling operation at high cutting speed the geometry of the chip section has to be carefully studied since the sectional area of the chip changes continuously as the cutter tooth proceeds. Furthermore, in the case of the helical cutter, the width as well as the thickness of the chip changes with the angle of advancement of the cutter tooth in the workpiece material. Therefore, for the purpose of this investigation, Fig 1a illustrates schematically the geometrical model of the cutting process employed, the model force resolution diagram is shown in Fig 1b whilst the velocities vector diagram is illustrated in Fig 1c. In order to simplify the model it was assumed that the operation is two dimensional peripheral milling and no cutting fluid is applied. It is further assumed that each chip particle formed follows an identical curved path through a shear deformation zone of finite thickness and its velocity changes progressively from the cutting velocity to shearing velocity and finally to chip velocity. The chip is formed in a plastic deformation zone which runs from the tool cutting edge to the chip/work free surface and further plastic flow occurs in a thin layer of chip adjacent to the tool/chip interface. From this geometric viewpoint the cutting ratio i.e. the ratio of depth of cut to the chip thickness

is the basic variable which defines the geometry of the cut needed to calculate the shear angle. The basic method of solution is to analyze the stresses along AB and the tool/chip interface in terms of the shear angle (Fig 1a), workpiece material properties and then to select the shear angle so that the resultant forces transmitted along AB and the tool/chip interface can be determined. Once the shear angle and the forces are known the corresponding temperature and other process parameters can be found.

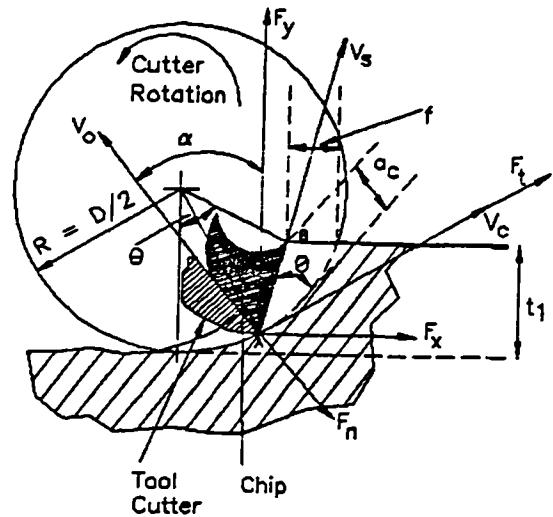


Fig 1a Developed peripheral geometrical two dimensional model

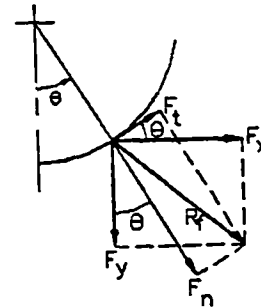


Fig 1b Model force resolution

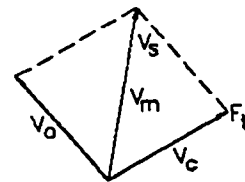


Fig 1c Velocities vector diagram

2.1 Work material properties

For the computer simulation model it is necessary to know the relevant tool/workpiece material properties such as flow stress, yield stress, brinell hardness, shear

stress etc. for the appropriate conditions of strain, strain rate and temperature. The dynamic behaviour of steel, aluminium and titanium alloys has been examined (6), and the following equations are shown to provide a good estimate of the dynamic strength as a function of Brinell hardness (BHN):

$$\sigma_y = 3.92 \text{ BHN} \quad (1)$$

$$\Psi = 4.55 \text{ BHN} \quad (2)$$

$$\sigma_s = \sigma_y + \Psi \epsilon_p \quad (3)$$

Where σ_y is the uni-axial tensile dynamic yield stress, σ_s is the true flow stress, ϵ_p is the natural plastic strain and Ψ is the work hardening coefficient. By applying the deformation theory of plasticity to equation (3), the dynamic shear stress, the shear strain and strain rate were computed by :

$$\tau_s = \frac{\sigma_y + \Psi \left(\frac{\gamma}{1.732} \right)}{1.732} \quad (4)$$

$$\gamma = \frac{1}{\tan(\phi)} + \tan(\phi - \alpha) \quad (5)$$

$$\dot{\gamma} = \frac{0.2 V_c \cos \alpha}{S_1 \cos(\phi - \alpha) 60000} \quad (6)$$

In a uniform continuous chip, if the total strain is given by equation (5), the maximum shear stress is computed using equation (4) and the shear yield stress τ_y is determined by setting $\gamma = 0$ in the equation, then the effective dynamic shear strength can be taken to be the average value by the following equation:

$$\tau = \frac{\tau_s + \tau_y}{2} \quad (7)$$

2.2 Cutting force derivations

The major significant difference between low speed machining and high speed machining is the influence of the cutting forces on the process parameters at high cutting speeds. Therefore it is vital to establish a theoretical foundation for cutting force at high cutting

speeds as it is the product of this force and the cutting speed which is the power at the cutting edge which in turn determines the metal removal rate and the required capacity of the machine tool. From established machining theory it is known that all forces created by interaction of the tool and chip are due to two main factors. Firstly, the shear deformation which in combination with the shear angle produces the shear force. Therefore, the magnitude of this shear force is computed by the following expression :

$$F_s = \frac{\tau t_1 b_1}{\sin(\phi)} \quad (8)$$

Secondly, since the uncut chip material passes through the shear plane, it gives rise to a momentum change and hence a momentum force acting parallel to the shear velocity vector or along the shear plane. The value of this force is given by :

$$F_m = \frac{b_1 t_1 V_c^2 \rho}{\cos(\phi)} \left(\frac{1}{1 + \tan(\phi) \tan(\alpha)} \right) \quad (9)$$

When machining at low speed the inertia force (momentum force) may be neglected as its value is insignificant compared to the shear force and other cutting forces. However, at high cutting speed its value may become exceedingly high since it varies with the square of cutting speed (4).

A possible combination of momentum and conventional forces have been developed by (4) as illustrated in Figure 2 where the momentum force and its resolved

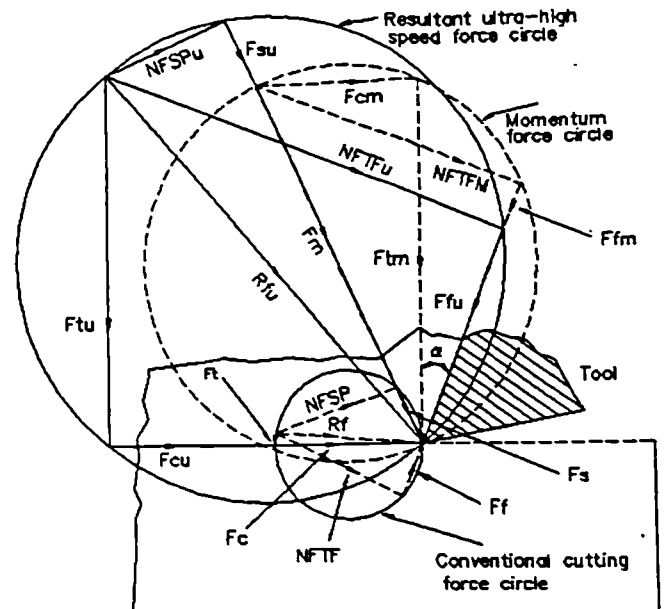


Fig 2 Force geometry for two dimensional low, high and ultra-high speed machining (4)

component have been added vectorially to the forces arising from the cutting mechanism to arrive at the resultant forces acting on the cutting tool. With increasing cutting speed, the ratio of F_m circle diameter to cutting force diameter would increase and R_n would more and more approach F_m in both magnitude and direction. The outstanding feature of the resultant force circle at high cutting speed is that both the normal cutting force F_{nu} and the friction force F_{fu} act in the direction opposite to their conventional directions, which would have repercussions on both tool and workpiece clamping arrangements.

If the value for the shear stress on the shear plane can be obtained from Equation 7 and the friction angle is known then from this investigation, it is possible to find other cutting forces by adding the momentum force values to the other forces found at low cutting speeds as shown below:

$$F_{cu} = \frac{\tau b_1 a_c \cos(\beta - \alpha)}{\sin(\phi) \cos(\phi + \beta - \alpha)} + F_m \quad (10)$$

$$F_{cu} = \frac{\tau b_1 a_c \sin(\beta - \alpha)}{\sin(\phi) \cos(\phi + \beta - \alpha)} + F_m \quad (11)$$

$$F_{nu} = F_c \cos(\alpha) - F_t \sin(\alpha) + F_m \quad (12)$$

$$F_{fu} = F_c \sin(\alpha) + F_t \cos(\alpha) + F_m \quad (13)$$

2.3 Cutting temperature derivations

The measurement and calculation of temperatures in any machining process is of utmost importance, however, it becomes even more imperative when high cutting speeds are involved. Heat is generated in the primary shear zone as the chip is first formed from the workpiece, and in the secondary zone as the chip interacts with the rake face of the tool. In conventional low speed machining the deformation rate is low and the process is considered to take place isothermally (7). However, with increased cutting speed, rapid plastic deformation occurs, and the local heat generation establishes steep temperature gradients. The physical features of these shear zones have been investigated by a number of workers (3, 7, 8), who show that seizure occurs at the tool rake face which has also been confirmed by other workers (9).

A set of equations has been presented (10) which allows the calculation of temperatures from readily measured cutting data. This approximate method is based on heat transfer in a moving material, the theory considers the heat generated in the primary zone and the standard heat transfer equations for a moving heat source with one boundary condition which is the heat flux due to secondary shear. This method gives rise to the following equations which were used in the mathematical model :

The thermal number of the material (Rt), is given by :

$$R_t = \frac{\rho V_c SHC a_c}{T_{con}} \quad (14)$$

The rate at which heat is generated by friction between the chip and tool is given by :

$$P_f = F_f V_o = F_f V_c r_c \quad (15)$$

However, if the rake angle (α) = 0, then $F_t = F_f$ and

$$P_f = F_t V_c r_c$$

The rate of total heat generated is given by :

$$P_m = F_{cu} V_c \quad (16)$$

The rate of heat generation by shearing is given by :

$$P_s = P_m - P_f \quad (17)$$

The average temperature of the chip resulting from the secondary deformation is given by:

$$T_f = \frac{P_f}{\rho SHC V_c a_c b_1} \quad (18)$$

The maximum temperature rise in the chip due to the frictional heat source in the secondary deformation zone is given by :

$$\delta T_m = T_f 1.13 \ln \left(\frac{R_s}{L_o} \right) \quad (19)$$

$$\text{where } L_o = \frac{(L_c r_c)}{a_c}$$

In developing a predictive theory for estimating the heat conducted into the workpiece (Hcw), it has been suggested (11-12) that an empirical equation (20) based on a compilation of experimental data by Boothroyd (13) can be used as shown:

$$H_{cw} = 0.5 - (0.35 \text{ Log } (R_t \tan \phi))$$

for $0.04 \leq R_t \tan \phi \leq 10.0$

and (20)

$$H_{cw} = 0.3 - (0.15 \text{ Log } (R_t \tan \phi))$$

for $R_t \tan \phi > 10.0$

The rate of heat generation in the primary deformation zone is P_s , and a fraction of this heat H_{cw} , is conducted into the workpiece, the remainder, $((1 - H_{cw}) P_s)$ is transported with the chip. Therefore, the average temperature rise δT_s , of the material passing through the primary deformation zone is given by :

$$\delta T_s = \frac{(1 - H_{cw}) P_s}{SHC V_c a_c b_1} \quad (21)$$

The maximum temperature along the tool rake face is given by :

$$T_{max} = T_m + T_s + T_o \quad (22)$$

2.4 Other process parameter derivations

It is important to establish the equations which relate to cutting parameters, such as metal removal rate, machining time and power. This will ensure a correct prediction of machining times, allow a comparison of selected cutting conditions and make a judgement as to whether the machine tool and available spindle power will withstand the selected cutting conditions. Therefore, the metal removal rate (ZW) can be expressed mathematically as:

$$ZW = t_1 b_1 f n Z \quad (23)$$

The power at the cut is computed by :

$$P_1 = \frac{F_{cu} V_c}{60\,000} \quad (24)$$

The specific metal removal rate is determined by:

$$ZWS = \frac{ZW}{P_1} \quad (25)$$

These equations are generally believed to describe adequately cutting process parameters at high cutting speed. However, experimental work is recommended to find the level of accuracy of these cutting equations.

3 THE NUMERICAL MODELLING OF HIGH SPEED MACHINING

Having derived the mathematical equations for the high

speed machining process, the task now is to develop a basic strategy to reformulate the developed equations into analytic expressions tailored for numerical modelling which are capable of predicting the torque and power characteristics for any given set of cutting conditions, spindle speed, metal removal rates, cutter specifications, cutting forces, cutting energy, and cutting temperature among other process parameters. However, to develop such a strategy will involve three main elements:

- (a) a determination of input parameters;
- (b) the selection of cutting equations that will meet the specified model requirements and
- (c) the presentation of the results.

Based on these criteria a theoretical modelling structure which forms the basis for the design and the development of the numerical model for cutting process evaluation in this study is shown in Fig 3. In order to

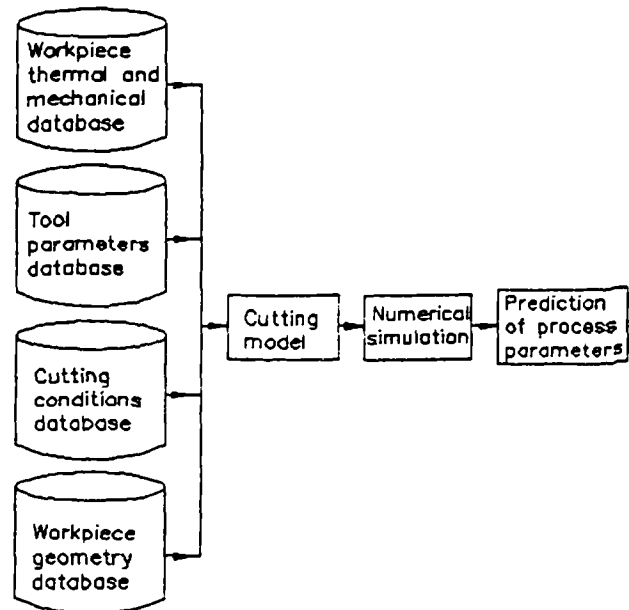


Fig 3 Flow diagram showing parameters for numerical simulation

make the modelling simple, this model has not included any constraints such as resource considerations, the manufacturing environment and tooling feasibility. The high speed milling computer model has been implemented in the Fortran programming language on the main Vax computer at Liverpool John Moores University. This model is illustrated in Fig 4. Databases were created for future access for the cutting conditions, the tool material and geometry data, the workpiece material geometry and the workpiece thermal and mechanical properties.

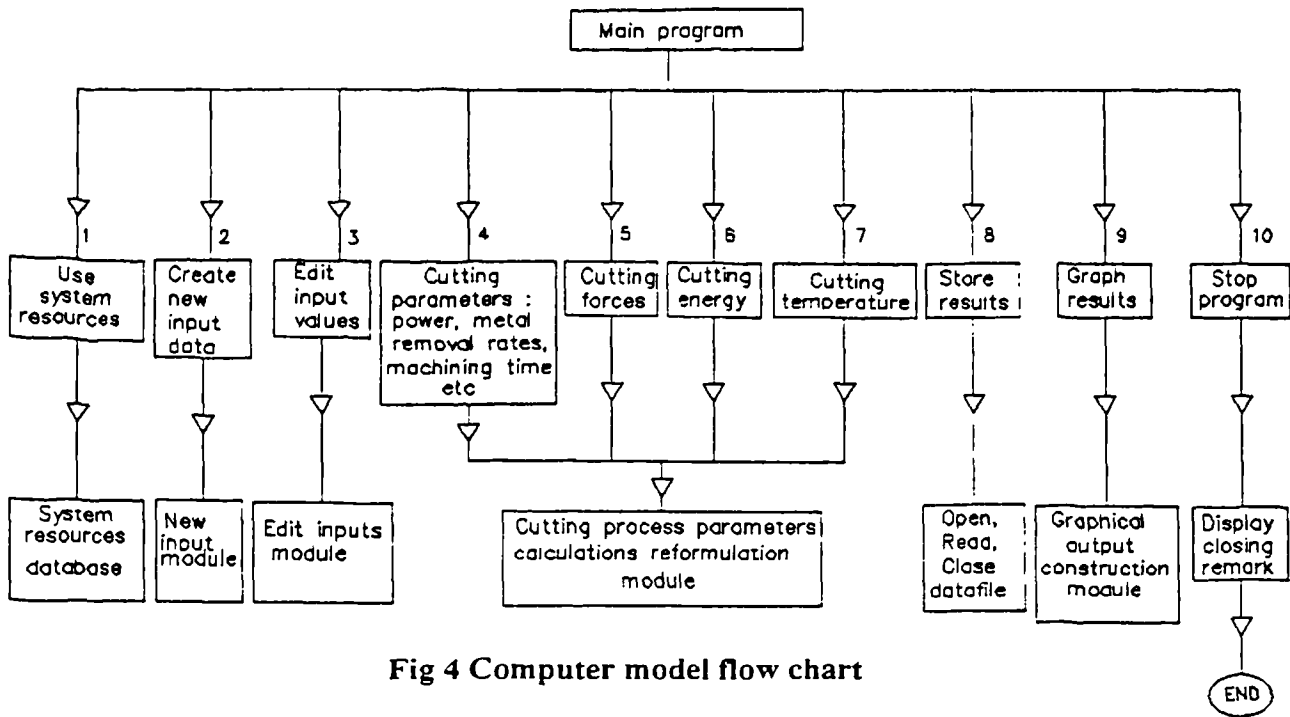


Fig 4 Computer model flow chart

4 SIMULATION RESULTS AND DISCUSSION

A number of simulations have been carried out to demonstrate and verify the model. Some of the results are presented below.

The relationship between the cutting speed and metal removal rate is illustrated in Fig 5 whilst Fig 6 shows typical relationship between the cutting speed and the volume of swarf removed per hour. It was observed in both figures that the metal removal rate and the volume of the metal removed increase linearly with increase in cutting speed, this can be ascribed to the fact that the metal removal rate is a function of the cutting speed. Fig 7 illustrates the relationship between the specific metal removal rate and the cutting speed. It was found that as the cutting speed increases the energy required to remove the deformed chips reduces, however not linearly, whilst the power required to remove the undeformed chips increases (14). This can be attributed to the effect of the momentum force which operates at high cutting speeds which requires an additional energy input. In depth experimental work is recommended to prove this theory.

From previous work (14) the relationship between the cutting speed and the cutting forces was simulated. It was observed that the cutting forces remained relatively constant at low cutting speed, ie. the magnitude of the momentum force is insignificant compared to the other cutting forces. However, as the cutting speed approaches 1 500 m/min, its magnitude starts to increase, consequently causing the other forces also to

increase. When the relationship between cutting speed and the cutting temperatures was simulated it was found that the workpiece and the average shear zone temperatures decrease with increasing cutting speed whilst chip and tool rake face temperatures increase. The increase in chip and tool rake face temperatures can be attributed to the increase in energy dissipation at the tool face. The decrease in the workpiece and shear zone temperature at high speed may be due to the fact that as the cutting speed increases there is less time available for the heat generated to conduct into the

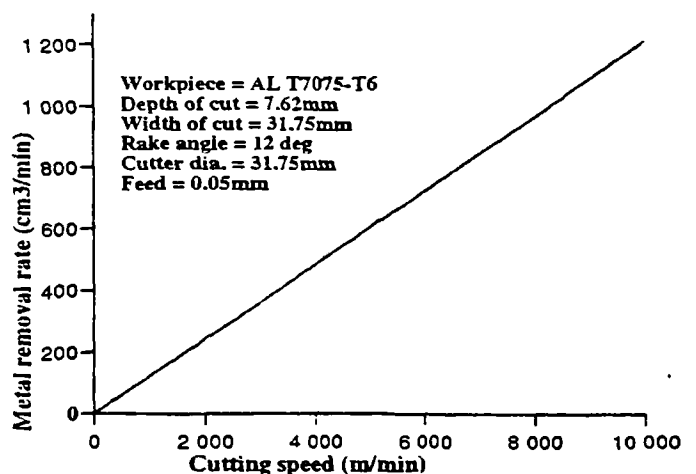


Fig 5 The relationship between the metal removal rate and cutting speed

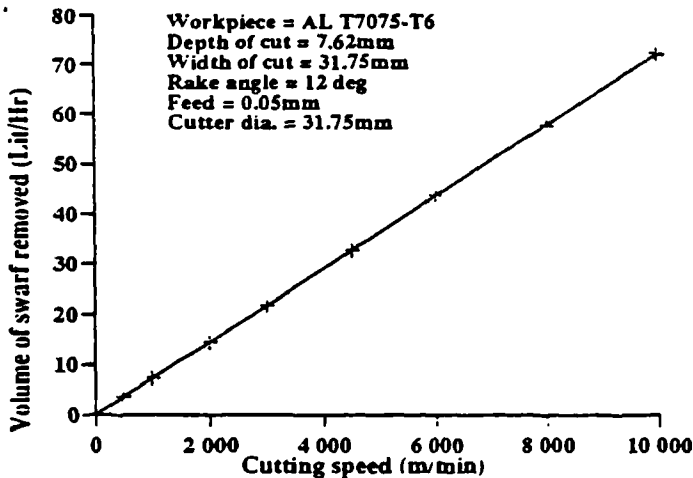


Fig 6 The relationship between the volumes of swarf removed and the cutting speed

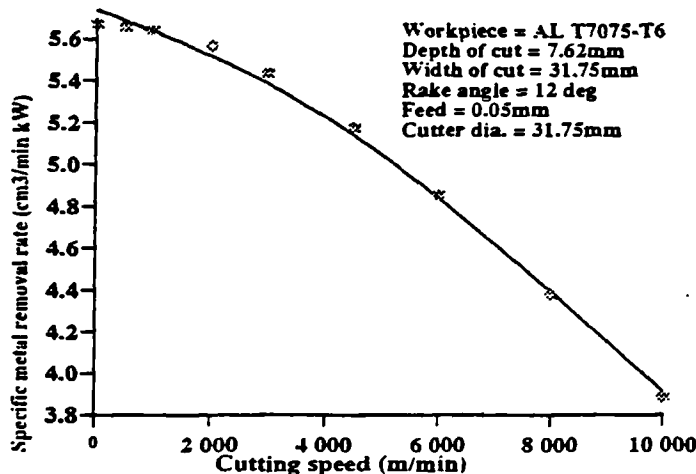


Fig 7 The relationship between the specific metal removal rate and the cutting speed

workpiece, so that the heat is effectively carried away with the chip. These simulated results of this model compared well with (4, 9, 15-19).

The model would certainly enable aerospace and other manufacturing industry to utilise fully their production facilities by allowing optimisation of the high speed cutting process parameters within the given limitation. To facilitate this, the model interactively allows for selection of the process parameters from the created database, or alternatively the user can input new cutting parameters if the available data from the system database is not suitable. In addition, the system database and the programming structure are designed to allow for future expansion, modifications and presently

the simulation results can be displayed numerically or graphically for real time analysis.

In any manufacturing environment the main objective has always been to be able to select the optimum cutting parameters in order to use the maximum available full spindle speed and machine tool power. This model has addressed these problems, also by the model's capability to compute the volume of metal removed and other process parameters instantaneously, specifications for the machine tool, the spindle and in particular the swarf removal techniques required to handle large volumes of swarf at high cutting speed can be determined at the product process planning stage. Therefore, this model will assist in the process planning, helping to reduce setup, tape proving time and production costs significantly.

5 CONCLUSION

In this paper a computer based mathematical model and associated software for the high speed milling process for cutting process predictions has been developed and assessed qualitatively and quantitatively by numerical simulation. Firstly, a theoretical analysis of the high speed machining process was carried out for the milling process. The developed equations were reformulated into analytic expressions tailored for numerical modeller use. The overall conclusions of this study are summarised below:

(a) It was established that the major significant difference between low speed machining and high speed machining is the influence of the cutting forces on the process parameters at high cutting speeds. From the resultant cutting force circle analysis it was found that both the normal cutting force and the friction force act in the direction opposite to their conventional directions which suggests that additional measures may be needed for both tool and workpiece clamping arrangements at high cutting speeds.

(b) This model provides a mechanism to predict cutting process parameters which will allow a comparison of selected cutting conditions and make a judgement as to whether the machine tool and available spindle power will withstand the selected cutting conditions.

(c) The model provides a foundation upon which adaptive optimisation strategies for high speed machining may be developed by integrating process parameters selection and manufacturing system elements constraints in the process planning.

REFERENCES

- (1) FLOM, D.G., KOMANDURI, R and LEE, M. High speed machining of metals, Annual Review of Materials Science, 1984, 4, 231.
- (2) SCHULTZ, H. High speed milling of aluminium alloys, Proc. of ASME high speed machining conf., 1984, PED 12, 241-244.
- (3) von TURKOVICH, B.F. Influence of Very High Cutting Speed on Chip Formation Mechanics, 7th NAMRC Proc. May 1979, 241-247.
- (4) ARNDT, G. Ultra-high Speed Machining : A Review and an Analysis of Cutting Forces. Proc. of Institute of Mech. Engineers (London), 1973, Vol 187, No 44/73, 625-634.
- (5) RECHT, R.F. A Dynamic Analysis of High Speed Machining, Proc. of SAME High Speed Machining Conf., 1984, PED 12, 83-93.
- (6) RECHT, R.F. Taylor Ballistic Impact Modelling Applied to Deformation and Mass Loss Determination. Int. J. Eng. Sci. 1978, 16, 809-827.
- (7) WRIGHT, P.K and ROBINSON, J.L. Material behaviour in deformation zone of machining, Journal of metal technology, 1977, 4, 240.
- (8) TANAKA, Y, TSUWA, H and KITANO, M. Cutting mechanism in Ultra-high speed machining, ASME, Proc. of Prod. Engineering Conf., Cleveland Ohio, May 2-4, 1967, 1-12.
- (9) WRIGHT, P.K and BAGCHI, A. Tool wear process in high speed machining, Manuf. Eng. Trans 1980 North America Manuf. Res. Conf. Proc. 8th, 1980, 277- 284.
- (10) BOOTHROYD, G and KNIGHT, W. A. Fundamentals of metal machining and machine tools, 2nd Ed, Marcel Dekker, Inc., 1989, 109-127.
- (11) TAY, A.O, STEVENSON, M.G, De VAHL DAVIS, G and OXLEY, P.L.B. A Numerical Method for Calculating Temperature distribution in Machining, From Force and Shear Angle Measurements, Int. J. of Machine Tool Des. and Res., 1978, 16, 335-349.
- (12) MATTHEW, P. Use of Predicted Cutting Temperatures in Determining Tool Performance, Int. J. of Mach. Tools Manufacturing, 1989, Vol. 29, No 4, 481-497.
- (13) BOOTHROYD, G. Temperatures in orthogonal metal cutting, Proc. Inst. Mech. Engineers, 1963, 177, 789-802.
- (14) DAGILOKE, I.F, KALDOS, A, DOUGLAS, S and MILLS, B. High Speed Machining: An Approach to Process Analysis. Int. Conf. on Advances in Materials & Processing Tech., Dublin, 1993, 63-70.
- (15) KING, R.I and McDONALD, J.G. Production Design Implications of New High-Speed Milling Techniques, Journal of Engineering for Industry, ASME, Nov. 1976, p176.
- (16) OKUSHIMA, K, HOTOMI, K., ITO, S and NARUTAKI, N. A Fundamental Study of Super-high Speed Machining, Bul. Japanese Society of Mechanical Engineers, 1965, 8, No 32, 702.
- (17) BER, A, ROTBERG, J and ZOMBACH, S. A Method for Cutting Force Evaluation of End Mills. Annals of the CIRP, 1988, 37/1, 39.
- (18) ARMAREGO, E.J.A and DESHPANDE, N.P. Computerized End-Milling Force Predictions with Cutting Models Allowing for Eccentricity and Cutter Deflections, Annals of the CIRP, 1991, 40/1, 27.
- (19) STOCK, T.A.C and THOMPSON, K.R.L. Penetration of Aluminium Alloys by Projectiles. Metall. Trans., 1970, 1, 219-224.

A GENERIC COMPUTER MODEL FOR HIGH SPEED MACHINING WITH AN INTEGRATED DATABASE

Mr Israel Dagiloke, Dr Andrew Kaldos, Dr Steve Douglas and Prof Ben Mills

*School of Engineering and Technology Management
Liverpool John Moores University, Liverpool, L3 3AF*

The selection of optimum cutting parameters for high speed machining (HSM) is absolutely critical and dependent on the adequacy of the cutting model employed. The general equations best describing the high speed machining process form a set of non-linear and partial differential equations which are too complex to solve analytically. A numerical solution is therefore required involving a reliable technique for developing an adequate computer model. In this paper an interactive generic computer model for evaluating the cutting process at high cutting speed complete with an integrated database is developed and discussed.

Introduction

The fundamental reason why there has been significant interest both in the metal cutting industry and research community in recent years in high speed machining technology is the claim that it can dramatically increase metal removal rates resulting in reduced machining times and increased productivity, Flom, Komanduri and Lee (1984). Despite the importance of the high speed machining process, very little has been published on the cutting process prediction at high cutting speed. This can be attributed to the fact that the high speed machining process is, perhaps, one of the most complex of the manufacturing methods employed today. It involves various input and output parameters linked together through a multitude of complex interactions.

It is well documented by King and Vaughn (1984), that as the cutting speed increases above the conventional speed range, new dynamic ranges are encountered, for example, in respect of the cutter and material interface, the basic chip morphology changes as new cutting phenomena are experienced which include the momentum force effects caused by momentum change of the chip from undeformed to deformed chip in the shear zone. The emergence of momentum force at high cutting speed causes an increase in the cutting forces and the cutting power. The

result of this is that machine tools must have adequate power, speed control and that the prediction of process parameters is vital in the machine tool design process.

Experimental data and a satisfactory mathematical simulation model are therefore vital in determining the factors which influence productivity at high cutting speed. Due to the complexity of the physical processes involved at cutting speeds above 600 m/min, reliable analytical and experimental data on cutting forces and temperatures are virtually non-existent or limited in the public domain. Information on cutting process parameters at high cutting speed is therefore of both practical and fundamental value.

An in-depth literature review and the study of the manufacture of large aerospace components suggests that efficiencies of HSM have been investigated to some extent by King and McDonald (1976). Although the purpose of HSM has been based on economies in production, most of the previously published work has focused on the difference in cutting mechanism between high speed and conventional low speed machining rather than in improving the economics of production von Turkovich, (1979), Arndt (1973), Okushima, Hotomi, Ito and Narutaki (1965). A neglected aspect of high speed machining technology has been the implementation of the technology in industry based on a systematically integrated total analysis of the high speed machining process.

The purpose of this paper is to describe a generic computer process model with integrated databases that can be used to predict the effects of the input cutting parameters (cutting speed, feed, rake angle and depth of cut) on the cutting process and on the selection of machine tools, cutting tools and workpiece materials in high speed machining in an interactive way.

Numerical modelling techniques of HSM and program design

In developing the cutting process model, several areas of workpiece behaviour and the mechanics of machining were explored. As an essential part of this research work, relevant cutting models related to this study were compiled and in some cases critically modified to suit conditions of the present application. The philosophy used was to create and implement an extensive and comprehensive theoretical model, based mathematically on basic cutting process parameters. Such a model makes it possible to show at a glance what the dependency of the cutting parameters and their effect within the simulated results. Further, by solving the equations, simultaneously as a set, it is possible to show how the user's choices affect the results of the model.

A computer program for modelling high speed machining processes partly based on general equations published by Dagiloke, Kaldos, Douglas and Mills (1994) and some other basic equations of the mechanics of cutting has been developed to obtain the cutting power, forces, temperature and other process parameters. To establish a broad data base for future access, all the data acquired for workpiece and tooling mechanical and thermal properties, cutting conditions, workpiece geometries, tooling geometries, machine tool parameters, generated

numerical and graphical results data were stored on a DEC Vax computer system.

Numerical modelling structure

Figure 1. illustrates the structure of the cutting simulation system which consists of three major modules: integrated input database, numerical simulation and output modules.

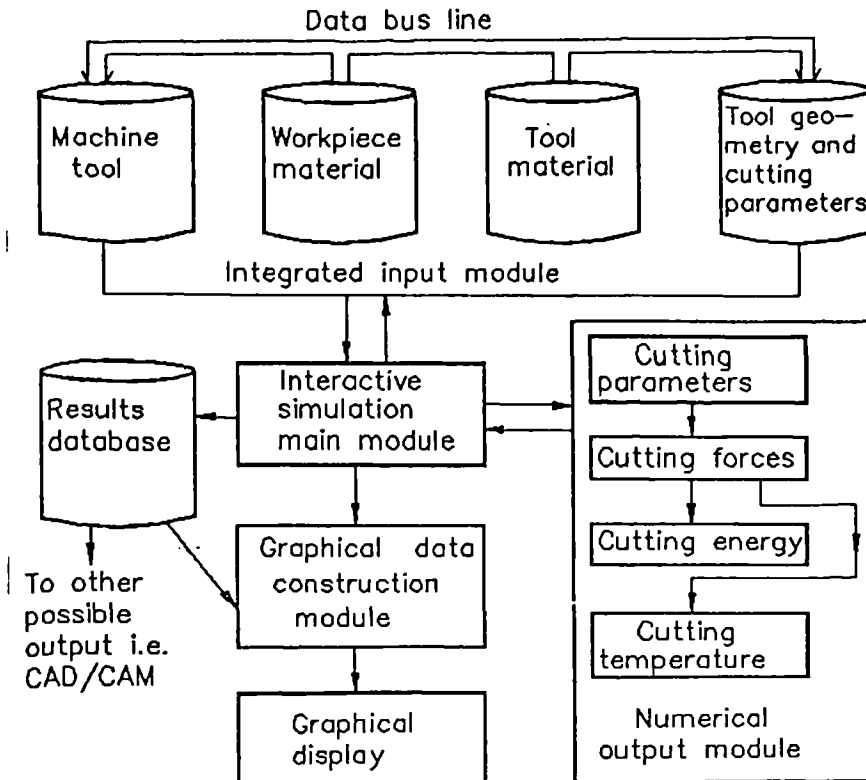


Figure 1. The structure of the cutting simulation model.

The input module has an integrated database on the following modules:

- (i) Workpiece and tool materials thermal and mechanical properties, e.g. workpiece density, thermal conductivity, specific heat capacity, initial workpiece temperature and Brinell hardness.
- (ii) Tool geometry: Tool diameter, number of teeth or flutes, tool shank diameter, rake angle and flute length.
- (iii) Workpiece geometry : Blank size, length, height, width and geometrical features.
- (iv) Cutting parameters : Feed, feed rate, depth of cut, width of cut and cutting speed.
- (v) Machine tool parameters: Range of operation for feed rate in x,y and z axes, spindle speed and power, tool length/diameter in x,y and z axes, i.e. working envelope.

Having identified the set of input information required, the program was

designed to transform the geometric, mechanical and thermal properties information of the workpiece, tools, machine tool and cutting conditions from the databases into a suitable form for simulation. Alternatively a new set of input data can be entered into the model. The workpiece, tool, machine tool and cutting conditions data files in the modules can be edited making it possible to update and expand the databases. The input module can also be edited prior to cutting simulation.

The numerical simulation module has a built-in numerical data controller with four sub-modules which are to be selected in pre-determined order. The output module generates the numerical output data and graphical representation of the cutting process based on the numerical data obtained through the "Results database". Typical examples of graphic outputs obtained during the cutting simulations are shown in Figure 2.

Numerical simulation results

Tool forces play an important role in the economics of the metal cutting process. They control the energy consumed as well as the power requirements of the process. Therefore, the chosen simulation results which demonstrate the capability of this cutting model is the relationship between the principal cutting force, the momentum force and the cutting speed as illustrated in Figure 2. It can be seen that at low cutting speed the principal cutting force remained relatively constant, whilst, the momentum force magnitude is very low. However, as the cutting speed approaches 1200 m/min, momentum magnitude starts to increase, consequently causing the principal cutting force to increase due to the fact that the vector sum of the momentum force has to be added to the values of the main cutting force. From previous work Dagiloke, Kaldos, Douglas and

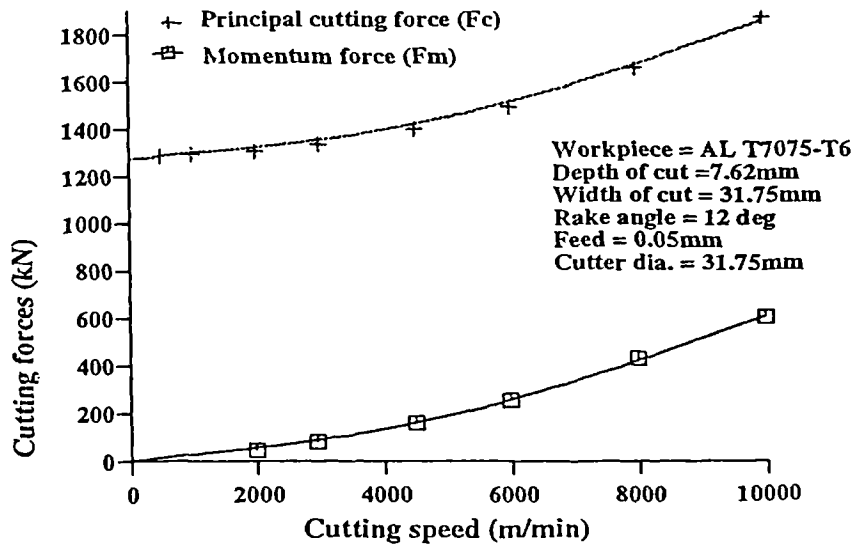


Figure 2. The relationship between the cutting speed and the cutting forces.

Mills (1993) the relationship between the cutting speed and the cutting temperatures was simulated. It was found that the workpiece and the average shear zone temperatures decrease with increasing cutting speed whilst chip and tool rake face temperatures increase. The increase in chip and tool rake temperatures can be attributed to the increase in energy dissipation at the tool face. Dagiloke et al (1994) suggested that as the cutting speed increases the energy required to remove the deformed chips reduces, however, not linearly, whilst the power required to remove the undeformed chips increases due to the effect of the momentum force. The simulated results of this model compared well with experimental data Arndt (1973), King et al (1976), Okushima et al (1965), Ber, Rotberg and Zombach (1988).

Conclusion

A generic computer model with an integrated database suitable for high speed machining has been developed and assessed by numerical simulation. Firstly all the necessary input elements were identified and discussed followed by the formulation of the required equations and programming design. In this study an extensive and comprehensive theoretical model, based mathematically on basic cutting process parameters has been created. This model makes it possible to show at a glance the dependency of the cutting parameters on cutting speed. Further, by solving the equations, simultaneously as a set, it is possible to show how the user's (process engineer) choices affect the results of the model.

References

- Arndt G. 1973, Ultra-high Speed Machining : A Review and an Analysis of Cutting Forces, *Proc. of Inst. of Mech. Eng. (London)*, 1973, Vol 187, No 44/73, 625-634.
- Ber A. Rotberg J and Zombach S.A. 1988, Method for Cutting Force Evaluation of End Mills, *Annals of the CIRP*, 37/1, 39.
- Dagiloke I.F., Kaldos A., Douglas S. and Mills B. 1994, Developing High Speed Cutting Simulation Suitable for Aerospace Components, *Aerotech '94*.
- Dagiloke I.F., Kaldos A., Douglas S. and Mills B. 1993, High Speed Machining: An Approach to Process Analysis, *Int. Conf. on Advances in Materials & Processing Tech.*, Dublin, 63-70.
- Flom D.G. Komanduri R. and Lee M. 1984, High Speed Machining (hsm) of Metals, *Ann.Rev.Materials Science*, Vol. 14, 231.
- King R.I. and Vaughn R.L. 1984, A Synoptic Review of High Speed Machining from Salomon to the Present, *Proc. of ASME HSM Conf. PED 12*, 2.
- Recht R.F. 1984 A Dynamic Analysis of High Speed Machining, *Proc. of ASME High Speed Machining Conf. PED 12*, 83-93.
- King R.I. and McDonald J.G. 1976, Production Design Implications of New High-Speed Milling Techniques, *Journal of Engineering for Industry*, ASME, 176.
- Turkovich von B.F. 1979, Influence of Very High Cutting Speed on Chip Formation Mechanics, *7th NAMRC Proc.*, 241-247.
- Okushima K, Hotomi K., Ito S and Narutaki N., 1965, A Fundamental Study of Super-high Speed Machining, *Bul. Jap. Soc. of Mech. Eng.*, 1965, 8, No 32, 702.

A GENERIC PROCESS MODEL FOR HIGH SPEED MILLING

Israel Dagiloke, Andrew Kaldos, Steve Douglas and Ben Mills
Liverpool John Moores University, Liverpool, England

SUMMARY

Process modelling and experimental data for the model database are of vital importance in determining the factors which influence productivity at high cutting speed. The simulation process model developed primarily for milling represents low cutting speed and high speed operations so that it can be applied to the whole cutting speed range. Applications of a generic computer model to the high speed milling process is described. The problems associated with the cutting process prediction at high cutting speeds are discussed.

1.0 INTRODUCTION

The implementation of high speed machining (HSM) presents a challenge since various factors limit the extent to which cutting speeds may be advantageously increased. These factors include the cutting temperature, the cutting tool material, the cutting geometry, the workpiece material, the machine tool design, the cutting power, the surface integrity and metallurgical condition of the workpiece.

It has been documented [1] that as the cutting speed increases above the conventional speed range, new dynamic effects are encountered as the basic chip morphology changes due to the momentum force. It has been suggested [2] that this momentum effect arises when additional energy has to be supplied to accelerate the chip past the shear zone.

Based on these problems, process modelling and experimental data are vital in determining the factors which influence productivity at high cutting speed. Detailed information on the cutting process is necessary to improve understanding of high

speed machining and enhance acceptance of the process.

An in-depth literature review indicates that the efficiency of HSM has been investigated to some extent for the machining of aluminium alloys, steels, iron and titanium alloys [3-7]. However, there has been no significant published work relating to simulation of the HSM process including cutting forces, momentum force, cutting energies and cutting temperatures. This can be attributed to the fact that the high speed machining process is one of the most complex manufacturing methods employed today. It involves various input and output parameters linked together through a multitude of complex internal interactions.

Therefore, the aim of this paper is to establish an analytical investigative technique and a generic process model that can be used to predict the effects of these independent cutting parameters on the milling process, the selection of machine tools and cutting tools and the effect on workpiece materials at high cutting speed.

2.0 THE PROCESS MODEL FOR MILLING

A complete description of the milling process requires the determination of the chip thickness and the shear angle produced when the cutting tool first penetrates the surface of the workpiece. The solution of this problem requires the establishment of a cutting model and selection of all the necessary equations that describes both low and high speed milling operations. The areas where process equations should be identified are: (i) strain and strain rate; (ii) machining stresses; (iii) cutting power and forces; (iv) cutting energies and temperatures.

It is also necessary for the process model to predict correctly the stress level at which material separation occurs, to determine the chip thickness and shear angle which can be used to calculate the cutting forces, energies and temperatures. However, to derive these required relationships it is vital to analyse the geometry of the chip section since the sectional area of the chip changes continuously as the cutter tooth moves along the workpiece. Furthermore, in the case of the helical cutter, the width as well as the thickness of the chip changes with the angle of advancement of the cutter tooth in the workpiece material.

Figure 1. illustrates the face milling process with associated cutting forces. Due to the intermittent material removal the cutting forces may vary between negative and positive values. This dynamic nature of the process makes the modelling technique very difficult. The generic force resolution diagram is shown in Figure 2. which applies to all conceivable milling operations. To determine the principal cutting force F_c and the cutting power P_c , the tangential force F_T needs to be found as a resultant force of F_x and F_y cutting force components in the work plane. The tangential force was obtained from equation:

$$F_T = F_x * \cos\alpha + F_y * \sin\alpha$$

and the cutting power is given by:

$$P_c = F_T * V_c$$

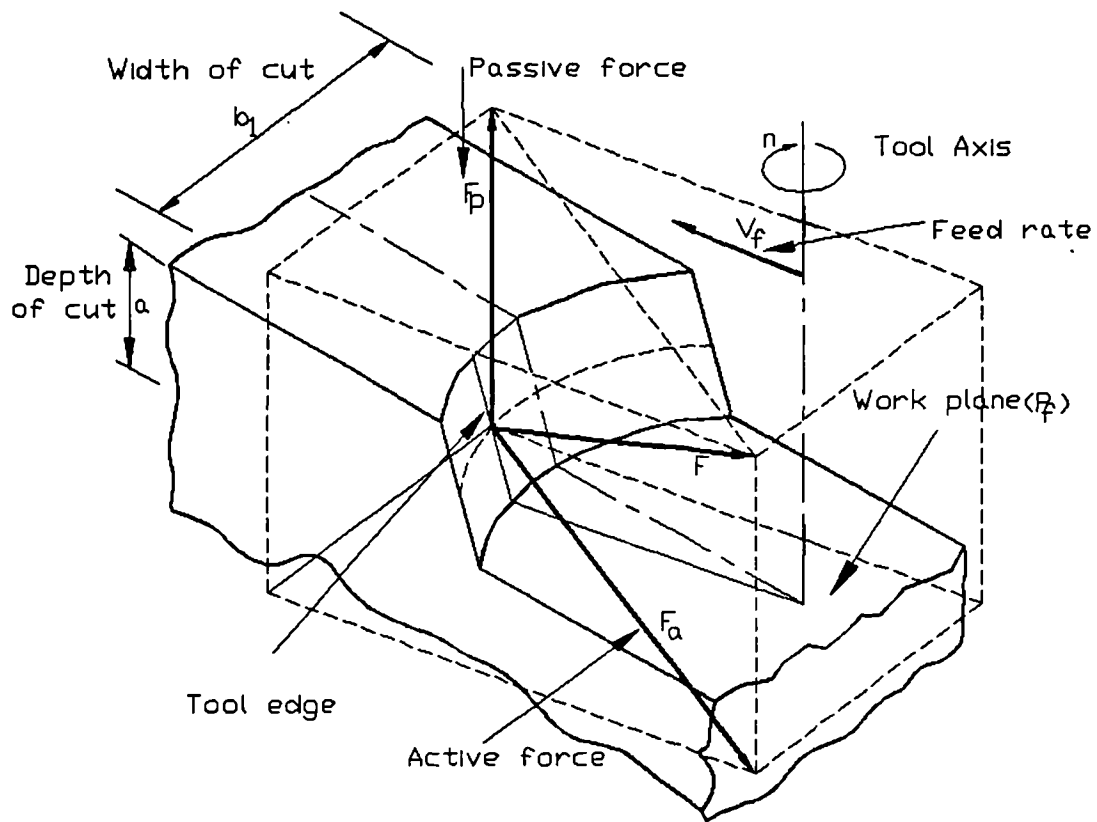


Figure 1: General milling geometrical model

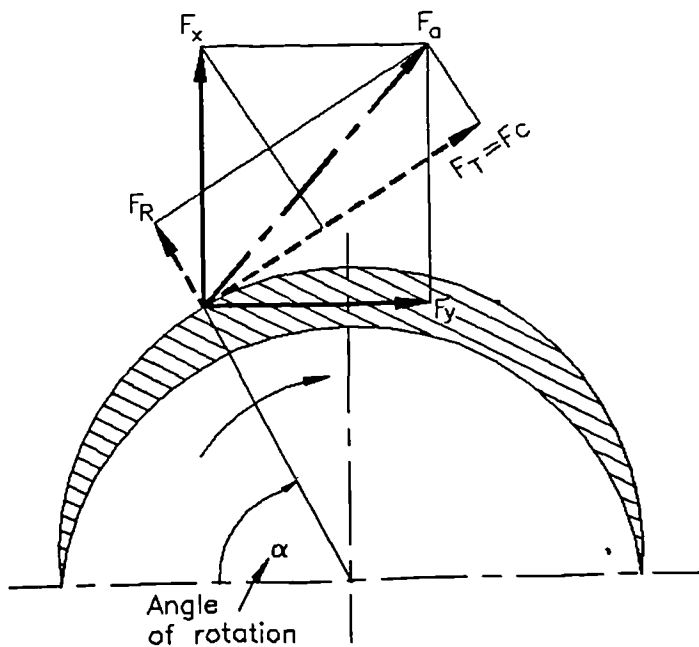


Figure 2: Force resolution

The aim now is to simulate the milling process to correlate with the measured data. The analysis used in this investigation is based on previously published work [8-11].

3.0 NUMERICAL MODELLING STRUCTURE

Figure 3. illustrates the structure of the cutting simulation model which consists of three major modules: integrated input database, numerical simulation and output modules.

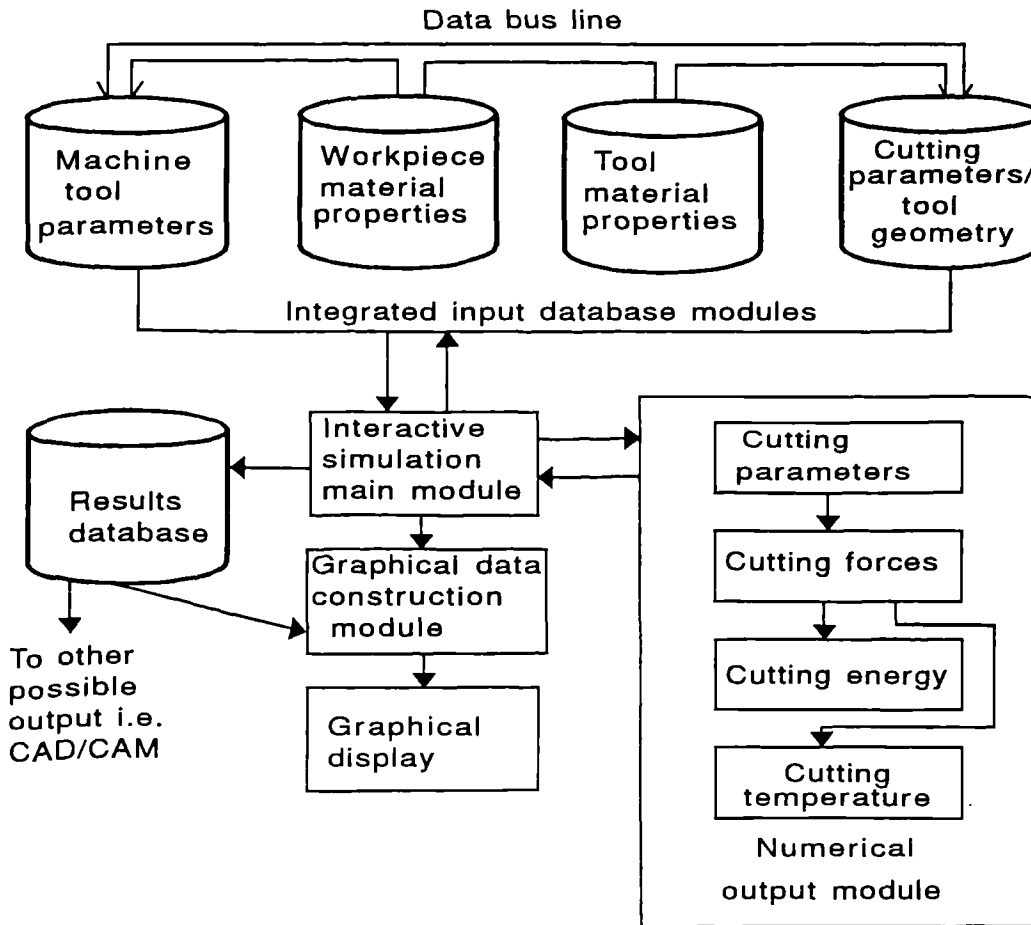


Figure 3: The structure of the simulation model

The input module has an integrated database including the following modules:

- (i) Workpiece materials: workpiece density, thermal conductivity, specific heat capacity, initial workpiece temperature and hardness.
- (ii) Tool materials: tool density, thermal conductivity, specific heat capacity, initial tool temperature.
- (iii) Tool geometry: tool diameter, number of teeth or flutes, tool shank diameter, rake angle and flute length.
- (iv) Workpiece geometry: blank size, length, height, width and geometrical features.
- (v) Cutting parameters: feed, feed rate, depth of cut, width of cut, and cutting speed.
- (vi) Machine tool parameters: range of operation for feed rate in x, y and z axes, spindle speed and power, tool length/diameter in x, y and z axes, i.e. working envelope.

The process model was designed to transform the geometric, mechanical and thermal properties information of the workpiece, tools, machine tool and cutting conditions from the databases into a suitable form for simulation. Alternatively, a new set of input data can be entered into the model. The workpiece, tools, machine tool and cutting conditions data files in the modules can be edited making it possible to update and expand the databases. The input module can also be edited prior to cutting simulation.

The numerical simulation output module has an in-built numerical data controller with four sub-modules, which determine the cutting parameters, cutting forces, cutting energy and cutting temperatures respectively. The simulation output module allows for the selection of sub-modules in a pre-determined order. The numerical output module generates both the numerical output and graphical representation of the milling process based on the numerical data obtained through the "Results database".

The philosophy used was to create and implement an extensive and comprehensive process model, based on milling cutting process parameters. Such a model makes it possible to show at a glance the dependency of the cutting parameters and their effect within the simulated results.

The full conceptual algorithm of the simulation model for the milling process analysis of both conventional and high speed machining is shown in Figure 4. The program is menu driven and designed to have a cutting speed flag indicator as part of its input subroutine. The objective of this cutting speed indicator is to alert the main program and the selection of the cutting equations to use every time there are changes in the input data that affect the value of the cutting speed. Also the main program itself has an in-built data pool controller subroutine to ensure that the correct data are retrieved and sent to the appropriate destination within the program. An in-built numeric data supervisor subroutine ensures that the simulated results data are sent to the appropriate output module.

4.0 RESULTS

To demonstrate the capabilities of the model the relationships between the principal cutting force, the cutting power and the cutting speed have been simulated as illustrated in Figure 5. The results suggest that at low cutting speed the principal cutting force remained relatively constant, whilst, the momentum force magnitude not shown in the figure is very low. However, as the cutting speed approaches 1200 m/min, the magnitude of the momentum force starts to increase, consequently causing the principal cutting force to increase due to the fact that the vector sum of the momentum force has to be added to the values of the main cutting force. It was observed that the cutting power increases almost linearly with an increase in cutting speed. Thus, when specifying the cutting speed for any given workpiece material, the power capability of the machine tool should be considered. The simulated results of this model compared well with other published experimental data[1] [6].

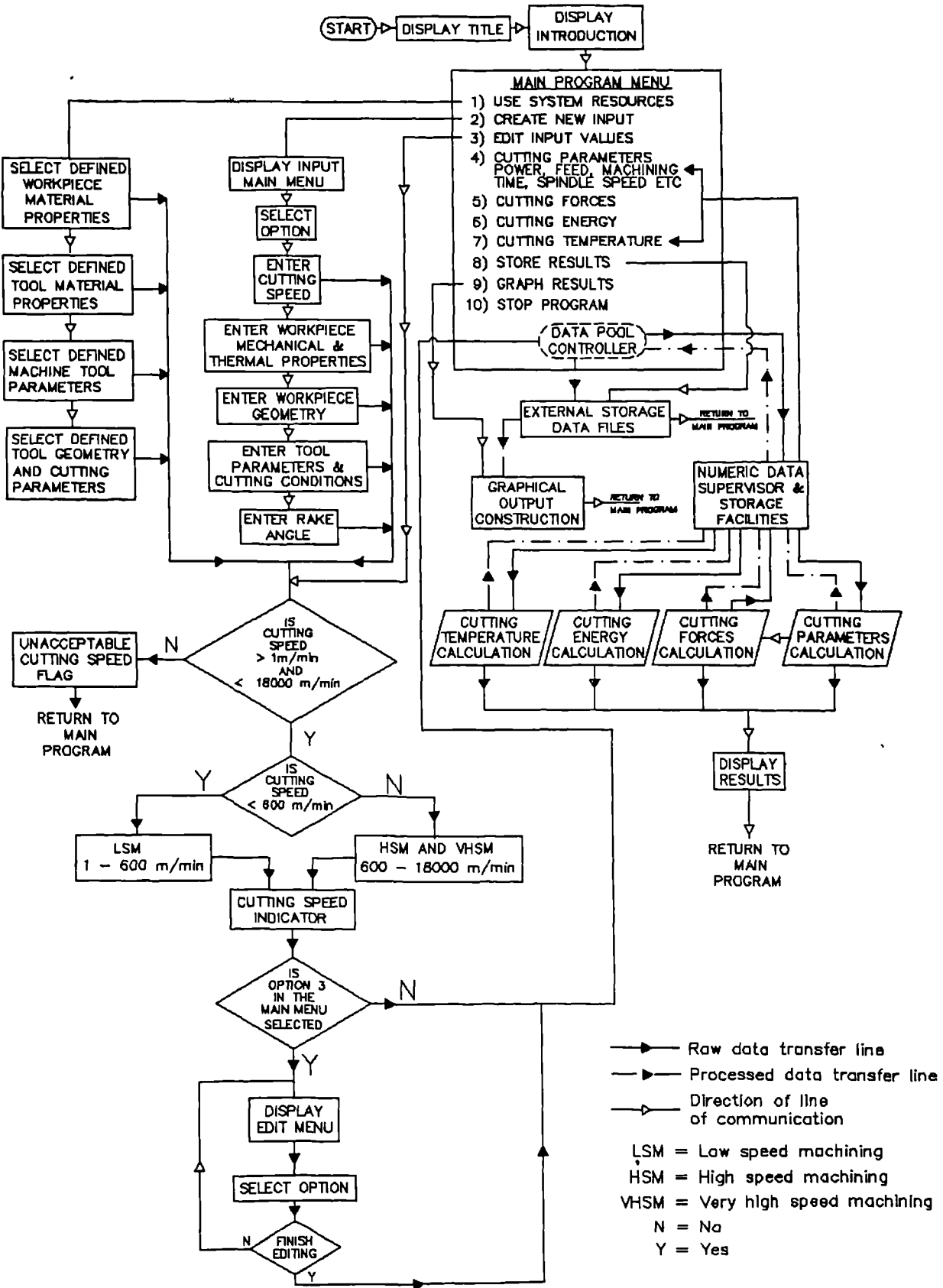


Figure 4: Modified conceptual algorithm for cutting process analysis

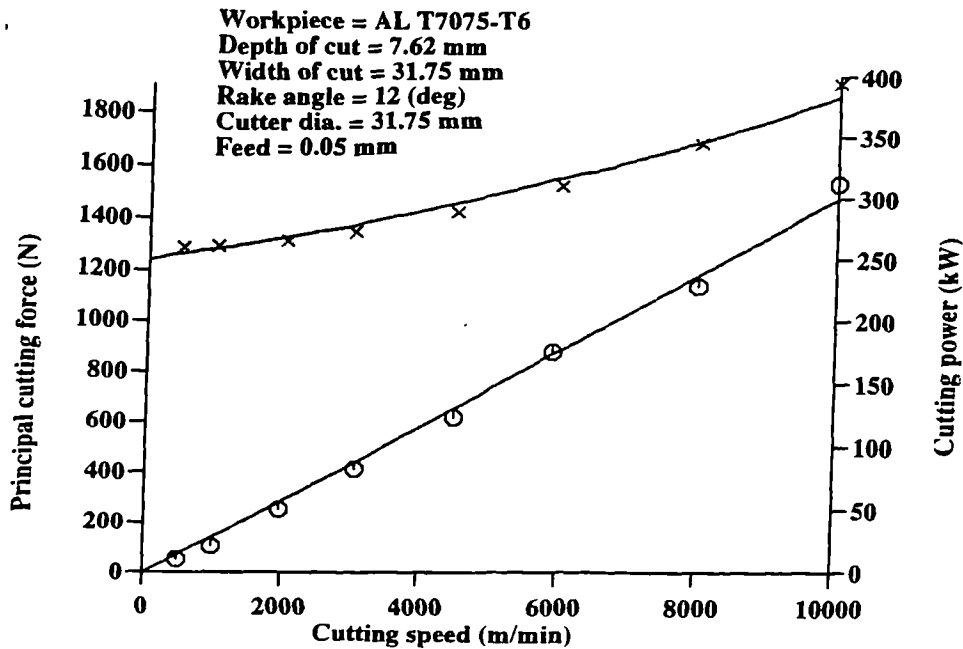


Figure 5: The relationship between the principal cutting force, cutting power and the cutting speed.

5.0 DISCUSSION AND CONCLUSIONS

In this paper a generic computer model with an integrated database suitable for high speed milling has been developed and assessed by numerical simulation. Firstly all the necessary input elements were identified and discussed followed by the formulation of the required equations and programming design. Also an extensive and comprehensive theoretical model, based mathematically on cutting process parameters has been created. This model makes it possible to show at a glance the dependency of the cutting parameters on cutting speed. Further, by solving the equations, simultaneously as a set, it is possible to show how the choice of the process engineer affects the results of the model.

The model certainly enables manufacturing industry to utilise fully their production facilities by allowing optimisation of the high speed cutting process parameters within the given limitation. To facilitate this, the model interactively allows for selection of the process parameters from the created database, or alternatively the user can input new cutting parameters if the available data from the system database is not suitable. In addition, the system database and the programming structure are designed to allow for future expansion, modifications and presently the simulation results can be displayed numerically or graphically for real time analysis.

In any manufacturing environment the main objective has always been to be able to

select the optimum cutting parameters in order to use the maximum available full spindle speed and machine tool power. This model has addressed these problems, also by the model's capability to compute the volume of metal removed and other process parameters instantaneously, specifications for the machine tool, the spindle and in particular the swarf removal techniques required to handle large volumes of swarf at high cutting speed can be determined at the product process planning stage. Therefore, this model will assist in the process planning, helping to reduce setup time, tape proving time and production costs significantly.

It has been established that the major significant difference between low speed machining and high speed machining is the influence of the cutting forces on the process parameters at high cutting speeds. From the resultant cutting force analysis it was found that both the normal cutting force and the friction force act in the direction opposite to their conventional directions which suggests that additional measures may be needed for both tool and workpiece clamping arrangements at high cutting speeds.

The model provides a foundation upon which adaptive optimisation strategies for high speed machining may be developed by integrating process parameter selection and manufacturing system constraints in the process planning.

REFERENCES

- [1] R.I.King and R.L.Vaughn: A Synoptic Review of High Speed Machining from Salomon to the Present, Proc. of ASME High Speed Machining Conf., PED 12, 1984, p.2.
- [2] H.Schulz and T.Moriwaki: High Speed Machining, CIRP General Assembly Annual Proceeding, August, 1992.
- [3] D.G.Flom, R.Komanduri and M.Lee: High Speed Machining of Metals, Annual Review of Materials Science, 1984, 4, p.231.
- [4] H.Schultz: High Speed Milling of Aluminium Alloys, Proc. of ASME High Speed Machining Conf., 1984, PED 12, 241-244.
- [5] B.F. von Turkovich: Influence of Very High Cutting Speed on Chip Formation Mechanics, 7th NAMRC Proc. May 1979, p.241-247.
- [6] G.Arndt: Ultra-High Speed Machining : A Review and an Analysis of Cutting Forces, Proc. of Institution of Mech. Engineers (London), 1973, Vol 187, No 44/73, p.625-634.
- [7] R.F.Recht: A Dynamic Analysis of High Speed Machining, Proc. of SAME High Speed Machining Conf., 1984, PED 12, p.83-93.
- [9] A.Kaldos, E.Nagy. and J.Takacs: Cutting Technology and Cutting Tools, Technical Publishing Company, Budapest, 1981, J4-790
- [8] I.F.Dagiloke, A. Kaldos, S. Douglas and B. Mills: Developing High Speed Cutting Simulation Suitable for Aerospace Components, AeroTech '94, Birmingham
- [10] I.F.Dagiloke, A.Kaldos, S.Douglas and B.Mills: High Speed Machining: An Approach to Process Analysis, Int. Conf. on Advances in Materials & Processing Technology, Dublin, 1993, p.63-70.
- [11] I.F.Dagiloke, A.Kaldos, S.Douglas and B.Mills: A Generic Approach to Process Modelling in High Speed Milling, 10th N.C.M.R. Conf., Loughborough, 13-15. September 1994, (accepted for publication)

Appendix: Experimental workpiece material properties

British Standard Aerospace Series : Specification for

Bars and extruded sections of aluminium – copper – magnesium – silicon – manganese alloy

(Solution treated and artificially aged)

(Not exceeding 200 mm diameter or minor sectional dimension)

(Cu 4.4, Mg 0.5, Si 0.7, Mn 0.8)

Série aérospatiale: Spécification des barres et profilés filés en alliage d'aluminium-cuivre-magnésium-silicium-manganèse (Traités pour mise en solution et vieillis artificiellement) (De diamètre ou de dimension sectionnelle mineure jusqu'à 200 mm)

Luft- und Raumfahrt-Reihe: Spezifikation für Stangen und Preßprofile aus Aluminium-Kupfer-Magnesium-Silizium-Mangan Legierung (Lösungsgeglüht und warmausgelagert) (Mit Durchmesser oder kleinerem der Querschnittsmaße von nicht mehr als 200 mm)

NOTE The chemical composition of this material complies with that registered as International Designation 2014A.

1. Inspection and testing procedure

This British Standard shall be used in conjunction with the relevant sections of the latest issue of British Standard L 100 as follows.

Bars for machining and extruded sections	sections one and five
Bars for machining and extruded sections highly stressed structures	sections one and six

2. Quality of material

The material shall be made from aluminium and alloying constituents, with or without approved scrap at the discretion of the manufacturer.

3. Chemical composition

The chemical composition of the material shall be:

Element	%	
	min.	max.
Silicon	0.50	0.9
Iron	—	0.50
Copper	3.9	5.0
Manganese	0.40	1.2
Magnesium	0.20	0.8
*Chromium	—	0.10
*Nickel	—	0.10
*Zinc	—	0.25
*Titanium	—	0.15
*Titanium plus zirconium	—	0.20
Others : each	—	0.05
Others : total	—	0.15
Aluminium	—	Remainder

*Subject to the discretion of the Quality Assurance Authority, determination of these elements need be made on a small proportion only of the samples analysed.

4. Condition

4.1 Bars and extruded sections (temper designation T6).

Unless otherwise agreed and stated on the order in accordance with L 100, section five, the material shall be supplied solution treated in accordance with 5.1, straightened and subsequently artificially aged in accordance with 5.2.

4.2 Bars and extruded sections for highly stressed structures (temper designation T651). Unless otherwise agreed and stated on the order in accordance with L 100, section six, the material shall be supplied solution treated in accordance with 5.1, controlled stretched and subsequently artificially aged in accordance with 5.2. Unless otherwise stated on the order, it may be straightened after controlled stretching.

5. Heat treatment

5.1 Solution treatment. The solution treatment shall consist of heating at a temperature of $505 \pm 5^\circ\text{C}$ and quenching in water at a temperature not exceeding 40°C .

5.2 Artificial ageing. Artificial ageing shall consist of heating at a temperature of $175 \pm 5^\circ\text{C}$ for 5 h to 12 h.

6. Mechanical properties

6.1 Tensile test. Unless they are required by L 100 to be fixed by agreement between the manufacturer and the purchaser, the mechanical properties obtained from test pieces selected and prepared in accordance with the relevant requirements of L 100 shall be not less than the following values.

Diameter or minor sectional dimension of the bar or extruded section		0.2 % proof stress	Tensile strength	Elongation on gauge length of 50 mm	
				$5.65\sqrt{S_0}$	
mm		MPa (= N/mm ²)	MPa (= N/mm ²)	%	%
Over	Up to and including				
—	2.5	370	415	6	7
2.5	10	385	435	6	7
10	25	415	460	—	7
25	75	440	490	—	7
75	100	435	480	—	7
100	150	420	465	—	7
150	200	390	435	—	7

NOTE. Information on SI units is given in BS 3763 'The International System of units (SI)' and BS 350 'Conversion factors and tables'.

Modulus = 72 GPa

6.2 Hardness test. The value of X shall be as shown in the following table.

Tensile strength of test piece*	Value of X
MPa	%
f_t to less than $f_t + 15$	5
$f_t + 15$ to less than $f_t + 30$	7.5
$f_t + 30$ to less than $f_t + 45$	10
$f_t + 45$ and over	12.5

* f_t = minimum value for the particular size of material as specified in 6.1.

7. Identification

The material shall be identified as follows.

- Material supplied as specified in 4.1 : L 168-T6.
- Material supplied as specified in 4.2, not straightened after controlled stretching : L 168-T6510.
- Material supplied as specified in 4.2, straightened after controlled stretching : L 168-T6511.



ALUMINIUM ALLOYS

L 168

BARS AND EXTRUDED SECTIONS
T8, T861

PREVIOUSLY: L 66

PHYSICAL PROPERTIES					PRINCIPAL ALLOYING ELEMENTS %		
Temperature °C	at 20	20-100	20-200	20-300	Element	Minimum	Maximum
α /°C		23.0×10^{-6}		23.8×10^{-6}			
k W/mK		159			Cu	3.9	5.0
ρ Mg/m ³	2.8				Mg	0.2	0.8
σ MS/m	23.2				Si	0.5	0.9
c kJ/kgK	0.92				Mn	0.4	1.2

MECHANICAL PROPERTIES AT ROOM TEMPERATURE

Orientation		Longitudinal						Transverse						Short Transverse					
Thickness mm	>	2.5	10	25	75	100	150		2.5	10	25	75	100	150	200	25	75	100	150
	≤	2.5	10	25	75	100	150	200	2.5	10	25	75	100	150	200	75	100	150	200
f_t MPa	A					480	468 (439)												397
	B					495	485 (460)												411
	S	415	435	460	490	480	465	435						411					394
t_2 MPa	A						410												351
	B						432												370
	S	370	385	415	440	435	420	390						364					360
t_1 MPa	A						403												
	B						425												
	S			406	432		413												
e		7	7	7	7	7	7												
E GPa		72	72	72	72	72	72	72	72	72	72	72	72	72	72	72	72	72	72
ν		0.33	0.33	0.33	0.33	0.33	0.33	0.33	0.33	0.33	0.33	0.33	0.33	0.33	0.33	0.33	0.33	0.33	0.33
c_1 MPa	A																		
	B																		
	S		391		450														
c_2 MPa	A																		
	B																		
	S		403		460														
E_c GPa		74	74	74	74	74	74	74	74	74	74	74	74	74	74	74	74	74	74
f_{50} MPa	A					254	248 (233)												210
	B					262	257 (244)												218
	S	220	231	244	260	254	246	231											209
Q_1 MPa	A						189												161
	B						199												170
	S	170	177	191	202	200	193	179											166
F_y MPa	A					346	337 (316)												286
	H					356	349 (331)												296
	S	299	313	331	353	346	335	313											284
G GPa		27	27	27	27	27	27	27	27	27	27	27	27	27	27	27	27	27	27
b_{10} MPa	A						504												432
	B						531												455
	S	455	474	510	541	535	517	480											443
f_b MPa	A																		
	B																		
	S																		

Toughness

K_{Ic} MPa m ^{1/2}	L-T	26.9-30.8-32.9(4)	T-L	18.5-22.1-25.7(5)	S-L	20.7-20.8-20.9(2)
	L-S	32.0-32.9-33.8(2)	T-S	18.3-19.9-21.5(2)	S-T	

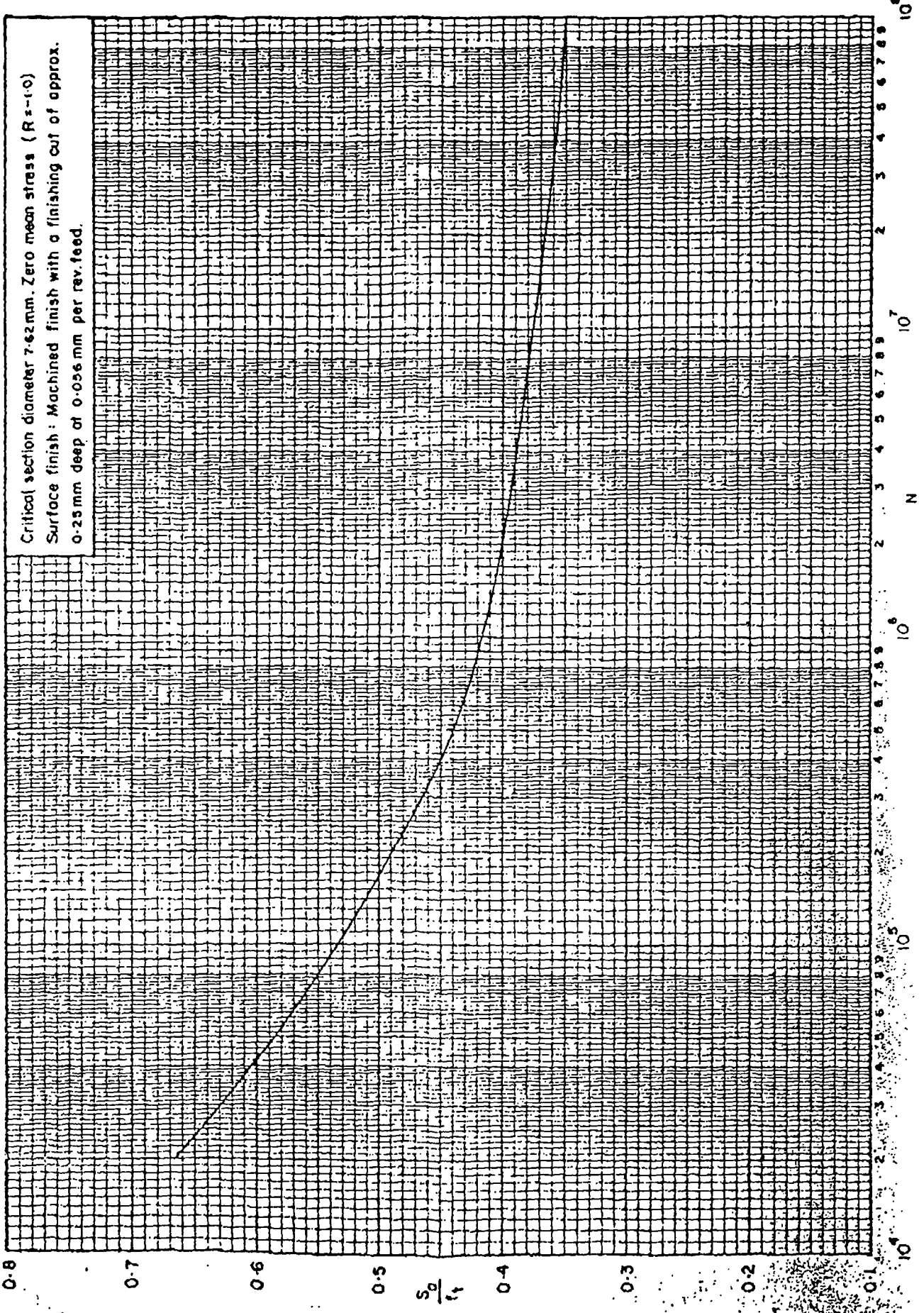


FIGURE 3. FATIGUE ENDURANCE IN ROTATING BENDING FOR PLAIN SPECIMENS

L 168

CHARACTERISTIC PROPERTIES

WELDABILITY	Electron Beam	Poor
	Arc (Inert Gas)	Very Poor
	Resistance (overlap joint)	Very Good
	Flame	Very Poor
	Brazing	Very Poor
RESISTANCE TO CORROSION		Susceptible
RESISTANCE TO STRESS CORROSION CRACKING		Resistant ^a
RESISTANCE TO EXFOLIATION CORROSION		Susceptible

(a) Aged at over 180°C (material aged at 160-170°C rated susceptible).

ADDITIONAL DATA

For data not provided on this specification some of the data for materials of similar composition may be used. The following properties may be taken from the specification listed against them and used for this material specification with the status (see Section 1, paragraph 2) indicated here.

PROPERTY	SPECIFICATION
Heat factor for t_2	1.65
Heat factor for f_t	1.65
Percentage elongation at temperature for e	1.65 (See note over Figure 3 on Page 4 of L65)
Heat factor for E	1.65
Heat factor for c_2	1.65